Assessment of Radiological Doses and Emergency Planning Zones of the Rooppur Nuclear Power Plant

by

Shafiqul Islam Faisal
Registration No.: 02
Session: 2020-2021

DOCTOR OF PHILOSOPHY IN NUCLEAR ENGINEERING

Department of Nuclear Engineering
UNIVERSITY OF DHAKA
December 2025

Assessment of Radiological Doses and Emergency Planning Zones of the Rooppur Nuclear Power Plant

Assessment of Radiological Doses and Emergency Planning Zones of the Rooppur Nuclear Power Plant

Supervisor : Professor Dr. Md. Shafiqul Islam

Co-Supervisor : Dr. Md. Abdul Malek Soner

by

Shafiqul Islam Faisal

Department of Nuclear Engineering

University of Dhaka

A thesis submitted to the University of Dhaka in partial fulfillment of the requirements for the degree of Doctor of Philosophy in the Department of Nuclear Engineering.

Statutory Declaration

The thesis titled "Assessment of Radiological Doses and Emergency Planning Zones of the Rooppur Nuclear Power Plant" submitted to the University of Dhaka in partial fulfillment of the requirements for the degree of Doctor of Philosophy in the Department of Nuclear Engineering. All published and unpublished writings referenced in this thesis have appropriately cited in the text. To the best of our knowledge, no part of the work presented herein have submitted for any other degree, qualification, or examination.

Dr. Md. Shafiqul Islam
Professor
Nuclear Engineering Department
University of Dhaka

Dr. Md. Abdul Malek Soner
Director
Center for Research Reactor
Bangladesh Atomic Energy Commission

CANDIDATE'S DECLARAION

It is hereby declared that this thesis or any part of it has not been submitted elsewhere for the award of any degree or diploma.

Shafiqul Islam Faisal

ACKNOWLEDGEMENTS

First and foremost, I express my deepest gratitude to Almighty Allah (SWT) for His guidance, blessings, and support throughout my academic journey.

My heartfelt thanks go to my supervisor, Prof. Dr. Md. Shafiqul Islam and co-supervisor Dr. Md. Abdul Malek Soner for their constant encouragement, valuable guidance, and constructive feedback, which have been instrumental in the successful completion of this work. I am also sincerely grateful to the Chairman of the Nuclear Engineering Department and the Dean of the Faculty of Engineering and Technology, University of Dhaka, for their continued administrative support. My appreciation extends to all faculty members of the Nuclear Engineering Department for their valuable insights during coursework and seminar sessions. I am equally thankful to the departmental staff, my colleagues, and well-wishers who have contributed in various ways to the success of this research.

Special thanks are due to the Radiation Safety Information Computational Center (RSICC) at Oak Ridge National Laboratory for providing access to the RASCAL 4.3 code, and to the National Atmospheric Advisory Release Center (NAARC) at Lawrence Livermore National Laboratory for the HotSpot code. I also gratefully acknowledge the NOAA Air Resources Laboratory (ARL) for the HYSPLIT transport and dispersion model and the READY website which were essential for meteorological data collection.

I am especially thankful to Dr. Ali Ayoub, Postdoctoral Fellow at the Massachusetts Institute of Technology (MIT), and Dr. Haruko Murakami Wainwright, Assistant Professor, Department of Nuclear Engineering, MIT, USA, for their insightful suggestions and thoughtful recommendations, which greatly enhanced the quality of this study. My sincere appreciation also goes to the journal reviewers for their constructive comments, which helped refine my methods and improve the interpretation of results.

Lastly, I am deeply obliged to my parents and family for their endless patience, encouragement, and unwavering support. My heartfelt thanks also go to my friends, who have stood beside me throughout this journey.

Yours, Faisal

ABSTRACT

Bangladesh is introducing nuclear power to meet rising energy demands and reduce reliance on fossil fuels, with the Rooppur Nuclear Power Plant (NPP) commissioning two 1,200 MWe VVER-1200 units in 2025 and 2026. While routine operations produce minimal radioactive releases, severe accidents, particularly long-term Station Blackout (LTSBO) events, can have significant radiological consequences, highlighting the need for robust emergency preparedness. Despite the use of advanced safety systems of housed VVER-1200 reactor, the adequacy of existing emergency planning zones (EPZ) and response measures at Rooppur NPP requires careful, site-specific evaluation to align with post-Fukushima IAEA safety requirements. Literature reviews point out research gaps, including limited analysis of beyond-design-basis accidents (BDBA), insufficient use of high-resolution atmospheric dispersion models, inadequate consideration of meteorological variability, lack of assessment of trans-boundary impacts, and the need for evidence-based EPZ design.

This study introduces several methodological advancements in radiological dose assessment for the Rooppur NPP. It extends previous work by analyzing BDBA, particularly LTSBO scenarios initiated by external events, and by employing plant-specific source terms derived from MELCOR-based SOARCA analyses. Radiological doses are evaluated across major exposure pathways while accounting for seasonal, diurnal, spatial variability using long-term (thirty-year), three-dimensional meteorological data and high-resolution atmospheric dispersion modeling. The study further applies post-Fukushima IAEA dosimetric criteria to reassess EPZs, evaluates the effectiveness of sheltering measures, and incorporates uncertainty analysis to ensure conservative and robust dose estimates. It uses modern accident consequence tools like Radiological Assessment System for Consequence Analysis (RASCAL 4.3), HotSpot 3.1.2, and Hybrid Single-Particle Lagrangian Integrated Trajectory (HYSPLIT) codes both in partial core melt (PCM) and complete core melt (CCM) under IAEA INES level 6 and 7 events. This also investigated the six LTSBO cases, both with and without passive safety systems like the Emergency Core Cooling System (ECCS), different leak rates and water uncovering times. Gaussian plume and puff models were used to simulate transport and dispersion of radioactive material for Monte Carlo randomly sampled yearly 360 possible weather scenarios considering the Rooppur region's (Ishurdi) meteorological data.

Results indicate that inhalation of I-131 dominates exposure near the plant immediately after release, while groundshine from deposited radionuclides, primarily Cs-137, becomes the main source over time. Meteorological conditions strongly affect dispersion: unstable conditions promote rapid dilution and shorter hazard distances, whereas stable conditions allow plumes to travel farther. Wet weather enhances deposition and groundshine, while dry conditions increase inhalation exposure. Deposition patterns peak close to the release point and are significantly higher during wet weather, with short-lived iodine and tellurium isotopes dominating early ground contamination. HotSpot predicts higher doses near the source but decreases faster with distance compared to RASCAL. In PCM scenarios, TEDE reached ~1,000 mSv, while CCM scenarios peaked at 11,000 mSv at 0.5 km, decreasing with smaller leaks or delayed containment failure. Simulations show that in the LTSBO event, sheltering-in-place or evacuation should be taken within 2 to 49 km of the Rooppur NPP reactor site based on criteria of TEDE 10 mSv for level 7, and within 0.7 to 14 km according to criteria of 100 mSv. Prophylactic measures to prevent radioiodine uptake by the thyroid may be necessary within a 3 to over 80 km radius for a threshold thyroid Committed Dose

Equivalent (CDE) of 50 mSv, depending on weather and accident conditions. The sensitivity results indicate that predicted air concentrations and ground deposition can increase by approximately four to six times when using a finer concentration grid of 0.010° (≈1 km × 1 km) compared to a coarser grid of 0.050° (≈5 km × 5 km), underscoring the strong dependence of results on spatial resolution. Long-range plume dispersion analysis revealed potential trans-boundary impacts; during a dry month of January, the plume moved south and then north, reaching the Bay of Bengal, Myanmar, and beyond, with heavy fallout near Ishurdi. During a wet month of July, the fallout was confined to a zone within 10-12 km, with ground deposition reaching above 1005 Bq/m2, primarily impacting Northwestern Bangladesh and parts of Eastern India in the initial days.

For 95% of the simulated weather scenarios, the maximum distance exceeding Precautionary Action Zone (PAZ) dose criteria was found to be approximately 3–4 km when sheltering in large buildings is available, increasing to 8–9 km when only residential houses are considered. Similarly, Urgent Protective Action Planning Zone (UPZ) criteria were exceeded at distances of about 20–25 km with large-building sheltering and 35–40 km with house-only sheltering. To balance public health protection with the practicality of emergency response, a PAZ radius of 5 km and a UPZ radius of 25 km are recommended for the Rooppur site. The analysis shows that taking shelter in large buildings can reduce radiation exposure much more effectively than staying in regular houses. Therefore, building large emergency shelters in nearby communities, especially in densely populated areas like Rooppur, Ishurdi, is recommended to improve public safety. Routine operation doses remain well below regulatory limits (<0.3% of the annual dose limit). Overall, the findings provide risk-informed guidance for emergency preparedness in Bangladesh, emphasizing sheltering, evacuation, iodine prophylaxis, strengthened infrastructure, and cross-border, weather-aware planning to ensure effective accident management and international safety compliance.

TABLE OF CONTENTS

CHAPTER 3.

FIGURES

LIST OF TABLES

ABBREVIATIONS

$AD_{fetus,inh}$	Absorbed Dose (RBE weighted) to the fetus from inhalation
$AD_{red\ bone\ marrow}$	Absorbed Dose (Average RBE-weighted) to red bone marrow
ARL	Air Resources Laboratory
ATDM	Atmospheric Transport and Dispersion Models
BDBA	Beyond Design-Basis Accident
BWR	Boiling Water Reactor
CCM	Complete Core Melt
CDC1	Climate Diagnostics Center
CDE	Committed Dose Equivalent
CDF	Core Damage Frequency
CEDE	Committed Effective Dose Equivalent
DALR	Dry Adiabatic Lapse Rate
DBA	Design Basis Accident
E_{inh}	Effective dose from inhalation (Committed)
ECCS	Emergency Core cooling System
EDE	Effective Dose Equivalent
ELR	Environmental Lapse Rate
EPA	Environmental Protection Agency
EPZ	Emergency Planning Zones
FGR	Federal Guidance Report
FSAR	Final Safety Analysis Report
GDAS	Global Data Assimilation System
GSR	General Safety Requirements
HYSPLIT	Hybrid Single-Particle Lagrangian Integrated Trajectory
IAEA	International Atomic Energy Agency
ICRP	International Commission on Radiological Protection

INES	International Nuclear and Radiological Event Scale
ITB	Iodine Thyroid Blocking
KI	Potassium Iodide
LBLOCA	Large Break Loss of Coolant Accident
LTSBO	Long-Term Station Blackout
MCCI	Molten corium concrete interaction
MOST	Ministry of Science and Technology
MTU	Metric ton of Uranium
MW_{th}	Mega Watt, thermal
MWd	Mega Watt day
NGas	Non-depositing Noble Gas
NOAA	National Oceanic and Atmospheric Administration
NNREPRP	National Nuclear and Radiological Emergency and Preparedness Response Plan
NPP	Nuclear Power Plant
PAG	Protective Action Guides
PAZ	Precautionary Action Zone
PBL	Planetary Boundary Layer
PCM	Partial Core Melt
PSAR	Preliminary Safety Analysis Report
PSD	Primary Side Depressurization
PWR	Pressurized Water Reactor
RASCAL	Radiological Assessment System for Consequence Analysis
RBE	Relative Biological Effectiveness
RCP	Reactor Coolant Pumps
RNUC	Particulate Radionuclide
SBO	Station Blackout
SG	Steam Generators

SOARCA	State-of-the-Art Reactor Consequence Analyses
STDose	Source Term to Dose
TBq	Tera Becquerel
TMI	Three Mile Island
TEDE	Total Effective Dose Equivalent
UPZ	Urgent Protective Action Planning Zone
VVER 1200	Water-Water Energy Reactor

CHAPTER 1.

INTRODUCTION

1.1 Background

Bangladesh is likely to incorporate nuclear power in its energy mix, in order to balance its growing energy needs and cut back on use of fossil fuels. The Rooppur Nuclear Power Plant (NPP), the country's first NPP, is scheduled to be commissioned with Unit 1 producing 1,200 MWe 1 in 2025 and Unit 2 producing an additional 1,200 MWe in 2026. The application of nuclear technology does involve thorough safety analyses, especially the whole reactor life cycle, starting from site selection, construction to operation and decommissioning (International Atomic Energy Agency (IAEA), 2015a). One aspect of this evaluation involves estimation of the radiological doses that may arise from hypothetical accidental releases of radioactive material.

The Rooppur site incorporates essential components and advanced safety systems implementing safety features based on lessons learned from the past three major accidents—the Three Mile Island (TMI), Chernobyl, and Fukushima—the VVER-1200 reactor ensures operational dependability even under extreme conditions by combining active and passive safety systems with multiple redundancies (two to four safety trains). These redundancies include containment spray systems, emergency boron injection systems, high-pressure Emergency Core Cooling System (ECCS), and hydrogen recombination units (Rooppur Nuclear Power Plant Construction Project, n.d.).

Nuclear events are ranked from Level 1 (anomaly) to Level 7 (severe accident) using the International Nuclear and Radiological Event Scale (INES) (IAEA, 2013a), which was created by the IAEA and Organization for Economic Co-operation and Development (OECD), Nuclear Energy Agency (NEA). When an event is rated Level 3 or higher, public concern usually increases. The seriousness of three significant nuclear accidents are frequently emphasized: 1. TMI in USA, 1979: A partial core meltdown and coolant loss resulted from an operator error and a stuck relief valve. Although some radioactive gases were released, the environmental impact was kept to a minimum by containment measures. INES assigned this accident a Level 5 rating. 2. Chernobyl in Ukraine, 1986: Unsafe testing practices and a defective RBMK reactor

design led to explosions and fires, which released a significant amount of radioactive material without any containment. The highest severity level, Level 7, was assigned to this accident. 3. Fukushima Daiichi in Japan, 2011: Core damage, hydrogen explosions, and extensive radioactive contamination resulted from a powerful earthquake and tsunami that cut off the reactors' cooling and power systems. The severity was upgraded from Level 5 to Level 7. **APPENDIX A** provides detailed explanations of the main causes behind these significant nuclear accidents and INES ratings procedure. These historical events emphasize the importance of accurate modeling and risk assessment to predict, evaluate, and response in severe scenarios, which is the basis of this study.

Emergency Planning Zones (EPZs) play a significant role in emergency preparedness. EPZs are areas surrounding a nuclear plant where pre-established protective measures, i.e., evacuation or sheltering, are taken in the event of an accident (IAEA, 2015a). The IAEA recommends two primary zones for protective measures: 1. Precautionary Action Zone (PAZ): Actions are taken before or soon after a radiation release to ensure safety. 2. Urgent Protective Action Planning Zone (UPZ): This zone focuses on minimizing long-term radiation exposure (IAEA, 2007) as shown in **Figure 1.1**. The IAEA recommendations have also been incorporated into Bangladesh law and regulation, including the Bangladesh Atomic Energy Regulatory Act 2012 (Ministry of Science and Technology (MOST), 2012) and the National Nuclear and Radiological Emergency Preparedness and Response Plan (NNREPRP) (MOST, 2020).

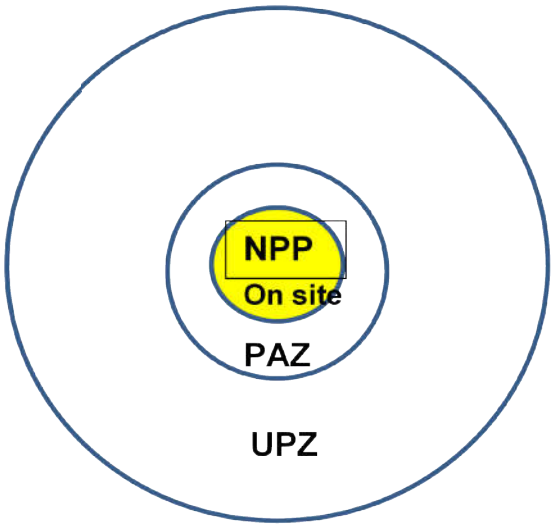

Figure 1.1: Primary Emergency Planning Zones

Both these emergency planning response and contamination/pollutant assessment rely on forecasting methods, which are based on mathematical modeling of atmospheric dispersion. They provide concentration field prediction and simulation of accident scenarios, combining emergency response with public and environmental safety. Over the years, different radiological dose assessment computer codes have been developed in an attempt to estimate plume paths, atmospheric transport, radiation doses, short-term health risks, long-term consequences, and effects of emergency countermeasures.

To assess potential radiation dispersion, two modeling approaches are commonly used: simple Gaussian models and more complex numerical simulations. Gaussian plume models are particularly effective in flat terrain and steady air conditions, typically for short distances—usually within 5 to 10 kilometers from the release point. These models are most effective when the emission source is small relative to the distance of interest and the local meteorology predominantly influences the dispersion. For short-range evaluations, HotSpot (Homann & Aluzzi, 2020) and Radiological Assessment System for Consequence Analysis (RASCAL) (Ramsdell et al., 2012) employ Gaussian plume models. Several research studies have been conducted using these two models in the assessment of different NPP's in several countries, which are presented in the next chapter. However, they have drawbacks when used in larger or more topographically varied regions. Long-range atmospheric transport models, like the Hybrid Single-Particle Lagrangian Integrated Trajectory (HYSPLIT) model (Stein et al., 2015), are better suited in these situations. These models provide more accurate predictions of radiological dispersion by taking into account vertical wind shear, surface roughness, and variable wind patterns.

1.2 Problem Statements

Although NPPs generally release minimal radioactivity during normal operations, severe accidents can lead to uncontrolled releases, posing significant risks to public health and the environment. Effective emergency protective measures—such as evacuation, sheltering, and iodine prophylaxis—require thorough analysis of potential accident scenarios to ensure adequate preparedness.

Despite advancements in reactor safety, such as redundant and passive safety systems in VVER-1000 reactors, Station Blackout (SBO) events remain a major contributor to core damage frequency, accounting for approximately 26% of total risk (Jabbari et al., 2019). Long-term SBOs, particularly those initiated by seismic events with 0.3–0.5 g Peak Ground Acceleration (PGA), can lead to core damage frequencies in the range of 1×10^{-5} to 2×10^{-5} per reactor-year (Chang et al., 2012). These highlight the critical need for effective safety measures, comprehensive accident analysis, and robust preparedness strategies.

For the Rooppur NPP, existing EPZs (PAZ and UPZ) and preparedness measures outlined in national guidelines of NNREPRP (MOST, 2020) requires closer evaluation to ensure alignment with post-Fukushima IAEA safety standards (IAEA, 2013b). Without comprehensive, site-specific radiological consequence analysis, Bangladesh's emergency response framework may remain insufficiently robust.

1.3 Research Gaps

The identified critical research gaps from the existing literature reviews discussed in chapter 2 are as follows:

(i) BDBA Analysis– No comprehensive study has assessed the radiological consequences of a BDBA-LTSBO event at Rooppur NPP using validated atmospheric dispersion models.

(ii) High-Resolution 3D Modeling– Absence of advanced tools like HYSPLIT for high-resolution and long-range (>200 km) dispersion analysis under diverse weather conditions.

(iii) Temporal and Meteorological Variability – Limited evaluation of how radionuclide transport differs between daytime and nighttime or under varying atmospheric stability classes.

(iv) Long-Term and Trans-boundary Effects– Lack of research on cross-border consequences of accidental releases.

(v) Evidence-Based Emergency Response Evaluation – Insufficient studies assessing the adequacy of emergency measures in light of IAEA's post-Fukushima safety standards.

(vi) PAZ and UPZ Design – Need for a technically justified approach to define EPZ sizes based on robust consequence analysis rather than indicative estimates.

1.4 Research Questions and Objectives

This study focuses on the following important research questions related to assessing the off-site radiological risks and emergency preparedness for the Rooppur NPP.

(i) What are the anticipated concentrations of radioactive materials, radiological dose distributions, airborne concentrations, and ground deposition in the vicinity of the Rooppur NPP during a BDBA scenario, such as an LTSBO? How do these change based on different weather conditions and the characteristics of the release?

(ii) What are the possible long-range environmental and public health effects of an accidental release from the Rooppur NPP? Which areas of Bangladesh and its neighbors might be affected by various weather patterns and release scenarios?

(iii) What are the appropriate sizes of off-site EPZs—specifically the PAZ and the UPZ—around the Rooppur NPP, as per post-Fukushima international guidelines? To what extent these zones prevent deterministic and reduce stochastic health effect ones?

The main objectives of this study are

- To investigate the radiological consequences of BDBA severe nuclear accidents at the Rooppur NPP by simulating public doses, analyzing radionuclide dispersion, and evaluating the effectiveness of protective measures.
- To verify the modeling results and sensitivity analysis of the used codes with long range accident impact assessment.
- To develop a methodology for determining EPZ sizes and to assess their potential impact on public health.
- To evaluate the routine release using 3-dimensional Meteorological Data.

1.5 Novelty of the Thesis

The current study provides several novel and significant advancements over previous studies in the estimation of radiological doses for the Rooppur NPP. The distinct characteristics and methodological developments outlined below establish the study's unique contributions.

(i) Broad Accident Scenario Coverage:

This study expands on BDBAs, particularly LTSBO events caused by external initiators. Previous studies only looked at DBAs, therefore they did not sufficiently represent all of the NPP's potential radiological hazards. The present study evaluates the scenarios considering with and without passive safety ECCS along with failure of all active safety ECCS, where as the previous study considered only the unavailability of active ECCS.

(ii) Updated Source Term Modeling

Unlike previous research that used generalized accident sequences from NUREG-1465 (Soffer et al., 1995) or analytical methodologies like Sahadat et al. (Sahadat & Fairuz, 2020a), present study uses source terms modeled using MELCOR (U.S. Nuclear Regulatory Commission (NRC), 2001) as reported in the NUREG-1935 State-of-the-Art Reactor Consequence Analyses (SOARCA) Report (Chang et al., 2012). This offers an assessment of radioactive emissions that is more accurate and plant-specific.

(iii) Comprehensive Exposure Pathway Analysis

The source term and radionuclide's contribution to three exposure pathways i.e. inhalation, cloudshine, and groundshine, and their time variation effects are investigated in this study, whereas no such assessment was in the previous study.

(iv) Consideration of Seasonal and Diurnal/Nocturnal Variability

The study incorporates seasonal variations, such as differences between dry and wet seasons, into the upper and lower bounds of atmospheric stability class. Furthermore, variations in exposure conditions during the day and at night are taken into account, whereas it was not part of the previous study.

(v) Use of Long-Term and 3-Dimensional Meteorological Data

Meteorological realism is enhanced by simulating 360 annual weather scenarios, based on 30 years of historical wind and rainfall data from the Ishurdi region in RASCAL. This approach surpasses earlier studies that used fewer or less representative meteorological samples. The 3-dimensional HYSPLIT dispersion model with compatible meteorological data of Global Reanalysis Climate Diagnostics Center (CDC1) and the Global Data Assimilation System (GDAS1) were used for long-range atmospheric transport effects of radionuclide dispersion, while all the prior studies used 2-D meteorological data.

(vi) Improved EPZ Dose Estimation Based on IAEA Criteria

Dose assessments for EPZs in this study adhere to the IAEA's post-Fukushima dosimetric thresholds, particularly focusing on red bone marrow and fetal thyroid doses (IAEA, 2013b). Prior studies have not analyzed the EPZ sizes under conservative accident scenarios.

(vii) Protective Measures Assessment

The current study examines the effectiveness of two protective measures—sheltering in a normal wooden house and in large buildings—under several accident scenarios. It is also examined how long-term sheltering (four days) affects dose reduction, especially for red bone marrow. Prior studies were not such specific assessments.

(viii) Uncertainty Analysis

This work, for the first time, applies an uncertainty analysis based on the 95th percentile of meteorological situations to improve the robustness and conservatism of dose estimations during the EPZ size estimation.

1.6 Significance of the Present Study

Although there have been some limitations, this study will provide essential baseline information for the Rooppur NPP for assessing various accident scenarios under diverse site-specific weather conditions. These findings could assist in estimating the potential impacts on the public and nearby areas, ultimately improving emergency preparedness and preventive measures. The public and relevant stakeholders will be informed about the potential impacts of a hypothetical catastrophic nuclear accident, the effectiveness of the current emergency response procedures, and the reliability of the safety features of the Rooppur NPP. The findings could be used for the development of evacuation plans and preparedness measures, eventually decreasing the detrimental consequences of such disasters on human health and the environment.

1.7 Thesis Layout

There are six chapters in the thesis. The issue of the current state of radiological dose assessment and EPZ size of the Rooppur NPP is briefly introduced in the first chapter. An overview of the previous research on the SBO event in VVER reactors and accident consequences of the Rooppur VVER-1200 reactors is provided in the second chapter. EPZ size assessment and routine operational studies of different reactors and different NPPs are also present in this chapter. In the third chapter, physical and meteorological aspects of atmospheric dispersion are briefly described. The theoretical bases of the three computational codes used in this study—

RASCAL, HotSpot, and HYSPLIT—are also discussed. The main emphasis is on the theoretical and mathematical implementations of the atmospheric dispersion modeling in the three codes, as well as the RASCAL source term calculation basis and its characteristics in Large Break Loss of Coolant Accident (LBLOCA) and LTSBO events.

The methodology for the analysis of the current study, the prerequisites for simulating severe initiating events, and their sensitivity test are all covered in the fourth chapter. Formulas for developed weather scenarios of the Rooppur sites, along with national and international guidelines and dosimetric criteria for intervention distances for various protective measures, are also presented in this chapter. Based on the three primary goals of the study—consequence analysis of LTSBO events, evaluation of EPZ size estimation and routine operational release analysis—this methodology chapter is divided into three parts. The calculated results and discussions based on the three-part methodology of chapter four are the main focus of chapter five. The source term of the six LTSBO cases, their release characteristics of various pathways, a comparative assessment of the protective measures in RASCAL and HotSpot, the estimation of PAZ and UPZ sizes with potential protective measures, and the annual effective dose during routine operation are all included in this chapter. The thesis's final chapter, chapter six, contains the key findings and some suggestions.

CHAPTER 2.

LITERATURE REVIEWS

2.1 Station Blackout Event Progression and Behavior

An SBO causes a loss of power, turbine trip, and simultaneous unavailability of on-site emergency AC power, which is the most dominating accident sequence in a VVER-1000 reactor. All of the main active safety systems, such as the Emergency Feedwater System (EFWS), Low-Pressure Injection System (LPIS), and High-Pressure Injection System (HPIS), become inoperable due to this condition (Tusheva & Reinke, 2007). As a result, the feedwater and primary coolant pumps trip when reactor SCRAM is activated, instantly reducing the forced coolant flow. Natural circulation initially removes the decay heat from the core, but as plant conditions deteriorate, this process progressively becomes worse.

As the turbine stop valves are shut, heat removal via steam dump to the condenser is avoided, leading to pressure rise in the secondary circuit. Relief of steam is provisionally given by the venting open of BRU-A valves, which maintain secondary pressure at approximately 6.67 MPa by flowing steam to atmosphere (Tusheva & Reinke, 2007). Without a constant feed-water supply, secondary-side water inventory continues to deplete through evaporation. When the steam generators are dehydrated, the plant has no ultimate effective heat sink, and the primary circuit begins to overheat.

In an SBO event, the time between reactor shutdown and the loss of cooling depends on whether the passive emergency cooling system is operational. If this system fails, cooling is lost immediately after shutdown. The escape of primary coolant through the Pressurizer (PZR) safety valve results in core uncover, overheating, and progression to a severe accident stage. With no additional safety systems engaged or accident management strategies applied, the Reactor Pressure Vessel (RPV) may fail under high pressure, compromising containment integrity. Furthermore, the high-pressure ejection of core melt, often accompanied by Direct Containment Heating (DCH), poses a significant threat to the containment structure (Tusheva et al., 2009).

The containment may fail before or shortly after the ejection of hot molten corium due to factors such as direct containment heating (DCH), steam explosions, hydrogen explosions, or containment isolation failure (Boeck, 2001). The location of a containment leak greatly affects the outcomes of severe accidents and the resulting dose rates. Leaks through penetrations into adjacent plant buildings release fewer fission products than direct leaks into the environment. Earlier studies assumed leaks at the top of the containment dome, but more accurate scenarios, focus on equipment hatches, airlocks, and penetrations where local strains are higher. Leak rates are difficult to predict due to differences in concrete placing, weld quality, and material properties (US NRC, 2013a).

Molten corium that breaches the pressure vessel in a catastrophic nuclear accident reacts with concrete to produce fission products and gases like hydrogen, which raises the containment pressure (Lee et al., 2016). Without cooling, this can damage containment and release radioactive material. Steam from molten corium entering the cavity or core-catcher is the main cause of rising pressure. Initially, pressure rises slowly but spikes when corium is released. Molten corium concrete interaction (MCCI) stops when water floods the cavity, but boiling water quickly raises pressure. During the early phase, steam condenses inside the containment due to the heat structures, reducing the pressure increase. Pressure gradually rises in the late phase as steam and gases are produced by MCCI and water evaporation, with MCCI accounting for two-thirds and evaporation accounting for one-third (Huong & Song, 2017).

The State-of-the-Art Reactor Consequence Analyses (SOARCA) project has demonstrated under unmitigated SBO conditions that core damage is to be expected in 9 to 16 hours, and reactor vessel rupture and off-site radioactive material releases within 45 hours (Chang et al., 2012). Esfandiari et al. (Esfandiari, et al., 2019) conducted a thermo-hydraulic analysis of loss-of-offsite-power accident scenarios. Jabbari et al. (Jabbari et al., 2019) examined SBO conditions in the VVER-1000 reactor, considering both the presence and absence of operator actions. Lee et al. (Lee et al., 2014) evaluated the extended SBO coping capability of the APR-1400 reactor, focusing on the effectiveness of external water injection strategies. Similarly, Darnowski et al. (Darnowski et al., 2015) studied the consequences of off-site power loss combined with total diesel generator failure in the European Pressurized Water Reactor (EPR).

Comparative assessments of SBO accidents using ATHLET for a German PWR-1300 MWe and a VVER-1000 demonstrate comparable key events, although changes in reactor power and steam generator design influence timing. The VVER-1000 allows more time for accident management. Without active ECCS, core dry-out is unavoidable; though the PSD procedure can delay it by two hr. Restoring power after accumulator depletion is essential to prevent severe core damage (Auria et al., 2008).

Auria et al. (Auria et al., 2008) found that depressurizing steam generators and the primary system in a VVER-1000 extended the plant's grace period from under 3 hr without accident management to 13 hr with accident management, and a theoretical maximum vessel failure time of 18 hr during SBO event. Another study using the ASTEC code (Tusheva et al., 2012) showed that without accident management, core heating begins approximately 2 hours and 26 minutes, with vessel failure at high pressure occurring after 4 hours and 18 minutes during an SBO. Depressurizing the primary system delays failure to about 5 hours and 48 minutes, but power restoration is still crucial for a VVER-1000/V-320 reactor.

Jabbari et al. (Jabbari et al., 2019) found that adding portable power sources and water supplies for the primary and secondary cooling systems significantly improves the VVER-1000's/V-446 resilience during SBO events using the Relap5 code. Besides, most of the studies including the mentioned above did not examine the core catcher system's role during accidents. However, Salari et al. (Salari et al, 2023) found that with a core-catcher during a SBO event reduces H_2 by 12.4%, CO and CO_2 by 100%, pressure by 14.34%, and temperature by 7.15% in the containment of a VVER- 1000 / v446 reactor using MELCOR code.

Battery-supported safety systems and passive heat removal capabilities need to be in place for much longer than a few hours, as the Fukushima Daiichi accident showed. Additionally, it noted the challenges of implementing emergency cooling in SBO conditions and restoring off-site power. Therefore, early depressurization, quick power supply restoration, and long-term passive heat removal are essential components of effective SBO accident management. In order to prevent re-criticality, containment flooding, ex-vessel cooling, and boron injection have also been proposed as ways to slow the core melt process and preserve fission products. (Tusheva et al., 2009).

2.2 Accident Analysis using RASCAL, HotSpot and HYSPLIT Codes

These codes have been widely applied in radiological dose assessments for various NPP scenarios in different countries. For a VVER-1200 reactor, Khai et al. (Khai & Cuong, 2015) modeled a Level 7 LBLOCA at the Ninh Thuan 1 NPP. They evaluated radiation doses within 40 km during the dry and rainy seasons. At the APR1400-based Shin Kori Unit 3, Muhammad et al. (Muhammad & Juyoul, 2019) assessed dose releases from hypothetiical LTSBO and LOCA events while taking seasonal effects into account. Similar to this, Gyamfi et al. (Gyamfi et al., 2020a) used a VVER-1000 model under a DBA involving a cold leg rupture and both InterRAS and HotSpot codes to evaluate radiological risks for a proposed site in Axim. Using RASCAL and GENII, Juyoul et al. (Juyoul & Moses, 2024) examined the radiological effects of accidents involving four different reactor types: APR1400, VVER1200, HPR1000, and APR1000. APR1000 presented the least risk to public health, according to their findings from LTSBO scenarios. Additionally, Juyoul et al. (Juyoul & Saleh, 2024) used ten years of meteorological data to model dispersion over a 40 km area in order to simulate LOCA and LTSBO at El Dabaa NPP.

In order to simulate a severe accident at Bushehr NPP, Ahangari et al. (Ahangari & Kalkhoran, 2019) used RASCAL to identify protective zones in accordance with EPA guidelines. They estimated Total Effective Dose Equivalent (TEDE) and thyroid doses under various weather conditions. Using RASCAL-4.2 and IAEA guidelines, Bakr et al. (Bakr & Abdien, 2018) conducted an assessment at El Dabaa to establish EPZs for a VVER reactor. Souissi et al. (Souissi et al., 2019) conducted seasonal LOCA simulations for a 3300 MW_t PWR at potential Tunisian sites—Marsa Dhouiba and Skhira. They estimated health impacts and determine appropriate protective measures using RASCAL.

Few research works have been done on consequence analysis for NPP accident using HotSpot code. Among them Cao et al. (Cao et al. , 2016) utilized HotSpot assess the radiological consequences of a hypothetical AP1000 SGTR event at Xianning NPP, calculating TEDE, air concentration, and ground deposition across stability classes A–F with site-specific meteorological data. Similarly, Gyamfi et al. (Gyamfi et al., 2020b) applied HotSpot to evaluate potential dispersion from a VVER-1000 accident at a proposed site in Axim, Ghana.

Shamsuddin (Shamsuddin et al., 2017) modeled radionuclide dispersion from a candidate nuclear site in Manjung, Malaysia.

The HYSPLIT code has been used in numerous studies in NPP scenarios and at different possible reactor locations. For instance, Pirouzmand et al. (Pirouzmand et al., 2018) examined the effects of an hypothetical SBO and LBLOCA accident scenario in Bushehr unit-1 (BNPP-1). Aliyu et al. (Aliyu et al., 2015) conducted hypothetical accident assessments at selected sites in Nigeria under different release conditions. Saeed et al. (Saeed et al., 2020) analyzed how radioactive plumes dispersed from a hypothetical accident in Baiji, Iraq. Omar et al. (Omar et al., 2019) modeled dispersion from a proposed site in Mersing, Johor, using HYSPLIT. In the meantime, HYSPLIT was used by Ireland's Radiological Protection Institute of Ireland (RPII) to evaluate the possible effects of UK-based NPPs on Irish territories (McMahon et al., 2013). Furthermore, HYSPLIT has been used in a number of studies to assess routine operational emissions.

2.3 Accident Analysis of the Rooppur NPP

There is limited research on the radiological risks associated with severe nuclear accidents at the Rooppur NPP in Bangladesh, particularly regarding Design Basis Accidents (DBAs) and the various modeling techniques that are applied. Sahadat et al. (Sahadat & Fairuz, 2020a) used the HotSpot 3.1 code to assess the Total Effective Dose (TED) and ground deposition in a hypothetical LBLOCA. They analyzed the radiological effects on the affected population in various seasonal weather conditions. Shiuli et al. (Shiuli et al., 2022) also evaluated the Rooppur reactor events that were at levels 5 to 7 on the INES. They used the RASCAL and HotSpot computer codes to model the LOCA events. Their assessments included TED, TEDE, Thyroid Committed Dose Equivalent (CDE), and Committed Effective Dose Equivalent (CEDE) from inhalation for a 40 km radius around the Rooppur NPP.

For Rooppur NPP, R. Alam (Alam, 2024) examined the LBLOCA without the ECCS under variations of weather and seasonal conditions. HotSpot (v3.1.2) and PCTRAN were used for the simulations within a 100 km radius. The radioactive releases and the associated external doses were measured with ground deposition, TED, plume area, and exposure pathways, all of which were evaluated seasonally. Altab et al. (Altab et al., 2020) used an atmospheric dispersion model

to study the potential radiation doses from a hypothetical release of radionuclides at the Rooppur NPP. They generate source term based on the Nuclear Regulation (NUREG-1228) using MATLAB. By adjusting uncertain input parameters, they conducted a sensitivity analysis for TEDE. Sahadat et al. (Sahadat & Fairuz, 2020b) evaluated the dose contours to track arrival times and plume direction in Rooppur. They used a source term comparable to that of the Fukushima accident and employed the HotSpot code. In case of an emergency evacuation, they also suggested possible shelter locations.

Nath et al. (Nath et al., 2020a; Nath et al., 2020b) examined the thermal-hydraulic behavior of VVER-1200 reactor cores during LOCA in conjunction with SBO scenarios. They analyzed various factors, including heat transfer, reactor pressure, coolant flow dynamics, critical heat flux, and temperature distribution, using the PCTRAN simulation both with and without the ECCS.

2.4 Previous Evaluations of EPZ

Several studies used different models and methodologies to evaluate the EPZs for different NPPs. The Swedish Radiation Safety Authority reassessed the EPZs for the Forsmark, Oskarshamn, and Ringhals sites using the RIMPUFF (Nielsen et al., 1999) and PIGLET (Young et al., 1990) models. Their evaluation led to a recommendation of revising the original 12–15 km EPZs to a 5 km radius PAZ and a 25 km radius UPZ (Johansson et al., 2018). Similarly, the German Commission on Radiological Protection reviewed EPZs (German Commission on Radiological Protection, 2014) using the Real-time Online Decision Support System (RODOS) framework (Raskob & Gering, 2010), incorporating lessons from the Fukushima accident. Based on emergency reference levels of 100 mSv for evacuation and 10 mSv for sheltering, they proposed defining a central zone extending up to 5 km and a medium zone reaching up to 20 km.

Sahin et al. (Sahin & Ali, 2016) evaluated EPZs for the ACP-1000 reactor in Karachi, Pakistan, using Gaussian plume and puff models within the RASCAL code (Ramsdell et al., 2012), following IAEA Post-Fukushima Guidelines. In the Czech Republic, EPZs for the Temelin VVER-1000 NPP were determined through a probabilistic approach for both DBA and BDBA (State Office for Nuclear Safety, 2001). These scenarios were derived from level 1 and level 2

probabilistic safety assessments (PSA) conducted with the MELCOR code (US NRC, 2001). Findings showed that beyond a 5 km radius, intervention thresholds for sheltering (50 mSv) and evacuation (500 mSv) were not exceeded. Likewise, at South Africa's Koeberg NPP (922 MWe Framatome), a combination of deterministic and probabilistic analyses was applied (Perryman, 2005). EPZs were calculated using the COSYMA code (National Radiological Protection Board, n.d.) for a reference scenario involving a 1% iodine release, recommending a PAZ of 3 km and a UPZ of 14 km. Additionally, Ali et al. (Ali & Kakosimos, 2023) proposed a receptor-centric decision support framework that integrates impact assessments from multiple NPPs for primary receptors (the State of Qatar) and secondary receptors (cities, transport hubs, industries, desalination plants, oil and gas fields). This system assesses potential consequences from three nearby NPPs—Barakah I in the UAE, Bushehr I (operational) in Iran, and Umm Huwayd (proposed) in Saudi Arabia—and prioritizes countermeasures for non-simultaneous accident scenarios.

According to the U.S. NRC, EPZs are tailored to site-specific factors such as local requirements, population density, terrain, access routes, and jurisdictional boundaries. A joint NRC-EPA task force established EPZ dimensions for plume exposure and ingestion pathways by evaluating risk, probability, cost-effectiveness, and potential accident consequences. Their findings indicated that, for most nuclear plants, EPA evacuation thresholds—250 mSv for thyroid exposure and 50 mSv for whole-body exposure—are unlikely to be exceeded beyond a 10-mile radius, even under conservative conditions (US NRC, 1980; US NRC, 2012). In a related study, Tang et al. (Tang et al., 2016) analyzed the evacuation zone requirements for a potential nuclear meltdown at the Longmen plant in Taiwan, using emission scenarios similar to those of the 2011 Fukushima accident. Results showed that the plume exposure pathway, accounting for inhalation and cloudshine with initial 7-day doses above 20 mSv, could extend from around 10 km in rainy conditions to as far as 100 km under sunny weather.

2.5 Routine Operations

Numerous studies have investigated the release of radioactive materials into the environment during the routine operation of various NPPs in different countries, employing a variety of computational codes. For instance, Sadhukhan et al. (Sadhukhan & Synzynys, 2023) studied routine operational impacts using the CROM code (CIEMAT, 2007). They assessed the

atmospheric dispersion of radionuclides and its impact on public radiation exposure both before and after the Rooppur plant was put into operation. Their model included a neutral atmospheric stability class (D) and a constant wind speed of 2.98 m/s during the dispersion process.

Sohrabi et al. (Sohrabi et al., 2013) used the PC-CEAM 98 code, while Pirouzmand et al. (Pirouzmand et al., 2015) applied the CAP88-PC code to evaluate radiation doses from routine releases at the Bushehr NPP-1, a VVER-1000 reactor. Similarly, Zubair et al. (Zubair et al., 2022) utilized the GALE code to assess radiation doses from gaseous emissions during the routine operation of the Barakah NPP of the APR-1400 reactor. The above studies utilize Gaussian dispersion models, which are among the simplest methods for simulating atmospheric dispersion and favored over numerical dispersion models due to their minimal data requirements, such as wind speed and source terms.

The HYSPLIT – a 3- D model has been widely utilized in scientific studies as well as examining dose assessment of the routine operations of NPPs in various locations of Korea (Kim et al., 2022), Saudi Arabia (Alramamah et al., 2022), Bushehr, Iran (Feyzinejad et al., 2019, Zali, et al. 2017), and Nigeria (Aliyu et al., 2015). Kim et al. (Kim et al., 2022) analyzed and compared radiation doses from operational NPPs in Korea and China, focusing on their impact on major cities in Korea. The study employed the HYSPLIT and SimPacts software packages to model the dispersion of airborne pollutants. Alrammah et al. (Alramamah et al., 2022) conducted a radiological impact assessment study for a proposed PWR at Umm Huwayd on the eastern coast of Saudi Arabia. The HYSPLIT tool was used to estimate the air concentration and ground deposition of radionuclides such as cesium-137 and iodine-131. Aliyu et al. (Aliyu et al., 2015) analyzed radionuclide air concentrations in air and surface depositions resulting from hypothetical NPP stack emissions in Nigeria. Feyzinejad et al. (Feyzinejad et al., 2019) validated the HYSPLIT model and conducted dispersion simulations using the integrated WRF-HYSPLIT framework to assess annual radiation doses from routine operational releases.

2.6 Criteria of Protective Actions

During a radiological accident involving uncontrolled radioactive material release, protective actions are necessary to prevent unnecessary radiation exposure, even if they disrupt normal life.

Early Phase Response

Table 2-1 lists protective actions for the early phase of a radiological accident as outlined in the Bangladesh NNREPRP (MOST, 2020), IAEA General Safety Requirements (GSR) Part 7 (IAEA, 2015a), and the Protective Action Guides (PAG) manual (US EPA, 2017). Key protective actions include sheltering in place, evacuation, and administering potassium iodide (KI) as a supplementary measure.

The projected early-phase PAG are usually calculated over the first four days after a release, covering exposure to both the plume and deposited materials before considering long-term protective actions like relocation (US EPA, 2017). PAGs outline dose thresholds that trigger protective actions to minimize radiation exposure and serve as advisory tools rather than regulatory limits; they do not classify exposure as safe or unsafe. PAG values are designed to aim a balance between practical considerations of health risks and cost-effectiveness (US EPA, 2017).

The EPA recommends sheltering-in-place or evacuation if TEDE exceeds 10–50 mSv, with evacuation generally starting at 10 mSv. However, evacuation may be unsuitable in cases like severe weather, concurrent disasters, or immobile individuals. Sheltering is often preferred for high-risk groups, with a recommendation to shelter in place for projected doses up to 50 mSv (US EPA, 2017). On the other hand, NNREPRP and GSR 7 recommend sheltering in place or evacuation for a 7-day whole body dose (TEDE).

If significant radioiodine is released and the projected thyroid dose exceeds 50 mSv, administering KI should be considered as an additional protective action. During the early phase of a radiological emergency, due to their sharp sensitivity to radioactive iodine exposure in children, the PAG Manual (US EPA, 2017) recommends the administration of potassium iodide (KI) when the projected thyroid dose to a child exceeds 5 rem (50 mSv). To support this recommendation, RASCAL 4.3 includes functionality for calculating child thyroid doses, specifically to inform decisions regarding KI distribution. These calculations are based on FGR 13 and ICRP Publication 72 dose coefficients, which provide age-specific parameters.

Table 2-1: Criteria for protective actions in National and International guidelines

Protective Actions	Intervention Levels		
	NNREPRP	GSR part-7	PAG Manual,

	(MOST, 2020)	(IAEA, 2015a)	(US EPA, 2017)
Sheltering-in-place or, Evacuation	100 mSv, whole body dose, first 7 days	100 mSv, Effective dose, first 7 days	10- 50 mSv, TEDE, first 4 days
Stable Iodine Administration (Iodine thyroid blocking)	50 mSv, Equivalent dose to the thyroid due to exposure from radioiodine, first 7 days ~ Thyroid committed dose equivalent	50 mSv, Equivalent dose to the thyroid due to exposure from radioiodine, first 7 days ~ Thyroid committed dose equivalent	50 mSv, Child thyroid dose from exposure to radioiodine~ Child Thyroid committed dose equivalent

Intermediate Phase Protective Actions

The intermediate phase lasts for weeks to months after an initial accident and focuses on three main areas 1. Limiting long-term radiation exposure, 2. controlling the spread of contamination, 3. preparing for recovery and potential reoccupation. Unlike the quick evacuation that occurs immediately after a release, relocation is a longer-term strategy aimed at reducing the risk of chronic exposure to radiation. This approach may involve moving residents from contaminated areas even after the initial evacuation has ended (US EPA, 2017).

For PAG, relocation thresholds are set at 5 mSv in each accomplishing year and 20 mSv in the first year. The 20 mSv annual threshold was selected as a compromise to guarantee safety while minimizing disturbance to impacted people and communities. Ingestion is usually excluded from these thresholds unless it substantially increases exposure, and they apply to future doses that can be prevented (US EPA, 2017).

Cleaning procedures like surface washing, soil removal, and debris disposal might be sufficient if anticipated radiation doses fall below specific relocation thresholds. In areas where short-lived radionuclides are present, natural decay and restricted access can help lower radiation exposure. For long-lasting contaminants, relocation might still be required.

2.7 Summary on Literature review and Identified Gaps

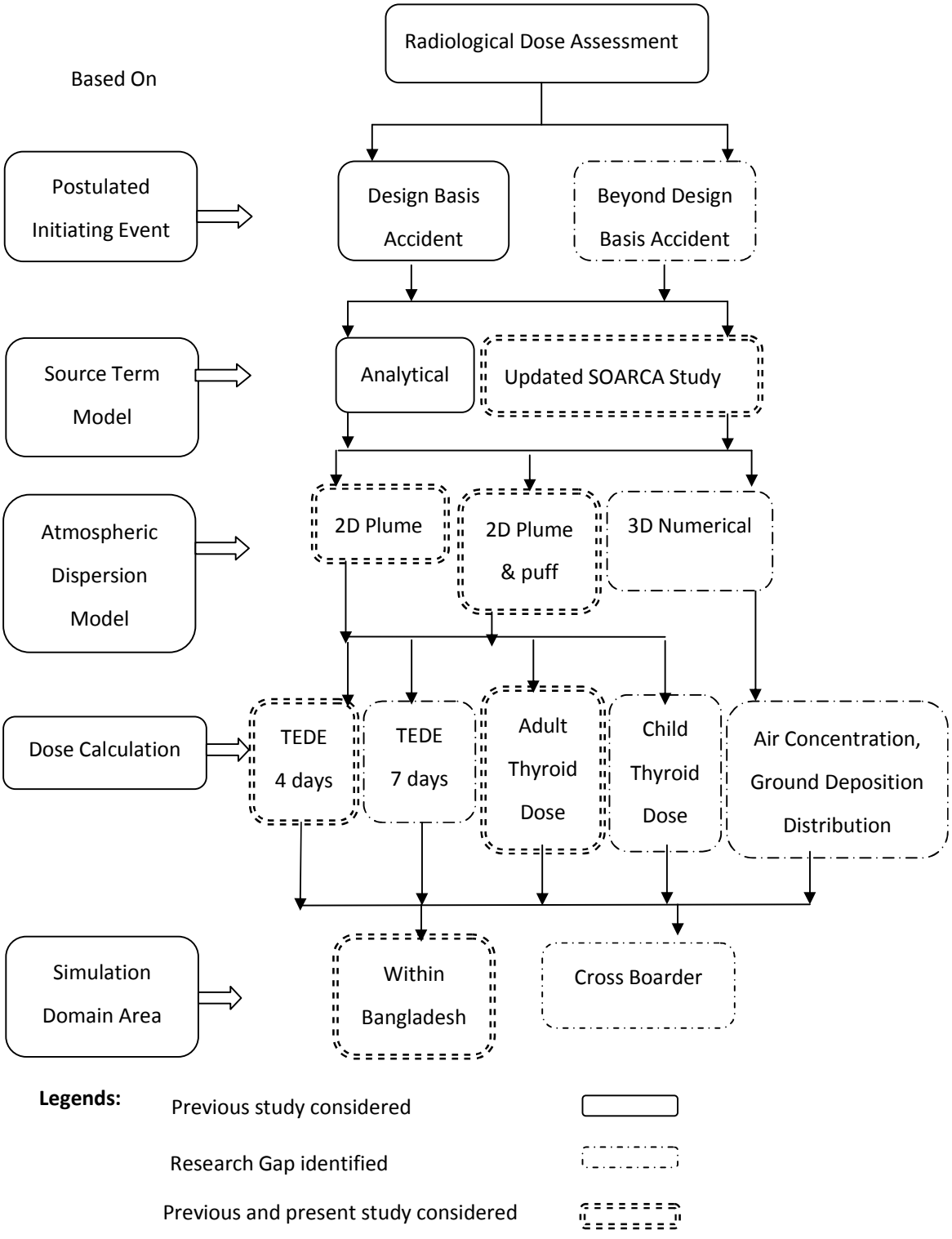

Figure 2-1: Summary on Literature Review and Identified Gaps
[19]

The review of existing literatures and identified gaps is shown in **Figure 2-1** indicates that several critical research gaps in the assessment of nuclear accident consequences at Rooppur NPP. Notably, there is no comprehensive evaluation of the radiological impacts of a BDBA involving a LTSBO using validated atmospheric dispersion models. Existing studies also lack high-resolution, three-dimensional dispersion analyses to capture long-range transport beyond 200 km under varying meteorological conditions. Moreover, limited attention has been given to temporal and atmospheric variability, particularly differences between daytime and nighttime releases and across stability classes. Research addressing long-term and trans-boundary impacts of accidental releases remain absence.

In addition, there is insufficient evidence-based evaluation of emergency protective actions in the context of post-Fukushima IAEA safety standards. Finally, the demarcation of PAZ and UPZ are largely based on indicative assumptions, highlighting the need for technically justified EPZ design grounded in robust radiological consequence analysis.

CHAPTER 3.

THEORETICAL ASPECTS OF ATMOSPHERIC DISPERSION AND USED CODES

3.1 Meteorological and Physical Aspects of Atmospheric Dispersion

Complex interactions between atmospheric physics and meteorological conditions control the dispersion of radioactive material in the atmosphere, especially during an NPP accident. These elements have a special impact on the planetary boundary layer (PBL), where surface-driven meteorological processes interact with the released pollutants.

3.1.1 Meteorology's Role in Atmospheric Dispersion

The way pollutants are dispersed and diluted in the atmosphere is greatly influenced by meteorology. From micrometers to thousands of kilometers, and from seconds to years, the atmosphere exhibits significant spatial and temporal variability. These differences have a direct impact on the movement and dispersion of gases and particles emitted from sources such as NPPs.

The spatial and temporal scales of atmospheric processes can be used to categorize them: Turbulence and eddy diffusion are examples of microscale phenomena (2 mm–2 km) that have a major impact on plume spread close to their source. Mesoscale (2 km–2,000 km): This includes regional wind patterns like thunderstorms, sea breezes, and mountain-valley winds. Larger weather patterns, such as fronts, major storm systems, and systems of high and low pressure, are covered by the synoptic scale (500–10,000 km) (Kiehl & Jacobson, 2001).

Different scales affect how pollutants spread in the environment. Important weather factors for dispersion are wind speed and direction, air stability, turbulence, temperature, humidity, and rainfall. Wind moves pollutants horizontally, while turbulence controls their spread. Air stability affects vertical dispersion and determines how much airborne contaminant get diluted (IAEA, 1986).

Understanding the weather is essential for forecasting the path of radioactive plumes and determining the possible radiation exposure of individuals in emergency situations, such as nuclear accidents.

3.1.2 The PBL and Its Influence on Dispersion

The PBL is the lowest part of the atmosphere that directly feels the effects of the Earth's surface. It reacts to things like heating, cooling, and friction within about an hour or less (Stull, 1988). The way the PBL is structured and moves plays a big role in how air spreads near the ground.

Inside the PBL, air mixes vertically because of two main reasons: Thermal convection happens when different parts of the surface heat up unevenly, causing warm air to rise. Mechanical turbulence is caused by wind changes near the surface or rough land. On sunny days with light winds, thermal turbulence is more prevalent, whereas mechanical turbulence is more intense when winds are high (Schulze & Turner, 1996).

Over land, the PBL changes a lot between day and night and can be divided into layers Surface layer: From the ground up to about 10% of the PBL height, where temperature and wind change quickly with height. Mixed layer: Forms during the day due to sunlight heating; well-mixed and topped by a layer that stops air from rising further. Residual layer: available from the mixed layer after sunset; less turbulent but can still move pollutants sideways. Stable layer (or nocturnal boundary layer): Forms at night when the surface cools; reduces vertical movement and causes pollutants to build up near the ground. The PBL's depth usually ranges from 100 to 3000 meters, depending on time, weather, and surface type.

3.1.3 Wind Profile and Surface Roughness

The main force behind the horizontal movement of pollutants in the atmosphere is wind. Pressure gradients create it, and surface friction and the Coriolis force alter it. Because frictional influence decreases with height, wind speed typically increases. Wind shear, a change with altitude, influences the vertical distribution of plumes and intensifies mechanical turbulence.

Depending on the surface roughness length (z_o), the wind speed profile in the boundary layer usually follows a logarithmic or power-law function of height. Rougher surfaces, like urban

areas and forests, create more friction, which slows down winds and intensifies turbulence close to the ground. On the other hand, less turbulent mixing occurs on smooth surfaces, such as flat terrain or open water. In addition to influencing local wind direction, surface roughness and obstructions like trees or buildings can create mechanical turbulence, which alters plume spread patterns (Marshall & Plumb, 1965).

3.1.4 Atmospheric Stability and Vertical Temperature Structure

Atmospheric stability affects how pollutants move up and down in the air. Stability is assessed by comparing the environmental lapse rate (ELR)—the rate of temperature decrease with height in the atmosphere—to theoretical lapse rates: Dry Adiabatic Lapse Rate (DALR): Approximately 9.8°C/km for unsaturated air (Barry et. al, 2003). Saturated Adiabatic Lapse Rate (SALR): Ranges from about 4°C/km to 7°C/km depending on temperature and moisture.

The DALR correlation with the ELR establishes whether the atmosphere is: Stable: ELR < DALR; poor dispersion results from suppressed vertical motion. Unstable: ELR > DALR; improved vertical motion promotes effective mixing. Neutral: ELR ≈ DALR; when air parcels are displaced vertically, they do not accelerate or decelerate. Significant levels of pollutants can trapped near the ground resulting from temperature inversions, in which the temperature increases with altitude.

In 1961, Pasquill created a classification system based on surface wind speed, solar radiation during the day, and cloud cover at night to aid in estimating atmospheric stability (Pasquill, 1974). This system includes six stability classes: A: Very unstable, B: Unstable, C: Slightly unstable, D: Neutral, E: Slightly stable, F: Stable. The dispersion coefficients for Gaussian plume models are determined by these classes, which are frequently employed in regulatory dispersion models (US NRC, 1982a). Classes E and F, for example, suggest little vertical mixing, whereas Classes A–C show strong vertical dispersion. Increased turbulence favors pollutants to move upward and downward in unstable conditions, which helps in their dilution. Because there is less vertical mixing under stable conditions, pollutants stay nearer the surface, increasing local concentrations.

Potential temperature (θ) is an important thermodynamic measure for assessing atmospheric stability, particularly at varying heights. It represents the temperature an air parcel would reach

if it were brought adiabatically to a standard pressure level, usually 1000 hPa. In a stable atmosphere, potential temperature increases with height. A constant or decreasing potential temperature with altitude indicates a neutral or unstable profile.

3.1.5 Plume Behavior and Dispersion Patterns

The stability of the atmosphere and wind structure has a major impact on the form and motion of a radioactive plume. While wind speed affects the plume's travel time and degree of dilution, wind direction affects how the plume disperses. Emergency responses planning and simulating radiation exposure require an understanding of these dispersion behaviors.

Some typical plume behaviors are: 1. Looping: The plume travels widely up and down when there is strong vertical mixing and unstable conditions. 2. Coning: Under neutral conditions, with moderate and steady vertical and horizontal dispersion, this behavior is observed. 3. Fanning: The plume spreads out horizontally but stays confined vertically in stable atmospheres with weak vertical mixing. 4. Lofting: The plume can rise and disperse without coming into contact with the ground when the atmosphere is unstable above the source but stable below. 5. Fumigation: When the atmosphere is stable above but unstable below, the plume is trapped and rapidly mixed down, which can result in high concentrations at ground level. 6. Trapping: The plume remains contained in a narrow layer when stable layers are present both above and below the emission point (Lamarsh & Baratta, 2001).

3.2 Present Study Used CODES

The radiological impact of a nuclear accident depends on a range of parameters like meteorology, topography, type and quantity of radionuclide released. The radiological dispersion needs to be simulated on the computer code for modeling and calculating the probable exposure of the population. NPPs worldwide employ codes for evaluating the probable outcome of nuclear accidents. These codes are supported by regulatory organizations and are used primarily for the assessment of accident sequences, estimation of source term releases from containment structures, and prediction of radioactive material dispersal into the environment. It examines radiation doses to members of the public through different paths of exposure, such as cloudshine, groundshine, resuspension, and ingestion of radiologically contaminated food and water. Furthermore, the codes determine the geographical contamination ranges and can simulate environmental impact over large distances, e.g., spanning national boundaries.

3.2.1 RASCAL CODE and Models

The Radiological Assessment System for Consequence Analysis (RASCAL) code (Ramsdell et al., 2012; Ramsdell et al., 2015), developed by the U.S. NRC Emergency Operations Center, serves as a rapid assessment tool for performing independent dose projections during radiological emergencies. It is designed to evaluate potential radiological impacts both prior to and during a release or severe accident, particularly when environmental monitoring data are not yet available.

RASCAL supports emergency planners, responders, and analysts by estimating population exposure levels and assisting in determining appropriate protective measures. Its fast dose calculation capability is especially valuable to local emergency authorities when deciding between issuing evacuation orders or advising the public to shelter in place.

RASCAL version 4.3 includes a suite of seven analytical tools, with four specifically designed for consequence assessment. Among these, Source Term to Dose (STDose) and Field Measurement to Dose (FMDose) are the principal tools used for estimating radiation doses (Ramsdell et al., 2013; Athey et al., 2013). The most widely used tool, STDose, was utilized in this study with an ordered process that includes incident site, describing the nature of the issue, estimating radionuclide releases, and assessing the dose consequences.

The tool simulates a number of scenarios including accidents involving nuclear reactors, spent fuel pools, radioactive material transportation accidents, and incidents involving radiological dispersal devices. RASCAL 4.3 can simulate events for up to 96 hours and has an extended calculation range of up to 160 kilometers (Ramsdell et al., 2015). To evaluate radiation doses, it uses two modeling techniques: a puff model on a Cartesian grid for longer distances and the Gaussian Plume Model (GPM) for short distances.

RASCAL employs a number of models to predict the consequences of an accidental release. The first set of models assesses the quantity of activity emitted into the environment over time. The second set of models distributes the activity in the environment; the third set of models determines the impact of the activity in the environment. (Ramsdell et al., 2013).

The STDose model is utilized when users need to input data regarding reactor or accident conditions to estimate the projected radiation dose to individuals located downwind of a release. Initially, STDose generates a time-dependent source term, which specifies the release rate of each radionuclide over time considering radioactive decay chains to track radionuclide behavior. An atmospheric dispersion and transport model that computes the movement and settling of radionuclides in the environment uses the source term from this tool as input. (Ramsdell et al., 2013). The transport, dispersion, and deposition model calculates the concentrations of radionuclides in the atmosphere and on the ground. Projected radiation doses through the three main exposure pathways—cloudshine (direct exposure from the radioactive plume), inhalation (intake of airborne radionuclides), and groundshine (external exposure from radionuclides deposited on the ground, usually assuming four days of exposure)—are then calculated using these concentrations (Ramsdell et al., 2013).

3.2.1.1 Source Term / Release Path Models

The initial models used in RASCAL simulations are the source term release path models. These models estimate which radionuclides are released and the quantity of each available for environmental release. They also define the transport mechanism of radioactive material from the source to the environment and quantify the release over time. Depending on the type of event, such as reactor accidents, spent fuel incidents, or events at fuel cycle facilities, different models are used (Ramsdell et al., 2013).

Reactors Models

A simplified model of nuclear reactors in RASCAL is made up of a number of connected compartments, or "boxes," that are used to transfer radioactive materials. The system begins with the reactor vessel and ends with the external environment. The number and arrangement of intermediate compartments, as well as the transfer pathways between them, vary depending on the specific type of reactor. The physical and chemical processes—such as radionuclide decay and the formation of decay products—can occur within any of these compartments. Each reactor type, such as a PWRs or Boiling Water Reactor (BWR), is characterized by a unique configuration of these boxes and transfer routes. RASCAL includes predefined configurations for several reactor types, including PWRs with U-tube and once-through steam generators, BWRs, and VVERs (Russian-designed PWR) (Ramsdell et al., 2013).

For identifying the source term in NPP accidents, RASCAL provides a number of techniques. These methods include approaches based on predetermined accident scenarios as well as sampling or monitoring data. In particular, RASCAL contains four predefined accident sequences: the LBLOCA, the LTSBO scenario based on the SOARCA study, Coolant Release Accidents, and scenarios utilizing data from the Containment Radiation Monitor (Ramsdell et al., 2012; Ramsdell et al., 2013). The LBLOCA and LTSBO are the two primary modeling sequences that RASCAL offers for core-melted accident scenarios. These are employed to model radionuclide release and the progression of severe accidents.

When modeling PWR scenarios where the source term is based on reactor conditions or derived from coolant or containment air samples, users can choose from three possible release pathways: Containment leakage or failure, Steam generator tube rupture, and Containment bypass (Ramsdell et al., 2012; Ramsdell et al., 2013).

To define the characteristics of a containment leak, users can select between two options: specifying the leak rate as a percentage of volume per unit time, which is used in this study or characterizing it based on containment pressure and hole size (Ramsdell et al., 2012; Ramsdell et al., 2013). For example, a 100% per hour leak rate equates to a 25% loss per 15-minute interval. RASCAL adjusts inventories at each step to account for decay, ongoing core damage, mitigation, and environmental release (Ramsdell et al., 2012).

In addition to these defined scenarios, there are five data-driven methods for estimating source terms: coolant sample, containment air sample, effluent discharge by mixes, effluent release rates by nuclide, and effluent release concentrations by nuclide. These allow users to specify or estimate source terms using radiological measurements or observable plant data (Ramsdell et al., 2012; Ramsdell et al., 2013).

3.2.1.1.1 Source Term Calculation Basis in RASCAL for PWRs

RASCAL 4's STDose module uses techniques primarily taken from NUREG-1228 (McKenna & Giitter, 1988) to estimate the source terms over time for NPP accidents. To better understand severe accident behaviors in light-water reactors, these techniques have been updated using timing and source term data from NUREG-1465 (Soffer et al., 1995).

For source terms involving core damage, radionuclide inventories are based on calculations by the U.S. NRC using the SAS2H module of the SCALE 4.4a (Standardized Computer Analyses for Licensing Evaluation) system, which employs ORIGEN-ARP for radionuclide concentration over time. These inventories are normalized in curies per megawatt thermal (Ci/MW_t) and a PWR with 193 fuel assemblies, a burnup of 38,585 MWd/MTU, 4.0% uranium-235 enrichment, and a total thermal output of 3,479 MW_t (Ramsdell et al., 2012).

Most radioactive material in a nuclear power plant is contained within the fuel rods, and significant releases typically occur only when severe fuel damage happens. The most common cause of this damage is coolant loss, which uncovers the fuel rods and prevents efficient heat removal. RASCAL simulates the release of fission products over time using the "time core uncovered" model, initially concentrating on noble gases and volatile radionuclides such as cesium and iodine. As a result, the fuel cladding melts first, followed by the fuel itself. If left uncovered, molten fuel may breach the reactor pressure vessel. Since predicting the timing and duration of core uncovering is more dependable than estimating the extent of core damage, RASCAL uses this parameter to estimate offsite consequences.

RASCAL simulates the release of fission products over time using the "time core uncovered" model, first focusing on noble gases and volatile radionuclides such as cesium and iodine (Ramsdell et al., 2012). This model estimates the amount of release based on how long the reactor core is without coolant. By providing the duration of core exposure, users can allow RASCAL 4 to estimate fuel damage according to specific timeframes in Table 3-13 of NUREG-1465 (Soffer et al., 1995).

In RASCAL version 4.3, the model includes a "core damage state" option for both LBLOCA and LTSBO scenarios. The “percent damage” input functions similarly to choosing the “core recovered” option with a specified recovery time. The correlations among the core damage phase, percentage of core damage, and the effective core recovery time in LBLOCA and LTSBO scenarios—for PWRs—are derived from the accident progression frameworks detailed in NUREG-7110 Volume 2, Revision 1 (US NRC, 2013a); and NUREG-1465 (Soffer et al., 1995). These relationships are implemented in RASCAL and are summarized in **Table 3-1**.

Table 3-1: Damage state and time of effective core recovery for LBLOCA and LTSBO events in PWR RASCAL Simulation (Ramsdell et al., 2015).

Core damage phase	Percent damage (%)	Core recovery time (min)* LBLOCA	Core recovery time (min)* LTSBO
Cladding failure	0 to 100	0 to 30†	0 to 90†
Core Melt	0 to 100	30 to 105†	90 to 300‡
Ex-vessel melt	Not applicable	240	360

* Time, following the onset of core damage
† Linear interpolation of time as a function of percent
‡ Linear interpolation of time as a function of percent, first sector, zero to seventy-five percent correspond to 90 to 240 minutes, and second sector, seventy-five to one hundred percent correspond to 240 to 300 minutes.

RASCAL 4 estimates source terms by dividing the facility into compartments and modeling radionuclide transfers between them in 15-minute time steps. Since fission ceases after shutdown, the fuel inventory declines over time due to decay and migration, although daughter nuclides may grow in from parent decay (Ramsdell et al., 2012). During a post-shutdown LBLOCA or an LTSBO in a PWR, radionuclides migrate from damaged fuel into the containment atmosphere. Within the containment compartment, radionuclides undergo radioactive decay, are subject to removal processes like spray systems and surface deposition, and may escape through leakage. These events are modeled in 15-minute intervals to match atmospheric dispersion calculations (Ramsdell et al., 2012).

RASCAL considers several release pathways in PWRs, including containment leakage, bypass routes, ruptures in steam generator tubes, and direct environmental releases. Each pathway includes attenuation mechanisms such as spray scrubbing, gravitational settling, and filtration, with the exception of noble gases, which are assumed to escape these reduction processes. Time-dependent exponential decay functions are used to model how effective these mechanisms are (Ramsdell et al., 2012). Using a number of reduction mechanisms, RASCAL 4.3 monitors radionuclide activity from the reactor core through plant systems and, eventually, to environmental release. First, activity is adjusted through decay and in growth from reactor shutdown until the final release applies the Bateman equations (Bateman, 1910; Ramsdell et al., 2012) along with decay chain data. Additionally, the code calculates decay and in growth factors for each radionuclide over a 5-minute interval and utilizes these factors to adjust the source term

during the release process. Second, while radionuclides remain in containment in the absence of sprays, natural mechanisms such as gravitational settling (Reduction factor multiplier, $exp(-\lambda_n t)$ where λ_n natural process reduction constant varying with time) and turbulent impaction on containment surfaces gradually reduce the airborne levels of particulates and reactive gases (US NRC, 1990; Ramsdell et al., 2012). When containment sprays are turned on, they use a decreasing reduction factor (multiplier, $exp(-\lambda_s t)$ where λ_s reduction constant for spray varies with time) that helps in the washout process of radionuclide removal (Sjoreen et al., 1987; Ramsdell et al., 2012). Additionally, filtration systems are employed to lower radionuclide concentrations when venting the containment atmosphere to the outside environment, using a multiplication factor of 0.01. (Ramsdell et al., 2012; Ramsdell et al., 2015).

In addition to plant design and accident scenario, source term assessment depends on various factors, including core degradation, molten core interaction with the concrete basement, and fission product removal in containment (US NRC, 2013a).

3.2.1.1.2 Source Term Basis for LBLOCA

The LBLOCA source term modeling in RASCAL 4.3 is based on the accident progression described in NUREG-1465 (Soffer et al., 1995), which describes the phases and timing of radionuclide release following a severe reactor event. In a LOCA scenario, coolant loss rapidly raises the core temperature, which ultimately leads to core degradation when the fuel is no longer adequately submerged. The reactor vessel's radionuclide releases are timed and scaled according to NUREG-1465 guidelines, specifically those listed in Table 3-13 from NUREG-1465 (Soffer et al., 1995)**.** Typically, releases last four to five hours. Based on how long the core is left exposed, RASCAL calculates the release of fission products. Cladding failure and fuel melting start about the moment the coolant falls below the active fuel height. Initial releases are dominated by gap activity, followed by progressive core melt and phase-specific radionuclide emissions.

The release fractions listed for each damage phase—cladding failure, core melt, and vessel melt-through—are phase-specific and not cumulative. To estimate the total release during a severe accident, these individual phase contributions are added. These values were derived through expert assessments of a variety of severe accident scenarios. While they don't capture every possible sequence, they reflect the most rapid progression of fuel damage, typically associated

with a LBLOCA at full reactor power and without ECCSs. Major fuel damage—and hence significant releases—occurs only when the reactor core is exposed. RASCAL correlates core exposure time with damage levels using timing data adapted from NUREG-1465 (Soffer et al., 1995). For instance, 15 minutes of exposure corresponds to approximately 50% cladding failure, and 30 minutes to full failure.

Gap release, early in-vessel release, ex-vessel release, and—beginning with version 4.3.1—late in-vessel release are the four primary release phases that RASCAL specifies for PWRs. As a result of updated source term modeling that incorporates additional fission product releases from halogens (like iodine and bromine), alkali metals (like cesium and rubidium), and tellurium group elements (like tellurium, antimony, and selenium), RASCAL 4.3.1 now includes the late in-vessel phase. NUREG-1465 (Soffer et al., 1995) is used to determine the release fractions for each radionuclide group and phase. RASCAL 4.3.1 uses updated values to account for the overlap between the ex-vessel and late in-vessel phases. The extended release behavior seen in serious accidents is partially explained by these modifications.

3.2.1.1.3 Source Term Basis for LTSBO

The LTSBO scenario is modeled by RASCAL as a slowly developing accident that is initiated by the complete loss of AC power, usually after an external effect. The reactor shuts down correctly at first, but when backup power systems fail and battery reserves run out (about 4 hours for PWRs), cooling is lost, and residual decay heat causes the reactor coolant to boil off. Core damage and radionuclide release start when the fuel becomes uncovered, usually 10 to 12 hours after the initiating event (Ramsdell et al., 2015).

In the case of LTSBO scenarios, the RASCAL source term model is structured around three principal components: the reactor, containment, and atmosphere. The reactor module evaluates the initial radionuclide inventory, accounts for radioactive decay, and models the initial release. The containment module, which includes the reactor vessel, associated piping, ducts, and the containment building, is treated as a single free-volume compartment in PWRs (Ramsdell et al., 2015). MELCOR simulations from the SOARCA project (Chang et al., 2012) serve as the foundation for the LTSBO source term model in RASCAL. The relative time-dependent fractional release behavior of eleven radionuclides groups where primary contribution from noble gases. Volatile radionuclides, such as iodine and cesium, come next. RASCAL makes the

assumption that radionuclides released from PWRs will mix instantly and evenly inside the containment area.

3.2.1.1.4 Comparison Between LBLOCA and LTSBO Source Terms

The release timing, radionuclide behavior, and ensuing radiological impact of the LBLOCA and LTSBO scenarios are very different. The time lag between the initiating event and the beginning of the radioactive release is one important difference. This delay enables more radioactive decay and in-growth prior to release, changing the emission's composition and magnitude in LTSBO events.

Figure 3-1 shows the relative time-dependent fractional releases of radionuclide groups for LBLOCA (dash lines) and LTSBO (solid lines) from the core. RASCAL integrates time-resolved release data from the SOARCA (Chang et al., 2012) simulations, in contrast to conventional LOCA models that employ fixed release phases. LOCAs produce a rapid release dominated by noble gases, LTSBOs result in delayed but more particle-rich emissions, especially for elements such as iodine, cesium, and tellurium. Additionally, LTSBO scenarios show higher release fractions for iodines and cesium due to extended core heating. These differences are important for dose assessment and emergency response planning. In RASCAL 4.3.1 modeling, LTSBO events typically release fewer noble gases compared to LOCAs. This is largely due to the decay of short-lived isotopes like Kr-87 and Xe-135m before LTSBO releases begin.

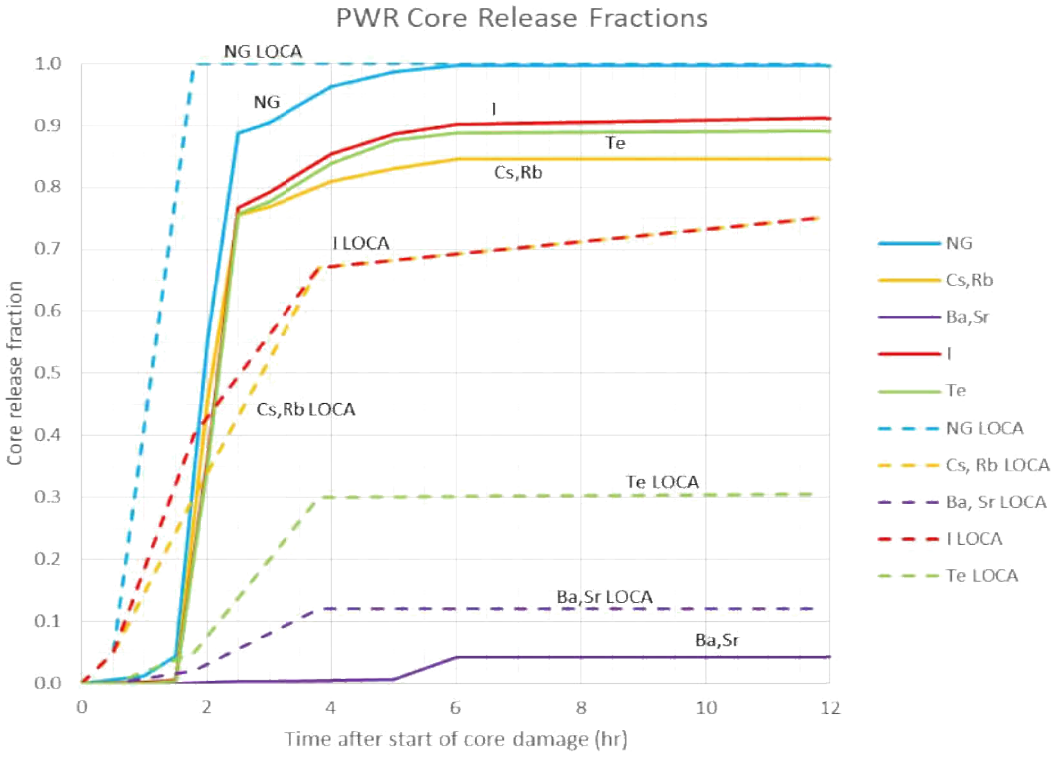

Figure 3-1: LBLOCA and LTSBO events release timing comparison for PWRs (Ramsdell et al., 2015).

3.2.1.1.5 Verification of the Source Term Calculations in RASCAL in light of Fukushima Daiichi Nuclear Accident

Table 3-2 compares observed radioactive releases reported by Japanese agencies (Inoue, 2012) and independent researchers (Chang et al., 2012) based on a MELCOR analysis of an unmitigated SBO for Peach Bottom Atomic Power Station. Estimates range from absolute activity values to fractions of the core inventory.

Table 3-2: Reported I-131 and Cs-137 Releases from Fukushima Units 1–3 (Ramsdell et al., 2012).

Source		I-131 (Bq)	Cs-137 (Bq)
Nuclear Safety Commission of Japan (#)		$1.3x10^{17}$	$1.1x10^{16}$
Nuclear and Industrial Safety Agency (#)		$1.6x10^{17}$	$1.5x10^{16}$
Japan Nuclear Energy Safety Organization (#)		$1.3x10^{17}$	$6.1x10^{15}$
(#) Inoue, 2012	Core inventory	<3%	<2%
Chang et al. ,2012		3% to 10%	2% to 3%

To evaluate RASCAL 4.2 performance, simulations were conducted using U.S. BWRs resembling Fukushima Daiichi Units 1–3. Duane Arnold Energy Center was used as a surrogate for Unit 1, and Cooper Nuclear Station for Units 2 and 3. Initial runs used default reactor settings and the NUREG-1465 (Soffer et al., 1995) release sequence to estimate iodine-131 (I-131) and cesium-137 (Cs-137) emissions over the first 48 hours following core uncover. Model results varied significantly depending on the assumed release path, with drywell releases. A more detailed simulation used a drywell pathway without spray mitigation. **Table 3-3** shows the parameters used for each reactor unit in the model. Simulations were initiated when fuel was no longer adequately covered. Leak rates were adjusted from the default 0.5%/day to reflect accident progression: 1%/hr during core damage, 25%/hr during venting, and 50%/hr after hydrogen explosions, then returned to 1%/hr (Institute of Nuclear Power Operations, 2011).

Table 3-3: Fukushima reactor parameters used for RASCAL accident simulations of source term verification and predicted releases of I-131 and Cs-137 (Institute of Nuclear Power Operations, 2011; Ramsdell et al. 2012)

	Unit 1	Unit 2	Unit 3	Total
Uranium (metric ton))	69	94	94	
Power (MWt))	1,380	2,381	2,381	
Last startup	9/27/2010	9/23/2010	11/18/2010	
Burnup (MWd/MTU)(*)	23,700	30,000	28,500	
I-131 inventory (Bq)	$1.36\times10^{+18}$	$2.35\times10^{+18}$	$2.35\times10^{+18}$	$6.07\times10^{+18}$
I-131 release (Bq)	$4.85\times10^{+16}$	$9.4\times10^{+16}$	$5.6\times10^{+16}$	$2.0\times10^{+17}$
I-131 release fraction	3.6%	4.0%	2.4%	3.3%
Cs-137 inventory (Bq)	$1.02\times10^{+17}$	$2.23\times10^{+17}$	$2.11\times10^{+17}$	$5.36\times10^{+17}$
Cs-137 release (Bq)	$4.10\times10^{+15}$	$1.13\times10^{+16}$	$6.28\times10^{+15}$	$2.17\times10^{+16}$
Cs-137 release fraction	4.0%	5.1%	3.0%	4.1%
(*) based on a 30-day shutdown and an 18-month refueling cycle, one third of the core is replaced.				

Even though **Table 3-3**'s RASCAL results slightly overestimated actual releases, the differences were still within allowable bounds of uncertainty. Interestingly, RASCAL assumes direct release from primary containment and does not take secondary containment in BWRs into account. However, in complicated accident scenarios like Fukushima, the RASCAL model showed respectable accuracy.

3.2.1.2 Atmospheric Transport, Dispersion, and Deposition Models

3.2.1.2.1 Atmospheric Dispersion Models

RASCAL calculates air transport, dispersion, and deposition based on time-dependent meteorological data. The data may be based on actual observations and projections. RASCAL has a meteorological data processing model that converts point observations into a structured grid format suited for modeling. RASCAL, the model used for emergency planning, relies on detailed wind data to make accurate calculations of how radioactive materials spread in the atmosphere. Simply using observational weather data is not enough. RASCAL uses Gaussian models to simulate the movement and dispersion of radioactive materials after a release, taking into account the weather conditions at that time. The simulation alternates between a straight-line Gaussian plume model and a Gaussian puff model (Ramsdell et al., 2012; Athey et al., 2013).

Near Field (Gaussian Plume/Polar Grid) RASCAL employs a straight-line Gaussian plume model for near-field computations. The model accounts for nuclide decay and in-growth, but not transit time. The release point is considered to be at the middle of a polar grid, and calculations are performed at 288 grid points (36 directions by 8 radii). The near field domain radii are keyed to the size of the far field domain, but the user can alter them (Ramsdell et al., 2013; Athey et al., 2013).

The straight-line Gaussian plume model is utilized when transit periods are short and plume depletion caused by dry deposition is minimal. For a straight-line Gaussian plume model at a release point, the assumptions are: a) meteorological conditions are constant as the puff proceeds from the source to the receiver; and b) meteorological variables are horizontally homogenous and stationary. b) Atmospheric conditions do not vary as a function of time during release and travel (Ramsdell et al., 2012). The simplified version of the straight-line Gaussian plume model used in RASCAL is given by equation 3.1.

$$\frac{\chi(x,y,z)}{Q`} = \frac{F_y F_z}{2\pi u\, \sigma_y \sigma_z} \qquad \text{.....} \quad (3.1)$$

Where χ is the mean concentration of diffusing material at a place (x, y, z). Q' represents the release rate, F_y and F_z are the lateral and vertical exponential terms, σ_y and σ_z are the horizontal

and vertical deviations of the plume concentration distribution (m), and u is the wind speed (m/s).

Far Field (Gaussian Puff/Cartesian Grid) RASCAL employs a Lagrangian Gaussian puff model for far field computations. The Gaussian puff model is entirely time-dependent. It addresses nuclide decay and in-growth, as well as the transport, dispersion, and deposition of activity in a puff, which can change in time and space as the puff moves over the model domain. Users can choose from four model domain sizes, ranging from 2 km to 160 km on a side. at all cases, the release point is assumed to be located at the domain's center. The calculations are performed at 1681 equally spaced nodes on a Cartesian grid (41 x 41). (Ramsdell et al., 2012; Athey et al., 2013).

The Gaussian puff model takes into account temporal and spatial fluctuations in meteorological circumstances, as well as the potential for significant plume depletion due to dry deposition. In a Cartesian coordinate system with x and y-axes in a horizontal plane and z in the vertical, the normalized concentrations (equation 3.2) near the puff are:

$$\frac{C(x,y,z)}{Q} = \frac{1}{\sqrt{(2\pi)^3}\sigma_x\sigma_y\sigma_z} e^{\left[-\frac{1}{2}\left(\frac{x-x_0}{\sigma_x}\right)^2\right]} e^{\left[-\frac{1}{2}\left(\frac{y-y_0}{\sigma_y}\right)^2\right]} e^{\left[-\frac{1}{2}\left(\frac{z-z_0}{\sigma_z}\right)^2\right]} \quad \text{.....(3.2)}$$

Where x-along wind coordinate (m), y-cross-wind coordinates (m), z-vertical coordinate (m), C (x, y, z) is the concentration (Ci/m^3 or g/m^3) at a puff position (x, y, z) from the center (x_0, y_0, z_0), Q is the amount of material released (Ci or g), and σ_x, σ_y, σ_z are the atmospheric dispersion parameters (m).

3.2.1.2.2 Dispersion Modeling Parameters

Radionuclides disperse as a result of atmospheric turbulence. RASCAL 4 makes use of updated dispersion algorithms that take turbulence parameters and transport time into account. (Ramsdell et al., 2012).

Horizontal Dispersion

The horizontal dispersion parameter (σ_y) rises in the first hour following a release in direct proportion to the horizontal turbulence (σ_v) and the amount of time that has passed since the release. This is calculated by integrating σ_v over time, making adjustments for atmospheric stability. After the first hour, the model shifts to a linear calculation based on travel time, using a

default speed of 0.2 m/s, which matches experimental results for longer transport times (Gifford, 1982, Ramsdell et al., 2012).

Vertical Dispersion

Vertical dispersion (σ_z) is influenced by the vertical turbulence component (σ_w), atmospheric stability, and a time-dependent function that diminishes turbulence's effectiveness over time. Under neutral and unstable conditions (Pasquill-Gifford classes A–D), vertical dispersion increases linearly with time. Conversely, under stable conditions (classes E–G), a correction function slows down the growth rate, using a default turbulence time scale of 50 seconds (Petersen & Lavdas, 1986, Ramsdell et al., 2012).

Using surface characteristics and meteorological data, the turbulence parameters σ_v and σ_w are dynamically determined. For instance, both σ_v and σ_w are modified according to surface friction velocity (u*) in stable conditions where plume heights are less than 90% of the mixing layer. Depending on whether the puff is in the lower or upper boundary layer, different equations are used to derive the parameters in unstable conditions from Monin-Obukhov similarity theory (Panofsky & Dutton, 1984; Hanna et al., 1982, Ramsdell et al., 2012).

Adjustments of Wind Speeds

Field studies have shown that dispersion is frequently underestimated near structures when wind speeds are low. To address this, RASCAL 4 improves dispersion parameters (Σy and Σz) by introducing empirical correction terms that account for increased diffusion not captured by traditional models. These enhancements grow with increasing travel time and are significant when wind speeds are below approximately 4 m/s but become negligible at higher speeds or further distances from the release site (Ramsdell & Fosmire, 1998, Ramsdell et al., 2012).

For elevated releases, RASCAL adjusts wind speed profiles based on release height and stability. It also accounts for mixing layer thickness, which defines how high released material can spread vertically. If the plume remains within this layer, it disperses horizontally and vertically; otherwise, vertical diffusion is limited. RASCAL estimates mixing height using either real-time or climatological data.

Stability Classes

Pasquill's stability classes are used by RASCAL to describe the atmospheric factors of dispersion. These classes change from unstable (A) to stable (G) depending on wind speed, solar radiation during the day, and cloud cover at night. For example, unstable conditions are indicated by strong sunlight and low wind, while neutral (D) conditions are often caused by cloud cover or high wind. Stability can also be estimated using temperature gradients ($\Delta T/\Delta z$) or the standard deviation of wind direction.

RASCAL incorporates different methods for classifying stability, including Pasquill-Gifford tables using observed weather parameters. If stability is not directly provided, RASCAL estimates it from available meteorological data such as wind speed, time of day, and precipitation (Ramsdell et al., 2012. **Table 3-4** shows the stability classification for RASCAL, when wind speed and precipitation data are available, if not directly provided.

Table 3-4: Estimated Atmospheric Stability Class used in RASCAL (Ramsdell et al., 2012).

	Daytime		Nighttime	
Wind speed (m/s)	No precipitation	Precipitation	No precipitation	Precipitation
=<2.0	B	C	F	E
2.01 to 3.0	B	C	E	E
3.01 to 5.0	C	D	E	D
>=5.01	D	D	D	D

3.2.1.2.3 Atmospheric Transport Mechanisms

Atmospheric transport refers to how airborne radioactive materials move from their release point to surrounding areas. RASCAL 4 includes two transport mechanisms: straight-line modeling and puff-based modeling. These methods are designed to handle the variability in wind conditions and the circumstances of material release.

TADPLUME Transport Model

TADPLUME is a straight-line Gaussian model that assumes the wind direction at the time of release determines the path taken by the radioactive plume. To make calculations easier, wind directions are rounded to the nearest 10 degrees. One drawback of this model is that it ignores the amount of time it takes for material to move from its source to its receptor. Dose rates are therefore computed as though the material arrived at every downwind location simultaneously.

This means TADPLUME cannot accurately predict when the plume will reach specific locations or match field measurements of dose rates (Ramsdell et al., 2012).

In situations where the wind speed at the release point drops below 0.447 m/s, TADPLUME behaves differently. Instead of moving horizontally, the material disperses through turbulent diffusion. In this case, the arrival time of radionuclides at various receptor locations is determined by how long it takes for diffusion to reach those points. The model takes into account radioactive decay and material depletion from both dry and wet deposition by assuming a specific travel time between the source and the receptor, with updates occurring every five minutes (Ramsdell et al., 2012).

TADPUFF Transport Model

TADPUFF, which depicts the release as a sequence of distinct "puffs" that vary over time, offers a more complex and accurate simulation of transport. Unlike TADPLUME, TADPUFF uses time-varying, two-dimensional wind patterns to track puff movement and directly accounts for travel time in its computations. Six iterative processes, including wind direction, height, and speed, are used to update the position of each puff every 15 minutes. This approach increases accuracy, especially in difficult terrain or when the weather is changing (Ramsdell et al., 2012).

Because TADPUFF maintains each puff separately, it can predict when a plume will reach a receptor as well as how concentrations and dose rates will alter over time and distance. It also considers topography by using wind fields generated by a meteorological preprocessor to model more realistic plume behavior in uneven landscapes. (Ramsdell et al., 2012).

3.2.1.2.4 Deposition Model:

RASCAL 4 estimates the deposition for iodine and particles using dry and wet deposition models adapted from MESORAD, incorporating updated algorithms (Scherpelz et al., 1986, Shipler et al., 1996).

Dry Deposition:

It is computed as the product of the airborne radionuclide concentration and a deposition velocity that changes according to the weather, surface properties, and radionuclide chemical form. Aerodynamic, surface, and transfer resistances are all included in the total resistance when

resistance-based approach is employed in RASCAL (Seinfeld, 1986). Deposition velocities for gases such as iodine (I_2) vary from 0.0021 to 0.016 m/s, based on atmospheric stability and wind speed. Fine particles, on the other hand, typically have slightly higher deposition velocities. (Ramsdell et al., 2012).

Wet deposition: Gases and particles are treated separately during wet deposition. For particles, deposition is based on washout coefficients that relate to the intensity and type of precipitation, following empirical models (Slinn, 1984). For gases, the wet deposition velocity is determined by solubility and rainfall rate. Reactive gases like I_2, which have high solubility, experience higher deposition rates, while non-reactive gases are less affected.

Projected doses are significantly impacted by precipitation. Snow and rain can remove radioactive particles from the plume, lowering airborne concentrations farther downwind and raising doses of groundshine closer to the source. RASCAL uses intensity to classify precipitation into three categories: light, moderate, and heavy (e.g., <1 mm/h rain as light rain). The model uses these inputs to adjust calculations of dispersion and doses accordingly. With a wet deposition velocity of 2.8×10^{-5} m/s and a washout coefficient of 0.25 h^{-1}(Ramsdell et al., 2012) , light rain suggests a comparatively slower rate of particle removal. On the other hand, moderate rain indicates a more effective removing process with a much higher washout coefficient of 3.3 h^{-1} and wet deposition velocity of 8.3×10^{-4} m/s (Ramsdell et al., 2012). This suggests that the rate at which pollutants from the atmosphere are deposited on the ground is directly influenced by the intensity of rainfall. The total surface contamination is calculated as the cumulative deposition from both dry and wet processes over time, excluding noble gases which do not deposit (Ramsdell et al., 2012).

3.2.1.3 Dose Models

RASCAL estimates doses for three exposure pathways: cloudshine/submersion, inhalation, and groundshine. It does not compute doses throughout the ingestion route. However, it does evaluate the radionuclide's contribution during discharged into the environment in terms of ingestion route doses.

Cloudshine: RASCAL computes external doses from nuclear accident plumes using both finite and semi-infinite plume models. As the horizontal dispersion of a plume increases (with σ_y

around 400 m), a model known as the infinite-slab or plane-source model is used. This model divides the plume into horizontal layers to simulate how the dose spreads vertically. When the vertical extent also becomes large (σ_z around 400 m) compared to the average gamma path, a different approach called the semi-infinite cloud model is applied (Ramsdell et al., 2012). This model assumes a uniform concentration of radioactivity throughout the space and utilizes updated dose conversion factors from Federal Guidance Report (FGR)-12 (Eckerman & Ryman, 1993).The TADPUFF and TADPLUME modules handle these cloudshine calculations in slightly different but consistent ways.

Inhalation: For inhalation dose calculations, RASCAL computes organ-committed dose equivalents and CEDEs from time-varying airborne activity concentrations at a point over 15-minute intervals using radionuclide-specific dose conversion factors and breathing rates (Eckerman et al., 1988; International Commission on Radiological Protection (ICRP), 1991). In particular, it computes acute bone marrow, lung, and colon doses, thyroid CDE, and adult inhalation CEDE. If the ICRP-60 inhalation dose conversion factors are chosen, it also determines the thyroid dose of iodines for a child aged one. The program includes updated dose factors reflecting the latest ICRP recommendations and extends dose calculations to 50 years, covering both early and intermediate phases of exposure (Ramsdell et al., 2012).

Two sets of inhalation dose conversion factors from ICRP-26/30 (FGR 11) and ICRP-60/72 (FGR 13) are included in RASCAL 4.3 in (Eckerman & Leggett., 2002). Commonly, the uncertainties in the source term and dispersion are much larger than the variations in CEDE dose conversion factors. The total CEDE doses are reduced by roughly 29% when the ICRP-60/72 dose conversion factors are used instead of the ICRP-26/30 dose conversion factors. The thyroid dose conversion factors vary more. Overall, the thyroid dose potential is reduced by roughly 3% when switching from ICRP-26/30 to ICRP-60/72 dose conversion factors (Ramsdell et al., 2012). If RASCAL 4.3 dose calculations are to be used to assess recommendations regarding the administration of KI, then the ICRP-60/72 inhalation dose conversion factors must be applied. The thyroid dose of children is the basis for the EPA PAGs associated with KI. Child thyroid dose conversion factors are not included in ICRP-26/30. The activity inhaled during plume passage is the source of the inhalation doses during the early stages of an accident.

Groundshine: RASCAL is used to calculate groundshine doses resulting from nuclide activity deposited on the ground. It corrects for radioactive decay and the growth of new isotopes since

the time of deposition. Groundshine doses are calculated by aggregating radionuclide-specific surface contamination, adjusted with dose conversion factors and a surface roughness factor to better reflect environmental conditions. The model tracks contamination over time, taking into account both radioactive decay and in-growth for the first four days following deposition (Eckerman et al., 1993).

Ingestion RASCAL only deals with ingestion doses in the context of determining the relative importance to ingestion dose of nuclides released to the environment.

Intermediate Phase Dose: Using the STDose and FMDose modules, RASCAL 4 computes intermediate-phase doses for comparison with the EPA's PAG Manual (US EPA, 2017). Based on ground contamination that remains after the early phase, it calculates doses for the first year, second year, and more than 50 years after a release. These values account for radioactive decay, in-growth, weathering, and re-suspension. During the intermediate phase, inhalation doses are derived from re-suspended deposited activities. Early phase inhalation doses are often several orders of magnitude higher than intermediate phase inhalation doses. Intermediate phase groundshine doses are calculated similarly to early phase groundshine doses, with the addition of a factor that compensates for activity diminished with time.

3.2.2 HotSpot CODE

HotSpot is a health physics modeling tool designed to quickly assess the radiological effects of releases of nuclear or hazardous materials. It provides an initial estimate of radiation impacts following short-term radioactive material releases, which typically last less than a few hours and occur within a 10-kilometer radius. The HotSpot atmospheric dispersion model is particularly effective for near-surface releases in flat terrain and under simplified weather conditions. (Homann & Aluzzi, 2020).

3.2.2.1 Dispersion Process

The Gaussian plume method, an established approach for simulating the spread of pollutants in the atmosphere, serves as the foundation for the model. This method, which is based on the assumption that pollutant concentrations follow a normal distribution both vertically and across wind directions, has been thoroughly validated through experiments and regulatory applications (Pasquill, 1974; Hanna et al., 1982; Homann & Aluzzi, 2020).

In the HotSpot modeling framework, the Coordinate System where it is centered at ground level directly below the release point of radionuclides, with coordinates (x = 0, y = 0, z = 0). The downwind direction, horizontally aligned with the dominant wind, is represented by the x-axis. The direction of the crosswind is indicated by the y-axis, which also extends horizontally but perpendicular to the x-axis. From the ground, the z-axis extends vertically upward. When the radioactive plume hits the ground, it reflects off the surface and travels downwind.

Using Gaussian equations and adjusting for vertical atmospheric mixing, HotSpot determines time-integrated air concentrations (equation 3.3 and 3.4). Vertical dispersion is restricted in the presence of a temperature inversion. HotSpot switches between open and limited dispersion regimes via interpolation if the plume height surpasses 70% of the inversion layer (Homann & Aluzzi, 2020).

$$C(x,y,z,H) = \frac{Q}{2\pi\sigma_y\sigma_z u}\exp\left[-\frac{1}{2}\left(\frac{y}{\sigma_y}\right)^2\right]\left\{\exp\left[-\frac{1}{2}\left(\frac{z-H}{\sigma_z}\right)^2\right] + \exp\left[-\frac{1}{2}\left(\frac{z+H}{\sigma_z}\right)^2\right]\right\}\exp\left[-\frac{\lambda x}{u}\right]DF(x) \quad (3.3)$$

$$C(x,y,z,H) = \frac{Q}{\sqrt{(2\pi)}\sigma_y L u}\exp\left[-\frac{1}{2}\left(\frac{y}{\sigma_y}\right)\right]\exp\left[-\frac{\lambda x}{u}\right]DF(x) \quad (3.4)$$

Where C = Time-integrated atmospheric concentration (Ci-s)/(m^3), Q = Source term (Ci), H = Effective release height (m), λ= Radioactive decay constant (s^{-1}), x = Downwind distance (m), y = Crosswind distance (m), z = Vertical axis distance (m), σ_y = Standard deviation of the integrated concentration distribution in the crosswind direction (m), σ_z = Standard deviation of the integrated concentration distribution in the vertical direction (m), u = Average wind speed at the effective release height (m/s), L = Inversion layer height (m), DF(x) = Plume Depletion factor.

HotSpot includes calculations for effective release height, taking into account both buoyancy and exit velocity, which decreases ground-level concentration. This adjustment helps avoid overestimating exposure at receptor locations by modeling the upward movement of the plume before horizontal dispersion.

3.2.2.2 Dispersion Coefficients and Surface Roughness:

Dispersion coefficients (σ_y and σ_z) in HotSpot are determined using Pasquill and Briggs formulations based on experimental data. HotSpot differentiates between standard terrain, which has a roughness height of 3 cm, and urban terrain, which increases turbulence and dispersion. The surface roughness impacts vertical dispersion, and correction factors are applied when the roughness exceeds the standard terrain assumption. However, since these factors are already incorporated into its parameters, no extra corrections are required for urban terrain (Homann & Aluzzi, 2020).

Although HotSpot's formulas are verified for up to 30 kilometers, the tool can be used for up to 200 kilometers with caution because its dependability decreases with distance. (Homann & Aluzzi, 2020).

Wind Speed Adjustment with Height: Pollutant dispersion in the atmosphere is influenced by wind speed, which typically rises with altitude. In HotSpot, the model uses a power-law relationship (equation 3.5) to modify wind speed when the release height rises above 2 meters. More realistic plume behavior results from this adjustment, which accounts for the vertical wind profile, especially for elevated or buoyant releases (Homann & Aluzzi, 2020).

$U(H)= U(z)(H/z)^p$ ……..(3.5)

Where, U(z) = wind speed (m/s), at reference height z (m), H = effective release height (m)

U(H) = wind speed (m/s), at height H (m), p = factor depends on stability class and terrain type

Atmospheric stability: In HotSpot, users have the option to manually choose atmospheric stability or base it on regional factors like wind speed and solar radiation. The stability classes go from A to G. Class G denotes extremely stable conditions, which are usually found at night with little wind.

Sampling Time: For short-term releases, HotSpot's default plume duration of 10 minutes is appropriate. With the exception of situations involving explosive releases, users can modify this time to suit their specific situation. Concentration calculations are impacted by sampling time; shorter sampling times record rapid concentration changes, whereas longer sampling times

average out these variations, producing lower peak concentration values (Homann & Aluzzi, 2020).

3.2.2.3 Deposition and Plume Depletion:

Dry Deposition: HotSpot accounts for dry deposition using two standard velocities: 0.3 cm/s for respirable particles (diameter <10 μm) and 8 cm/s for larger, non-respirable particles), following empirical comparisons with National Atmospheric Release Advisory Center (NARAC) (Hanna & Britter, 2002). The model accounts for the removal of pollutants by turbulence, impaction, and chemical processes. Users can modify default settings for chemically reactive substances.

Plume Depletion: HotSpot reduces airborne concentrations according to distance and deposition rate using a source-depletion factor derived from Van der Hoven's formulation (Van der Hoven, 1968). When assessing long-distance transportation and possible environmental contamination, this component is particularly crucial (Homann & Aluzzi, 2020). HotSpot makes use of the source-depletion factor equation of 3.6.

$$DF(x) = \left[\exp \int_0^x \frac{1}{\sigma_z(x)\exp\left[\frac{1}{2}\left(\frac{H}{\sigma_z(x)}\right)^2\right]} dx\right]^{-\frac{v}{u}\sqrt{\frac{2}{\pi}}} \quad \text{.....(3.6)}$$

Where DF(x) = Depletion factor, (dimensionless), x== Downwind distance (m), v= Deposition velocity (cm/s), *u*= average wind speed (m/s) at the effective release height, H= Effective release height, $\sigma_z(x)$ = standard deviation of the vertical air concentration distribution (z axis) for either standard terrain (adjusted for surface roughness height if applicable) or city terrain.

Wet Deposition: Wet deposition consists of two main processes: Rainout, which is the removal of particles that occur within clouds, and Washout, which is the removal of particles occurring below clouds. In HotSpot, these two processes are combined into a single removal mechanism. When wet deposition is activated, the concentration of radionuclides decreases exponentially with precipitation (equation 3.7) (Homann & Aluzzi, 2020) as follows:

$C'(x,y,z) = C(x,y,z)e^{(-\Lambda x/u)}$ .....(3.7)

where, C': radionuclide concentration (Ci/m³), Λ: washout coefficient (s^{-1}) and u: average wind speed (m/s). **Table 3-5** presents the typical washout coefficients by rain rate used in HotSpot.

Table 3-5 Typical washout coefficients by rain rate used in HotSpot (Homann & Aluzzi, 2020)

Rain Rate (mm/hr)	Coefficient (s^{-1})
0.5	0.0001
1.0	0.0002
5.0	0.0006
10.0	0.0010
15.0	0.0013
20.0	0.0017
25.0	0.0020

Ground Shine: Radionuclides that settle on the ground can expose people through direct radiation (referred to as ground shine) or by becoming airborne again (a process known as resuspension). HotSpot calculates ground shine assuming a flat surface.

3.2.2.4 HotSpot Dose:

HotSpot relies on five key parameters to estimate radiation doses downwind: 1) Material at Risk (MAR), 2) Damage Ratio (DR), 3) Airborne Release Fraction (ARF), 4. Leak Path Factor (LPF), 5) Respirable Fraction (RF). They are combined to calculate downwind concentrations and dose estimates, taking into account the depletion of the source, atmospheric dispersion, and deposition effects for radiological safety analysis. The relative biological effectiveness (RBE) of various radiation types is taken into account by HotSpot when calculating the RBE-weighted absorbed dose, particularly for deterministic effects during early exposure periods. It is expressed in rad-equivalent or gray-equivalent. HotSpot offers two calculation modes that follow ICRP guidelines: 1. FGR-11 Option: Utilizes ICRP Publication 30 (the older lung model), along with ICRP-26 weighting factors 2. FGR-13 Option: Uses ICRP Publications 60 and 66 (the newer lung model), updated tissue weighting factors (Homann & Aluzzi, 2020).

3.2.3 HYSPLIT CODE

The Hybrid Single-Particle Lagrangian Integrated Trajectory (HYSPLIT) model (Stein et al., 2015), developed by the National Oceanic and Atmospheric Administration's (NOAA) Air Resources Laboratory (ARL), is a popular tool for simulating how pollutants disperse and deposit in the atmosphere (Draxler et al., 2018). HYSPLIT functions as a 3-dimensional particle or puff model that uses variable meteorological data to track the movement of gases and aerosols in the atmosphere.

Users can create multiple concentration grids, each with specific time, horizontal, and vertical resolutions, which can operate independently of the meteorological grid. This flexibility allows for effective tracking of pollutant levels and deposition patterns over time and different locations (Draxler & Hess, 2015). Compared to conventional Gaussian plume models, HYSPLIT is especially helpful for modeling complex environmental conditions because it accounts for important atmospheric factors like wind shear, terrain effects, surface roughness, and atmospheric stability in addition to wind in both horizontal and vertical directions.

From straightforward air parcel trajectories to complex scenarios involving dispersion and deposition, the model supports a wide range of simulation types. A fixed number of particles, the puff method, or a hybrid approach is the options available to users for dispersion modeling. By treating pollutants as both vertical and horizontal puffs, the hybrid approach preserves the spatial benefits of horizontal puff dispersion while increasing the accuracy of vertical dispersion (Draxler & Hess, 2015).

HYSPLIT effectively simulates the distribution of pollutants under various weather conditions by combining elements of the Eulerian and Lagrangian modeling frameworks. Numerous vertical coordinate systems, including pressure-sigma, absolute pressure, terrain-sigma, and mixed configurations, are supported by it, along with a variety of other meteorological data formats. Better integration of atmospheric data is made possible by this flexibility. The characteristics of pollutant species, emission rates, grids of meteorological data, and user-defined deposition regions are important input parameters.

A number of variables, such as data resolution, turbulent kinetic energy, vertical atmospheric profiles, and meteorological fluxes, can influence the model's results. Additionally, environmental aspects like seasonal weather variations, topography, and rainfall patterns have a significant impact on dispersion results (Draxler & Hess, 2015). Consequently, HYSPLIT is a powerful and versatile tool for atmospheric dispersion modeling, especially useful for emergency response, air quality forecasting, and radiological dose assessments.

Even with the same meteorological inputs, Draxler et al. (Draxler et al., 2015) discovered that different Atmospheric Transport and Dispersion Modeling (ATDMs) yielded different deposition results. Although the optimal deposition model did not always work best for air

concentration, smoother deposition patterns were generally more accurate. While detailed precipitation data had minimal impact, high-resolution mesoscale data increased model accuracy. For both metrics, the most accurate results were obtained using ensemble averages. When Connan et al. (Connan et al., 2013) compared HYSPLIT, RIMPUFF, and ADMS, they discovered that HYSPLIT and RIMPUFF produced more accurate results, whereas ADMS underestimated radioactive concentrations.

3.2.3.1 Trajectories and Air concentration Calculations

HYSPLIT models based on focusing on three main processes: advection by the wind, turbulent diffusion, and estimating atmospheric concentrations. It calculates the paths of particles by integrating wind data over both space and time. Turbulent transport is represented by adding random variations to the mean wind speed across three dimensions (Challa et al., 2008).

The movement of each particle or puff primarily depends on advection. This is determined by averaging the wind velocity vectors at the starting point, P (t), and the estimated point, P'(t+Δt) The velocity vectors are linearly interpolated in both space and time, with the initial position defined by equation 3.8 (Draxler & Hess, 1998).

$$P'(t + \Delta t) = P(t) + V(P, t)\Delta t \quad \text{.....(3.8)}$$

and the final position is

$$P(t + \Delta t) = P(t) + 0.5[V(P, t) + V(P', t + \Delta t)]\Delta t \quad \text{.....(3.9)}$$

After determining the wind velocities at a specific time step, the path of each released particle is calculated using a small time interval Δt, representing the Lagrangian step.

To describe how puffs and particles disperse, the model uses equations that include turbulent velocity components based on turbulent diffusivities. In this particle-based approach, dispersion is simulated by adding a turbulence-induced velocity to the mean wind speed obtained from meteorological data. This method can be applied in vertical, horizontal, or combined directions. After calculating the new position of the particle through wind advection at each time step, the new position of particles or puffs has computed by adding the turbulent component to the mean position (X) and (Z) (Draxler & Hess, 1998), as expressed in equation 3.10 and 3.11 respectively.

$$X_{final}(t + \Delta t) = X_{mean}(t + \Delta t) + U'(t + \Delta t)\Delta t\, G \quad \text{.....(3.10)}$$

$$Z_{final}(t + \Delta t) = Z_{mean}(t + \Delta t) + W'(t + \Delta t)\Delta t\, Z^{-1}{}_{top} \quad \text{.....(3.11)}$$

The horizontal and vertical positions are expressed in grid and sigma coordinates, respectively, while the turbulent velocity components are measured in m/s. The constants G and Z_{top} are used for unit conversion. The final particle position is calculated by adding the horizontal (U') and vertical (W') turbulent wind components to the mean position. This updated position serves as the starting point for advection in the next time step. If a particle reaches the ground or the top of the model domain, it is fully reflected. The time step for integration is determined by ensuring that the change in the vertical extent of the plume remains within a specified limit (Draxler & Hess, 1998).

$\Delta t = (\Delta z)^2 / (8\sigma_w^2 T_{Lw})$.....(3.12)

Where σ_w^2 vertical velocity variance and T_{Lw} Larangian time scale.

In the particle-based model, the air concentration (C) is calculated by adding the mass (m) of all 3D particles within a grid cell at each time step. This total is then divided by the volume of the cell, which is determined by its dimensions in the x, y, and z directions. The concentration distribution by each puff of mass (m) to a grid point, increase according to equation 3.13 (Draxler & Hess, 1998).

$\Delta C = m(\Delta x \Delta y \Delta z)^{-1}$.....(3.13)

To simplify calculations, total pollutant removal through dry and wet deposition is expressed using reciprocal time constants. The mass (m) of a particle or puff is reduced based on these processes. The model accounts for different types of deposition, including dry deposition (β_{dry}), wet gas removal (β_{gas}), in-cloud (β_{inc}), and below-cloud (β_{bel}) particle removal (Draxler & Hess, 1998). $D_{wet+drey} = m\{1- \exp[-\Delta t(\beta_{dry} + \beta_{gas} + \beta_{inc} + \beta_{bel}]\}$.....(3.14)

While decay itself does not cause deposition, radioactive materials that have already been deposited will continue to decay. Thus, the model adjusts deposited mass for radioactive decay at every time step. The decay constant is derived from the radionuclide's half-life ($T_{1/2}$) and is defined by $\beta_{rad} = \ln 2 / T_{1/2}$..... (3.15)

The updated mass of the pollutant—whether in the air or deposited—is then computed using the decay relationship (Draxler & Hess, 1998).

$m_2 = m_1 \exp(-\beta_{rad}\Delta t)$.....(3.16)

where m_1 is initial mass and m_2 is the new mass.

Beyond the core trajectory and dispersion model, HYSPLIT includes nearly 100 additional tools for pre- and post-processing. These utilities help prepare input data before running simulations and allow for processing or visualizing results afterward, including converting outputs into PostScript images. A typical HYSPLIT simulation framework is shown in Figure 3-2. The setup starts with a CONTROL file, which defines the main simulation parameters, and a NAMELIST file (commonly called SETUP.CFG), which explains these parameters and allows adjustments to the model's physical settings. A gridded meteorological dataset is also needed to simulate dispersion and deposition. HYSPLIT produces air concentration and deposition results in binary format (big-endian), which can then be post-processed using tools to extract predictions for specific locations (CON2STN), create concentration or deposition maps (CONCPLOT), or convert the data into radiological dose estimates (CON2REM) (Faisal & Islam, 2025*).

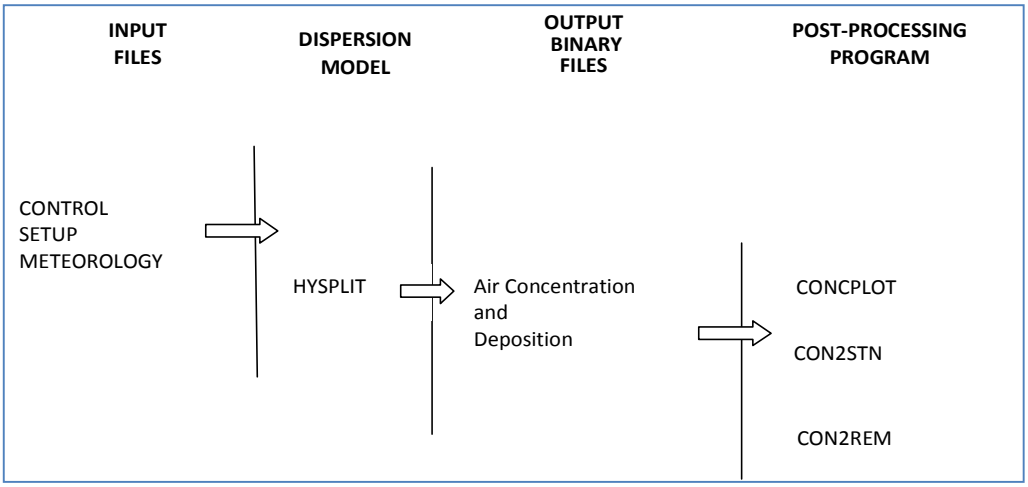

Figure 3-2: Computational frameworks in HYSPLIT simulation (Faisal & Islam, 2025*).

3.3 Comparative dispersion models for present study

Table 3-6 summarizes key atmospheric dispersion models and their applications in present study used codes. The Gaussian plume model uses basic surface meteorological data and is widely applied to estimate concentrations from continuous releases over flat, homogeneous terrain, as implemented in HotSpot. The Gaussian puff model uses similar inputs but better represents time-varying meteorological conditions and short-term releases, making it suitable for

* Article published from this thesis

mesoscale applications, although it performs poorly under strong wind shear; RASCAL is a common example where Gaussian plume model is also applicable in near field. The particle trajectory model incorporates atmospheric stability, wind, and turbulence data and is well suited for dispersion over complex terrain, with HYSPLIT being a widely used code.

Table 3-6: Comparative dispersion models in present study used codes

Model	**Type**	**Input data needed**	**Application**	**Remarks**	**Codes**
Gaussian Plume Model	Combined meteorology and diffusion Model	Surface wind speed, direction, insolation, cloud cover	Point, area, volume source	Widely used Gives concentration estimates for continuous releases over homogeneous terrain	**HotSpot**
Gaussian puff Model	Dispersion model	Surface wind speed, direction, insolation, cloud cover	Dispersion under time varying meteorological conditions, continuous short term releases	Used in mesoscale Models Better than Gaussian plume model for time varying meteorology. Not satisfactory under strong wind shear	**RASCAL** (also includes Gaussian plume model in the near field)
Particle trajectory model	Dispersion model	Atmospheric stability, wind and turbulence data	Dispersion over Complex terrine	Used in mesoscale Models Good for complex terrain	**HYSPLIT**

CHAPTER 4.
METHODS

4.1 Workflow of the present study

Figure 4-1 illustrates the overall framework and schematic of the modeling and computational procedure adopted in this work, with additional details in the following subsections.

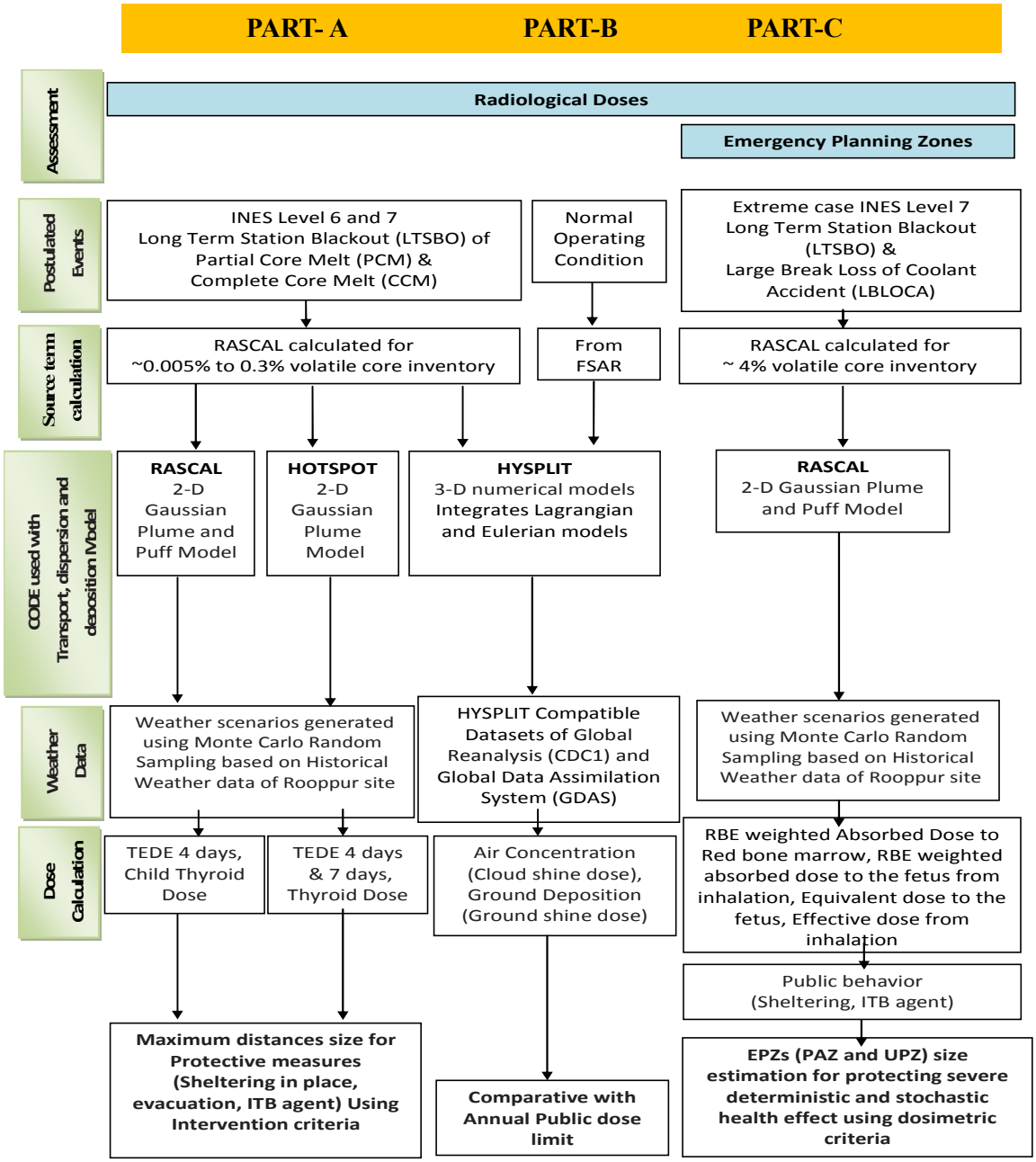

Figure 4-1: Workflow diagram of Radiological Doses and EPZ assessment.

The study is divides into three main parts.

- Consequences Analysis of LTSBO events (Part-A)
- Assessment of Emergency Planning Zones (Part-B)
- Consequences Analysis during Routine Operation (Part-C)

Each part covers: the relevant input technical parameters of the VVER-1200 reactor, the different computational tools (i.e., RASCAL, HotSpot, and HYSPLIT codes) that are used Accident scenarios and assumptions, Source terms of the events, Site-specific meteorological data, Atmospheric dispersion models. The **APPENDIX B** discusses the simulated site (Rooppur NPP) current state and geographical location.

4.2 PART- A: Consequences Analysis of LTSBO events

The following aims are set to simulate hypothetical BDBA INES Level 6 and 7 LTSBO events using the RASCAL 4.3 code (Ramsdell et al., 2012; Ramsdell et al., 2015), HotSpot 3.1.2 (Homann & Aluzzi, 2020) and the HYSPLIT Codes under dry and wet meteorological conditions. RASCAL code is used to model accident scenarios, calculate source terms, and perform radiological dose assessments. The source term generated by RASCAL serves as input for HotSpot and HYSPLIT, enabling a comparative analysis of results from both codes under similar conditions.

(a) Assessment of Radiological Consequences from Severe Accidents

- To compare the radiological impact of accident scenarios with and without the function of Passive ECCS.
- To calculate the TEDE and their contribution with time-delayed effects of three exposure pathways: cloudshine, inhalation, and 4-day groundshine.
- To analyze the spatial distribution of airborne radionuclide concentrations and ground deposition of released radionuclides under varying accidental cases and weather conditions.
- To analyze long-range atmospheric transport effects, taking into account topographical complexity, vertical wind shear, and seasonal fluctuations using the 3-D HYSPLIT dispersion model.

(b) Verification of Modeling Results and Sensitivity Analysis

- Compare RASCAL and HotSpot models with the same source terms to identify discrepancies in dose and dispersion predictions.
- To assess the effectiveness of protective measures—evacuation, sheltering-in-place, and KI administration—based on dose thresholds from the IAEA GSR Part 7 (IAEA, 2015a), Bangladesh's NNREPRP (MOST, 2020), and the PAG manual (U.S. Environmental Protection Agency (EPA), 2017).
- To perform the HYSPLIT model sensitivity through various input parameterizations.

4.2.1 Technical Parameters of the VVER-1200 Reactor used in RASCAL Simulation

Table 4-1 provides technical information on the Rooppur VVER-1200 reactor for the RASCAL 4.3 computations. In addition of this, the Rooppur site incorporates essential components and advanced safety systems, as outlined in **APPENDIX C**.

Table 4-1: Technical parameters of VVER-1200 reactor for RASCAL simulation (Faisal et al., 2023*).

Reactor power	3,212 MW_{th} (IAEA, 2011)
Average burn-up in the reactor core	30,000 MWd/MTU (Rascal default) (Ramsdell et al., 2012)
Primary containment type	PWR Dry Ambient
Primary containment volume	7.08E+4 m^3
Design pressure of primary containment	5.09E+4 kgf/m^2 (IAEA, 2011)
Design leak rate	0.2 volume % /day (IAEA, 2011)
Primary coolant mass	2.36E+05 kg (Calculated based on Rascal typical PWR for 3212 MW_{th}) (Ramsdell et al., 2012)
Number of fuel assemblies in the core	163 (IAEA, 2011)
Steam generator shape	U-type
Steam generator water mass	42,184 kg (Rascal default) (Ramsdell et al., 2012)
Primary containment height	42.2 meters (IAEA, 2011)

4.2.2 Accidental Release Scenarios

The Rooppur NPP of the VVER-1200 reactors is designed with safety features like active or passive ECCSs, containment systems, and core catchers to accident management. However, the performance of the passive heat removal system and core melt retention function of the VVER-1200 reactor might be impaired by various failure modes of passive safety systems-such as reduced heat exchange efficiency, diminished heat convection, valve blockages, corrosion, and

* Article published from this thesis

impurities (Burgazzi, 1998). Furthermore, the limited information in the open literature on the behavior of the core catcher under dry and wet conditions creates uncertainty about its effectiveness. Although the design includes additional technical measures in response to Fukushima accident- to improve stability and operational independence during BDBA (Asmolov et al., 2017), a severe earthquake or internal flooding could initiate a postulated event. Such an event may lead to both loss of offsite power and residual heat removal in the VVER-1200 reactor at the Rooppur site. So, the LTSBO event considered in this study could result from a sequence of more extensively severe events than those occurred at Fukushima.

In the LTSBO accident, both offsite power and all four emergency diesel generators (EDG) are lost with the reactor shut down. This stops the feed-water supply to the steam generators (SG), trips the reactor coolant pumps (RCP), and initiates a reactor scram. As the SG drains, the primary coolant heats up, increasing pressure and potentially leading to core damage without intervention. **Table 4-2** outlines six LTSBO accident cases and key input parameters for RASCAL simulations of the events. It is assumed that the LTSBO occurred in one unit of the RNPP in six cases. The reactor core was uncovered for 3 hr in the first three cases and 10 hr in the second three cases. Based on Table 2-9 of NUREG-1940 Supplement 1 presented in the previous chapter on **Table 3-1** (Ramsdell et al., 2015), the 3-hr and 10-hr uncovered reactor core scenarios on **Table 4.2** corresponds to 42.85% and 100% of core melt respectively for PCM and CCM. They are respectively identified as partial core melt (PCM) and complete core melt (CCM) for 3 hr and 10 hr uncovering time. In Case PCM_7c, the operator opens the pressurizer primary side depressurization and the emergency gas removal system valves, reducing primary pressure and allowing water to be supplied from the accumulators of the passive ECCS. After 24 hr, these systems failed, causing coolant to boil away.

For PWR-like VVER-1200 reactors, RASCAL assumes a boil-off time of 8 hr (Ramsdell et al., 2015). Radioactive materials are contained in the reactor pressure vessel and containment for 24 hr in the PCM_7c and CCM_6b cases, respectively. The radioactive leakage in these two cases started (8+24)=32 hours after reactor shutdown. In contrast, it happened after 8 hr in other cases. Containment pressure increased as a result of containment sprays failing in all cases. Radioactive materials were released into the environment through the containment at leakage rates of 0.2% per day (design leakage rate) in CCM_6a case and 3% per day in the other five cases. The sprays were activated after 3 hr in PCM cases and after 10 hr in the CCM cases;

subsequently, the core was recovered.

RASCAL does not fully account for specific advanced engineered safety features, such as the core catcher and passive safety system, of the VVER-1200 in accident scenarios, making highly severe cases, even though their likelihood is extremely low.

Table 4-2: RASCAL input parameters for six accident cases.

Accident Stage	**Partial Core Melt (PCM) (42.85%)**			**Complete Core Melt (CCM) (100%)**		
INES (Detailed in Section 5.1)	Level 7	Level 7	Level 7	Level 6	Level 6	Level 7
Case ID	PCM_ 7a	PCM_ 7b	PCM_ 7c	CCM_ 6a	CCM_ 6b	CCM_ 7c
ECCS available	No	No	24 hr	No	No	No
Reactor Uncovered for	3 hr	3 hr	3 hr	10 hr	10 hr	10 hr
Radioactive material in containment for release	0 hr	0 hr	0 hr	0 hr	24 hr	0 hr
Environment release start after shutdown	8 hr	8 hr	8hr+24hr	8 hr	8hr+24hr	8 hr
Sprays during release start	off	off	off	off	off	off
Sprays On after	3 hr	3 hr	3 hr	10 hr	10 hr	10 hr
Leak rate (volume % per day	3.0	3.0	3.0	0.2	3.0	3.0
Release height/containment leak location	10 m	30 m	30 m	10 m	10m	10 m
End of Calculation at	Start of release +24 hr					

4.2.3 Weather Scenarios

4.2.3.1 Regional Meteorological Characteristics

In the Rooppur region and Bangladesh in general, the seasonal air temperature fluctuates just slightly from season to season, with rainfall serving as the primary determinant of when each season begins and finishes. In this study two distinct seasons were taken in account: the dry season (September/October to April/May), characterized by the absence of rain, and the wet season (May/June to September/October) marked by rainfall.

The average mean hourly wind speed at 10 meters above ground at the closest weather station, Ishurdi, which is 10 kilometers from the Rooppur NPP site, is shown in **Figure 4-2**. The statistical study of historical hourly weather reports and model reconstructions covering meteorological data from January 1, 1980, to December 31, 2016 produced this wind speed data (Average-Weather-in-Ishurdi-BangladeshYear-Round#Figures-Summary, 2023). It also includes the 25th to 75th and the 10th to 90th percentile bands (Faisal et al., 2025*).

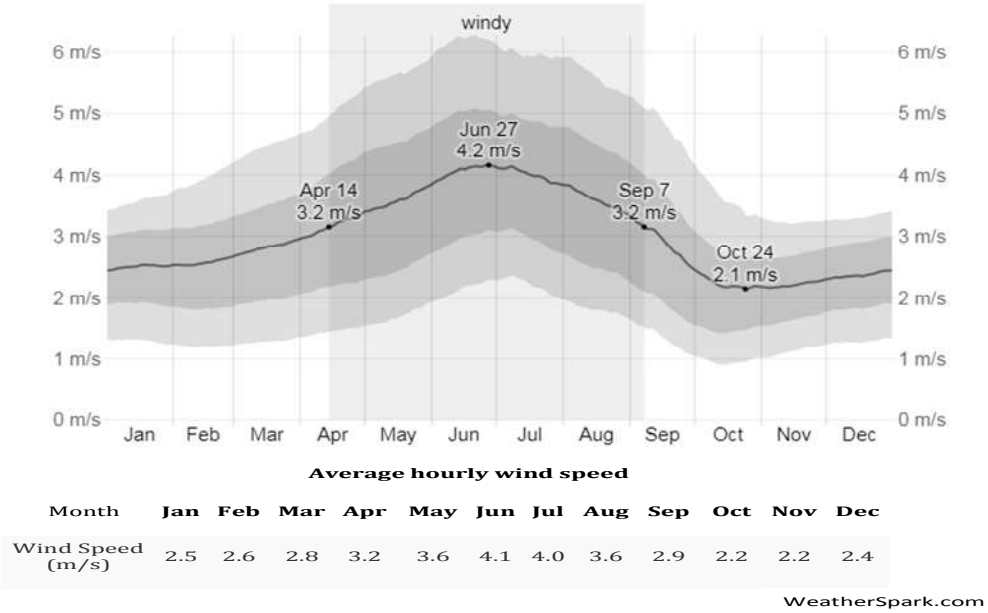

Figure 4-2: Individual 12 Months average of mean hourly wind speed (solid line) with 25th to 75th and 10th to 90th percentile bands and monthly mean wind speed in Ishuardi station (Average-Weather-in-Ishurdi-Bangladesh-Year-Round#Figures-Summary, 2023) (Faisal et al., 2025*).

Figure 4-2 indicates that the windiest period spans from April 14 to September 7, with average wind speeds surpassing 3.2 m/s. In contrast, the calmer season lasts from September 7 to April 14. June records the highest average hourly wind speed at 4.1 m/s, while October and November are the calmest months, with wind speeds averaging 2.2 m/s (Faisal et al., 2025*).

Since rainfall is a key driver of seasonal variation, data from the Bangladesh Meteorological Department's Ishurdi station (1981–2010) (Khatun et al., 2016), summarized in **Table 4-3**, show the distribution of dry and wet days across different rainfall categories throughout the year. Dry days dominate from November to March (90–97%), with December having the lowest

* Article published from this thesis

proportion of rainy days (2.7%). Conversely, wet conditions prevail from May to September, peaking in July when about 65% of the days experience rainfall. In Ishurdi, as in Bangladesh, no snow is observed yearly, with only rain contributing to precipitation (Faisal et al., 2025*). RASCAL defined three equivalent precipitation types based on hourly rainfall: light rain, rain, and heavy rain. The last column of the table represents RASCAL's classified three equivalent precipitation types.

4.2.3.2 Developed FORMULA for Sampling Data of Wind Speed and Precipitation Type

RASCAL's meteorological data processor enables users to input weather data and format it for use in atmospheric transport and diffusion modeling. To run simulations, the program requires key parameters such as wind speed, wind direction, release timing (day or night), and precipitation type. For this study, thirty weather scenarios were randomly generated for each month using wind speed and rainfall data specific to the Ishurdi region (Faisal et al., 2025*). Wind speeds for these scenarios were sampled from the assumed normal distribution ranges presented in **Figure 4-2**. **Table 4-4** shows the month-wise wind speed data for the Monte Carlo random sampling wind speed FORMULA and precipitation type distribution CONDITIONAL FORMULA, respectively, based on the historical wind speed of **Figure 4-2** and the historical rainfall data of **Table 4-3** at the Ishurdi region Rooppur site for 360 weather scenarios. Wind speed is computed using mean and standard deviation [(95 percentile values - mean)/2] data from **Figure 4-2** of each months.

* Article published from this thesis

Table 4-3: Frequency and percentage of dry and rainy days by rainfall ranges over 12 months of 30 years (1981-2010) in Ishurdi (Khatun et al., 2016; Faisal et al., 2025*).

Rainfall (mm) per day	Jan	Feb	Mar	Apr	May	Jun	Jul	Aug	Sep	Oct	Nov	Dec	Total days	RASCAL Equivalent Precipitation type
Dry days	893 (96%)	777 (91.8%)	832 (89.6%)	727 (80.9%)	593 (63.8%)	472 (52.8%)	321 (34.6%)	416 (44.8%)	434 48.2%)	713 (76.8%)	854 (95%)	905 (97.3%)	7937 (72.6%)	No precipitation
1-10	31 (3.4%)	45 (5.3%)	56 (6.0%)	91 (10.1%)	167 (18%)	232 (26.0%)	349 (37.6%)	311 (33.5%)	241 (26.8%)	136 (14.7%)	32 (3.5%)	18 (2.0%)	1709 (15.6%)	Light rain (< 1 mm/h)
11-22	5 (0.5%)	18 (2.2%)	29 (3.1%)	47 (5.2%)	82 (8.8%)	85 (9.5%)	128 (13.8%)	113 (12.2%)	108 (12.0%)	34 (3.7%)	6 (0.7%)	3 (0.3%)	658 (6.0%)	
23-43	1 (0.1%)	6 (0.7%)	11 (1.2%)	24 (2.7%)	61 (6.6%)	64 (7.2%)	82 (8.9%)	57 (6.2%)	63 (7.0%)	26 (2.8%)	5 (0.6%)	3 (0.3%)	403 (3.4%)	Rain (1 - 5 mm/h)
44-88			1 (0.1%)	9 (1.0%)	26 (2.8%)	35 (3.9%)	39 (4.2%)	27 (2.9%)	41 (4.5%)	14 (1.5%)	2 (0.2%)	1 (0.1%)	195 (1.8%)	
89-99						1 (0.1%)	3 (0.3%)		5 (0.6%)	2 (0.2%)			11 (0.1%)	
100-199				1 (0.1%)		5 (0.5%)	6 (0.6%)	4 (0.4%)	8 (0.9%)	2 (0.2%)			26 (0.2%)	Heavy rain (> 5 mm/h)
200-299										1 (0.1%)			1 (0.01%)	
Total days	930 (100%)	846 (100%)	929 (100%)	899 (100%)	929 (100%)	894 (100%)	928 (100%)	928 (100%)	900 (100%)	928 (100%)	899 (100%)	930 (100%)	10,940 (100%)	

* Article published from this thesis

Table 4-4: 12 Months wind speed data for Monte Carlo Random Sampling wind speed FORMULA and Precipitation type distribution CONDITIONAL FORMULA for 360 weather scenarios for Rooppur site.

	Wind speed (m/s)				Precipitation type	
Month	**95 percentile wind speed**	**Mean, μ**	**Standard Deviation, σ**	**Monte Carlo random sampling**	**Random values (0-1) for rainfall**	**CONDITIONAL FORMULA**
Jan	3.5	2.5	0.50	=NORMINV(RAND(),2.5,0.5)	'R' = RAND()	=IF((AND(R>=0.96,R<=0.998)),"light",IF(AND(R>0.998,R<=1),"moderate","No Precipitation"))
Feb	3.8	2.6	0.6	=NORMINV(RAND(),2.6,0.6)	'R'= RAND()	=IF((AND(R>0.918,R<=0.993)),"light",IF(AND(R>0.993,R<=1),"moderate","No Precipitation"))
Mar	4.5	2.8	0.85	=NORMINV(RAND(),2.8, 0.85)	'R'= RAND()	=IF((AND(R>0.896,R<=0.987)),"light",IF(AND(R>0.987,R<=1),"moderate","No Precipitation"))
Apr	5	3.2	0.9	=NORMINV(RAND(),3.2,0.9)	'R'= RAND()	=IF((AND(R>0.809,R<=0.962)),"light",IF(AND(R>0.962,R<=0.999),"moderate",IF(R>0.999,"Heavy","No Precipitation")))
May	5.6	3.6	1.0	=NORMINV(RAND(),3.6,1.0)	'R'= RAND()	=IF((AND(R>0.638,R<=0.906)),"light",IF(AND(R>0.906,R<=1),"moderate","No Precipitation"))
Jun	6.4	4.1	1.15	=NORMINV(RAND(),4.1,1.15)	'R'= RAND()	=IF((AND(R>=0.528,R<=0.883)),"light",IF(AND(R>0.883, R<=0.995),"moderate",IF(R>0.995,"Heavy","No Precipitation")))
Jul	5.9	4	0.95	=NORMINV(RAND(),4,0.95)	'R'= RAND()	=IF((AND(R>0.346,R<=0.86)),"light",IF(AND(R>0.86,R<=0.996),"moderate",IF(R>0.996,"Heavy","No Precipitation")))

Aug	5.4	3.6	0.9	=NORMINV(RAND(),3.6,0.9)	'R'= RAND()	=IF((AND(R>0.448,R<=0.905)),"light",IF(AND(R>0.905,R<=0.996),"moderate",IF(R>0.996,"Heavy","No Precipitation")))
Sep	4.6	2.9	0.85	=NORMINV(RAND(),2.9,0.85)	'R'= RAND()	=IF((AND(R>0.482,R<=0.87)),"light",IF(AND(R>0.87,R<=0.991),"moderate",IF(R>0.991,"Heavy","No Precipitation")))
Oct	3.5	2.2	0.65	=NORMINV(RAND(),2.2,0.65)	'R'= RAND()	=IF((AND(R>0.768,R<=0.952)),"light",IF(AND(R>0.952,R<=0.997),"moderate",IF(R>0.997,"Heavy","No Precipitation")))
Nov	3.3	2.2	0.55	=NORMINV(RAND(),2.2,0.55)	'R'= RAND()	=IF((AND(R>0.95,R<=0.992)),"light",IF(AND(R>0.992,R<=1),"moderate","No Precipitation"))
Dec	3.4	2.4	0.5	=NORMINV(RAND(),2.4,0.5)	'R'= RAND()	=IF((AND(R>0.973,R<=0.996)),"light",IF(AND(R>0.996,R<=1),"moderate","No Precipitation"))

4.2.3.3 Generated Weather Scenarios for RASCAL and HotSpot Simulation

According to **Table 3.4** FORMULA, a total of 360 scenarios (30 per month across 12 months) were developed to represent the potential weather conditions at the Rooppur site throughout the year, as detailed in **APPENDIX-D**. Wind direction variability was not included, as the analysis focuses exclusively on dose estimation, applying uniform EPZ distances in all directions. For RASCAL meteorological input, wind was assumed to blow consistently from 0 degrees in all scenarios. Additionally, release periods were set at 10:00 for daytime and 22:00 for nighttime, with these times randomly assigned across the 360 sampled weather conditions. Precipitation types in weather scenarios are distributed by comparing each month's contribution of dry days, light rain, rain, and heavy rain frequencies from **Table 4-3**'s historical rainfall data to their corresponding random values in each scenario. The weather scenarios stability class employs the Pasquill-Gifford stability classification, as indicated in **Table 3-4**. The stability class ranges from 'B' to 'D' during the day and from 'D' to 'F' at night.

The current study's weather parameters, such as wind speed, precipitation type, release time, and stability class, are presented in **Figure 4-3** for the 360 weather scenarios in **APPENDIX-D**. The percentages in **Table 4-3's** historical rainfall statistics roughly correspond to the distribution of precipitation types: There was 1% heavy rain, 21% light rain, 4% rain, and 74% no precipitation. The two most often observed stability classes out of the 360 situations are 'E' (34%) and 'B' (27%). In the dry season (October to May), most situations show stability classes 'B' and 'E,' however in the rainy season (June to September), the dominating classes change to 'C' and 'D' (Faisal et al., 2025*). These scenarios give a sufficient statistical basis to account for varying weather conditions around the plants.

* Article published from this thesis

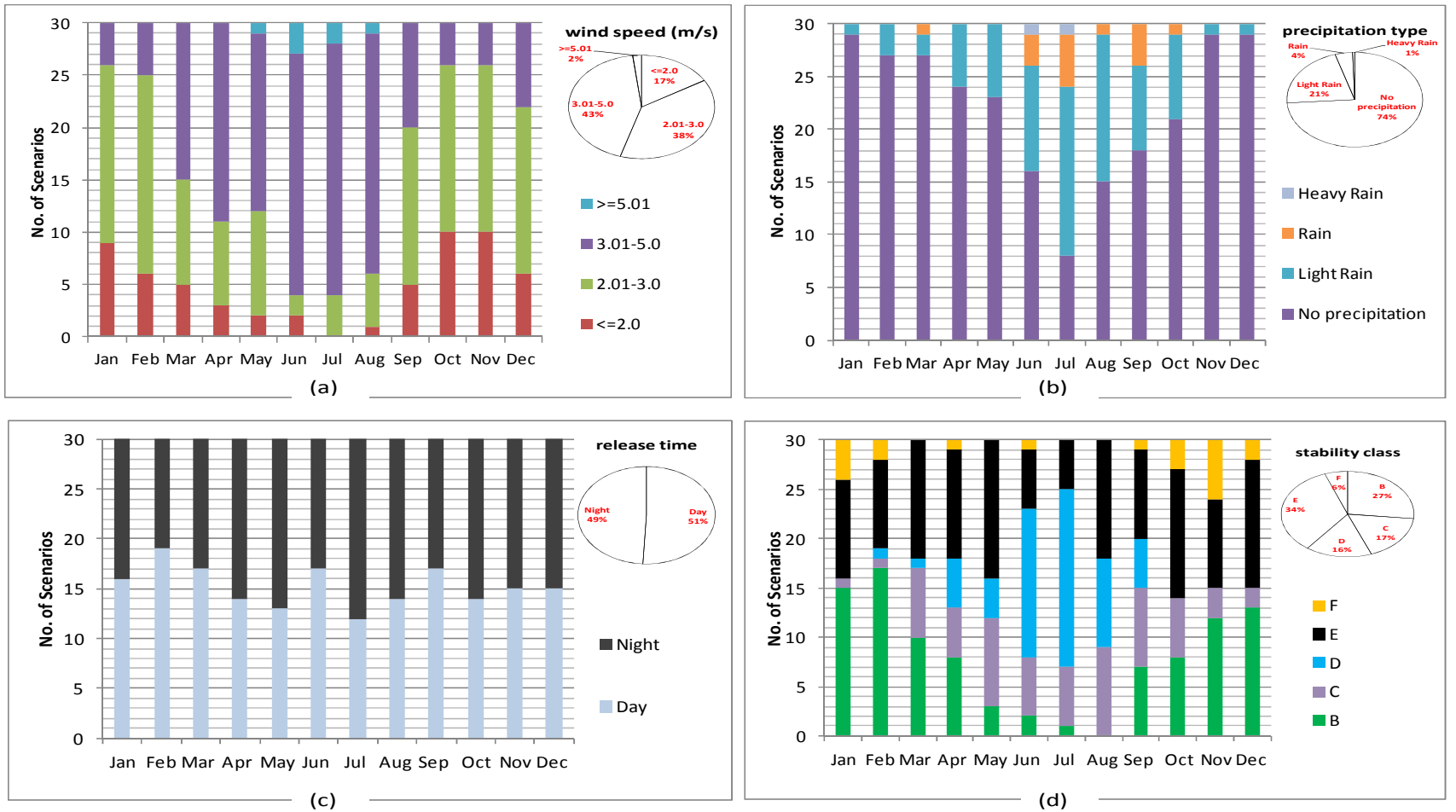

Figure 4-3: Individual 12 Months Frequency distribution of (a) wind speed (b) precipitation type (c) release time and (d) stability class for the 360 Monte Carlo Random sampled weather scenarios (Faisal et al., 2025*).

* Article published from this thesis

4.2.4 RASCAL and HotSpot Dose Calculation

The following presumptions are considered while calculating doses in RASCAL: i) There are no buildings or other topographical features in the area close to the dose measurement; ii) the meteorological station has a uniform surface roughness of 0.2; and iii) people stay outside for the duration of the plume passage and for four days in order to be exposed to radionuclides that have been deposited on the ground (Faisal et al., 2025*). TEDE is computed up to 80 kilometers from the discharge location in this part. The straight-line Gaussian plume model is used to compute the close-in doses (area up to 20 km) on a polar grid. Assuming that the release point is near the grid's center, the far-field doses are computed using the Gaussian puff model on an 80 km Cartesian grid distance.

Inhalation, cloudshine, and ground shine are the three exposure paths by which RASCAL determines doses. The radioactivity absorbed during plume passage in the early stages of the disaster is the source of the inhalation doses. For an adult male, the inhalation Committed Effective dose Equivalent (CEDE) is a committed dose of 50 years. An external dose of radiation from the plume is known as the cloudshine dose. Based on the radioactive activity deposited on the surface, RASCAL determines a 4-day dose of groundshine. It is the total of the doses of groundshine received during the model computation period and the doses that would be received within the first 96 hr after the calculation was completed. Cloud shine dose, inhalation CEDE, and groundshine dose accrued within the first 96 hours from the onset of release to the environment are all included in the early phase TEDE, as defined by the US EPA. Individuals who are engaged in traditional activities (spending a lot of time indoors) and evacuated or relocated for four days after plume passage would receive lower doses than the plume phase doses that RASCAL calculates (Ramsdell et al., 2012, Faisal et al., 2023*).

RASCAL's child thyroid dose modeling assumes parameters for a 1-year-old child, applying weighted averages to represent the distribution of iodine in the atmosphere. The calculations focus solely on exposure to iodine isotopes to remain consistent with EPA's KI-specific dose guidance. RASCAL 4.3's dose estimates serve to evaluate whether the KI threshold is met, enabling prompt and informed decisions during emergencies involving radioactive iodine releases.

* Article published from this thesis

To assess whole-body exposure, HotSpot uses the effective dose equivalent (EDE), which aggregates organ-specific dose equivalents using tissue weighting factors. When radioactive material is inhaled or ingested and retained within the body, it continues to deliver a dose over time. The committed dose equivalent (CDE) represents this long-term organ-specific dose, typically projected over 50 years. HotSpot calculates the 50-year committed dose equivalent for each target organ using site-specific integrated air concentrations and dose conversion factors (DCF). 50-year CDE(T) = C × DCF(T) where C is the integrated air concentration ([Ci-s/m³]), and DCF(T) is the dose conversion factor [rem-m^3]/[Ci-s] for the target organ. The CEDE is the sum of weighted CDEs across all organs, representing total internal exposure. When external exposure (e.g., from ground or air submersion) is also included, then TEDE = CEDE (inhalation) + EDE (submersion) + EDE (groundshine) + EDE (resuspension).

APPENDIX-E, Figure E-1 and E-2 present the simulation steps in the RASCAL and HotSpot codes used in this study.

4.2.5 Input Meteorological Data Model in HYSPLIT

The HYSPLIT model can utilize different meteorological datasets to improve its predictions. Draxler et al. suggested that combining the ATDM with a suitable meteorological model would enhance predictions of how particles disperse and deposit (Draxler et al., 2015). Their research shows that linking dispersion models with the GDAS weather framework yields better results than other combinations. In this study, two global reanalysis meteorological datasets, CDC1 and GDAS1, were used and converted into formats compatible with HYSPLIT. While the CDC1 dataset has a coarser spatial and temporal resolution, it is widely used in regulatory screening models because of its easy availability. To improve the realism and spatial accuracy of the simulations, the higher-resolution GDAS1 dataset was also included (Faisal & Islam, 2025*).

4.2.5.1 NCAR/NCEP Global Reanalysis Climate Diagnostics Center (CDC1)

Climate Diagnostics Center (CDC1) meteorological data is an archived pressure-level reanalysis dataset from the NOAA Climate Diagnostics Center. It includes global and regional climate variables. This meteorological input dataset was obtained from a reanalysis by the National Center for Environmental Prediction (NCEP) and the National Center for Atmospheric Research (NCAR) (Draxler et al., 2018). Global 2.5° meteorological data with a 6-hr time resolution was

* Article published from this thesis

retrieved from the NOAA ARL server (https://www.ready.noaa.gov/ready2-bin/extract/extracta.pl). This dataset includes surface-level information such as surface pressure (PRSS), 2-meter air temperature (T02M), 10-meter horizontal wind components (U10M and V10M), and 6-hour accumulated precipitation (TPP6). Vertically, it provides data at 17 pressure levels, ranging from 1000 to 10 hPa, including height (HGTS), temperature (TEMP), horizontal wind components (UWND and VWND), vertical wind velocity (WWND), and relative humidity (RELH). Each month's meteorological data is saved as a separate file (Faisal & Islam, 2025*).

4.2.5.2 Global Data Assimilation System (GDAS1)

NOAA's GDAS dataset (https://www.ready.noaa.gov/ready2-bin/extract/extracta.pl) provides meteorological data on a pressure-coordinate system with a 1° horizontal resolution, which is roughly 100 km × 100 km, at 3-hour intervals. It includes 23 vertical layers and provides weekly values for 32 different meteorological parameters across the globe. Each week's data is saved as a separate file. Compared to the CDC1 dataset, GDAS offers finer spatial detail. Both datasets were used in this study to compare results and to see how the resolution of meteorological input influences the patterns of dispersion and deposition. (Faisal & Islam, 2025*). **Table 4-6** shows the available comparative meteorological parameters of the two datasets.

Table 4-6: Available parameters of the GDAS1 and CDC1 Meteorological datasets (Faisal & Islam, 2025*).

Meteorological Data	CDC1	GDAS1
1. Ten meter wind	√	√
2. Two meter temp	√	√
3. Heat flux	x	√
4. Momentum flux	x	√
5. Terrain height	x	√
6. Surface pressure	√	√
7. Mixed layer depth	x	√
8. Convective mixing	x	√
9. Meteorological Grid	2.5°	1°

4.2.6 HYSPLIT simulation Configuration for LTSBO event

4.2.6.1 Sensitivity Run for Particle Number, Concentration Grid and Release Height

The concentration pattern in HYSPLIT shows a relationship among particle number, the

* Article published from this thesis

concentration grid cell, and sampling average time (Draxler et al., 2019). So it is important to understand the concentration pattern in different combinations of particle number and concentration grid to obtain a realistic representation. **Table 4-7** shows the parameters used in the sensitivity tests for particle numbers and concentration grid resolutions, along with the symbols representing each combination. The simulations were carried out using 100, 1,000, 10,000, and 100,000 particles, with concentration grids of 0.01°, 0.025°, 0.05°, and 0.1°, assuming a stack height of 100 meters. Case C3 represents a scenario where 10,000 particles are released per hour using a concentration grid of 0.050° × 0.050° (Faisal & Islam, 2025*). Variation of release height effects were also analyzed at 10m, 30 m and 200 m, where H30 ($_{0\text{-}100}$) indicates radionucles were released at 30 m height and air concentration were estimated at a grid cell of 0m and 100m.

For all combinations, the sensitivity simulations were run over a 12-hour period, with a single output representing the entire 12 hours. A unit release rate of 100 Bq/hr was used over 0.01 hours. Meteorological data for January 2021 from the CDC1 and GDAS1 datasets were applied, with the simulations starting at 00:00 UTC on the first day of the month (Faisal & Islam, 2025*). Detailed results of the sensitivity analysis can be found in the Results section. A concentration grid of 0.05°X0.05° and approximately 1000 particles discharged in each emission hour offer the best possible balance between accuracy, calculation time, and a more even distribution of air concentration and ground deposition for LTSBO accident simulation.

Table 4-7: Parameters along with symbols of particle number, concentration grid and release height used in HYSPLIT sensitivity run (Faisal & Islam, 2025*).

Meteorology data source	a) Global Reanalysis (CDC1) b) GDAS1 (1-degree, global, 2006 - present) (NOAA)	**Concentration grid**	**1) 0.01° X 0.01°**	**2) 0.025° X 0.025°**	**3) 0.05° X 0.05°**	**4) 0.1° X 0.1°**	Height
Met. Data:	Jan 2021	Number of particles per cyclic					

* Article published from this thesis

<table>
<tr><td>Start of simulation: Release starting time:</td><td>01-01-2021 at 00:00</td><td>A) 100 (8.3/hr)</td><td>A1</td><td>A2</td><td>A3</td><td>A4</td><td rowspan="4">H100 = 100m (stack release)</td></tr>
<tr><td>Simulation run time:</td><td>12 hr</td><td>B) 1000 (83.3/hr)</td><td>B1</td><td>B2</td><td>B3</td><td>B4</td></tr>
<tr><td>End of simulation:</td><td>01-01-2021 at 12:00</td><td>C) 100000 (833.3/hr)</td><td>C1</td><td>C2</td><td>C3</td><td>C4</td></tr>
<tr><td>Radionuclide:</td><td>RNUC and NGas</td><td>D) 100000 (8333.3/hr)</td><td>D1</td><td>D2</td><td>D3</td><td>D4</td></tr>
<tr><td>Release rate:</td><td>100Bq/hr</td><td rowspan="4">Concentration grid:
0.05°X0.05°
Number of particle:
100</td><td colspan="2">H200 (0-100)</td><td>H200 (0-200)</td><td>H200</td><td>200m</td></tr>
<tr><td>Release duration:</td><td>0.01 hr</td><td colspan="2">H30 (0-100)</td><td>H30 (0-30)</td><td>H30</td><td>30m</td></tr>
<tr><td>Top of averaged layer:</td><td>100 m (Above Ground Level)</td><td colspan="2">H10 (0-100)</td><td>H10 (0-10)</td><td>H10</td><td>10m (ground level)</td></tr>
<tr><td>Sampling interval:</td><td>12 hr</td></tr>
</table>

4.2.6.2 Computational Domain and Simulation Run Time

Computational Domain

The computational domain, which includes Bangladesh and its surrounding areas, is depicted in **Figure 4-4**. Its center is near Rooppur NPP (24.07°N, 89.10°E), and it extends over 50° in longitude (from west to east) and 50° in latitude (from south to north). The domain's output concentration field was computed across a vertical layer that was 100 meters deep, and the computational grid's spatial resolution was 0.05° (~5 km).

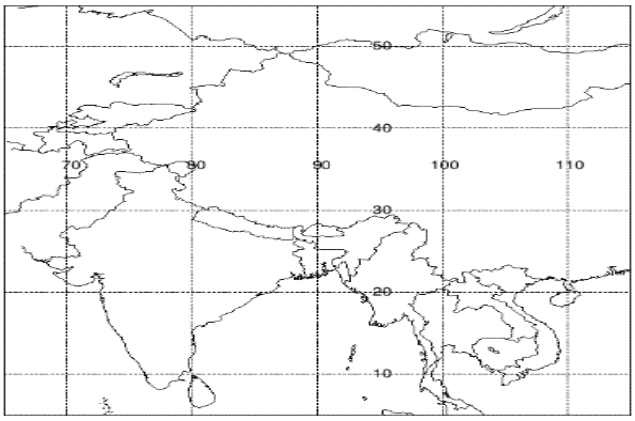

Figure 4-4: Model domains mapping (generated from NOAA ARL server) in HYSPLIT simulation for LTSBO event.

Simulation Run Time

APPENDIX F of Figures F-1 to F-12 represent 12 monthly (January–December) wind rose diagrams for the years 2021 and 2022 of GDAS1 and CDC1 meteorological datasets over 84 hours starting on the 15th day of each months. **APPENDIX G of Figures G-1** shows Pasquill stability class and boundary layer depth variations over 84 hr starting from 15th of the month of January & July of the years 2021 and 2022 for GDAS1 and CDC1 meteorological data. To determine the appropriate simulation duration, air concentration, and ground deposition distribution characteristics for the LTSBO accident scenario study, the model was executed based on the worst-case 10-hr CCM accidental release from the Rooppur NPP during two representative months of 2022: January and July. These months were selected to represent typical dry and wet weather conditions, respectively, using two distinct meteorological datasets of GDAS1 and CDC1. Based on this sensitivity analysis result presented in the next chapter—and recognizing that radionuclides can be transported over long distances from the accident site—the simulation run time was set at 15 days to evaluate long-range consequences.

4.2.6.3 Accident Simulation Pollutant and Concentration Grid Setting

Table 4-8 shows the parameters for the HYSPLIT dispersion model used in this study for the LTSBO accidental release. Monthly simulation ran were performed for 360 hours, using CDC1 and GDAS1 meteorological data files, with the release starting on the 15th day at 00:00 hr of the respective month. Air concentration results were averaged between 0 and 100 m above ground level, and 15 days of cumulative ground depositions were calculated. Dispersion was simulated over a 2000 km radius around the source, with a horizontal grid of 50° × 50° and a concentration grid resolution of 0.05° × 0.05° (approximately 5 × 5 km). The model includes two vertical levels: 0 and 100 m AGL. For simplicity, a release height of 30m and 500 m at coordinates 24.07°E and 89.1°N (Rooppur NPP 1) was used for the emission location. Other model parameters were set to their default values. **APPENDIX-E, Figure E-3** presents the simulation steps in the HYSPLIT code used in this study.

Table 4-8: Input parameters for the LTSBO event in HYSPLIT Simulation.

Parameter	**CCM (10 hr release)**	**PCM (3 hr release)**
Meteorology Data source	a) Global Reanalysis (CDC1) b) GDAS1 (1-degree, Global, 2006 - present)	
Met. Data year	2022	

Vertical motion method	Input model data	
Start of simulation	From the 15th day of months January (Dry weather condition) and July (Wet weather condition) of the years at 00:00	
Simulation run time	360 hr (15 Days)	
End of simulation	30th day of respective month 00:00	
Release starting time (UTC)	From the 15th day of months January (Dry weather condition) and July (Wet weather condition) of the years at 00:00	
Release height	30 m, 500m	
Release rate	1Bq/hr	
Radionuclide	RNUC and NGas	
Release duration	10 hr	3 hr
Top of averaged layer	100 m	
Number of release particles per cycle	10000	3000
Number of release particles per hour	1000	
Grid span	50 degree × 50 degree	
Concentration grid resolution	$0.05^{o} \times 0.05^{o}$	
Sampling interval	24 hr and 360 hr	

4.2.6.4 Deposition Parameter Setup

Each model run included deposition characteristics separately for two surrogate radionuclides. Key data for deposition characteristics used in HYSPLIT are listed in **Table 4-9**.

Table 4-9: Deposition characteristics values used in present HYSPLIT simulation (Faisal & Islam, 2025*).

Parameter	Values
Density, shape, and particle diameter	'0' treats as a gas, while '1' flags as a particle
Dry deposition rates	0.001 m/s
Wet deposition	In-cloud and below-cloud removal, same scavenging constant ($8 \times 10^{-5} s^{-1}$)
Henry's constant	noble gases - zero
Re-suspension factor	zero for both surrogate

Density, shape, and particle diameter define pollutants subject to gravitational settling and wet removal. **Dry deposition rates** are highly uncertain due to varying interactions between radioisotopes and ground cover over time and space. For the Rooppur site, this study uses a constant dry deposition velocity of 0.001 m/s, applied with its associated uncertainties. During a LTSBO accident scenario at the NPP, various radionuclides may be released. These include non-depositing noble gases like Xenon-133, iodine-131 in both gaseous and particulate forms, and

* Article published from this thesis

particulate-bound isotopes such as cesium-137, which have moderate dry deposition velocities of about 0.001–0.01 m/s. The deposition behavior depends on the chemical form and particle size. A typical velocity of 0.001 m/s is used as a representative value, especially for small particles and semi-volatile substances. This fixed value also provides an average across different land surfaces—including grasslands, agricultural areas, soil, and the Padma River—offering a balanced estimate that avoids overestimating deposition on rough surfaces like forests or underestimating it over smooth surfaces like water (Faisal & Islam, 2025*).

Wet deposition involves the removal of pollutants from the atmosphere via precipitation. The HYSPLIT 854 version (January 2017 release), which was used in this present study, uses a simplified approach for in-cloud and below-cloud removal, defined by the same scavenging constant (8×10^{-5} s^{-1}) (Draxler et al., 2019). Pollutants reach the ground when rain forms within clouds or below clouds, when falling droplets collide with aerosols through processes like Brownian diffusion, interception, impaction, and turbulent diffusion. **Henry's constant** for noble gases was set to zero, implying their health effects stem only from inhalation or external exposure in the plume (cloud submersion). Studies show noble gases do not undergo dry or wet deposition but remain airborne until they decay radioactively (Draxler and Hess, 1998). The **Re-suspension factor** for deposited particles was assumed to be zero for both surrogate radionuclides in this study.

4.2.6.5 Air Concentration and Ground Deposition Calculations

In HYSPLIT, each particle represents a portion of the total pollutant mass. As the particles move through the computational domain, their masses are summed and divided by the volume of each grid cell to determine the air concentration. This calculation takes into account particle radioactivity, the duration of the release, and the deposition rate. For simplicity, no specific half-lives are assigned in this study, assuming that all particulate radionuclides behave like cesium-137 in terms of deposition. Finally, the air concentration and ground deposition are adjusted during post-processing to account for the radioactive decay of all released radionuclides (Faisal & Islam, 2025*).

The unit release concentration output file is read by the program named CON2REM. The air concentration is calculated by multiplying the normalized concentration output from the model,

* Article published from this thesis

the dilution factors, and the dispersion factors by the source term in the post-processing phase (CON2REM software) using the ACTIVITY.TXT file. Additionally, the half-life decays it to provide the air concentration for this radionuclide at that specific sample output time. (Draxler et al., 2019). Adding all the species give, a total air concentration from cloud-shine and a total ground deposition from the ground-shine.

APPENDIX H of **Figures H-1 and H-2** shows the ACTIVITY.TXT file, which lists the radionuclides that are considered for volumetric air concentration and volumetric ground deposition, respectively, for the 10 hr CCM state and 3 hr PCM state. This file contains several columns. The radionuclides' half-lives are listed in the first column. The highest emission rate (Bq/hr) of that specific radionuclide for 10 and 3 hour accidental LTSBO emissions from the VVER-1200 reactor at the RNPP site is shown in the following four columns, which are identical for a reactor accident.

4.2.7 Air Concentration Uncertainty in HYSPLIT

There are various reasons of air concentration uncertainty, such as how well the meteorological data represent the real flow field, inaccuracies in the parameterization of physical processes in the model, and even the impacts of atmospheric turbulence that the model does not account for. (Draxler et al., 2019). This study used two methods of uncertainty analysis: (a) Meteorological Data Ensemble, which examines gradients in meteorological data not captured by grid points, and (b) Model Physics Ensemble, which tests different physical representations of dispersion. These methods assess variability in model concentration predictions. Each analysis uses a script to automate steps, running HYSPLIT for each model variation with suffixes like .001, .002…… The output files include prob05, prob10, prob25, prob50, prob75, prob90, and prob95, representing concentrations at probability levels ranging from 5% to 95% (Draxler et al., 2018).

4.2.7.1 Meteorological Data Ensemble

In the ensemble model, the meteorological grid is shifted in the X, Y, and Z directions for each member. Each member runs sequentially. Offsets are defined by the SETUP.CFG file, with default values of one grid point horizontally and 0.01 sigma vertically, resulting in 27 ensemble members (Draxler et al., 2018). For valid vertical offsets, the starting height is at least 0.01 sigma (250 m) above the ground. The model generates 27 output files; only one offset (X, Y, or

Z) is applied per member, with ranges of 1-9 for no vertical shift, 10-18 for a positive shift, and 19-27 for a negative shift.

4.2.7.2 Model Physics Ensemble

Unless a SETUP.CFG file with parameter modifications appears, the model runs with the default values. A script in the model physics ensemble performs 20 various computations, including 3D-particle, Gaussian, and top-hat puffs; modifications in mixed layer depth calculation; turbulence and stability equations; vertical-to-horizontal turbulence ratio; and Lagrangian time scale adjustments (Draxler et al., 2019). HYSPLIT is a dispersion modeling tool that can simulate the spread of pollutants using either a three-dimensional particle method (ensemble no. 01) or a puff-based approach (ensemble no. 02 and 03). The particle method follows the turbulent motion of individual particles, while the puff method estimates dispersion growth rates (ensemble no. 04). The boundary layer depth is usually taken from the meteorological model (ensemble no. 05), but it can also be estimated as the height where the potential temperature increases by 2°C above the near-ground minimum. Alternatively, a fixed boundary layer height can be used (ensemble no. 06–08). Vertical turbulence changes with height, though it can be simplified using a constant vertical diffusivity (ensemble no. 09–11). Turbulence can be calculated using methods such as Kantha-Clayson, the Beljaars-Holtslag scheme (ensemble no. 014), or based on low-level wind and temperature profiles (ensemble no. 013), and it can also be derived from the turbulent kinetic energy field (ensemble no. 12, 15, 16). Horizontal and vertical turbulent length scales are typically set at 10,800 s and 200 s, respectively (ensemble no. 17–20), with dynamic calculations allowing for additional variability (Faisal & Islam, 2025*).

* Article published from this thesis

4.3 PART- B: Assessment of Emergency Planning Zones

This part describes the method to estimate the EPZ (PAZ and the UPZ) sizes of the under-construction Rooppur NPP site based on conservative assumptions aligned with the post-Fukushima IAEA guidelines (IAEA, 2013b). The specific aims of this part are to

- Propose a scientific methodology to determine the sizes of the EPZ by developing source terms and weather scenarios.
- Analyze and compare the EPZ protective requirements for both DBA and BDBA.
- Assess the validity of the proposed EPZ sizes and protective measures under different scenarios.

To do so, it accounts for an environmental release of 4% volatile fission products (Kr, Xe, I, Cs, and Te) from each DBA and BDBA event. Radiological doses for the LBLOCA and LTSBO occurrences are assessed yearly using 360 different weather scenarios (Faisal et al., 2025*). EPZs are then established using dosimetric criteria (IAEA, 2013b) that account for more than 95% of all meteorological conditions (Faisal et al., 2025*). Appropriate protection measures are also defined inside these zones to keep doses below the deterministic and stochastic health effects criteria.

4.3.1 Postulated Initiating Events

In the Rooppur NPP feasibility study, the frequency of fuel damage in the core caused by internal starting events in all operating modes was determined to be less than 5.9E-07. According to the Preliminary Safety Analysis Report (PSAR) for the Rooppur project, the most serious DBA is an LBLOCA produced by a pipeline rupture larger than 100 mm in diameter (Environmental Impact Assessment, 2017). A breach of this magnitude leads to a rapid and substantial loss of coolant. This can overheat the reactor core, which may damage or even melt the fuel, resulting in radioactive fission products leaking into the reactor coolant system and potentially into the environment. The radioactive leak poses serious radiological dangers, including contamination of the environment and extensive health effects, resulting in significant public and environmental consequences (Faisal et al., 2025*). According to the feasibility assessment for the Ostrovets' VVER-1200 NPP project in Belarus, the reactor's core meltdown probability is 1E-6 per reactor year. In a BDBA event, large radionuclides are released into the environment with a likelihood of 1E-7 per reactor-year, possibly totaling to 100 TBq for ^{137}Cs.

* Article published from this thesis

(Belarussian NPP, Environmental Impact Assessment, 2010). NPP, including VVER-1200 reactors, are designed to handle DBAs using advanced safety features like active and passive ECCSs, containment structures, and core catchers. However, the RASCAL model takes a conservative approach by assuming a complete failure of these safety systems. This assumption helps assess the worst-case scenario for radiological release, which is crucial for determining the size of the EPZ (Faisal et al., 2025*). By preparing for such unlikely failures that ensure the EPZ is large enough to handle even the most severe events.

To define the boundaries of the EPZ, two hypothetical events from both DBA and BDBA categories are considered. In the DBA category, a LBLOCA is a significant event where a major rupture in the primary cooling system causes rapid depressurization and makes it difficult to maintain core cooling. If no action is taken, the coolant will be depleted within three hours, exposing the reactor core. This could lead to severe overheating, a core meltdown, and ultimately, the failure of the reactor vessel.

In the BDBA scenario, a LTSBO is characterized by the simultaneous loss of both off-site and on-site power. This typically occurs due to an external event like an earthquake (Faisal et al., 2025*). In this situation, it is assumed that neither active nor passive ECCSs or portable mitigation equipment are available. As a result, the coolant will evaporate, causing damage to the reactor core.

Table 4-10 provides a summary of the timing and release sequences used in the RASCAL model, based on conservative accident assumptions. Both scenarios initiate environmental releases at the same times: 10:00 AM (10:00) for daytime and 10:00 PM (22:00) for nighttime. However, in the LTSBO scenario, the loss of ECCS functionality is assumed to start five hours earlier than in the LBLOCA scenario for considering releasing radionuclides in a same weather conditions. In both cases, the reactor core remains exposed for 10 hours until the progression of damage stops and the release of fission products ceases, indicating the beginning of core recovery. Radiological releases are expected to occur at ground level (10 meters) due to leaks in containment, without any spray or filtration systems to limit the dispersion of fission products. A conservative leakage rate of 1% volume per hour is assumed for both events. This leads to the

* Article published from this thesis

release of about 3.60% of volatile and gaseous fission products (such as Krypton, Xenon, Iodine, Cesium, and Tellurium) into the atmosphere over a 10-hour period during the LBLOCA scenario, and approximately 3.88% for the LTSBO scenario (Faisal et al., 2025*).

Table 4-10: Timing of LBLOCA and LTSBO postulated initiating events used for source term and release pathways in RASCAL simulation (Faisal et al., 2025*).

Parameter	LBLOCA	LTSBO
Shutdown time (hr: min)	T_{sd}	T_{sd}
Core uncovered / Core Release start / Relese to the containment start (hr: min)	Tsd + 3hr	T_{sd} + 8hr (For PWRs, RASCAL assums an 8- hr delay between loss of cooling and the onset of core damage)
Start of release to environment (hr: min) (no containment holdup time assumed for maximum release)	Tsd + 3hr	T_{sd} + 8hr
Containment leak rate to environment (% vol)	1.0 %/ hr	1.0 %/ hr
Core recovered /Core damage stops (core damage state remains the same) (hr: min)	T_{sd} + 3 hr +10 hr	T_{sd} + 8 hr +10 hr
Sprays off (hr: min)	During core uncover time	During core uncover time
Sprays on (hr: min)	During core recover time	During core recover time
Release height (m)	10 m (ground level)	
End of calculation/simulation (hr: min)	Start of release to environment +24 hr	Start of release to environment +24 hr

4.3.2 Radionuclides Release Characteristics of the Postulated Events

The RASCAL model evaluates the severity of core damage and the amount of fission products released, depending on the duration of time the reactor core is exposed without water coverage. Core inventory data, measured in curies per megawatt thermal (MWt), is sourced from NUREG-1940 (Ramsdell et al., 2012) and used in RASCAL's source term calculations. These values come from the SAS2H control module of the SCALE (Standardized Computer Analyses for Licensing Evaluation) code, Version 4.4a. For LBLOCA scenarios in PWRs, RASCAL follows the accident sequences and release schedules outlined in Table 3.6 of NUREG-1465 (Soffer et

* Article published from this thesis

al., 1995). In the RASCAL for LTSBO events, the source of radioactive releases were modeled from NUREG-1935 (Chang et al., 2012) along with accident progression information based on MELCOR. This includes radioactive release fractions and timing for 11 groups of radionuclides.

Volatile fission products, such as iodine (I), cesium (Cs), tellurium (Te), and noble gases like krypton (Kr) and xenon (Xe), play a significant role in radioactive releases (US NRC, 1982b). **Figure 4-5 (a & b)** shows the time-dependent release profiles for four important radionuclides—Xe-133, I-131, Cs-137, and Te-132—over a 10-hour period for both LBLOCA and LTSBO scenarios. According to the LTSBO event timing outlined in **Table 4-10**, the reactor was shut down five hours before the LBLOCA event, with both LBLOCA and LTSBO releases beginning at 10:00 and ending at 20:00. In the LBLOCA event, the highest release of radionuclides occurs about three hours after the start of the discharge, while in the LTSBO scenario, the peak is reached in approximately two hours. LTSBO events result in higher release rates of iodine, cesium, and tellurium because a larger proportion of these radionuclides is released from the reactor core.

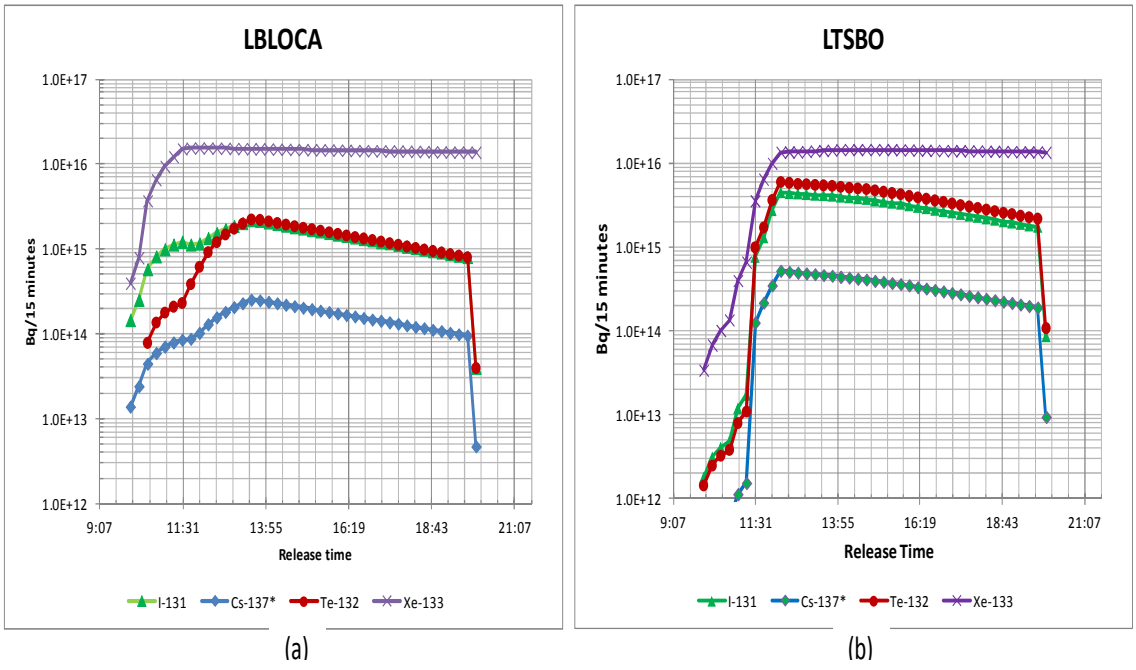

Figure 4-5: Time-dependent release rates from containment to the environment for (a) LBLOCA and (b) LTSBO (Faisal et al., 2025*).

* Article published from this thesis

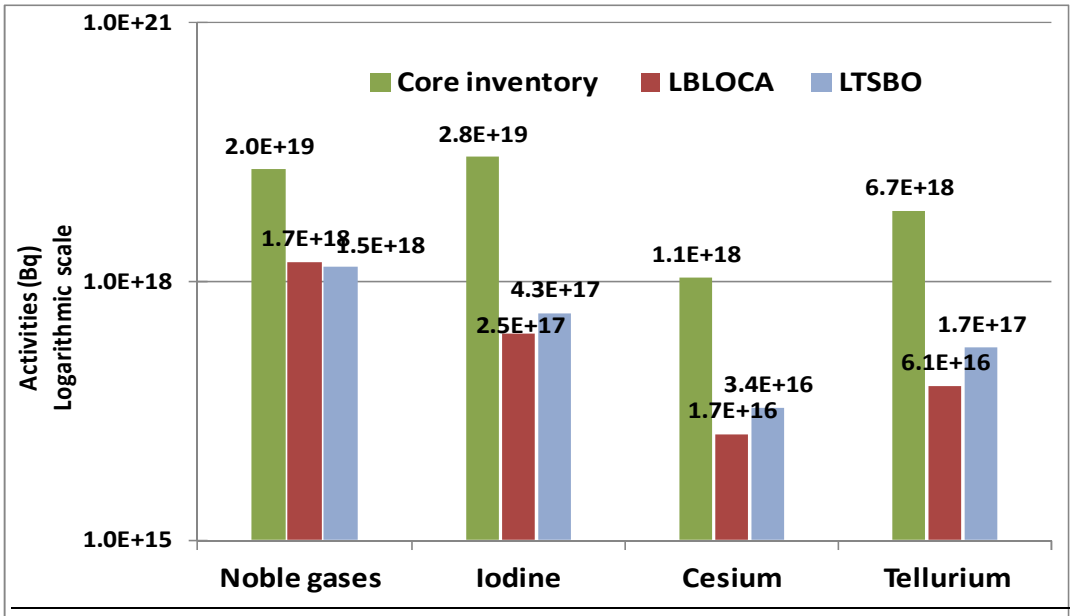

Environment release percentage of their core inventory

Radionuclide's	Noble gases (Kr,Xe)	Iodine	Cesium	Tellurium	Total
LBLOCA	8.9%	0.9%	1.5%	0.9%	3.60%
LTSBO	7.8%	1.6%	3.0%	2.6%	3.88%

Figure 4-6: Total volatile fission product released activities to the environment and their percentage to core inventories during LBLOCA and LTSBO events (Faisal et al., 2025*).

Figure 4-6 illustrates the initial core inventory of four volatile radionuclides and their corresponding environmental release levels for both LBLOCA and LTSBO scenarios. The results indicate that LTSBO events lead to higher releases of iodine, cesium, and tellurium compared to LBLOCA events, while noble gas releases are slightly lower (Faisal et al., 2025*). This variation is attributed to the larger core release fractions assumed for these radionuclides during LTSBO conditions (Ramsdell et al., 2015).

Table 4-11 presents a comparison of the environmental release activities (Bq) for key volatile radionuclides predicted by RASCAL for the two scenarios and those reported for the Fukushima Daiichi nuclear accident. The calculated releases for the Rooppur NPP show close agreement with values from the multi-unit Fukushima event, underscoring the conservative nature of the assumptions applied in this study.

* Article published from this thesis

Table 4-11: Released volatile radionuclides comparative activities for LBLOCA and LTSBO postulated events with the Fukushima accident (Faisal et al., 2025*).

Radionuclides	Activity (Bq)		
	Postulated events (Rooppur NPP)		Fukushima Diachi accident (IAEA , 2015b ,Volume 4, Page 7)
	LBLOCA	LTSBO	
Xe-133	1.2E+18	1.1E+18	6.0E+18 – 1.2E+19
Xe-135	3.4E+17	2.9E+17	-
Kr-85	5.3E+15	6.5E+15	6.4E+15–3.2E+16
I-131	5.3E+16	1.0E+17	1.0E+17 – 4.0E+17
I-132	6.8E+16	1.4E+17	-
I-133	8.4E+16	1.4E+17	6.8E+14–3.0E+17
I-134	9.7E+14	2.1E+13	-
I-135	4.7E+16	5.3E+16	-
Cs-134	8.3E+15	1.7E+16	8.3E+15 – 5.0E+16
Cs-136	3.3E+15	5.1E+15	-
Cs-137	5.8E+15	1.2E+16	7.0E+15 – 2.0E+16
Cs-138	5.3E+13	6.1E+10	-
Te-127	3.3E+15	9.8E+15	-
Te-127m	5.2E+14	1.6E+15	-
Te-129	1.5E+15	4.3E+15	-
Te-129m	2.2E+15	6.5E+15	3.3E+15 – 1.2E+16
Te-131	1.3E+15	3.5E+15	-
Te-131m	5.8E+15	1.6E+16	-
Te-132	4.6E+16	1.3E+17	7.6E+14 – 1.6E+17

4.3.3 Weather Scenarios for EPZ at the Rooppur NPP Site

The weather scenarios discussed in Section 3.2.3 were used in the LBLOCA and LTSBO event simulations for EPZ size estimation.

4.3.4 Protective Measures Dose Reduction Factors and Reference Dose Level

Table 4-12 presents the dose reduction factors applied to account for different protective measures during an emergency. When implemented, these measures decrease cloud shine exposure, inhalation CEDE, ground shine from deposited radionuclides, and acute inhalation doses to the red bone marrow. The adjusted dose values represent the actual radiation doses individuals would receive under each protective action (Faisal et al., 2025*).

* Article published from this thesis

House sheltering assumes occupants remain inside a wooden structure, while large-building sheltering refers to staying within a multi-story building during and after the release. Iodine Thyroid Blocking (ITB) involves taking a blocking agent prior to, or within one to two hours of, inhaling radioactive iodine to reduce thyroid exposure (IAEA, 2013b).

Table 4-12: Dose reduction factor for different protective measures (Faisal et al., 2025*).

Protective measure	Dose Reduction Factor	Exposure pathway
House sheltering	0.4 (Burson, 1975)	External exposure to ground deposition
	0.6 (US NRC, 2010)	External exposure to a radioactive cloud
	0.5 (US NRC, 2010)	Internal exposure from inhalation
Large building sheltering	0.02 (US NRC, 2010)	External exposure to ground deposition
	0.3 (US NRC, 2010)	External exposure to a radioactive cloud
	0.2 (US NRC, 2010)	Internal exposure from inhalation
Taking ITB agent	0.1 (US NRC, 2010)	Thyroid and fetal dose from inhalation of radioiodine

The GSR Part 3 (IAEA, 2014), GSR Part 7 (IAEA, 2015), and NNREPR (MOST, 2020) suggested a reference dose level that should be applied to utilize protective measures in emergency exposure scenarios to assure that the public dose is less than the chosen reference level. This dose level is expressed as a residual dose, usually an effective dose in the range of 20-100 mSv, acute or annual, which includes dose contributions from all exposure pathways. It represents the cumulative dose that is expected to be received by an individual from the start of the event up until the protective measures have been lifted (or following the decision not to take protective measures). A 20-100 mSv per year reference dose level is adopted by the NNREPRP for an emergency phase (MOST, 2020).

4.3.5 Dosimetric Criteria for PAZ and UPZ Sizes

Table 4-13 presents the IAEA dosimetric criteria used to define the sizes of the PAZ and UPZ. These criteria are based on threshold doses intended to prevent significant deterministic health effects and substantially reduce the probability of stochastic effects. The thresholds are applied to critical organs, such as the red bone marrow, and sensitive groups, including fetuses of pregnant women (IAEA, 2013b). For the red bone marrow, the total acute dose is calculated as the sum of cloud shine exposure, ground shine dose over the specified duration (one day for

* Article published from this thesis

PAZ assessment), and acute inhalation dose.

The RBE-weighted absorbed dose (Gy) to the fetus (AD_{fetus}) is equal in numerical terms to the equivalent dose (Sv) in the fetus (H_{fetus}), assuming RBE_{fetus}=1 for internal exposure to the fetal thyroid (IAEA, 2013b). In $AD_{fetus,\ inh}$, only the inhalation exposure pathway is considered (IAEA, 2013b). The RASCAL thyroid CDE represents a 50-year committed dose to an adult man, encompassing contributions from all radionuclides. Radioiodines with short half-lives are the primary source of thyroid dose, making the thyroid CDE comparable to acute thyroid dose. Thyroid CDE in RASCAL was utilized to assess $AD_{fetus,inh}$ and $H_{fetus,inh}$ when a pregnant woman was house-sheltered. Radiation doses were calculated using the ICRP-60 dose conversion factor.

Table 4-13: IAEA dosimetric criteria for the EPZ size (IAEA, 2013b, Faisal et al., 2025*).

Zone	Actions are taken based on plant conditions to prevent	Dosimetric quantity	Dose criterion	Considered exposure pathways		
PAZ	Severe deterministic effects	Average RBE-weighted absorbed dose to red bone marrow ($AD_{red\ bonemarrow}$)[a]	1 Gy[d]	Inhalation	Cloud shine	Ground shine[g]
		RBE weighted absorbed dose to the fetus from inhalation ($AD_{fetus,inh}$) [b]	1 Gy[e]	Inhalation		
UPZ	Stochastic effects	Equivalent dose to the fetus from inhalation by the pregnant woman ($H_{fetus,inh}$) [b,c]	100 mSv[f]	Inhalation		
		Committed effective dose from inhalation (E_{inh})	100 mSv[f]	Inhalation		

a. Internal tissues or organs i.e. red bone marrow are exposed to a uniform field of strongly penetrating radiation.
b. Dominated by the dose to the fetal thyroid.
c. The equivalent dose to an adult from inhalation is approximately equal to the equivalent dose to the fetal thyroid.
d. If the dose is kept below this threshold, no severe deterministic effects, such as permanently decreased sperm or ovulation rates, will result from external exposure to the whole body.
e. Above this, higher probability of severe mental retardation for the fetus.
f. Criteria at which, if projected, protective measures and other response actions are to be taken to reduce the risk of stochastic effects.
g. 1-day exposure from the beginning of the release

* Article published from this thesis

4.4 PART- C: Consequences Analysis during Routine Operation

This part describes the methodology to simulate dispersion for routine operation of the Rooppur NPP using the HYSPLIT model and to quantify air concentrations (Bq/m³) and ground depositions (Bq/m²) from routine gaseous radioactive discharges and assess their potential impact on public annual doses. For this purpose, HYSPLIT-compatible 3-Dimensional meteorological datasets of CDC1 and GDAS1 were used for dispersion modeling.

4.4.1 HYSPLIT Simulation Configuration for Routine Operation

4.4.1.1 Computational Domain

Figure 4-7 shows the study's computational domain, covering Bangladesh and nearby areas of neighboring countries. The domain extends about 10° in both longitude (west to east) and latitude (south to north), with the Rooppur NPP (24.07°N, 89.10°E) positioned at the center (Faisal & Islam, 2025*).

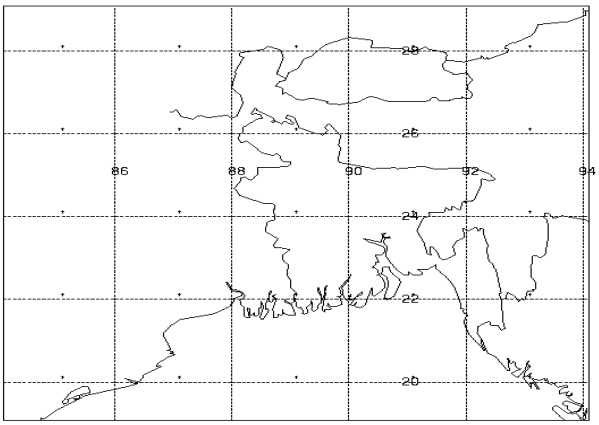

Figure 4-7: Model domains mapping (generated from NOAA ARL server) HYSPLIT simulation for Routine operation (Faisal & Islam, 2025*).

4.4.1.2 Simulation Run Time and Concentration Grid Setting

Table 4-14 outlines the HYSPLIT dispersion model settings used in this study to simulate routine operational releases. Monthly simulations were run for 672, 720, or 744 hours using CDC1 and GDAS1 meteorological data, while year-long simulations covered 8,759 hours for 2021–2023 and 8,783 hours for 2020. For the annual runs, twelve monthly CDC1 files were

* Article published from this thesis

required, whereas the GDAS1 dataset needed sixty weekly files. Because the HYSPLIT graphical user interface limits the number of input files that can be used, only the CDC1 dataset was applied in the year-long simulations. In all cases, the release began at the first hour of the first day of the relevant month or year. Dispersion was simulated within a 500 km radius of the release point over a 10° × 10° horizontal grid. The model considered two vertical levels, at ground level (0 m) and 100 m above ground level. Air concentrations were averaged at 100 m, while ground deposition was evaluated at the surface (Faisal & Islam, 2025*).

To keep the modeling approach straightforward, HYSPLIT was set up to simulate continuous releases using two representative radionuclides, treated as surrogate pollutants: a generic particulate radionuclide (RNUC) and a non-depositing noble gas (NGas). Both were released at a unit rate of 1 Bq/hr, and the results were later scaled during post-processing to reflect the actual release rates. All emissions were assumed to come from a single stack at a height of 100 m, located at 24.07°N and 89.1°E at the Rooppur NPP-1 site. Sensitivity analyses showed that using a concentration grid of 0.05° × 0.05° (about 5 km × 5 km) together with a three-dimensional particle mode provided a good balance between computational efficiency, accuracy, and smooth spatial patterns of air concentration and ground deposition. Based on this, around 403, 417, or 447 particles were released each hour for the monthly simulations, depending on the month, while about 114 particles per hour were used for the year-long continuous release simulations (Faisal & Islam, 2025*).

Table 4-14: Input parameters for routine operation release in HYSPLIT Simulation (Faisal & Islam, 2025*).

Parameter	Month-wise simulation	Year-wise simulation
Meteorology Data source:	a) Global Reanalysis (CDC1) b) GDAS1 (1-degree, Global, 2006 - present) (NOAA)	Global Reanalysis (CDC1)
Met. Data year:	2021, 2022	2020, 2021, 2022, 2023
Start of simulation:	From First day of each months of the years at 00:00	From First day of each year at 00:00
Simulation run time:	Whole months 744 hr/720 hr/ 672 hr(Feb) depends on month	Whole years 8759 hr/8783 hr(2020) depends on year
End of simulation:	Last day of each month 24:00	Last day of each year at 23:00
Release starting	From First day of each months at	From First day of each year at

* Article published from this thesis

time (UTC):	00:00	00:00
Release height:	100 m (Above Ground Level)	100 m (Above Ground Level)
Release rate:	1Bq/hr	1Bq/hr
Release duration:	744 hr/720 hr/ 672 hr (Feb) depends on month	8759 hr/8783 hr (2020) depends on year
Top of averaged layer:	100 m	100 m
Number of release particles per cycle:	300000	1000000
Number of release particles per hour:	~ 403/417/447 depends on month	~114
Grid span:	10degree × 10 degree	10degree × 10 degree
Concentration grid resolution:	$0.05^{o} \times 0.05^{o}$	$0.05^{o} \times 0.05^{o}$
Sampling interval:	744 hr/720 hr/ 672 hr (Feb) depends on month	8759 hr/8783 hr (2020) depends on year

4.4.1.3 Deposition Parameter Setup

The deposition parameter described in Section 4.2.7.5 was used in the routine operation simulations. During routine operations, NPPs can release small amounts of radionuclides. Some, like the noble gases krypton-85 and xenon-133, do not deposit, while others, such as iodine-131 and cesium-137, have moderate dry deposition velocities of around 0.001–0.01 m/s. For routine release scenarios, a dry deposition velocity of 0.001 m/s is typically used as a median estimate, especially for small particles and semi-volatile substances released over long-term and low-level (Faisal & Islam, 2025*).

4.4.2 Annual Routine Operational Release Activities

Table 4-15 presents a list of radionuclides annually released under routine operation of the VVER-1200 reactor of Rooppur power plant units 1 and 2, as given by PSAR (Environmental Impact Assessment, 2017).

Table 4-15: Annual Routine operation release activities (Environmental Impact Assessment, 2017) (Faisal & Islam, 2025*).

Radionuclides	Annual release Activity (Bq)	Radionuclides	Annual release Activity (Bq)	Radionuclides	Annual release Activity (Bq)	Radionuclides	Annual release Activity (Bq)
^{85m}Kr	1.04E+12	$^{131}I_{aerosol}$	4.30E+07	$^{131}I_{molecular}$	5.15E+07	$^{131}I_{organic}$	7.11E+07

* Article published from this thesis

^{85}Kr	3.08E+09	$^{132}I_{aerosol}$	1.10E+08	$^{132}I_{molecular}$	1.31E+08	$^{132}_{organic}$	1.81E+08
^{87}Kr	1.08E+12	$^{133}I_{aerosol}$	1.06E+08	$^{133}I_{molecular}$	1.27E+08	$^{133}I_{organic}$	1.75E+08
^{88}Kr	2.73E+12	$^{134}I_{aerosol}$	5.70E+07	$^{134}I_{molecular}$	6.82E+07	$^{134}I_{organic}$	9.41E+07
^{133}Xe	1.43E+13	$^{135}I_{aerosol}$	3.36E+07	$^{135}I_{molecular}$	4.01E+07	$^{135}I_{organic}$	5.54E+07
^{135}Xe	1.44E+12	^{138}Xe	5.50E+11	^{134}Cs	9.27E+06	^{137}Cs	1.31E+07

4.4.3 Dose Calculations in HYSPLIT

Radiation exposure generally occurs in two ways: internal and external. Internal exposure happens through inhalation or ingestion, while external exposure comes from cloudshine and groundshine radiation. In this study, the ingestion pathway is not included, as accurately estimating it would require detailed information on population habits and food consumption, which is often difficult to obtain. As a result, only external exposure pathways are considered. Cumulative doses are calculated using air concentrations (cloudshine) and ground deposition (groundshine) of radioactive materials. To keep the assessment conservative, factors like whether people are indoors or outdoors and the shielding effect of buildings are not accounted for (Faisal & Islam, 2025*).

In HYSPLIT, the CON2REM program processes the unit release concentration output file. Using the ACTIVITY.TXT file and specified switches, CON2REM generates a dose file. During post-processing, the program extracts air concentration values at specific sampling times and multiplies them by the corresponding dose conversion factors to calculate doses for individual radionuclides (Draxler et al., 2019). Summing the contributions from all radionuclides provides the total dose from cloud-shine and ground-shine.

APPENDIX H (**Figure H-3**) presents the ACTIVITY.TXT file used in this study, listing the radionuclides included in the dose calculations. The file contains several columns: the first lists radionuclide half-lives, while the next four specify the maximum emission rates (Bq/hr) for each radionuclide during routine operational releases from the VVER-1200 reactor at the Rooppur NPP site. The final two columns provide dose conversion factors for cloud-shine and ground-shine, which are used to compute radiation doses. These conversion factors were obtained from the Radiological Toolbox (US NRC, 2013b) and based on FGR-12 (Eckerman & Ryman, 1993).

* Article published from this thesis

CHAPTER 5.
RESULTS AND DISCUSSIONS

5.1 PART- A: Consequences Analysis of LTSBO events

5.1.1 LTSBO Cases Source Term and Corresponding INES Accident Level

In LTSBO scenarios, RASCAL generates approximately fifty radionuclides for PCM and sixty for CCM accidents at the VVER-1200 reactor. In HotSpot, six radionuclide mixtures were created based on the RASCAL source terms for each accident case. Due to limitations in HotSpot radionuclide mixtures, not all radionuclides from RASCAL are included. To make a mixture, up to 50 radionuclides can be added (Homann & Aluzzi, 2020), some less significant radionuclides being excluded. **Table 5-1** lists important radionuclides and their I-131 equivalent activity. Each released radionuclide activity (Ai) must be associated to I-131 equivalent activities by multiplying it by an I-131 radiological equivalence factor (Fi). To determine the INES accident level, the acquired I-131equivalence activities for each scenario are added up as (Ai*Fi) (IAEA, 2013a). These I-131 equivalence activities (several tens of thousands of TBq) indicate that the considered 4 LTSBO accident scenarios are graded as the highest INES level of 7, which is termed a major accident (IAEA, 2013a). The highest total I-131 equivalence activity is 1.27E+17 Bq for CCM_7c, the worst-case scenario. Cases CCM_6a and CCM_6b are classified as CCM at INES Level 6. Despite a 10-hr core uncovering in Cases CCM_6a and CCM_6b, the accident level remains at Level 6 due to the low leak rates in CCM_6a and radionuclide confinement within the containment for 24 hr in CCM_6b, allowing short half-life radionuclides to decay. The differences in radionuclide activities between the PCM and the CCM are due to varying accident severities, including core uncovering time, passive ECCS availability, and containment leakage rates.

Noble gases and iodine are the main contributors to released activities in all accident scenarios. The noble gas to I-131 ratio is crucial for understanding dose projections and guiding protective actions, as I-131 significantly impacts thyroid dose (Athey et al., 2013). Cases CCM_6a and CCM_7c show comparatively higher I-131 releases, with a ratio of 16:1, compared to a 79:1 ratio in PCM_7a and PCM_7b, which could influence protective actions

based on thyroid dose. This lower ratio is due to a higher iodine release fraction of 90% after 10 hr, compared to 80% after 3 hr in PWR LTSBO scenarios, according to Figure 2-1 of Nuclear Regulatory Commission Regulation (NUREG)-1940 Supplement 1 (Ramsdell et al., 2015). However, if the radionuclides are confined for a day in containment, as in CCM_6b, iodine can plate out or wash out, where I-131 contributes only 1%. This increases the noble gas to iodine ratio, making TEDE the primary factor in determining protective actions instead of the thyroid CDE dose.

For the two PCM and CCM accidental scenarios, **Figure 5-1** displays the activities of the released radionuclide ranked by contributing dose potential (TEDE) during plume passage (0-day). Among the more than fifty radionuclides in the source terms, only 19 and 28 significantly contribute to the total dose fraction in PCM and CCM scenarios, respectively. The remaining radionuclides in the source term have negligible impact on the overall dose. As illustrated in **Figure 5-1(a),** the activity of most radionuclides decreases as the passive ECCS continues to operate over 24 hours, with the exception of Cs-137, Cs-134, Ru-106, Te-127m, and Sr-90. These five radionuclides show minimal change in activity due to their relatively long half-lives—30 years, 2.062 years, 368.2 days, 109 days, and 29.12 years, respectively—compared to the delay time between reactor shutdown and release (Faisal et al., 2023*). In the CCM state, due to the long time of 10 hr uncovering the reactor core and based on the release timing for a PWR LTSBO accident of Figure 2.6, some rare earth metals like La, Ce, Cm, Pu, Np, and Sb are released.

* Article published from this thesis

Table 5-1: Radiologically important released radionuclides activities and their I-131 Equivalence activities with corresponding INES for six LTSBO accident scenarios.

Core Melt State		Partial Core Melt (42.85%)						Complete Core Melt (100%)					
Case Scenario		**PCM_7a (No_ECCS_ No Containment hold)**		**PCM_7b (No_ECCS_ No Containment hold)**		**PCM_7c (24hr_ECCS_No Containment hold)**		**CCM_6a (No_ECCS No Containment hold)**		**CCM_6b (No_ECCS_ 24 hr Containment hold)**		**CCM_7c (No_ECCS_ No Containment hold)**	
Radionuclide	Radiological Equivalence to I-131, Fi	Activity, A(Bq)	I-131 Equivalence Activity [A*F] (Bq)	Activity, A(Bq)	I-131 Equivalence Activity [A*F] (Bq)	Activity, A(Bq)	I-131 Equivalence Activity [A*F] (Bq)	Activity, A(Bq)	I-131 Equivalence Activity [A*F] (Bq)	Activity, A(Bq)	I-131 Equivalence Activity [A*F] (Bq)	Activity, A(Bq)	I-131 Equivalence Activity [A*F] (Bq)
Sr-90	20	1.11E+12	2.22E+13	1.11E+12	2.22E+13	1.11E+12	2.22E+13	3.40E+12	6.81E+13	-	-	5.18E+13	1.04E+15
Mo-99	0.08	9.62E+14	7.70E+13	9.62E+14	7.70E+13	7.40E+14	5.92E+13	3.26E+14	2.60E+13	1.67E+14	1.33E+13	4.81E+15	3.85E+14
Ru-106	6	1.89E+13	1.13E+14	1.89E+13	1.13E+14	1.89E+13	1.13E+14	1.22E+13	7.33E+13	9.62E+12	5.77E+13	1.81E+14	1.09E+15
I-131	1	2.29E+15	2.29E+15	2.29E+15	2.29E+15	2.15E+15	2.15E+15	8.88E+14	8.88E+14	5.55E+14	5.55E+14	1.30E+16	1.30E+16
Te-132	0.3	3.03E+15	9.10E+14	3.03E+15	9.10E+14	2.44E+15	7.33E+14	1.15E+15	3.44E+14	6.29E+14	1.89E+14	1.70E+16	5.11E+15
Xe-133	0	1.4E+17	-	1.41E+17	-	1.26E+17	-	1.1E+16	-	1.1E+16	-	1.6E+17	-
Cs-134	17	4.07E	6.92E	4.07E	6.92E	4.07E	6.92E+	1.44E	2.45E	9.25E	1.57E	2.15E	3.65E

		+14	+15	+14	+15	+14	15	+14	+15	+13	+15	+15	+16
Cs-137	40	2.85E +14	1.14E +16	2.85E +14	1.14E +16	2.85E +14	1.14E+ 16	9.99E +13	4.00E +15	6.66E +13	2.66E +15	1.48E +15	5.92E +16
Total			2.20E +16		2.20E +16		2.16E+ 16		8.53E +15		5.05E +15		1.27E +17
INES		Level 7		Level 7		Level 7		Level 6		Level 6		Level 7	
Released Radionuclides contributions		Noble gas -91% Iodine-5.2% Others-3.7%		Noble gas -91% Iodine -5.2% Others-3.7%		Noble gas -92% Iodine -4.2% Others-3.8%		Noble gas -67% Iodine -18% Others-15%		Noble gas - 97.9% Iodine-1% Others-1.2%		Noble gas - 66.8% Iodine-18.1% Others-15.1%	
Noble gas/I-131		79:1		79:1		65:1		16:1		296:1		16:1	
I & Cs fraction to core inventory (%)		0.04		0.04		0.025		0.013		0.006		0.28	

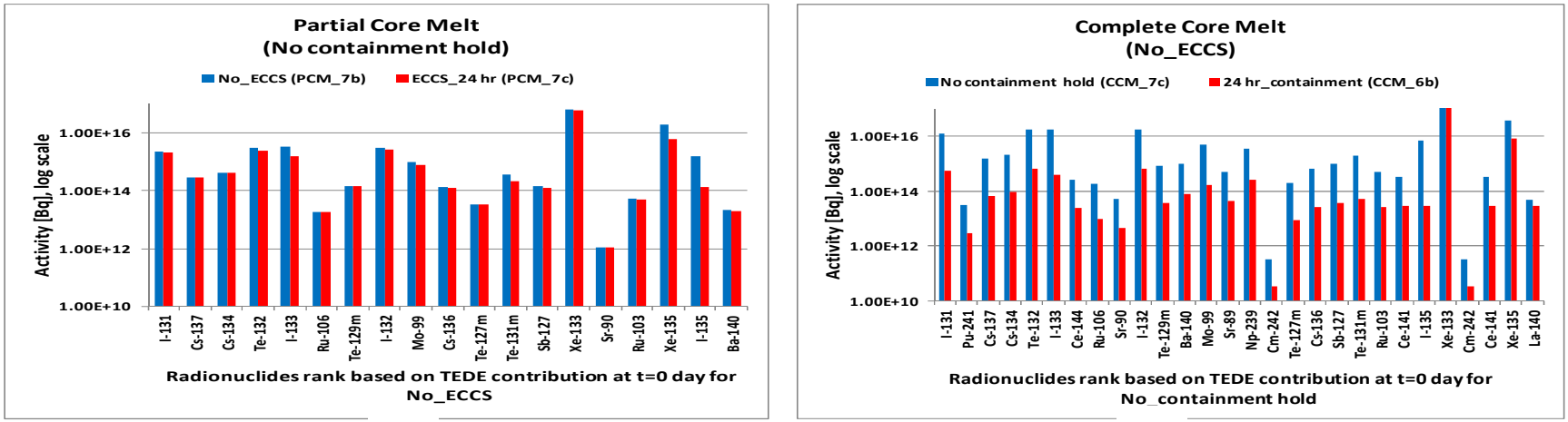

Figure 5-1: Comparative environment released radionuclides activities for (a) PCM and (b) CCM state in different LTSBO cases.

5.1.2 Release Characteristic of LTSBO event

Figure 5-2 illustrates the estimated total release of radionuclide activities at the end of the RASCAL simulation. About 0.1% and 0.25% of the reactor core inventory are released into the environment for PCM and CCM scenarios, respectively. After 3 hours for PCM and 10 hours for CCM, the reactor core begins to recovered. A substantial portion of activity, on the order of 10^{18} Bq, remains trapped within the containment. The activity levels in the reactor core, containment, and environment decrease as the passive safety ECCS continues to function over a 24-hour period.

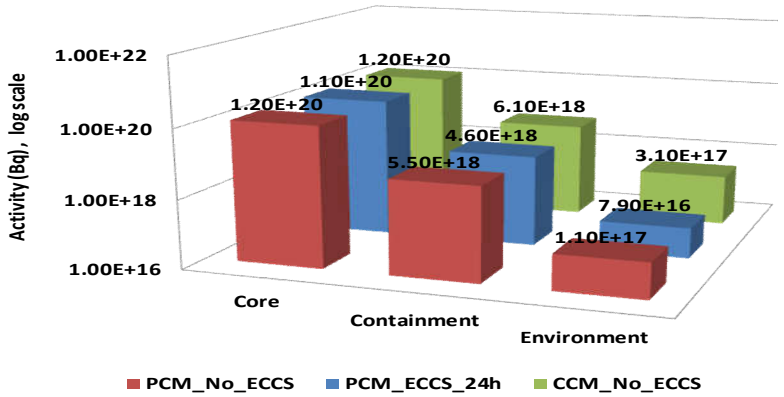

Figure 5-2: Core, Containment and Environment activities at end of the simulation for PCM and CCM state in different LTSBO scenarios.

Figure 5-3 illustrates the time-dependent release rates of the five radionuclides contributing most to TEDE. For PCM, releases occur from 10:00 to 13:00, while for CCM, they continue until 20:00. Among all radionuclides, I-131, I-132, I-133, and Te-132 exhibit the highest release rates for both PCM and CCM scenarios. This is attributed to the relatively high core release fractions of iodine and cesium groups during the LTSBO-PWR event, as shown in **Figure 3-1**.

In both PCM and CCM, the release rate rises rapidly after approximately two hours (around 12:15), reaching peak values. I-133 and I-132 record the highest release rates in PCM and CCM, respectively, under conditions without ECCS. As the passive safety ECCS continues to operate over 24 hours, the release rates decline significantly. For PCM, the reduction continues steadily until around 12:45, and for CCM until about 19:45. A sharp drop is observed at 13:00 for PCM and 20:00 for CCM, corresponding to core recovery and the ending of radionuclide release.

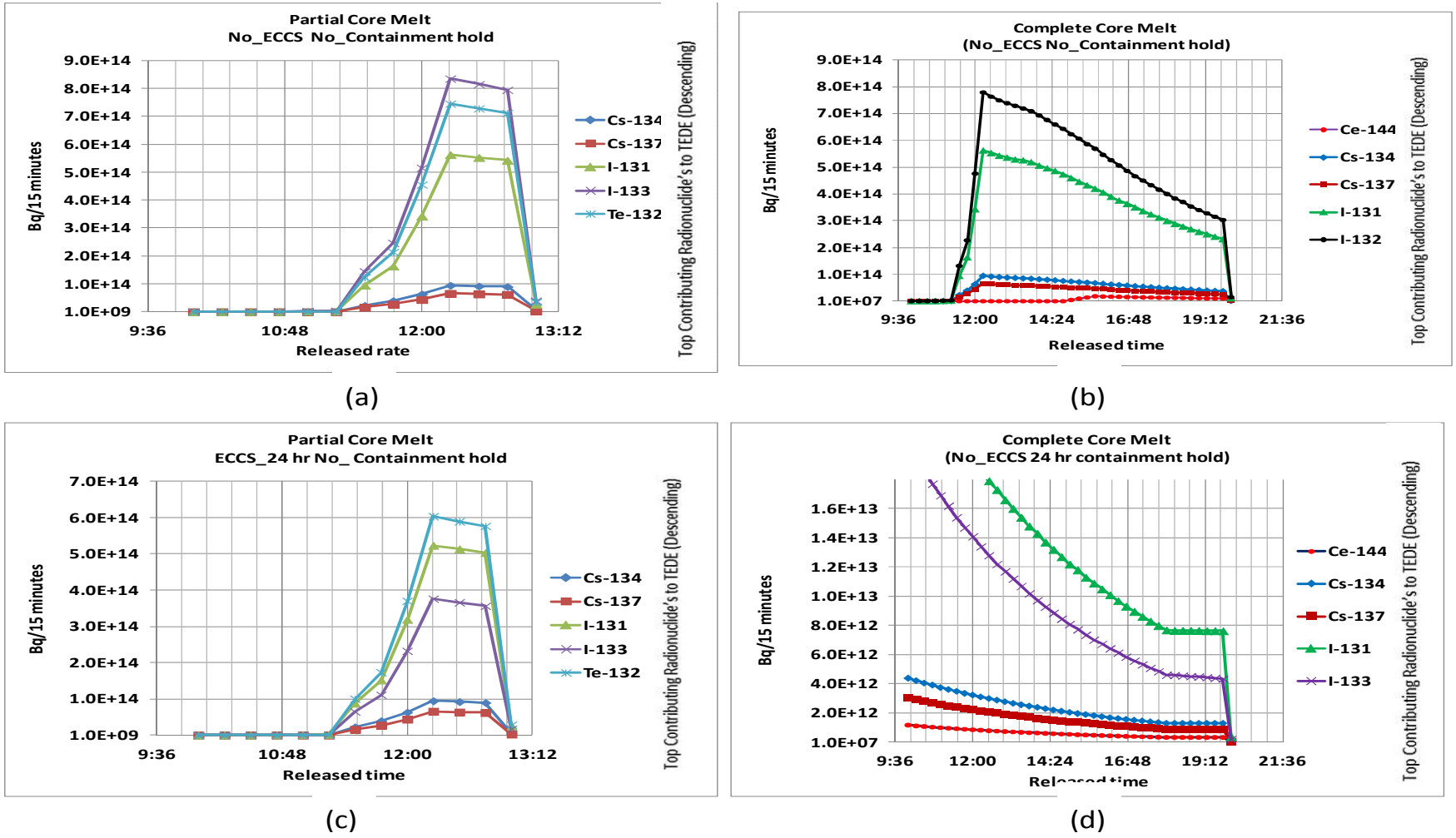

Figure 5-3: Activity release rate to the environment for top 05 contributing radionuclide to TEDE for (a & c) PCM and (b & d) CCM state in different LTSBO cases.

5.1.3 Relative Importance of Pathways and Radionuclide's contribution to TEDE

Figure 5-4 shows the variation in TEDE contributions through three exposure pathways at different post-accident decay times near the release point for both PCM and CCM scenarios. During plume passage (day 0), inhalation is the predominant pathway, accounting for approximately 98% of the total dose potential in PCM, while submersion contributes about 1.8%, and groundshine remains negligible. The dominance of inhalation is primarily due to the significant presence of I-131, which contributes about 47% at day 0, as illustrated in **Figure 5-8(a).** In contrast, isotopes such as Xe-133 and Xe-135, which mainly contribute to submersion, represent only about 1% of the dose, resulting in a smaller submersion pathway contribution.

After the plume passage, groundshine from deposited radionuclide activity becomes the primary contributor to TEDE. For PCM, the groundshine fraction rises to approximately 0.95 at 1 day, 0.95 at 7 days, 0.99 at 30 days, and reaches 1.0 by 183 days. During these later periods, inhalation plays a secondary role, while submersion remains negligible.

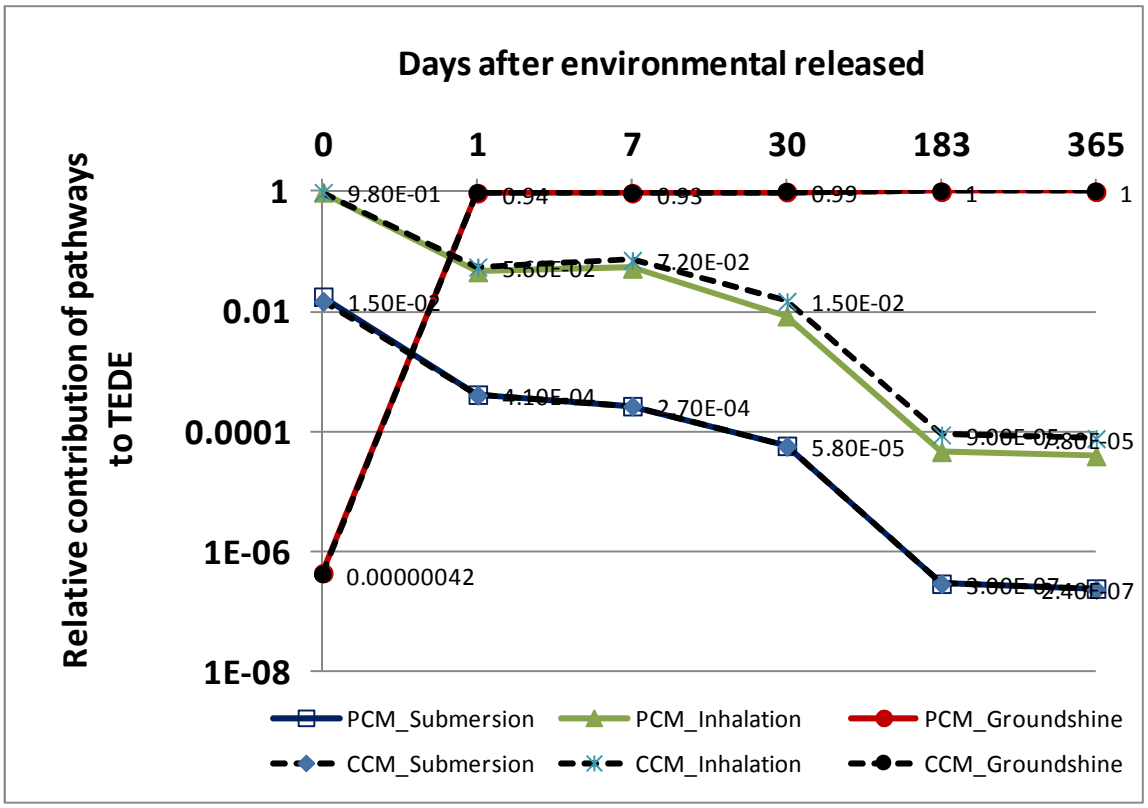

Figure 5-4: Three dose pathways contributions to TEDE for PCM and CCM in LTSBO at different post-accident decay times.

Calculating radionuclide importance helps identify which radionuclides contribute the most to the overall dose. **Figure 5-5(a & b)** shows the contributing released radionuclides and their cumulative involvement in TEDE dose potential, respectively, for PCM and CCM states in each of two accident cases with comparative contribution during plume passage (t=0 day). The y-axis represents the cumulative fraction of the dose potential contributed by a given radionuclide, along with all preceding radionuclides ranked as more significant. The most contributing radionuclide is I-131 in both states, while the second most contributors are Cs-137 for PCM and Pu-241 for CCM.

The contributing released radionuclides, their time delay effects for one day, seven days, thirty days, 183 days, and 365 days, as well as the cumulative involvement to TEDE dose potential for PCM and CCM states, are displayed in **Figure 5-6(a & b).** After a day, I-132 is the radionuclide that contributes the most in both states. It makes up 70% of the TEDE dose for PCM when combined with I-131, Te-132, and Cs-134, whereas in the case of CCM, these four nuclides contribute 64%. After 7 days, Cs-134, Cs-136, and Cs-137 contribute 65 percent of TEDE during the PCM state, while for the CCM state, the same contribution comes from Cs-14, Cs-137, and I-131. After 365 days, above 98 percent contribution comes from Cs-137 for both PCM and CCM states.

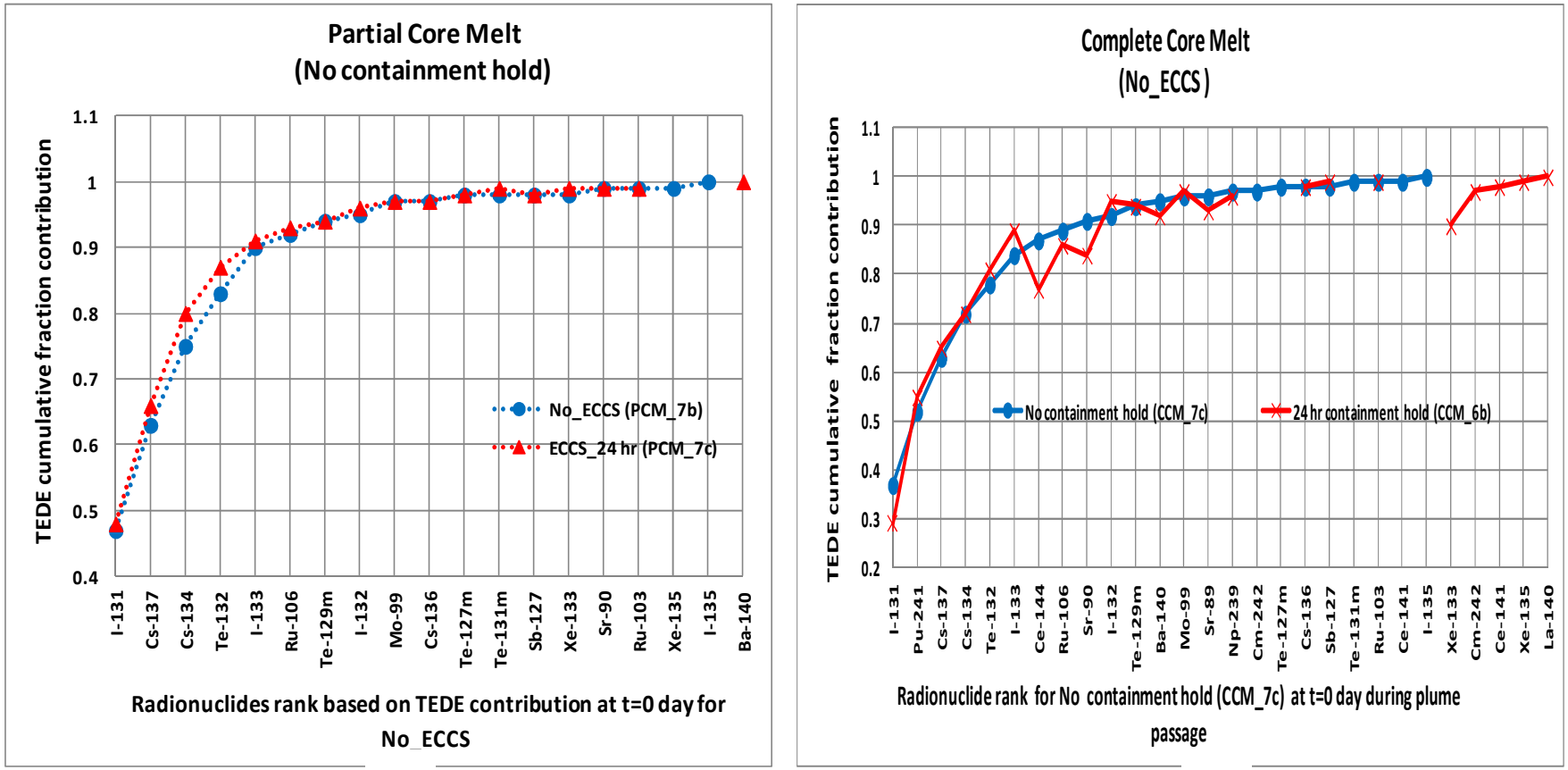

Figure: 5-5: Cumulative Radionuclides contribution to TEDE for (a) PCM and (b) CCM states in different LTSBO cases during plume passage (t= 0-day).

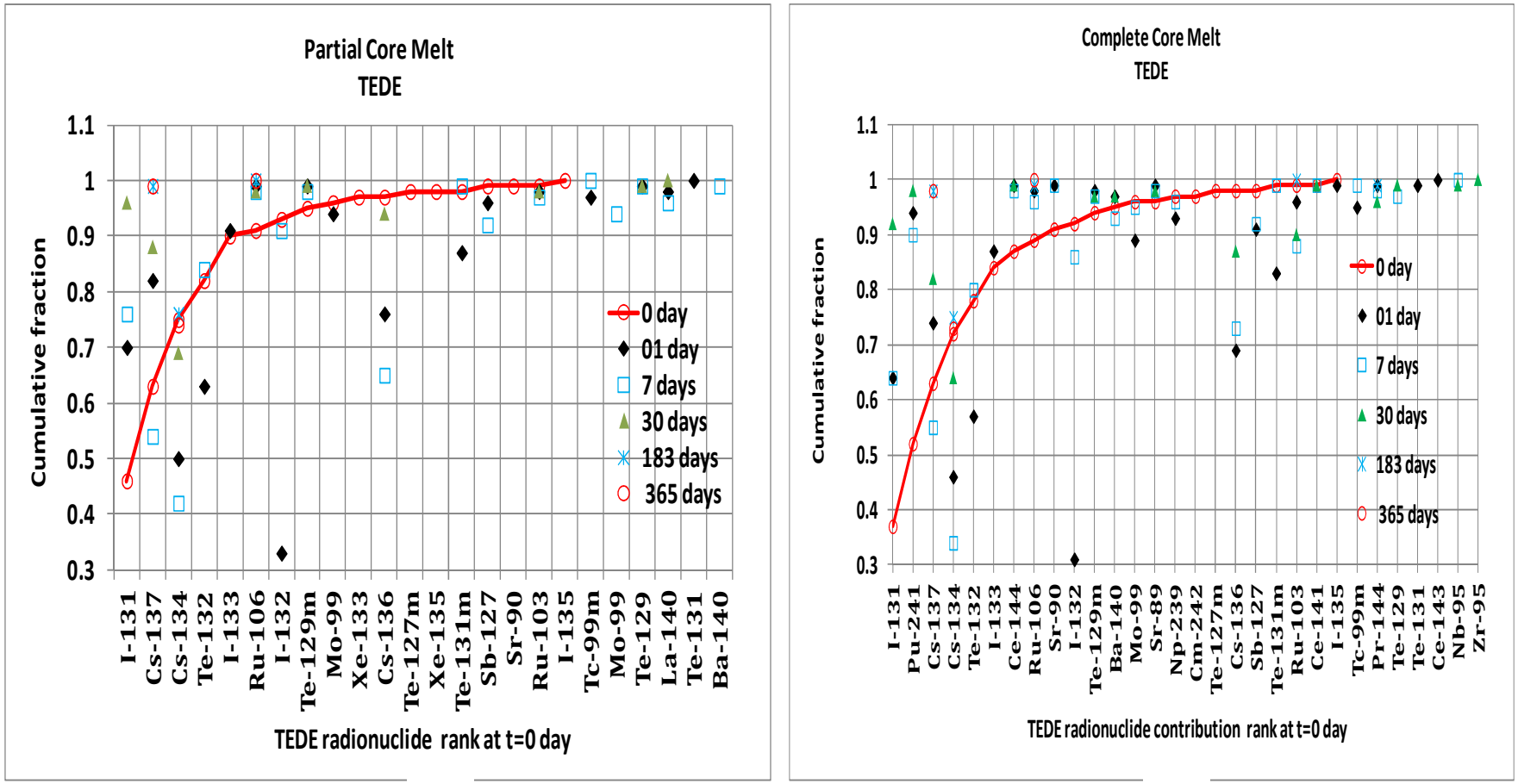

Figure 5-6: Cumulative radionuclide contribution to TEDE from (a) PCM and (b) CCM states in LTSBO at varying post-accident delay times.

5.1.4 Radionuclides contribution to Submersion, Inhalation, Groundshine and Ingestion Dose

The effects of radionuclide time delay are assessed using a reference importance diagram. In this diagram, red represents submersion and inhalation at day 0, while black corresponds to groundshine at day 1, as shown in **Figures 5-7, 5-8, and 5-9** respectively. The results highlight two key observations common to all three dose pathways. First, the radionuclides with the highest importance vary depending on the pathway. For instance, **Figure 5-7** shows that at day 0, I-132 is the primary contributor to submersion (48%), whereas **Figure 5-8** indicates that I-131 dominates inhalation (49%) in the PCM state. The second notable trend across these diagrams is that the number of radionuclides contributing significantly to dose potential decreases as delay time increases. **In Figure 5-9**, at day 1 in PCM, the top 10 radionuclides account for 96% of the dose potential. By day 183, only two radionuclides—Cs-134 and Cs-137—contribute 99% of the groundshine dose. Short-lived radionuclides decay over time, while radionuclide decay and in-growth processes alter the dominant contributors to inhalation and groundshine doses at later stages.

In the CCM state, radionuclides with varying contribution fractions, along with additional radionuclides such as Np, Ba, Sr, and Ce, contribute to the submersion dose beyond those observed in the PCM state. Similarly, Pu, Np, Cm, Ce, La, and Am provide additional contributions to inhalation doses during CCM. For groundshine, **Figure 5-9** shows that at day 1, I-132 accounts for the highest contribution (33%), and while by day 7, Cs-134 dominates with 45% in the PCM scenario. In the CCM state, radionuclides such as Np, Pr, Sr, Ce, Nb, and Zr, along with those from PCM, further contribute to the groundshine dose with varying fractions. **Figure 5-10** highlights the radionuclides that contribute most significantly to ingestion doses through the food pathway. As the time delay increases, the number of contributing radionuclides decreases. By 365 days, only three radionuclides—Cs-134, Cs-137, and Sr-90—remain as major contributors to ingestion doses (Faisal et al., 2023*). However, because RASCAL 4.3 does not account for variations in dose coefficients or food consumption patterns across different age groups, there is some uncertainty in the ingestion importance analysis (Ramsdell et al., 2015).

* Article published from this thesis

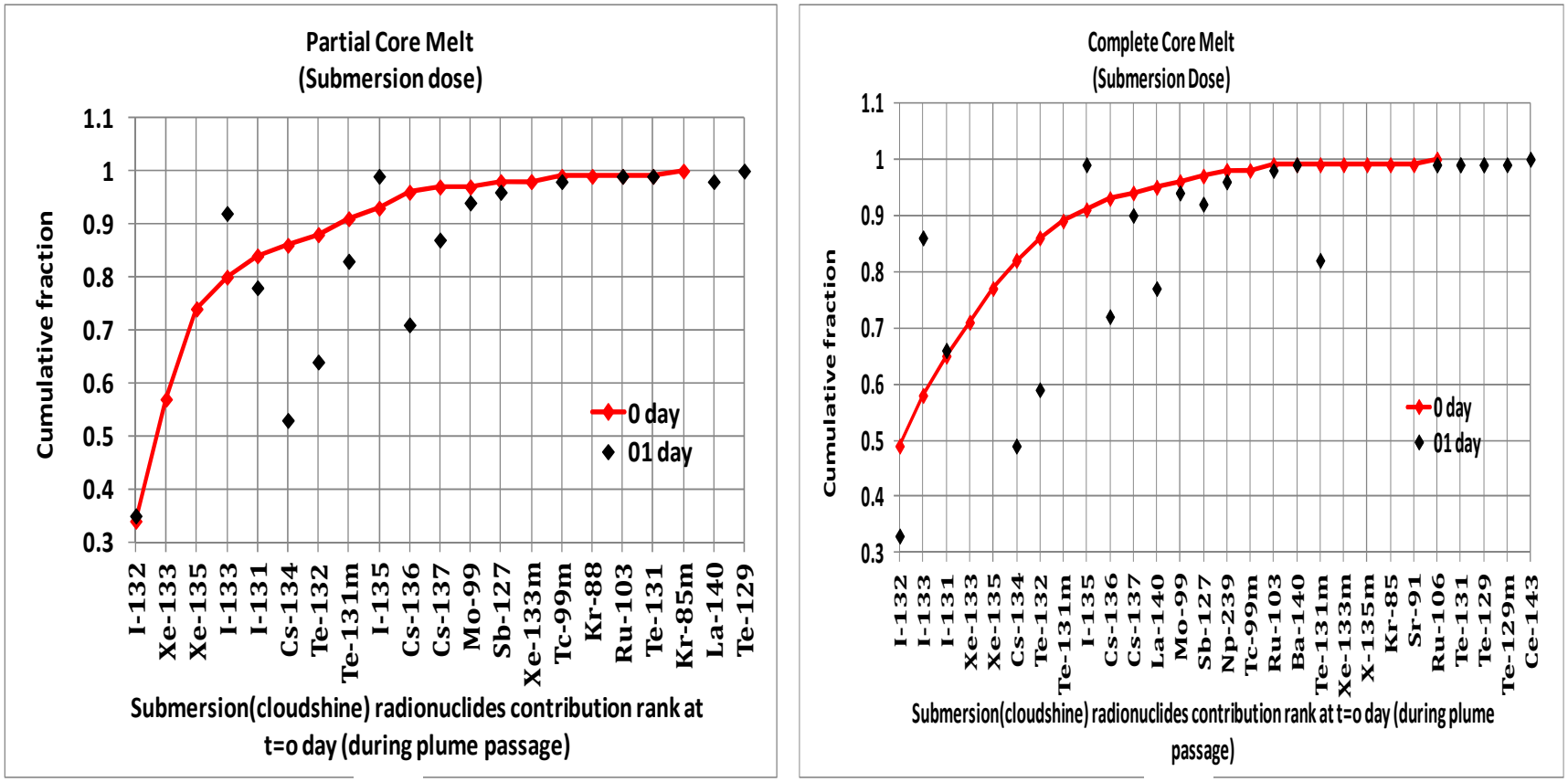

(a) (b)

Figure 5-7: Cumulative radionuclides contribution for Submersion dose from (a) PCM and (b) CCM states in LTSBO during plume passage and first day of post-accident.

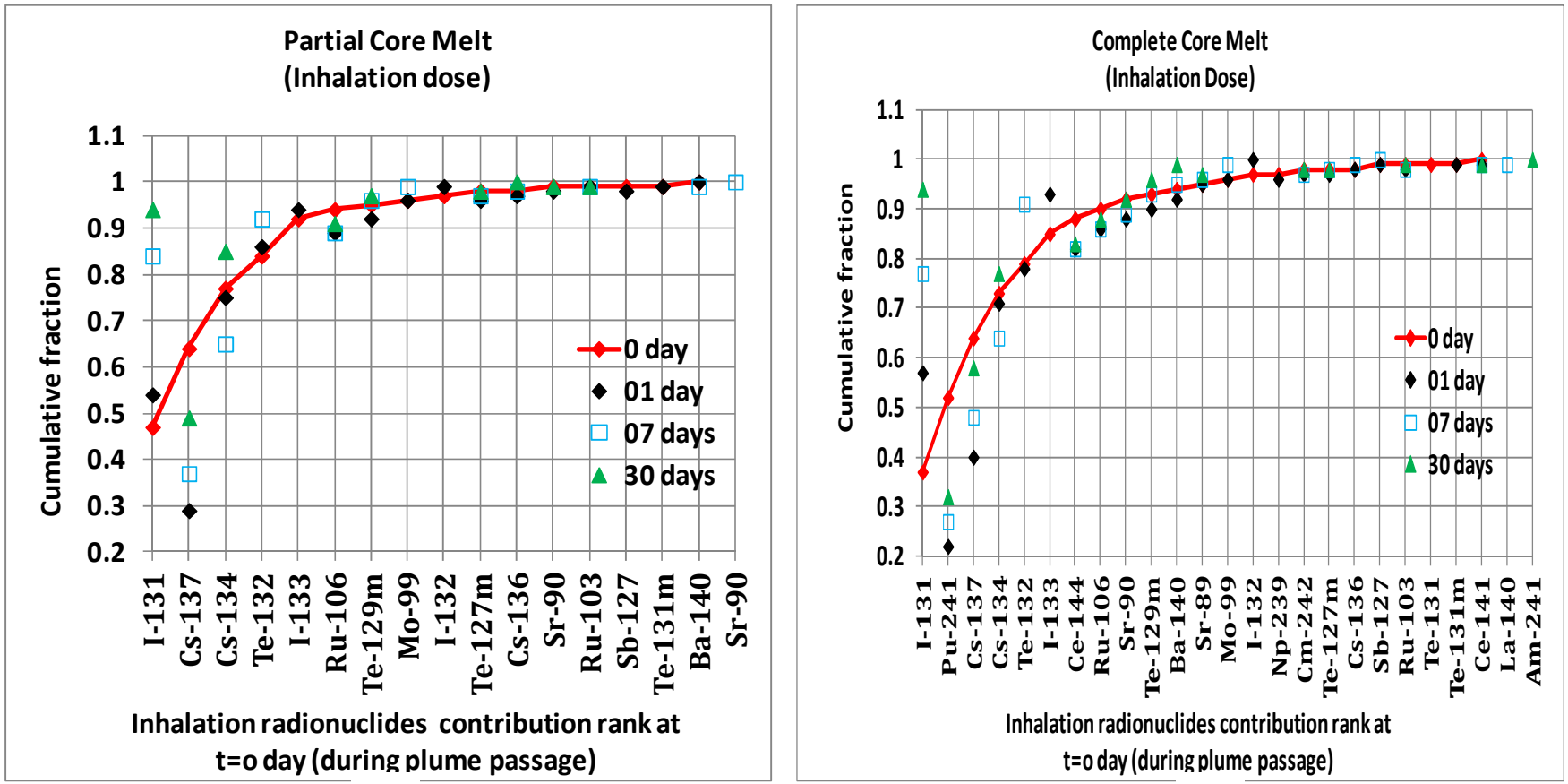

Figure 5-8: Cumulative radionuclide contribution Inhalation dose from (a) PCM and (b) CCM states in LTSBO at varying post-accident delay times.

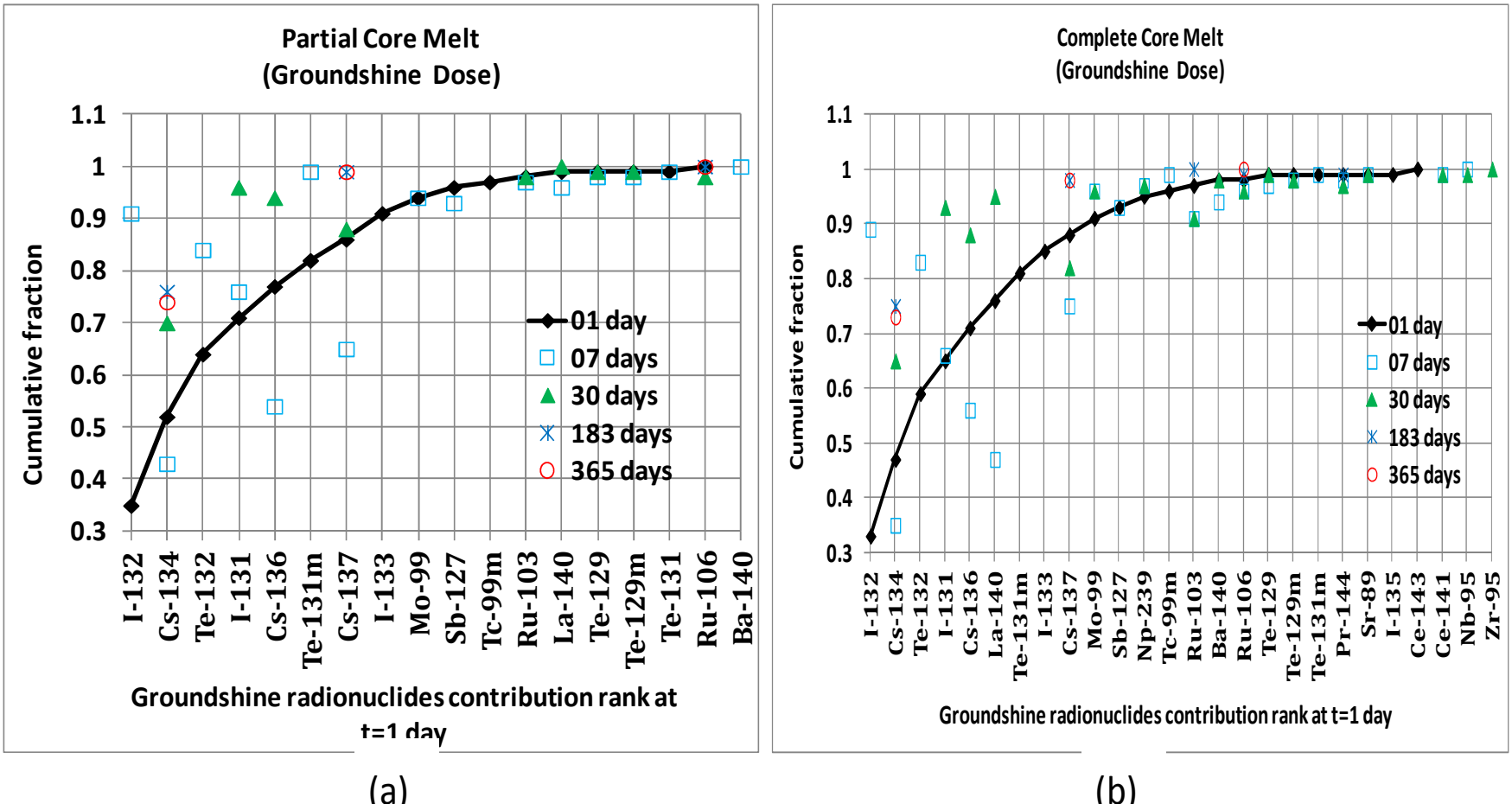

Figure 5-9: Cumulative radionuclide contribution groundshine from (a) PCM and (a) CCM states in LTSBO at varying post-accident delay times.

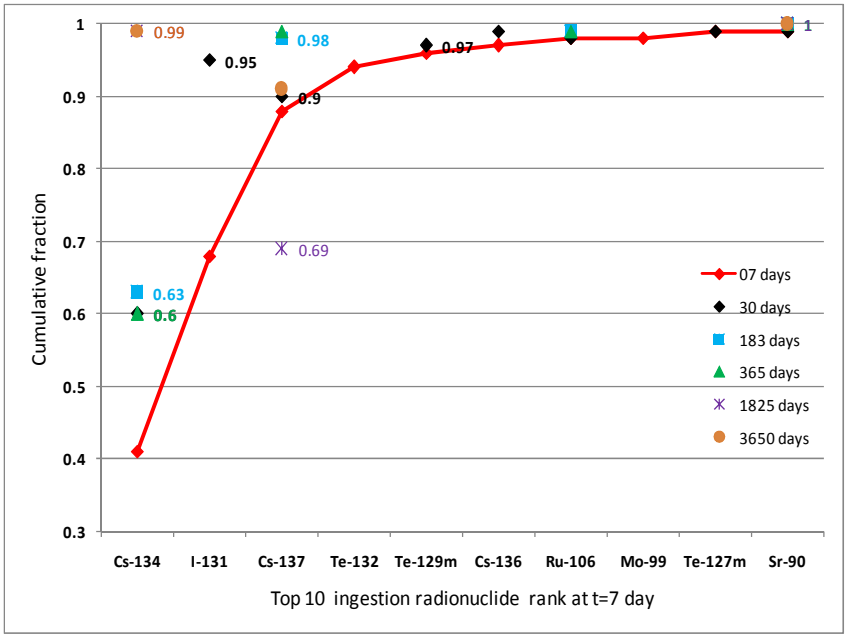

Figure 5-10: Cumulative radionuclide contribution Ingestion dose from PCM state in LTSBO at varying post-accident delay times.

5.1.5 Weather Scenarios Effects

5.1.5.1 Weather Scenario Bound for Different Stability Classes

For the worst-case scenarios of CCM_7c, **Figure 5-11** shows the exceeded distance limits of the threshold 4-day exposure TEDE calculated from RASCAL based on EPA PAG criteria. It shows the necessary distances for the various stability classes 'B,' 'C,' 'D,' 'E,' and 'F' of 360 weather scenarios where sheltering-in-place or evacuation is required when projected doses reach 10 mSv or 50 mSv. The black color legend indicates wet weather, while the other colors indicate dry weather. Unstable conditions 'B' and 'C,' often caused by solar heating, enhance horizontal and vertical mixing and speed up dispersion, dilution, and shorter travel distances for threshold dosages (Hanna et al., 1982). While stable conditions 'E' and 'F' retain plumes closer to the ground with less dilution, allowing for longer transit. Low wind speeds and temperature inversions, which limit vertical mixing and allow contaminants to spread horizontally over longer distances for threshold dosages, are characteristics of the 'E' and 'F' classes.

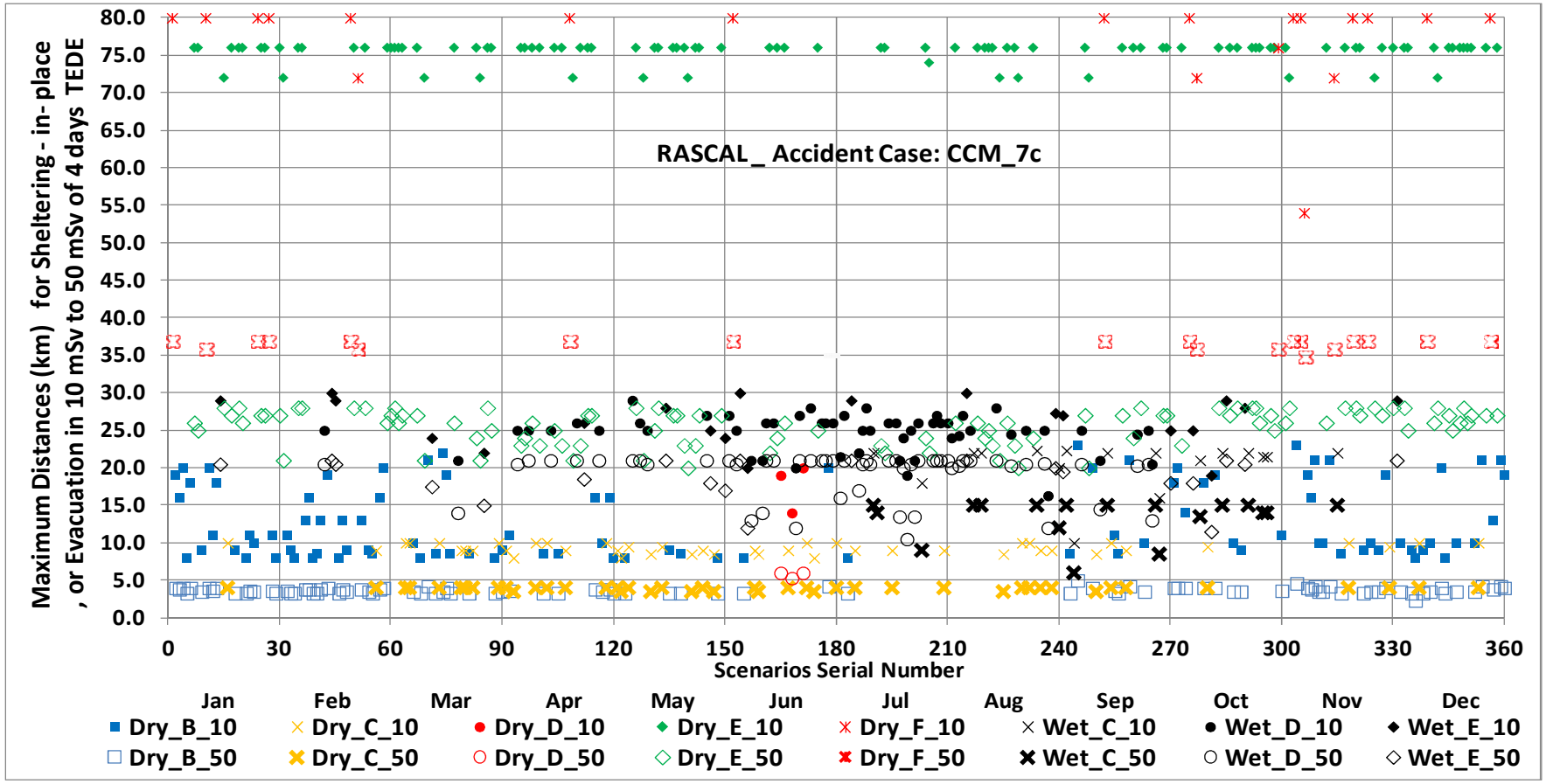

Figure 5-11: Month-wise 360 weather scenarios distance limits for sheltering or evacuation based on 4-day TEDE (10–50 mSv) PAG criteria during worst-case in LTSBO.

Table 5-2 summarizes the yearly weather scenarios at the Rooppur site for different stability classes, based on the 10 mSv EPA PAG criteria across 360 scenarios, as shown in **Figure 5-11**. It lists the upper and lower bounds of each stability class with the exceeded distance limits for a projected dose of 10 mSv, along with wind speeds, precipitation types and intensities.

Table 5-2: Weather scenarios bound in different Stability classes for Rooppur site.

Weather conditions / Stability class	Range	Distances bound from **Figure 5.11** (worst accident case)	Weather scenarios meteorological parameter			Weather scenarios percentage contribution
			Release time	Wind speed (m/s)	Precipitation type & intensity	
Dry B	Upper bound	23 km	day	1.1	No	26.7%
	Lower bound	8 km	day	2.9	No	
Dry C	Upper bound	10 km	day	3.1	No	12.7%
	Lower bound	8 km	day	5.0	No	
Dry E	Upper bound	76 km	night	2.2	No	28.6%
	Lower bound	72 km	night	4.9	No	
Dry F	Upper bound	80 km	night	2.0	No	5.6%
	Lower bound	54 km	night	0.7	No	
Wet C	Upper bound	22.3 km	day	2.8	Light rain	4.7%
	Lower bound	10 km	day	1.0	Moderate Rain	
Wet D	Upper bound	29 km	night	5.5	Light rain (< 1 mm/h)	15%
	Lower bound	16.3 km	day	3.8	Heavy rain	
Wet E	Upper bound	30 km	night	3	Light rain (< 1 mm/h)	5.6%
	Lower bound	19 km	night	2.1	Moderate Rain (1 - 5 mm/h)	

5.1.5.2 Weather Effects in Pathways Contributions to 4-day exposure TEDE

Figure 5-12 represents the TEDE contribution for the three dose pathways—cloudshine, inhalation, and groundshine—for four stability class weather scenarios of the Rooppur site. This evaluation is performed at six distances (0.5 km and 1-5 km) from the release point of the site. For dry weather conditions, 'B' & 'E' and in wet weather, 'D' & 'E' stability classes were considered. In dry weather, 72-75% of doses are derived from inhalation, while groundshine accounts for 24-26%, and cloudshine contributes the remaining 1-2%. Both accident scenarios of the PCM and CCM cases exhibit similar behavior during the PCM phase, although there is a slight variation in the contribution of pathways during the wet weather 'D' and 'E' conditions of the CCM scenario.

Under wet weather conditions, groundshine accounts for the majority of the dose contribution (70–92%). This occurs because precipitation removes particulates from the plume, resulting in substantial ground deposition of radioactive material and consequently higher groundshine doses. Inhalation contributes the remaining 8–30%, while cloudshine has an insignificant impact. These percentage distributions show slight variation with increasing distance from the release point. During wet weather, the contribution of groundshine, as illustrated in **Figure 5-12(c & d)**, particularly in 'D' class, gradually increases with the increasing distance downwind for both PCM and CCM states. When the plume moves, precipitation during wet weather depletes the plume, resulting in lower concentrations downwind. Additionally, at greater distances, precipitation reduces the levels of cloudshine, groundshine, and inhalation doses (Ramsdell et al., 2012).

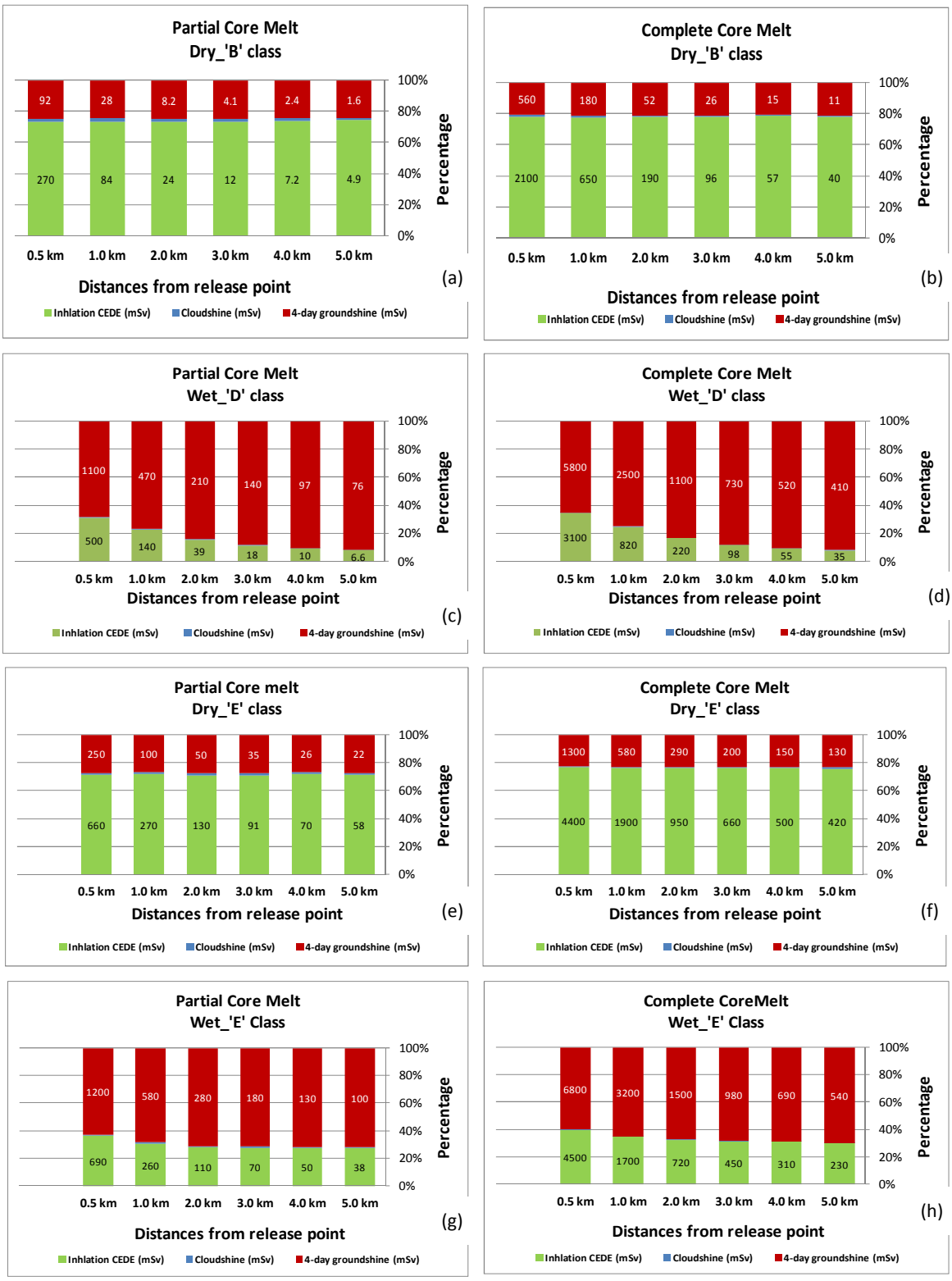

Figure 5-12: Three pathway contributions to TEDE for different stability classes (a & b) dry 'B' (c & d) wet 'D' (e & f) dry 'E' (g & h) wet 'E' in (a, c, e, g) PCM and (b, d, f, h) CCM states of LTSBO.

5.1.5.3 Weather Effects in Surface Concentration

Figure 5-13 illustrates the downwind spatial variation of deposited surface concentrations under dry and wet weather conditions, considering different stability classes for PCM and CCM scenarios. These values represent the highest total surface concentration recorded at each distance during the 24-hour deposition period. Along the plume path, surface concentration quickly rises to a peak at approximately 0.16 km before sharply declining. Under wet weather conditions, deposition levels are higher than in dry weather due to rain washing particulates from the plume, resulting in increased ground deposition.

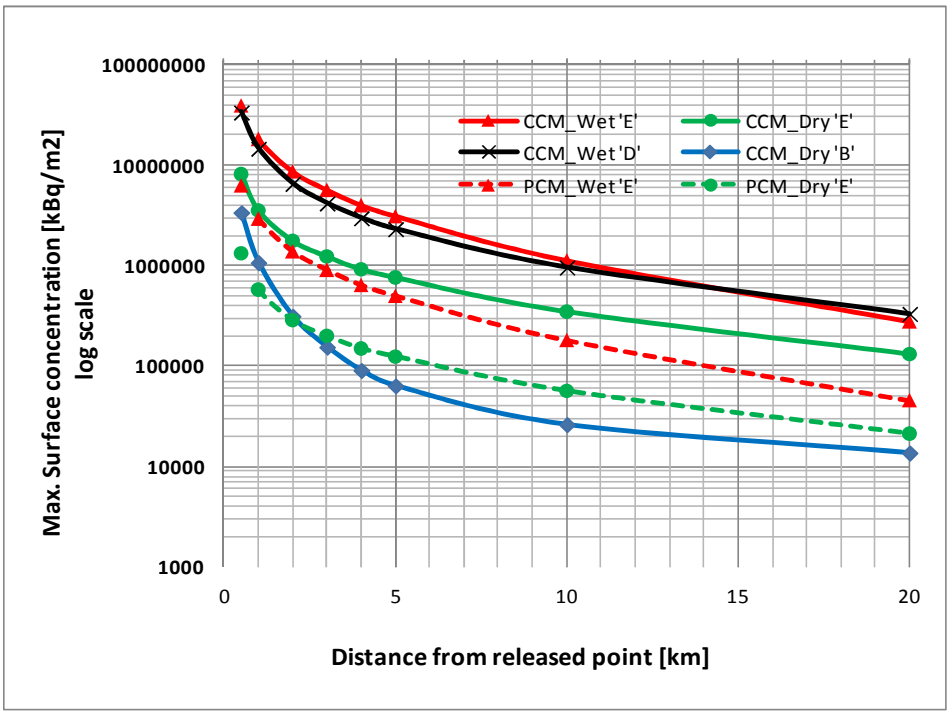

Figure 5-13: Spatial distribution of peak surface concentrations for PCM and CCM during LTSBO under dry and wet conditions of different stability classes.

Figure 5-14(a & b) presents the activities of the top ten radionuclides and their percentage contributions to surface concentrations under dry and wet weather conditions for the 'E' stability class in PCM and CCM scenarios. For PCM, the maximum total ground deposition is 2.05×10^6 kBq/m² in dry weather and 4.76×10^7 kBq/m² in wet weather, measured at 0.16 km from the release point. In dry weather, I-131 is the primary contributor at 21%, while in wet

weather its contribution decreases to 8%. Te-132 and I-133 also contribute significantly in dry conditions, whereas I-132 dominates in wet weather with 27%, followed by Te-132 (26%) and I-133 (3%). Contributions from other radionuclides remain similar across both weather conditions. Due to its short half-life of 8 days, I-131 decays from the ground after a few half-lives. Cs-137 contributes only 3–4%, indicating a minimal environmental impact at the Rooppur NPP site.

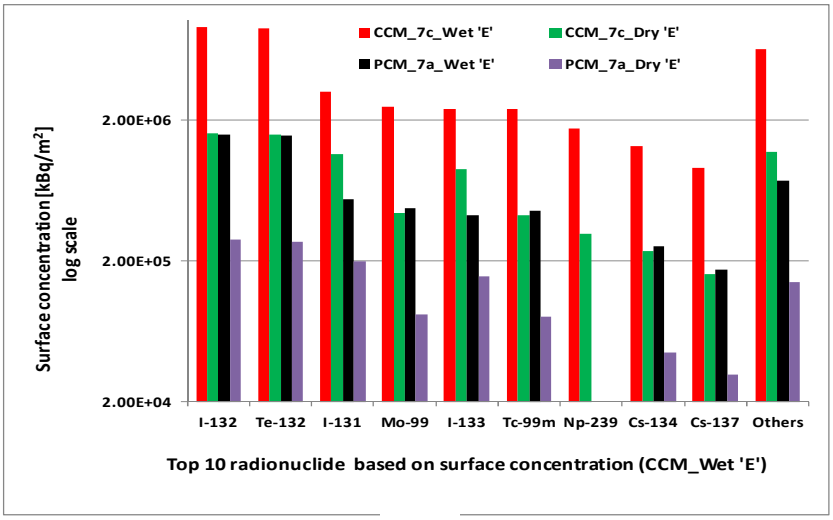

(a)

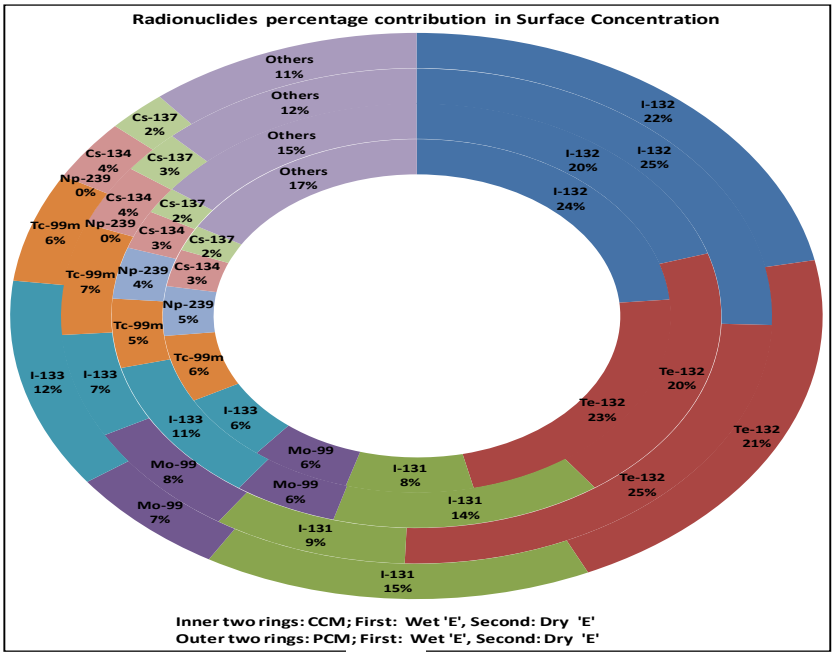

(b)

Figure 5-14: (a)Top-10 radionuclides contributing surface concentration and (b) Radionuclides percentage contributions to total surface concentration for PCM and CCM in LTSBO under dry and wet 'E' stability

Surface concentration footprints shown in Figure 5-15(a) and (b) illustrate the affected areas along the predefined 0^o downwind direction, with deposited ground concentration around the Rooppur NPP site under dry and wet weather conditions, respectively for the most severe accident scenario with the stability class 'E'. Under wet weather conditions, the plume affects a narrower region compared to dry conditions, with much higher concentrations near the release point.

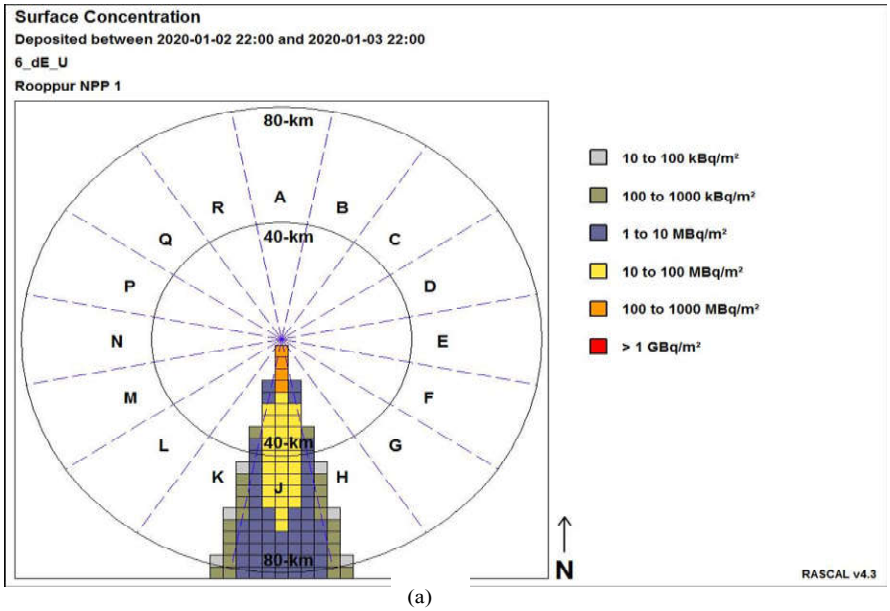

(a)

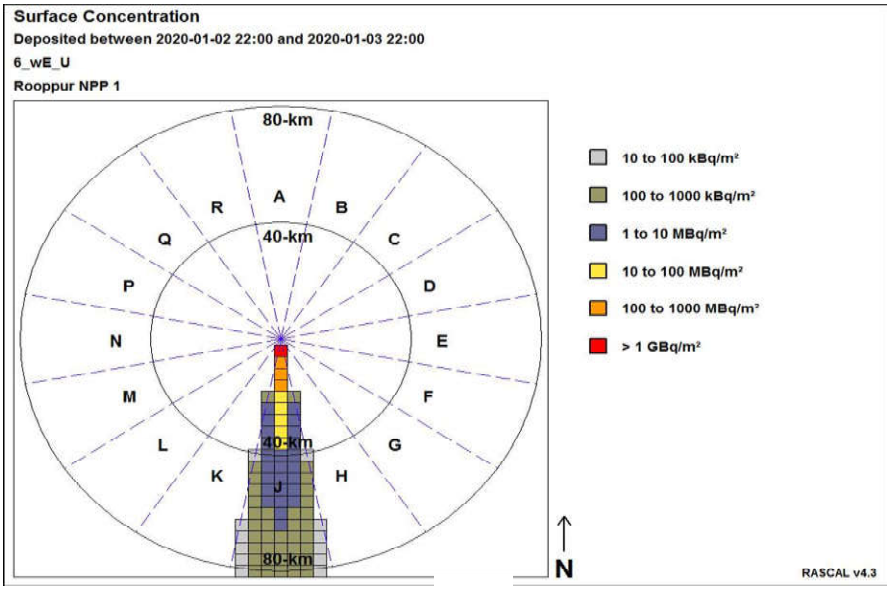

(b)

Figure 5-15: Surface concentration footprint for (a) dry weather and (b) wet weather of 'E'stability class of most severe accident scenario

5.1.6 Comparative Analysis of TEDE exposure in RASCAL and HotSpot

5.1.6.1 Four Days Exposure Distance vs. Dose in Different Accidental Cases and Weather Conditions

In RASCAL and HotSpot, the early-phase TEDE accounts for doses from cloudshine/submersion, inhalation CEDE, and groundshine accumulated during the first four days following the release. RASCAL assumes that individuals remain outdoors during the plume passage and throughout the subsequent four days to capture the contribution from groundshine due to deposited radionuclides. HotSpot also includes re-suspension doses. **Figure 5-16(a & b**) shows the spatial distribution of the dry and wet weather conditions' average 4-day exposure TEDE for RASCAL and HotSpot in six accident scenarios, focusing on the dominant weather scenario of stability class 'E' with uncertainty of the calculated RASCAL and HotSpot TEDE. The U.S. EPA's dose intervention levels (10-50 mSv) for sheltering-in-place or evacuation are indicated by blue dotted arrows. **Figure 5-16(c & d)** shows the normalized variation of the two codes, where distances corresponding to negative values indicate higher HotSpot-calculated values, while positive values indicate higher RASCAL-calculated values. Initially, HotSpot estimates a higher TEDE than RASCAL, but in dry weather, it declines more rapidly with distance (not shown in the Figure) due to the source-depletion factor incorporated in its calculations. This means the plume's radioactive concentration decreases more quickly with distance in HotSpot than in RASCAL, which uses a time-dependent model, leading to slower dose reduction.

For three PCM cases, the TEDE in RASCAL approached 1000 mSv. However, PCM_7c displayed relatively lower doses because of the 24-hour activation of passive ECCS, which decayed some radionuclides during this time after shutdown. Other than the radionuclide release height, which is 10 m in PCM_7a and 30 m in PCM_7b, the RASCAL input parameters in the two situations are identical. Because of the lower release height, PCM_7a exhibits a higher TEDE even though the same quantity of radionuclides is released in both scenarios. As the release height increases, radionuclides are affected by more diverse wind patterns, which results in wider spatial dispersion and a decrease in near-ground doses. On the other hand, due to the plume staying closer to the ground for a lower release height, it results in higher exposure to inhalation and deposition.

For CCM of case CCM_7c, the TEDE at 0.5 km was 5700 to 11000 mSv, but in CCM_6a, due to a small leak rate, and in CCM_6b, due to prolonged containment confinement, the TEDE was 500 to 700 mSv at 0.5 km. For both codes near the release point for the same stability class, the TEDE is higher in the wet season than in the dry season because precipitation and increased atmospheric moisture promote greater deposition of radioactive particles near the release site. Since the two codes make different assumptions about the distribution and intensity of precipitation, there are higher uncertainties during wet weather, which leads to uneven wet deposition rates. With its higher rain washout coefficient, HotSpot's doses decrease more rapidly than RASCAL's in wet conditions. HotSpot uses 2E-4 s^{-1} (~0.72 h^{-1}) (Homann & Aluzzi, 2020), which causes a faster drop in airborne radionuclide concentration than RASCAL, which uses a default value of 0.25 h^{-1}(Ramsdell et al., 2012) for light rain.

Figure 5-17(a & b) compares the dry and wet weather conditions average 4-day TEDE results from RASCAL and HotSpot, and **Figure 5-17 (c & d)** shows the normalized variation of the two codes for the worst-case scenario of CCM_7c under different upper-bound stability classes. More uncertainty was observed in stability classes 'E' and 'F' during dry weather, with TEDEs reaching roughly 5000 to 6000 mSv with RASCAL and 11000 mSv to 25000 mSv with HotSpot at 0.5 km. HotSpot's plume depletion factor (DF) has an impact on stable stability classes as distance rises, leading to lower concentration and subsequently lower dosages than RASCAL. Stable classes 'E' and 'F' had higher doses than unstable classes 'B' and 'C' due to less atmospheric vertical mixing; consequently, radionuclides trapped near the surface for extended times causeed higher concentrations near the source. On the other hand, due to moderate convective mixing caused by ground heating, vertical turbulence is relatively strong in stability classes ‘B’ and ‘C’, which dilutes the concentration of pollutants near the ground. In both RASCAL and HotSpot, wet conditions, where rainfall enhances the removal of airborne radionuclides, lead to increased groundshine. As a result, TEDEs are higher in wet conditions than in dry conditions within the same stability classes, depending on the balance between reduced airborne exposure (inhalation and cloudshine doses) and increased surface exposure (groundshine). Particularly in wet conditions and at distances above 20 km, where RASCAL transitions from a plume dispersion model to a puff model, the TEDE estimations of the two codes are different. The two codes use different dispersion models, which causes this discrepancy. Moreover, the varying wet deposition coefficients employed by RASCAL and HotSpot increase the degree of uncertainty in dosage estimates.

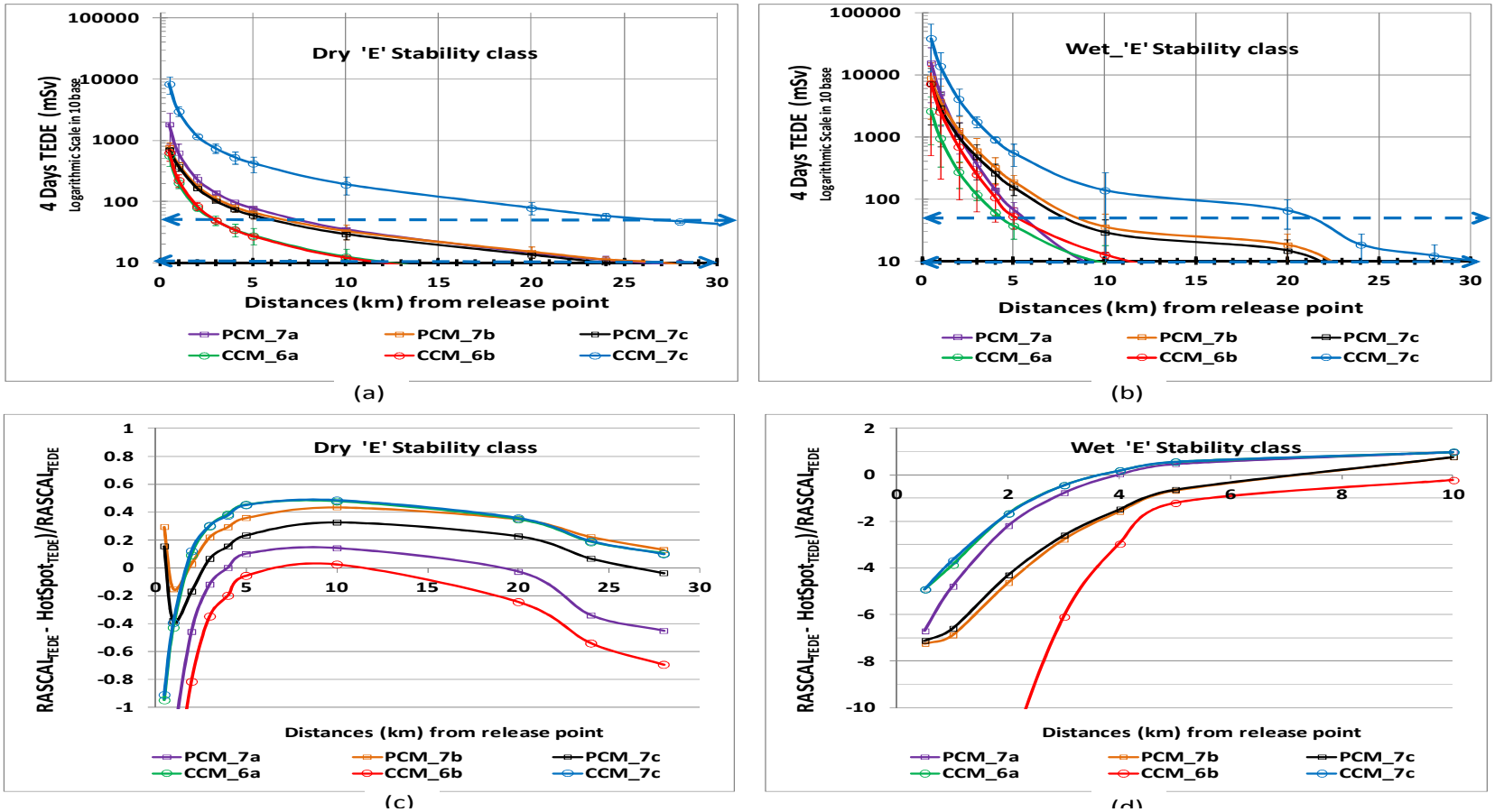

Figure 5-16: (a & b) Average RASCAL and HotSpot calculated 4 days TEDE vs. distances for six accident cases (with uncertainty), ◄- - - - - ► indicate EPA sheltering-in-place, or evacuation thresholds; (c & d) Percentage deviation of HotSpot from RASCAL in dry and wet conditions for the dominating stability class of 'E'.

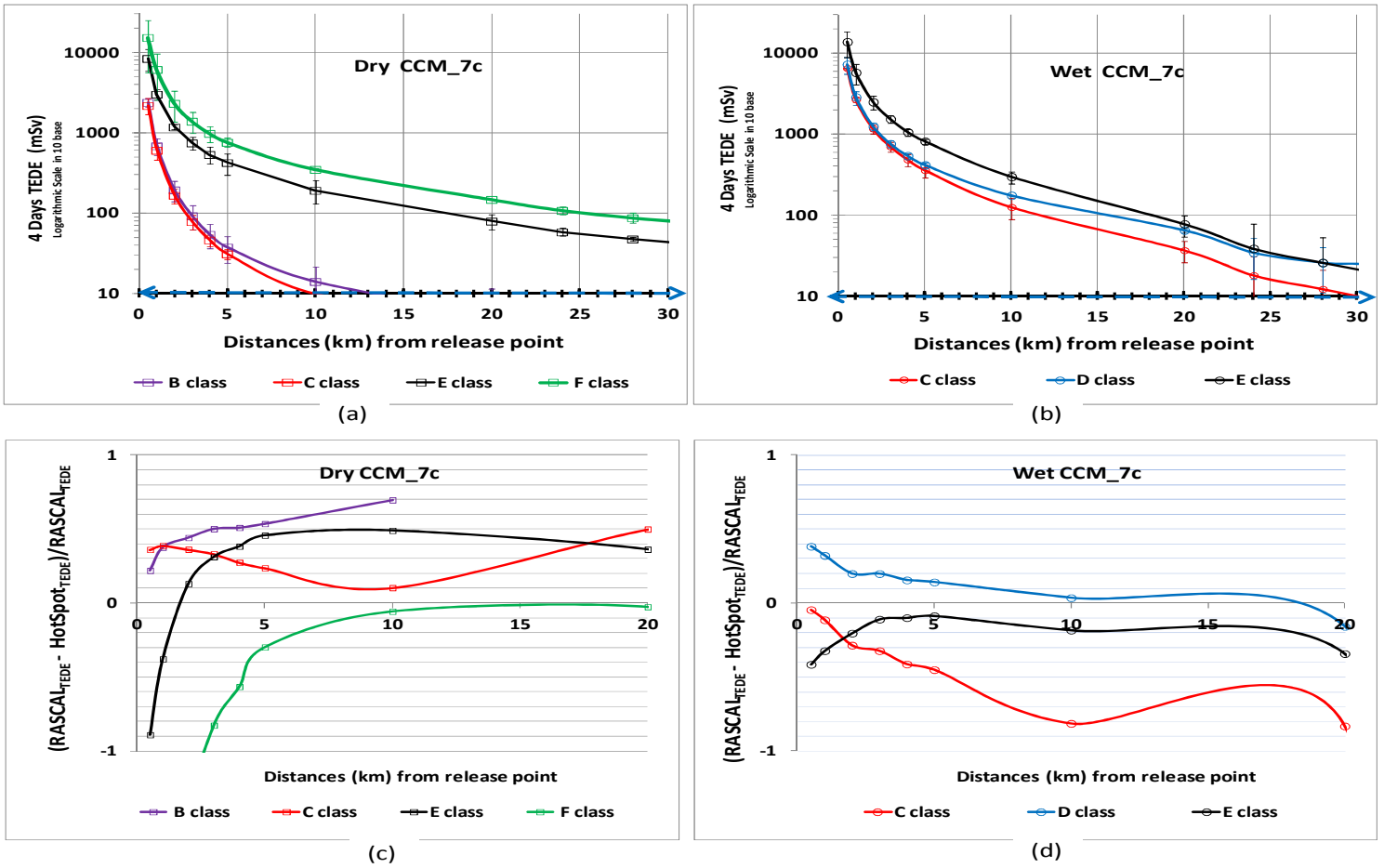

Figure 5-17: (a & b) Average RASCAL and HotSpot calculated 4 days TEDE vs. distances for various upper bound stability classes (with uncertainty), ◄- - - - - ► indicate EPA sheltering-in-place, or evacuation threshold; (c & d) Normalized deviation of HotSpot from RASCAL in dry and wet weather for worst CCM state LTSBO accident case.

5.1.6.2 Intervention Distances for Sheltering-in-Place, or Evacuation

The corresponding distance limits for initiating sheltering-in-place or evacuation measures at the lower (10 mSv) and upper (50 mSv) dose criteria, respectively, in various atmospheric stability classes across different accident cases for EPA PAG dose criteria, are shown in **Figures 5-18 and 5-19.** In **Figure 5-18(a)**, for the PCM with INES level 7 of PCM_7a, the calculated distance limit for stability class 'B' in the dry season is 2-3.7 km, while in Dry 'E', it is 16-30 km. For CCM of INES level 7 in CCM_7c, the stability class 'B' during dry conditions, the area up to 5-23 km around the release point requires these protective measures, and it is greater than 70 km for dry 'E' conditions. In **Figure 5-18(b)**, for stability classes 'D' and 'E' under wet conditions, the sheltering-in-place or evacuation zone extends up to 19-30 km in RASCAL and 17-53 km in HotSpot, based on wind speed and precipitation type. For the CCM of INES level 6 in the accident of CCM_6a and CCM_6b, in **Figure 5-18(a)**, for stability class B in the dry season, it exceeds between 1 and 2 km, while in Dry 'E', it is 15-30 km. Protective intervention measures are limited to shorter distances for these two cases due to their ability to confine the radionuclides within the reactor and containment, compared to the CCM_7c cases, although the reactor cores in these cases were completely melted down. Thus, sheltering-in-place or evacuation should be implemented depending on plant status and atmospheric conditions at the site. **Figure 5-19(a & b)** apparently shows that comparatively lower initiating distances are required for the upper PAG intervention criteria of 50 mSv than for 10 mSv, as shown in Figure **5-17(a & b).**

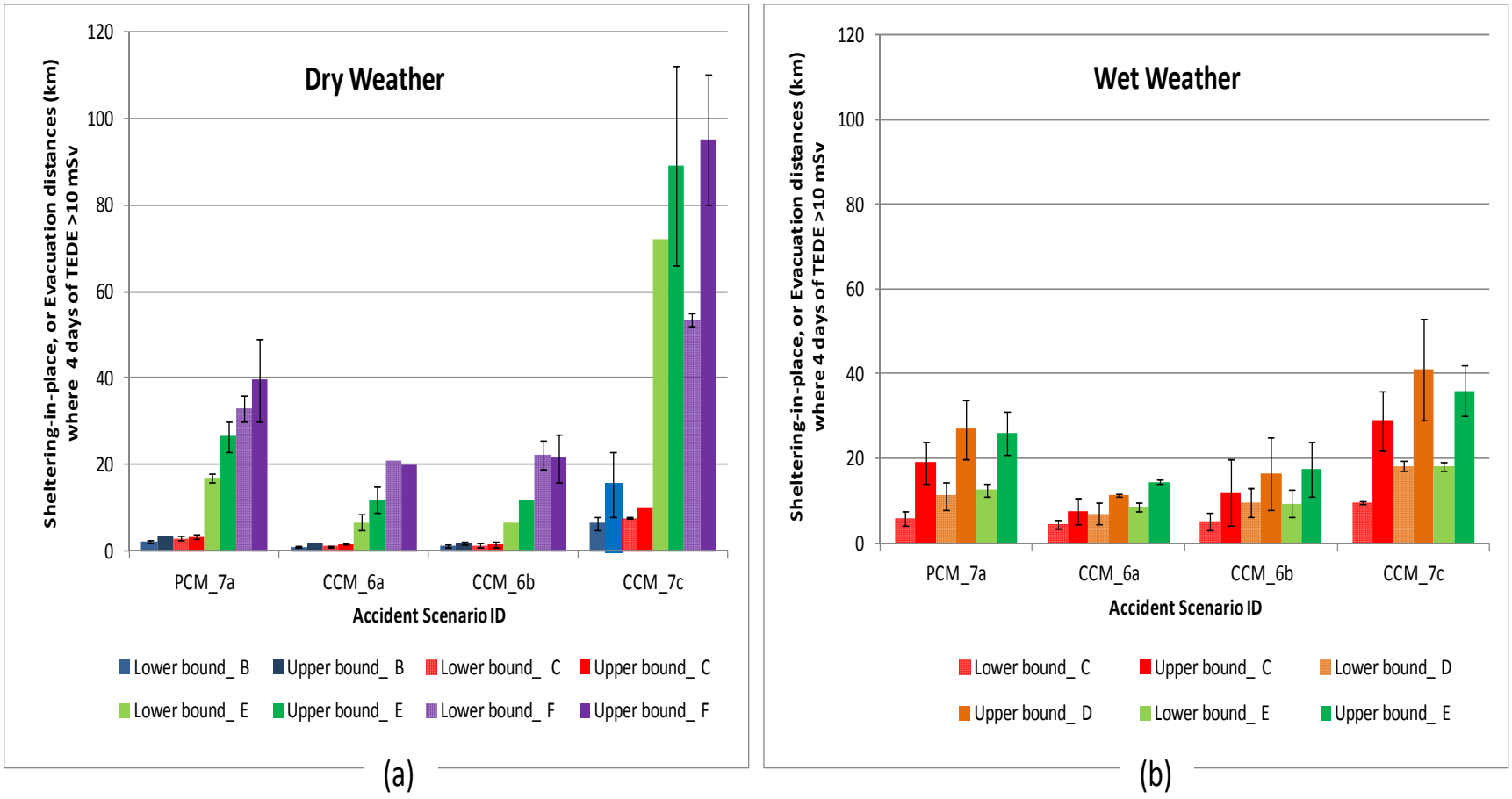

Figure 5-18: Average RASCAL & HotSpot estimated EPA PAG (4 Days TEDE >10 mSv) threshold distances (km) limit along prevailing wind for Sheltering-in-place, or Evacuation with uncertainties in (a) dry and (b) wet weather of various stability classes from PCM and CCM state in LTSBO.

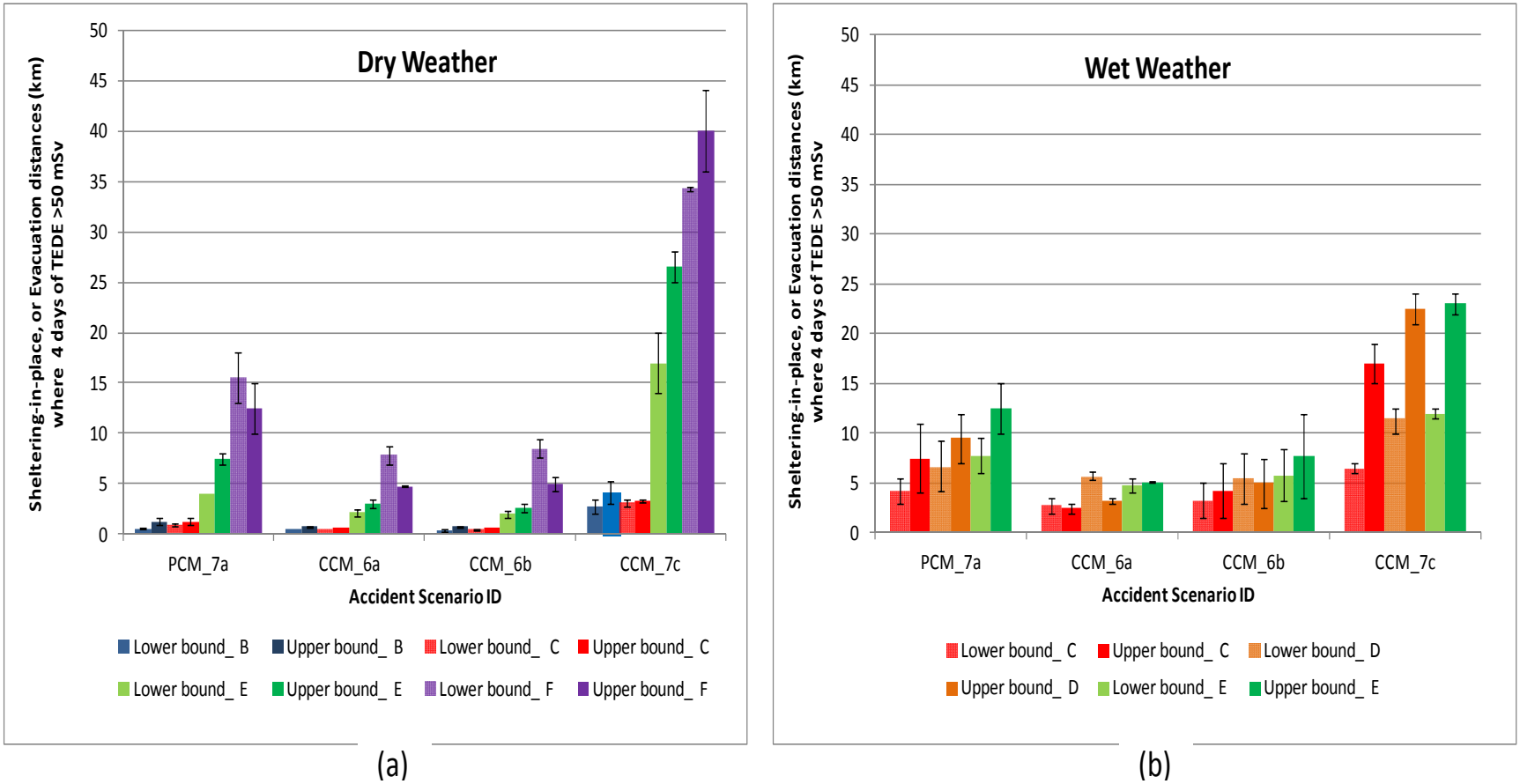

Figure 5-19: Average RASCAL & HotSpot estimated EPA PAG (4 Days TEDE >50 mSv) threshold distances (km) limit along prevailing wind for Sheltering-in-place, or Evacuation with uncertainties in (a) dry and (b) wet weather of various stability classes from PCM and CCM state in LTSBO.

5.1.7 Seven days Exposure TEDE and Intervention Distances for Sheltering-in-Place, or Evacuation

Cloudshine/submersion doses, inhalation CEDE, and 7-day groundshine are all included in the 7-day exposure TEDE, which was computed using HotSpot. In a stability class of "E," **Figure 5-20 (a to c)** displays the TEDE variation over distances for various accident cases in both dry and wet conditions. Due to higher deposited radionuclides to groundshine, the 7-day TEDE is higher in wet conditions than in dry ones in the same accidental case.

The distance limits for different accident cases and stability classes are displayed in **Figure 5-21 (a & b).** The Bangladesh NNREPRP and IAEA GSR Part 7 criteria require sheltering-in-place or evacuation at a dose of 100 mSv. The TEDE values for the CCM_7c case in dry conditions (stability class 'E') went over the limit by 9.5 km. The 21-km radius needs to be protected during wet conditions. The required distance for PCM level 7 accidents is 3.5 km in dry conditions and 12 km in wet conditions. Differences in dose calculations, especially far field in stable 'F' class, between the HotSpot and RASCAL codes result in disparities in intervention distances between the lower and upper bound dry F weather conditions. The main cause of these discrepancies is the way each model (plume and puff) addresses radionuclide deposition, dispersion, and ground-level concentration in HotSpot and RASCAL. The upper and lower bound dry stability class F weather scenarios in **Table 5-2** are based on 10 mSv dose distances determined using the RASCAL far-field puff model, whereas **Figure 5-21** displays the plume model based on HotSpot outputs.

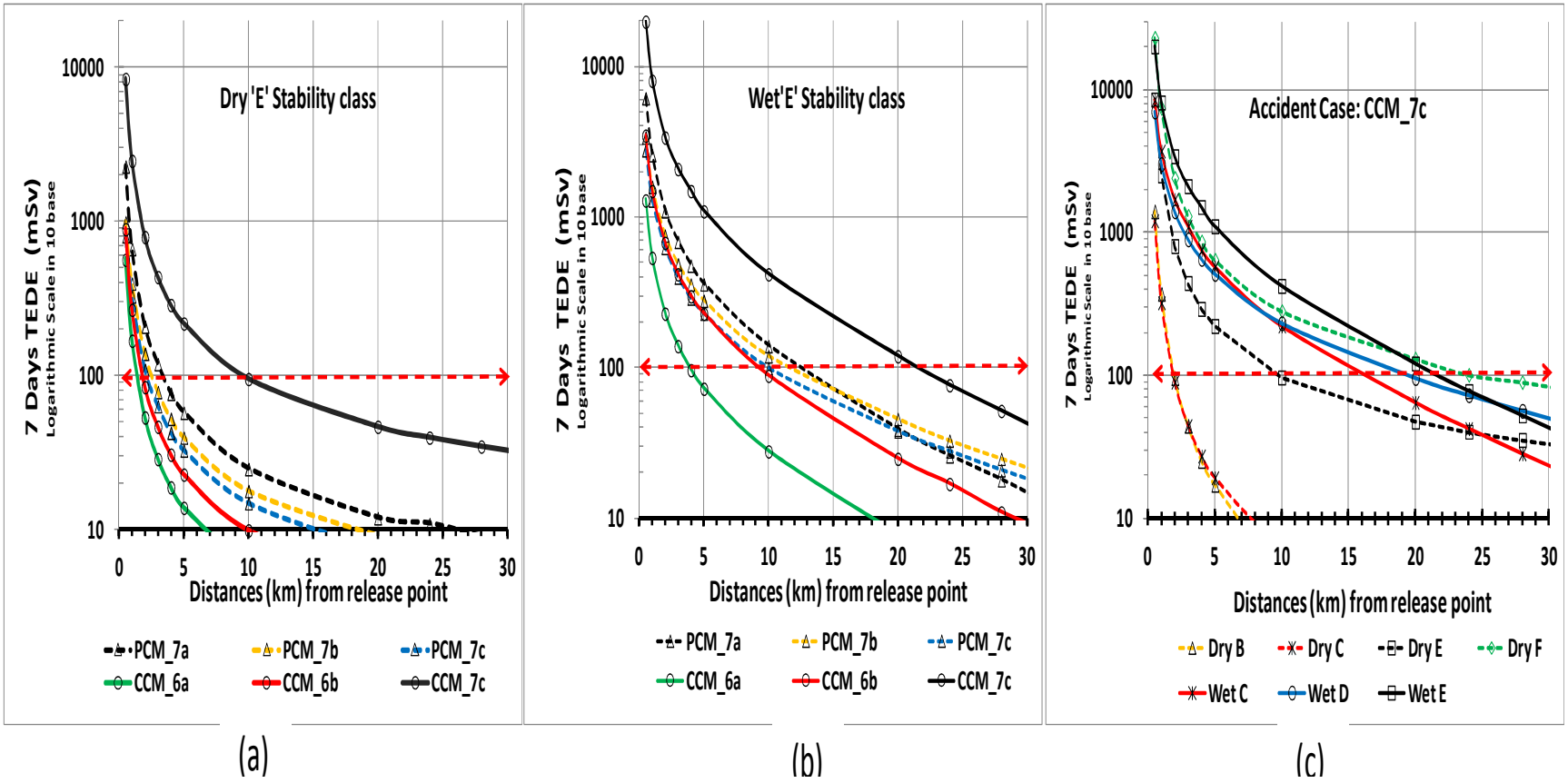

Figure 5-20: 7 days TEDE vs. distances: Comparison under (a) dry and (b)wet weather condition in six PCM and CCM states LTSBO cases for dominant stability class of 'E'; (c) Comparison across upper bound stability classes for worst-case accident; ◄- - - - - ► indicate NNREPRP and GSR Part 7 sheltering-in-place, or evacuation threshold.

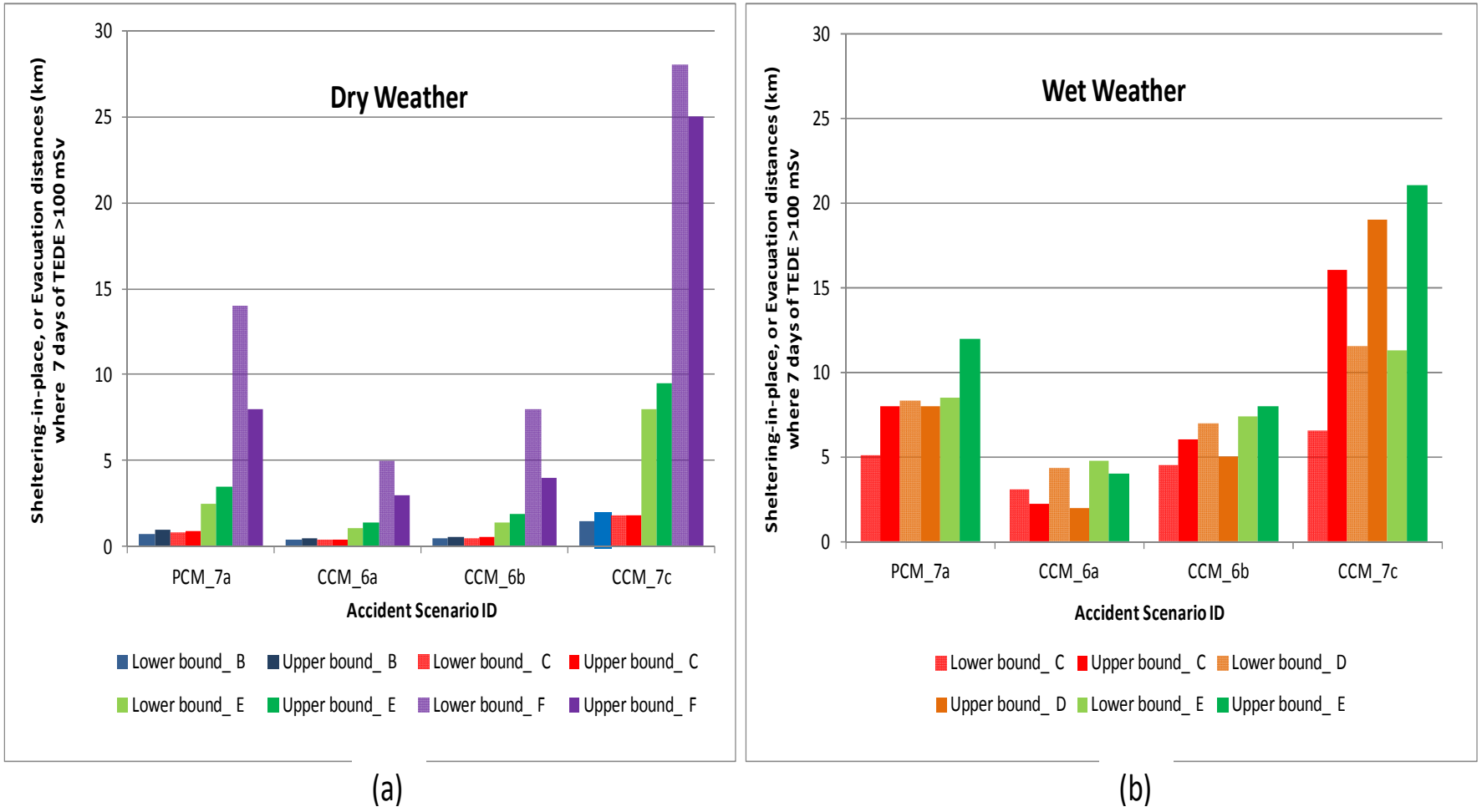

Figure 5-21: NNREPRP and GSR Part 7 (7 Days TEDE>100 mSv) threshold distances (km) along prevailing wind for sheltering-in-place or evacuation in (a) dry and (b) wet weather of various stability classes from PCM and CCM state in LTSBO.

5.1.8 Contour Area for Sheltering-in-place and Evacuation

The **Table 5-3** shows how the size of areas requiring sheltering-in-place or evacuation changes for different accident cases, based on HotSpot calculations for doses exceeding 10 mSv over 4 days TEDE and 100 mSv over 7 days TEDE, under a range of dry and wet weather conditions. In general, the results highlight that both accident severity and meteorological conditions strongly influence how large the protective zones become.

Table 5-3: HotSpot calculated Sheltering-in-place, or Evacuation contour area (km^2) for >10 mSv of 4 Days TEDE & >100 mSv of 7 days TEDE [underline]

Accident Case ID	Upper bound **Dry B**	Upper bound **Dry C**	Upper bound **Dry E**	Upper bound **Dry F**	Upper bound **Wet C**	Upper bound **Wet D**	Upper bound **Wet E**
PCM_7a	2.6 0.19	1.8 0.11	33 0.67	59 2	56 6.4	62 4.2	48 7.7
CCM_6a	0.68 0.047	0.42 0.026	3.9 0.12	11 0.31	10 0.48	7.8 0.25	12 0.82
CCM_6b	0.95 0.076	0.6 0.042	6.6 0.21	19 0.56	37 3.4	37 1.9	33 4.3
CCM_7c	10 0.72	9.1 0.44	332 4.4	239 15	119 24	156 21	93 23

For PCM_7a**,** the affected area remains relatively small under most dry conditions, typically within a few square kilometers. However, when wet conditions are considered, the contour areas increase noticeably, in some cases reaching several tens of square kilometers. This reflects the added effect of rainfall, which enhances deposition and leads to higher accumulated doses over a wider area.

The CCM_6a case consistently shows the least impact among all scenarios. Across both dry and wet conditions, the sheltering or evacuation areas remain very limited, generally below a few square kilometers, suggesting that protective actions would be confined to a small zone close to the plant. CCM_6b represents a moderate case, with larger contour areas than CCM_6a. While still limited under stable dry conditions, the affected area expands significantly under unfavorable dry or wet weather, in some instances exceeding 30 km².

The sheltering and evacuation areas expand rapidly, reaching very large extents under the stable E and F meteorological classes of the CCM_7c scenario. Under wet conditions, these areas remain extensive, covering well over 100 km² in some cases. **Figure 5-22** shows the plume contours generated using HotSpot and the dose footprints produced by RASCAL for the most severe CCM_7c scenario, assuming a predefined wind direction of 0° under dry conditions.

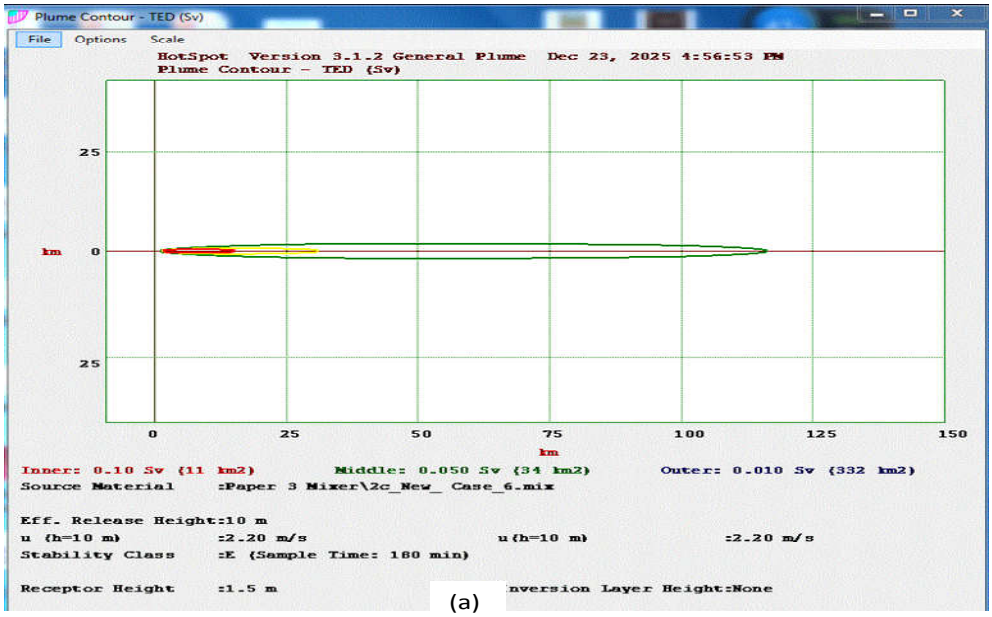

(a)

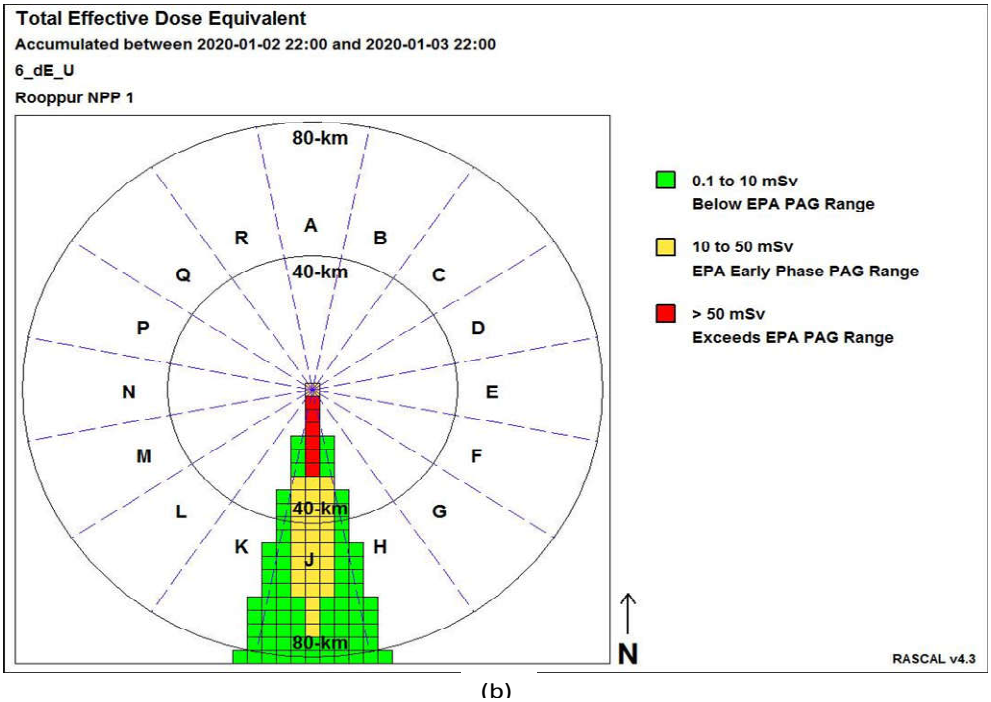

(b)

Figure 5-22: (a) Plume contour generated using HotSpot and (b) dose footprint produced using the RASCAL code for the most severe scenario under dry E stability class

5.1.9 Comparative Analysis of Thyroid Dose in RASCAL and HotSpot

5.1.9.1 Distance vs. Thyroid Dose in Different Accidental Cases and Weather Conditions

For the dominant stability class 'E', **Figure 5-23(a to d)** shows the committed thyroid dose by HotSpot and the child thyroid CDEs calculated by RASCAL for various incidents in both dry and wet situations. RASCAL declined gradually with distance; however, HotSpot shows a somewhat faster reduction due to plume depletion factor accounting. Both models initially report higher thyroid doses in wet settings than in dry ones because of increased exposure to groundshine from deposited iodine.

The spatial variation in thyroid dose for various stability classes in the worst CCM level 7 accident is depicted in **Figure 5-24(a & b)**. The committed thyroid dose (70000 mSv) in HotSpot at 0.5 km is lower than the child thyroid CDE (85300 mSv) in dry weather. Since children's thyroids retain more radioactive iodine than adults', RASCAL accounts for higher iodine absorption in children one year of age when calculating thyroid doses for them. RASCAL incorporates cloudshine, and inhalation exposure pathways, while HotSpot primarily takes inhalation into account. However, HotSpot does not distinguish between children and adults, which could result in an underestimation of children's exposure.

Based on the child thyroid CDE of EPA PAG criteria, **Figure 5-25** displays the distance limits for iodine prophylaxis using the RASCAL code under 360 weather conditions. In both dry and wet conditions, it shows different stability classes ‘B’, ‘C’, ‘D’, ‘E’, and ‘F’. Iodine prophylaxis is required when projected doses for CCM_7c reach 50 mSv. Black indicates wet weather, while other colors indicate dry conditions. The distance needed for iodine prophylaxis ranges from 10 km to more than 80 km, depending on the stability class and weather.

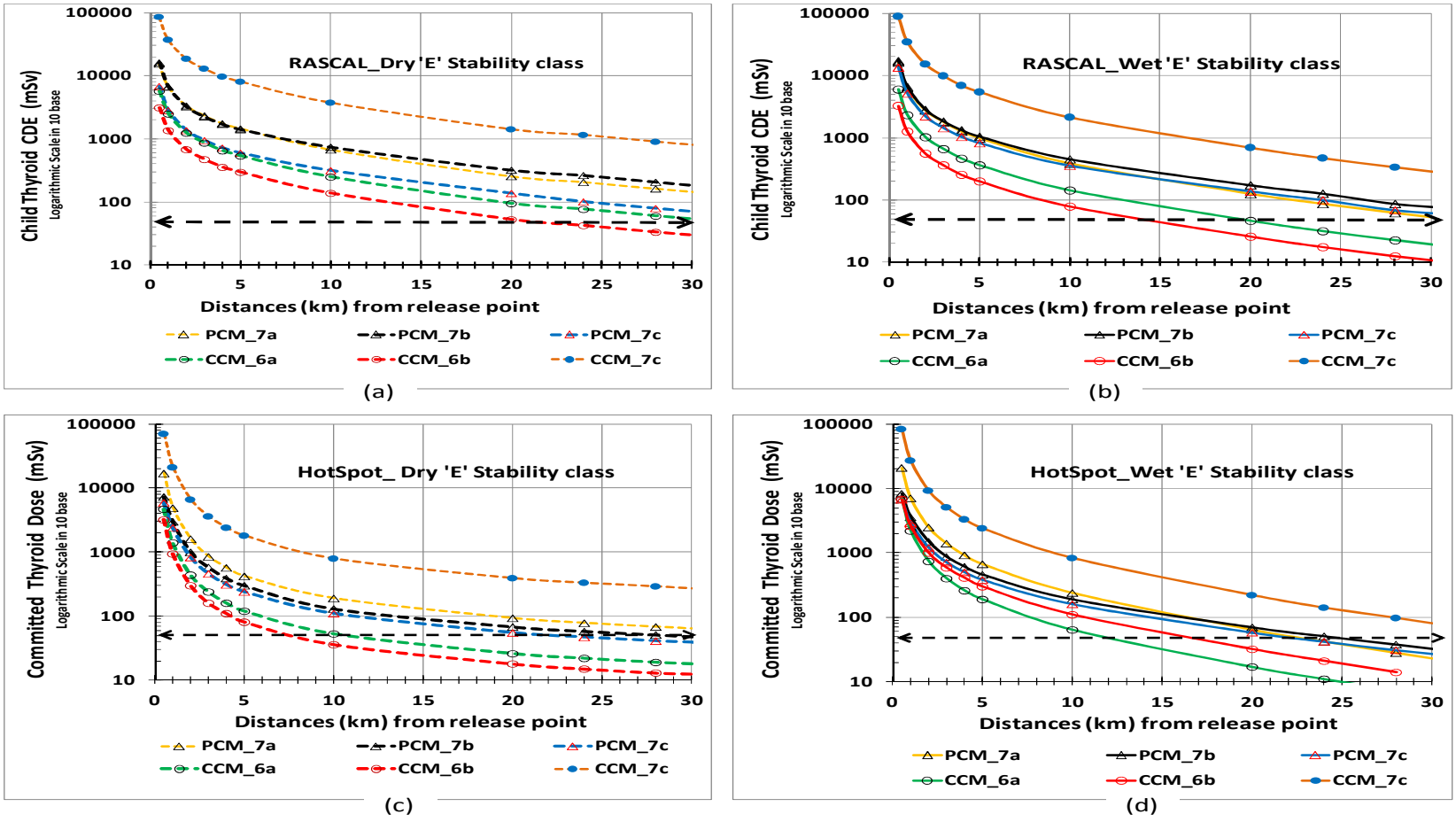

Figure 5-23: Thyroid dose vs. distance comparison: (a, c) dry and (b, d) wet weather for dominant stability class of 'E' from PCM and CCM state in six LTSBO cases; where (a, b) RASCAL child thyroid CDE and (c, d) HotSpot committed thyroid dose; ◄- - - - - - - ► indicate NNREPRP, IAEA GSR Part 7, and EPR PAG threshold dose for iodine administration.

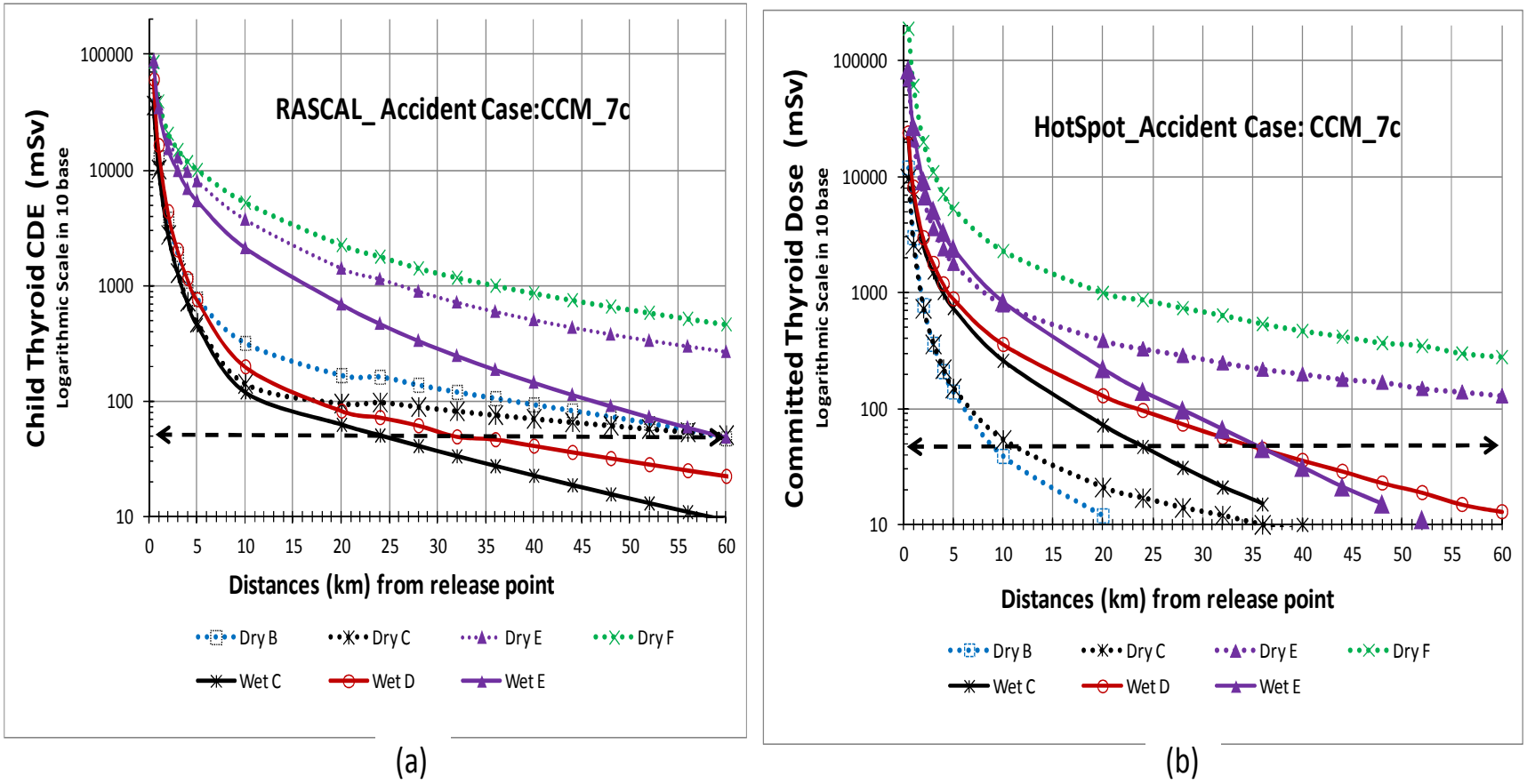

Figure 5-24: Thyroid dose vs. distances comparison: (a) RASCAL calculated Child thyroid CDE and (b) HotSpot calculated committed thyroid dose for various stability classes in worst accident case; ◄- - - - - - - - ► indicate NNREPRP, IAEA GSR Part 7, and EPR PAG threshold dose for Iodine administration.

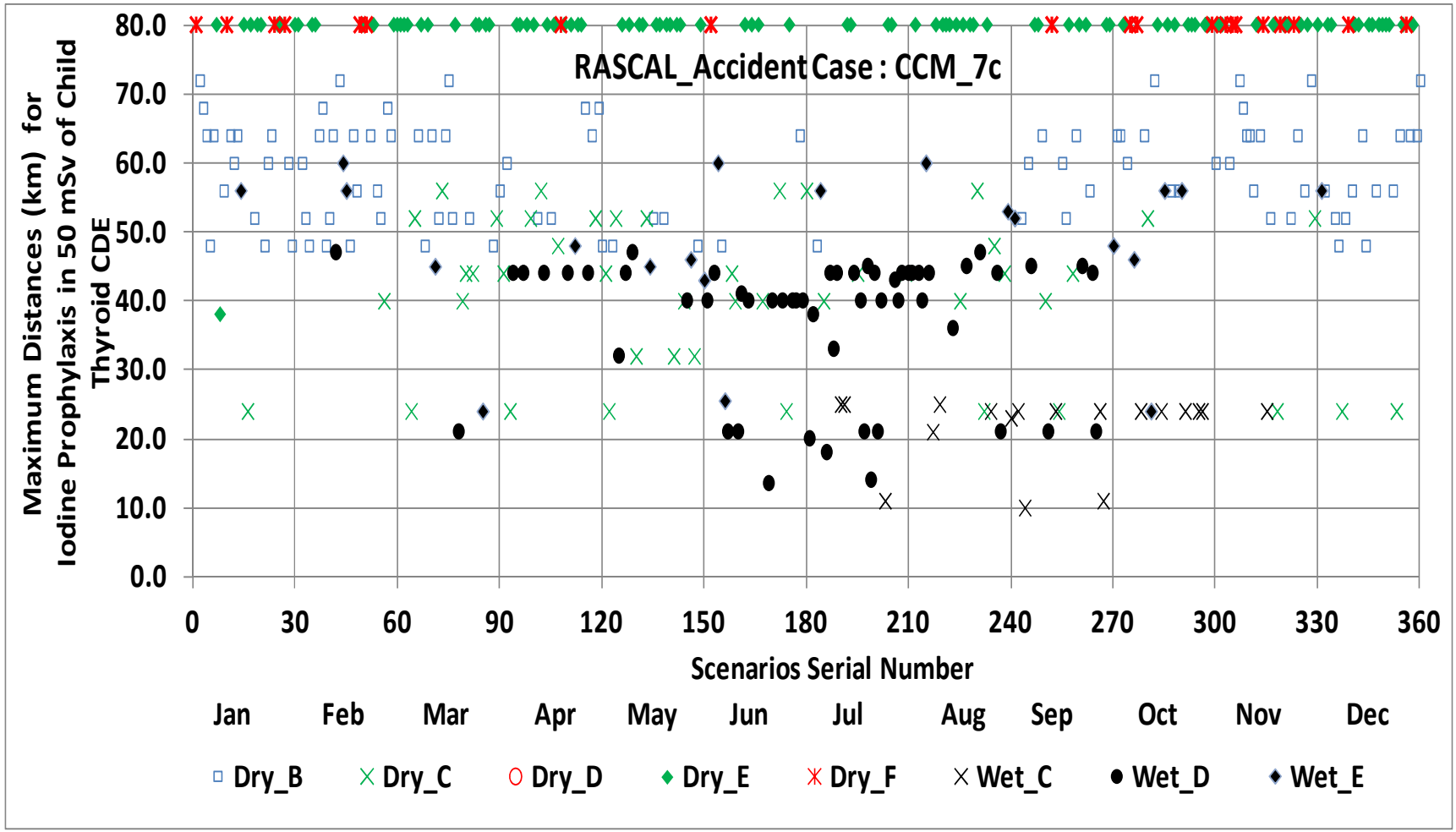

Figure 5-25: Month-wise 360 weather scenarios distances limit for Iodine prophylaxis based on PAG criteria of 50 mSv child thyroid CDE during worst-case in LTSBO.

5.1.9.2 Intervention Distances for ITB Agent

According to Bangladesh NNREPRP, IAEA GSR Part 7, and EPA PAG criteria for 50 mSv, iodine prophylaxis is needed within the distances listed in **Figure 5-26(a & b)** for RASCAL and HotSpot codes across various accident cases and stability classes. For the dominant dry weather condition (stability class 'E'), figures show that thyroid doses exceed the criteria at distances of 30-56 km for a level 7 accident with PCM (case PCM_7a) and over 80 km for CCM (case CCM_7c). In contrast, under dominant wet weather conditions (stability class 'D'), the distance limits are 14-34 km for CCM and 4-18 km for PCM for level 7 accidents, depending on wind speed and precipitation type.

INES Level 6 accidents of cases CCM_6a and CCM_6b are due to their comparatively lower iodine release activities than other cases, smaller thyroid doses, and shorter intervention distances. The distance limits are 8.5-31 km for CCM_6a and 6-20 km for CCM_6b. The relatively smaller distances in CCM_6b are due to radionuclides being contained for 24 hours before release, and only 1% of the release consists of iodine, resulting in a noble gas to iodine ratio of 296:1. In this case, protective measures are based on TEDE rather than thyroid doses.

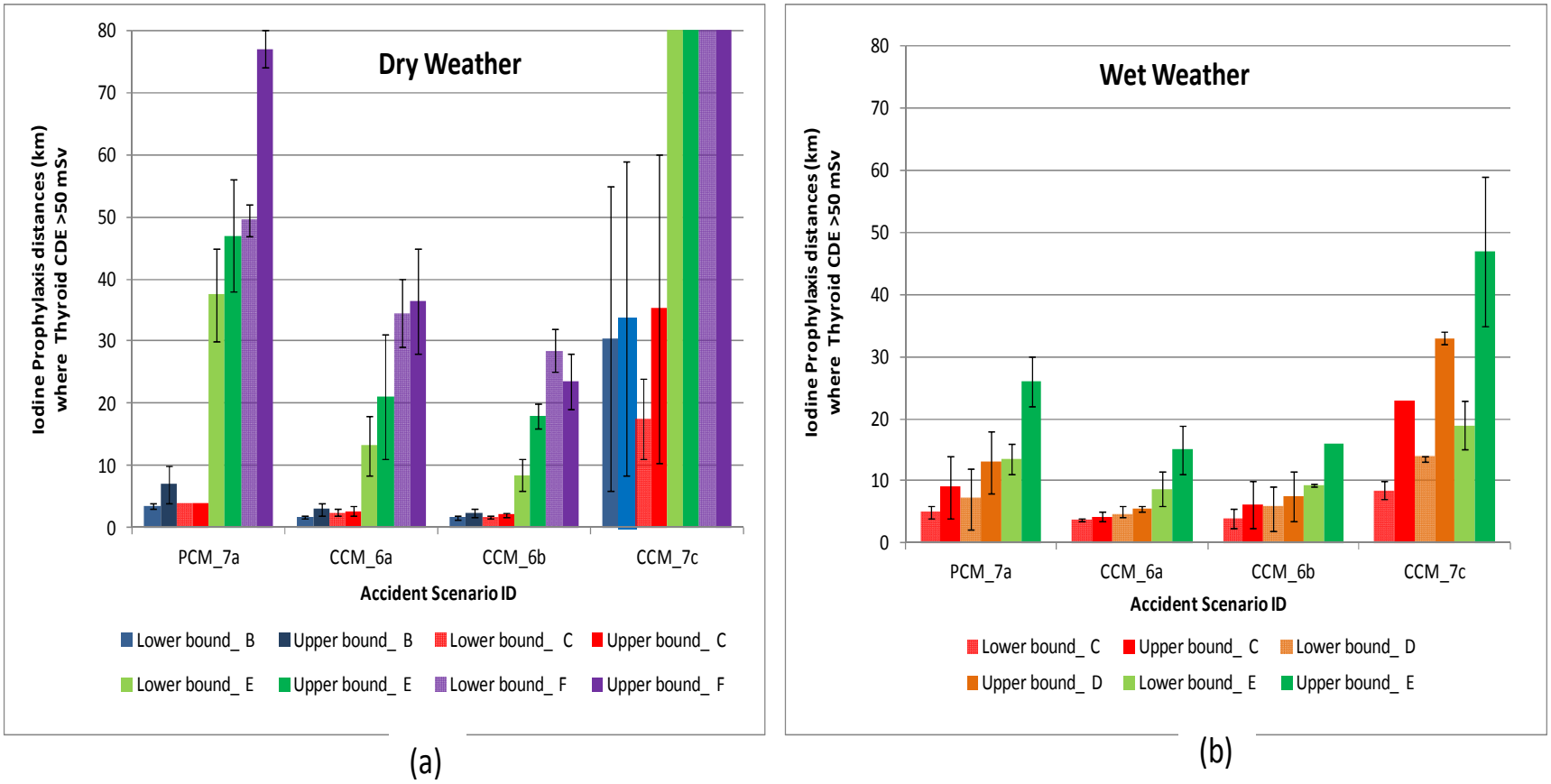

Figure 5-26: Average child thyroid CDE (RASCAL) and committed thyroid dose (HotSpot) threshold dose (>50 mSv) distances (km) limit along prevailing wind for Iodine prophylaxis with uncertainty in (a) dry and (b) wet weather of various stability classes from PCM and CCM state in LTSBO.

5.1.10 First Year Intermediate Phase TEDE and Relocation Distances

Figure 5-27 shows how the first-year intermediate-phase TEDE varies in different stability classes during the PCM and CCM states in the LTSBO event, with a relocation dose limit of 20 mSv. During CCM state for dry weather conditions of 'E and 'D,' stability class first-year intermediate projected doses are approximately 1000 to 10000 mSv near the plant site, while in wet weather for the same stability class, it is nearly 100000 mSv with higher projected intermediate doses near the site area compared to dry weather. In the PCM state, the projected doses are nearly 1000 mSv for dry conditions, while the doses are nearly 10000 mSv for wet conditions. The relocation threshold distance for different scenarios is presented in **Figure 5-28**.

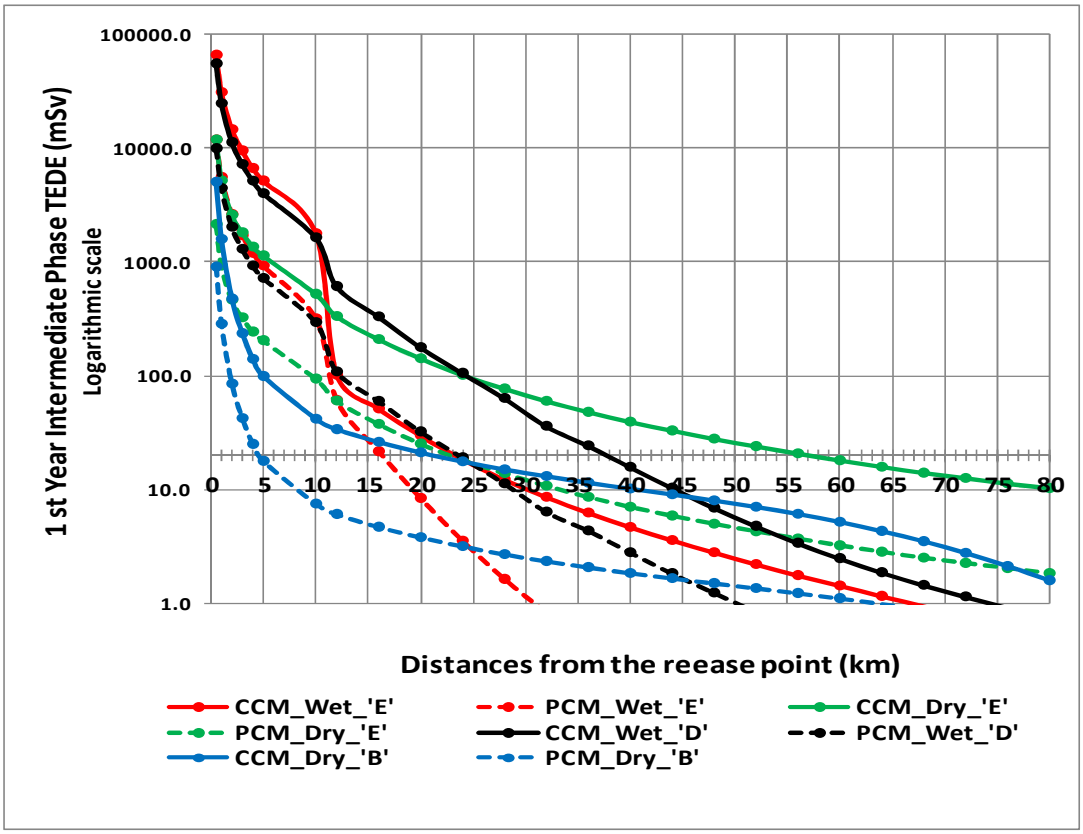

Figure 5-27: 1st year Intermediate phase TEDE vs. distances for various stability classes from PCM and CCM state in LTSBO where intersect of horizontal axis indicate EPA PAG threshold dose (20 mSv) for relocation.

Figure 5-28 shows the comparative relocation distance with corresponding impact areas that exceeded the relocation threshold of 20 mSv for various stability classes in PCM and CCM

states during the LTSBO event. A larger relocation distance is required for dry, stable weather conditions of the 'E' stability class, approximately 56 km (impact area above 400 km²), while for wet weather of the same stability class, it is 23 km (impact area above 250 km²) during the CCM state. In the PCM state, the required relocation distances are 22 km and 16 km, respectively, for dry and wet 'E' stability classes. For the stability class 'B,' the required relocation distances are much shorter than for the 'E' stability class. Relocating people in densely populated areas like Rooppur could be challenging. Emergency planners need to focus on areas with high exposure risks while also considering vulnerable populations, the needs for infrastructure, and how long displacement may last. In addition, environmental conditions, shielding, and cleanup efforts play a critical role in relocation decisions (US EPA, 2017).

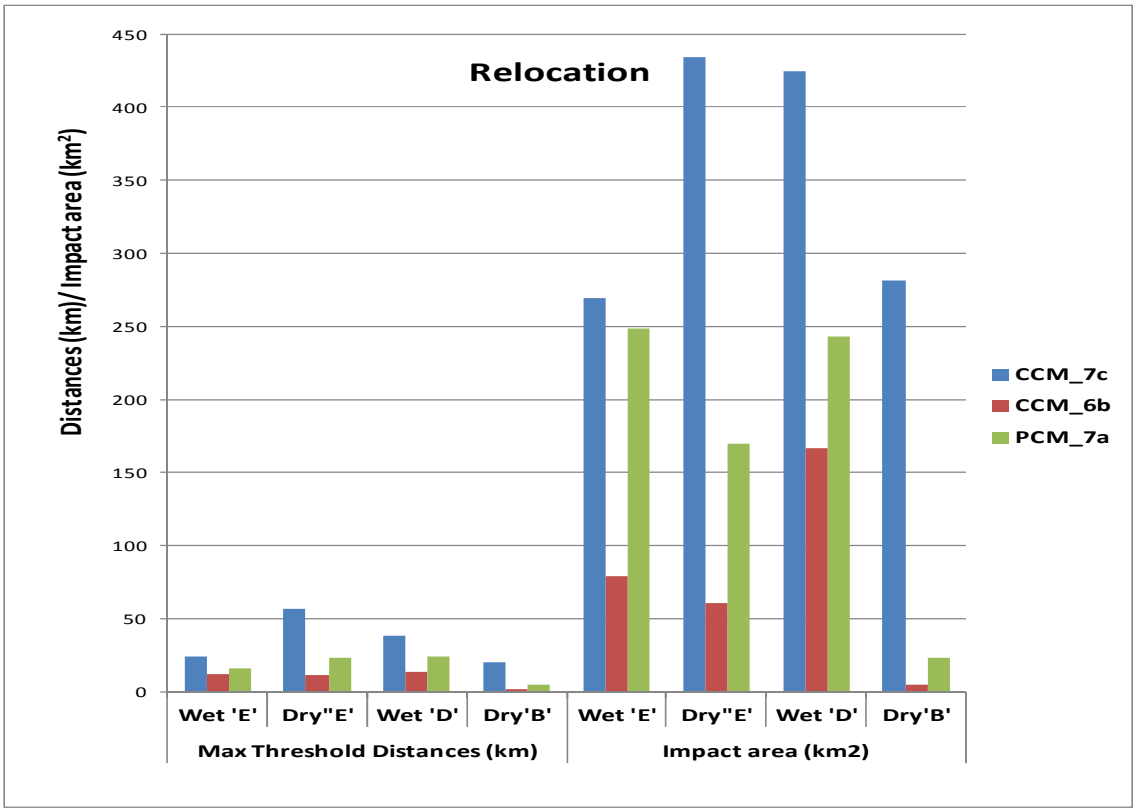

Figure 5-28: Maximum threshold distances and Impact area for relocation for various stability classes from PCM and CCM state in LTSBO.

5.1.11 Sensitivity Results of Particle Numbers, Concentration Grid and Release Height in HYSPLIT

Figure 5-29 shows the time-averaged normalized air concentration distribution pattern for different particle numbers and concentration grid combinations. According to the HYSPLIT User's Guide and in **Figure 5-29**, finer grid resolutions (e.g., 0.01°) can offer more detailed spatial representation of the particles but be associated with significantly increased computational and storage demands. Conversely, coarser grids (e.g., 0.1°) excessively smooth spatial gradients and reduce the accuracy of local concentration, deposition, and dose estimates—especially in areas with complex terrain or variable meteorological conditions (Stein et al., 2015). Using a grid resolution of 0.05° × 0.05°, which is roughly 5–6 km, strikes a good balance between capturing spatial details and keeping computations manageable. This resolution is sufficient to represent local variations in both air concentration and ground deposition (Faisal & Islam, 2025*).

When looking at a specific concentration grid, increasing the number of particles from 100 to 1,000 produces a noticeably smoother distribution. At 10,000 particles, the distribution becomes very smooth with a clearly defined center, though the edges remain slightly uneven. Increasing the particle count beyond this does not significantly change the concentration patterns but does add considerably to computational time. On the other hand, using fewer than 10,000 particles—around 83 per hour, for example—can lead to sampling errors and inconsistencies (Faisal & Islam, 2025*).

Figure 5-30 (a & b) shows how peak time-averaged normalized air concentrations and peak cumulative normalized ground deposition vary across different test runs. Four particle counts were used—100 (8.3/hr), 1,000 (83.3/hr), 10,000 (833.3/hr), and 100,000 (8,333.3/hr)—along with four concentration grid sizes: 0.01°, 0.025°, 0.05°, and 0.1°. To provide a conservative estimate, the analysis did not focus on any specific receptor location. Instead, the highest values within the modeled domain were considered to represent maximum potential exposure (Faisal & Islam, 2025*).

* Article published from this thesis

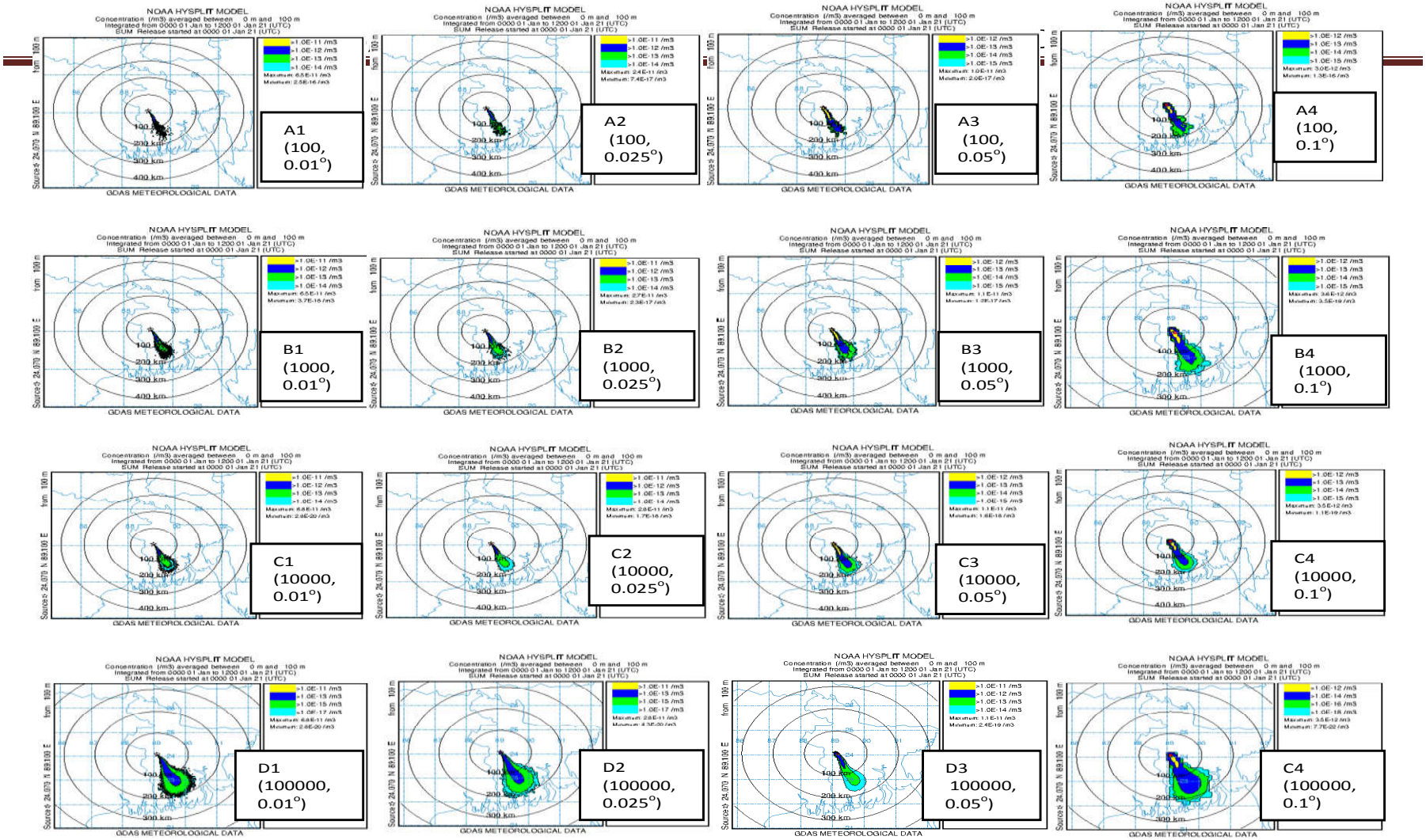

Figure 5-29: Time-averaged Normalized air concentration distribution pattern for different particle numbers and concentration grid combination in HYSPLIT sensitivity test (Faisal & Islam, 2025*).

* Article published from this thesis

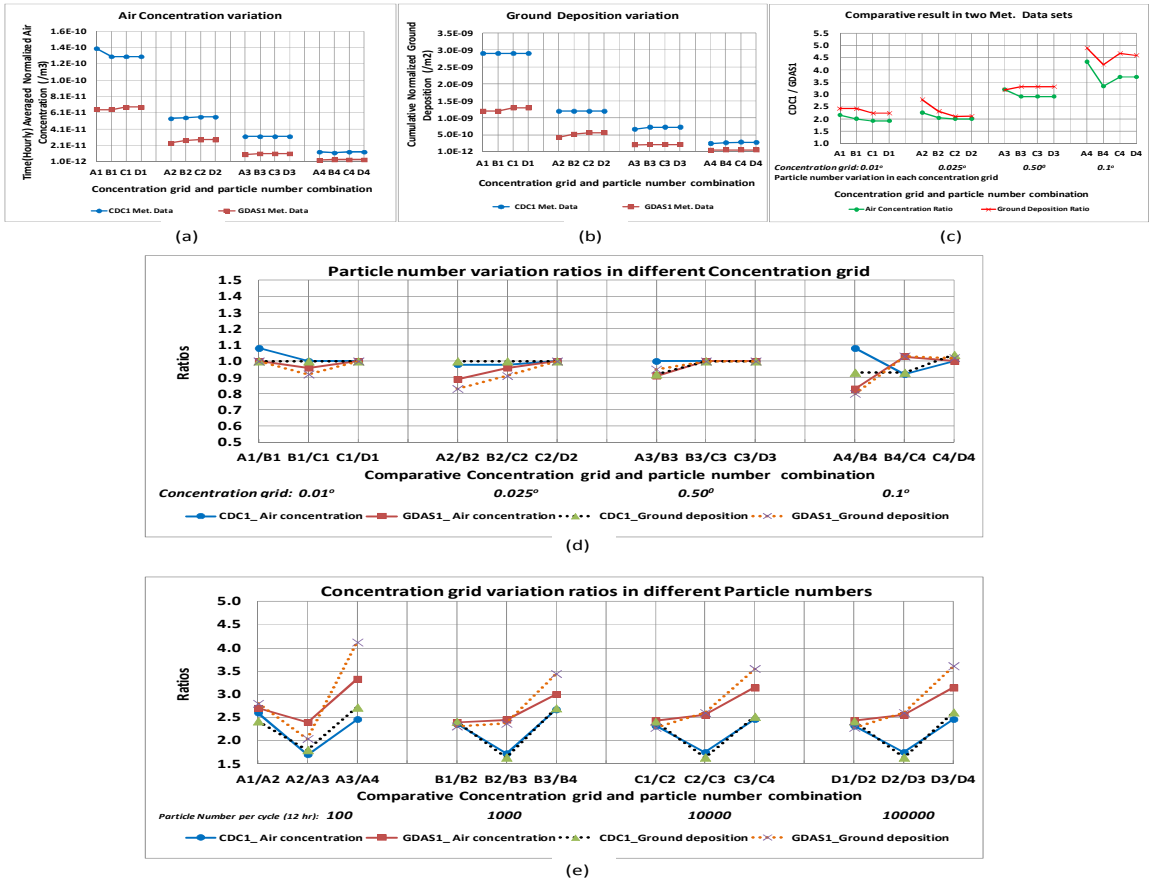

Figure 5-30: Comparative HYSPLIT sensitivity tests showing (a) time-averaged normalized air concentration and (b) cumulative normalized ground deposition across grid resolutions and particle numbers; (c) CDC1-to-GDAS1air concentration/ ground deposition ratios; peak air concentration/ground deposition variations with (d) grid resolution and (e) particle number changes under both datasets (Faisal & Islam, 2025*).

Figure 5-30(c) shows that normalized air concentrations are 2 to 3 times higher when using the CDC1 meteorological dataset compared to GDAS1. This is because CDC1 uses a coarser grid of 2.5° with 6-hour intervals, while GDAS1 provides a finer 1° grid with 3-hour intervals. Coarser grids tend to smooth out variations in wind speed, precipitation, and turbulence over large areas, which can make pollution levels appear higher. This happens because smaller-scale weather patterns, which influence how pollutants spread, are not captured in the coarser data (Faisal & Islam, 2025*). They may also underestimate how much pollutants are removed by rain, spread emissions over larger areas, and ignore the effects of terrain and weather. As a

* Article published from this thesis

result, the observed pollution levels may be uncertain (Draxler & Hess, 1998; Stein et al., 2015).

Figure 5-30(d & e) shows how peak time-averaged normalized air concentrations and cumulative normalized ground deposition change when either the concentration grid or the particle number is varied. In **Figure 5-30(d),** the ratios B1/B2 and B2/B3 represent the change in maximum normalized air concentration or ground deposition as the grid resolution shifts from 0.01° to 0.025° (B1/B2) and from 0.025° to 0.05° (B2/B3), using 1,000 particles (83.3/hr). For a 0.01° grid, the air concentration is 4.4 times higher (2.6 × 1.7) than for a 0.05° grid in the CDC1 dataset, while in the GDAS1 dataset, it increases by 6.5 times (2.7 × 2.4) (Faisal & Islam, 2025*). Pollutant dispersion in a finer (1-degree for GDAS1) concentration grid captures localized concentration peaks more accurately, allowing smaller areas to reflect higher concentrations (Stein et al., 2015).

In Figure 5-30(e), the ratio at points B3/C3 shows how the maximum normalized air concentration or ground deposition changes when the particle number increases from 100 (8.3/hr) to 1,000 (83.3/hr), while the C3/D3 ratio reflects the change from 1,000 to 10,000 particles, using a 0.05° concentration grid. Ratios close to one for these particle increases—especially on 0.01°, 0.025°, and 0.05° grids—indicate that the simulations are numerically converging. The sensitivity tests in **Figure 5-29** further show that increasing the number of particles produces smoother air concentration distributions, with counts between 1,000 (83.3/hr) and 10,000 (833.3/hr) per hour resulting in stable and uniform concentration fields. (Faisal & Islam, 2025*).

The modeling parameters—particle numbers between 1,000 (83.3/hr) and 10,000 (833.3/hr) along with a 0.05° concentration grid—offer a practical balance between simulation accuracy and computational effort. The chosen grid resolution allows for spatially detailed results, while the selected particle count provides stable and reliable representations of atmospheric dispersion without placing excessive demands on computing resources (Faisal & Islam, 2025*).

Figure 5-31(a to c) shows sensitivity results for release height variation using 100 particles

* Article published from this thesis

(8.33/hr) and a 0.05° concentration grid. For each release height, air concentration was measured within 0–200 m and 0–100 m vertical grids, while ground deposition was evaluated at 0 m. As release height increases, both air concentration and ground deposition decrease (**Figure 5-31(a)**. Narrower measurement grids result in higher observed concentrations due to reduced vertical dispersion. Higher-altitude releases encounter stronger, more variable winds, spreading pollutants over a wider area and reducing ground-level impact (Draxler & Hess, 1998; Stein et al., 2015). **Figure 5-31(b)** shows air concentration and ground deposition values are about three times higher with the CDC1 dataset compared to GDAS1. **Figure 5-31(c)** further illustrates how much variation of peak air concentration and ground deposition with release height variation.

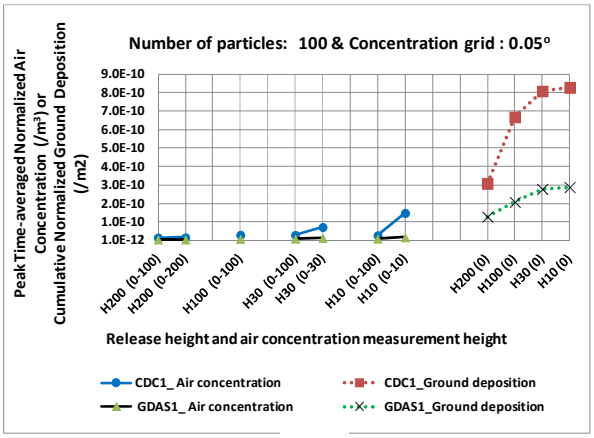

(a)

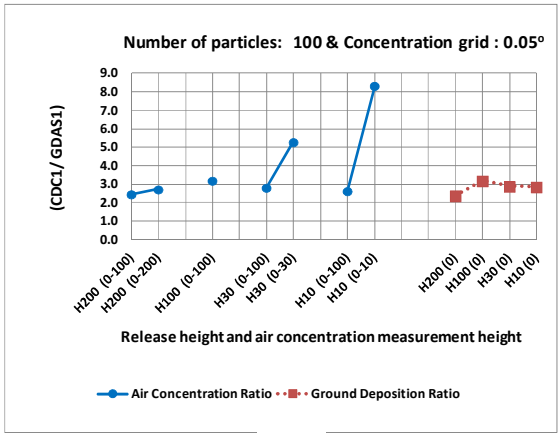

(b)

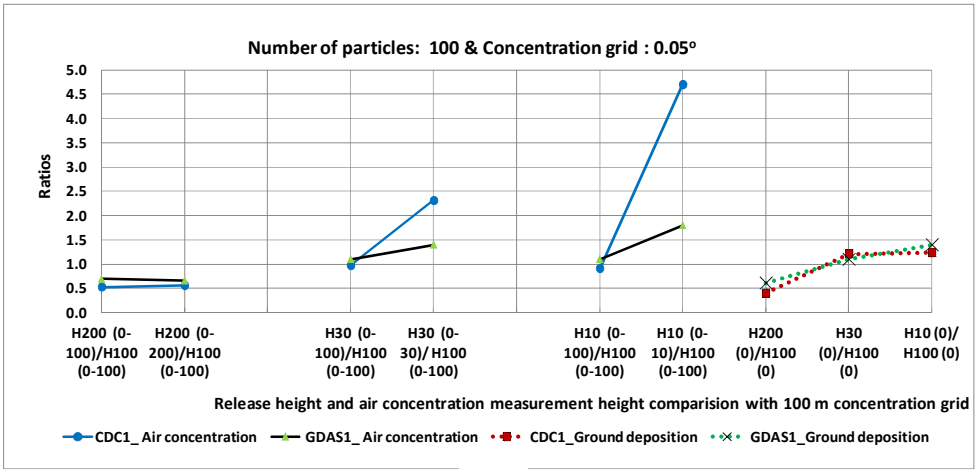

(c)

Figure 5-31: (a) Time-averaged normalized air concentration and cumulative normalized ground deposition variation for different release height in CDC1 and GDAS1 meteorological data; (b) CDC1 to GDAS1 simulation ratio; (c) Ratios of simulation outputs for varying release heights to 100 m concentration grid in HYSPLIT sensitivity testing.

5.1.12 Selection of Simulation Run Time in HYSPLIT during LTSBO Accident

Figure 5-32 shows how the highest ground deposition changed over simulation run time after a CCM accidental 10 hr release. It uses weather data from two sources (GDAS1 and CDC1) for January and July 2022. The amount of deposited material initially increased over several days. The observed peak ground deposition values leveled off between 312 and 360 simulation hours (about 13 to 15 days). For this reason, a 15 days (360 hr) simulation run time was selected for these LTSBO accident cases.

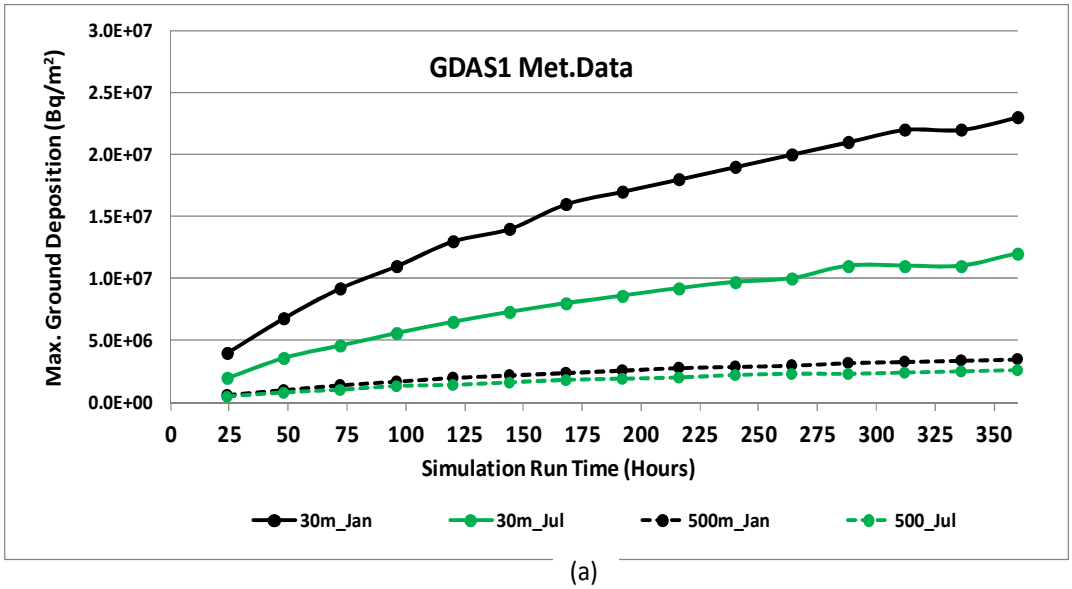

(a)

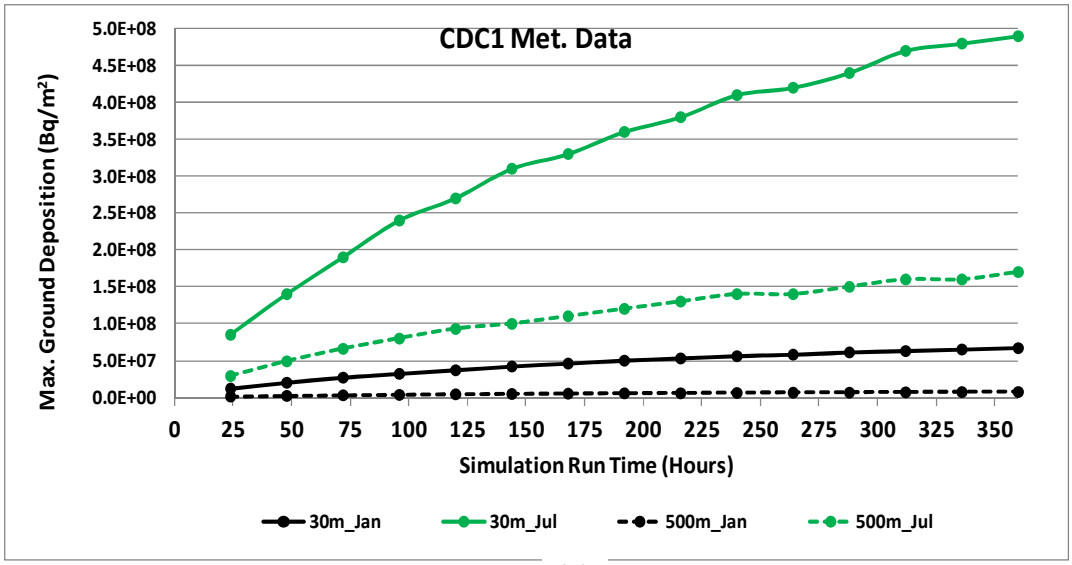

(b)

Figure 5-32: Max. cumulative ground deposition (Bq/m^2) as a function of simulation time.

5.1.13 Air Concentration and Ground Deposition Distribution of LTSBO event

APPENDIX F presents the monthly wind rose diagram from January to December for the years 2021 and 2022 using GDAS1 and CDC1 meteorological datasets. The diagrams are based on 84- hour wind speed and wind direction data starting on the 15th of each month, collected from the NOAA Air Research Laboratory Ready web server (https://www.ready.noaa.gov/ready2-bin/mainarc.pl) for the Rooppur site at latitude 24.07^{o} and longitude 89.1^{o}. During the dry weather of months from November to April, the wind predominantly blows from northwest to southwest, as shown in the wind rose diagrams. While, during the wet weather months from May to October, the dominant wind direction is southeast. For air concentration and ground deposition distribution during the LTSBO event, Janauary was selected to represent dry weather and July for wet weather conditions. **APPENDIX G** presents the Pasquill Stability Class variations over 84 hours starting from the 15th of January and July for the years 2021 and 2022, based on GDAS1 and CDC1 Meteorological Data, can also affects the air concentration and ground deposition distribution.

5.1.13.1 Distribution Pattern in Dry Weather Month of January

Figure 5-33 shows how the radioactive plume from the LTSBO CCM accident evolved and moved during dry weather month of January for GDAS1 meteorological dataset. According to **Figure 5-33(a),** within the first day, the plume left the southern part of Bangladesh and spread over 400 km into the Bay of Bengal. From **Figure 5-33(h)** as expected, extremely high activity levels were observed at the accident site, reaching volumetric air concentration of 9.9×10^{4} Bq/m³. Increased activity levels over 10,000 Bq/m³ were also found more than 50 km from the site, mainly in the direction of the prevailing southerly winds. The areas of Kushtia, Kumarkhali, Jhenaidah, Jashore, and the surrounding areas had the highest levels of airborne radioactivity on the first day of the release. With volumetric air concentrations ranging from 10 to 10^{3} Bq/m³, contamination was found throughout the entire southwestern region of Bangladesh.

However, due to the short half-life of the iodine-131 isotope—responsible for the increased radioactivity—a rapid decline in airborne activity was expected over the following days. For example, on the first and second days after the accident as shown in **Figure 5-33(b & c)**, peak

activity levels differed by about two orders of magnitude. While activity levels continued to decline, they did so at an uneven rate. During plume moving to the south, other regions of Bangladesh were unaffected by the radioactive cloud. By the second day, the plume had traveled more than 1,000 km from the accident site. By the third day, the most radioactive part of the plume had traveled approximately 1,500 km from the accident site and was positioned over the central Bay of Bengal. On the fourth day as shown in **Figure 5-33(d)**, the plume's highest activity concentration was located over Sri Lanka, and the maximum time-averaged normalized air concentration had dropped from 5.2×10^{-10} m^{-3} on the first day to 2.7×10^{-12} m^{-3}.

From the second day, a significant change in weather occurred, as upper-level winds shifted part of the plume's direction, causing it to move back north along with continuing out to sea. As a result, the plume spread across large areas of Myanmar and into Thailand. In the following days, persistent northerly winds at higher altitudes caused the radioactive cloud to shift back and forth, expanding the affected area from parts of western Thailand to southern regions of China. The time-averaged normalized air concentration of airborne activity in the most radioactive part had dropped to 2.3×10^{-12} m^{-3}.

Figure 5-34(a to e) shows the cumulative distribution patterns of radioactivity deposition for a release rate of 1 Bq/hr on the first, second, third, fifth, and seventh days. During this time, the radioactive cloud impacted southern Bangladesh, extending beyond Satkhira and Khulna to the western and southern coastal areas of the Sundarbans. According to **Figure 34(f & g)** for the accidental release rate of CCM release duration for 10 hours, cumulative ground deposition levels in southward regions of 100 km after the first and seventh days ranged from 104 to 105 Bq/m2. However, a 40 km-wide area in southwestern Bangladesh had levels as high as 10^6 Bq/m^2. In addition, the cumulative ground deposition levels after seven days were roughly 10^7 Bq/m^2 in a smaller area of about 5 to 7 km, which includes the southern part of the Ishurdi region. The immediate fallout of radioactive material was responsible for most of the deposition at the accident site before the wind dispersed the plume.

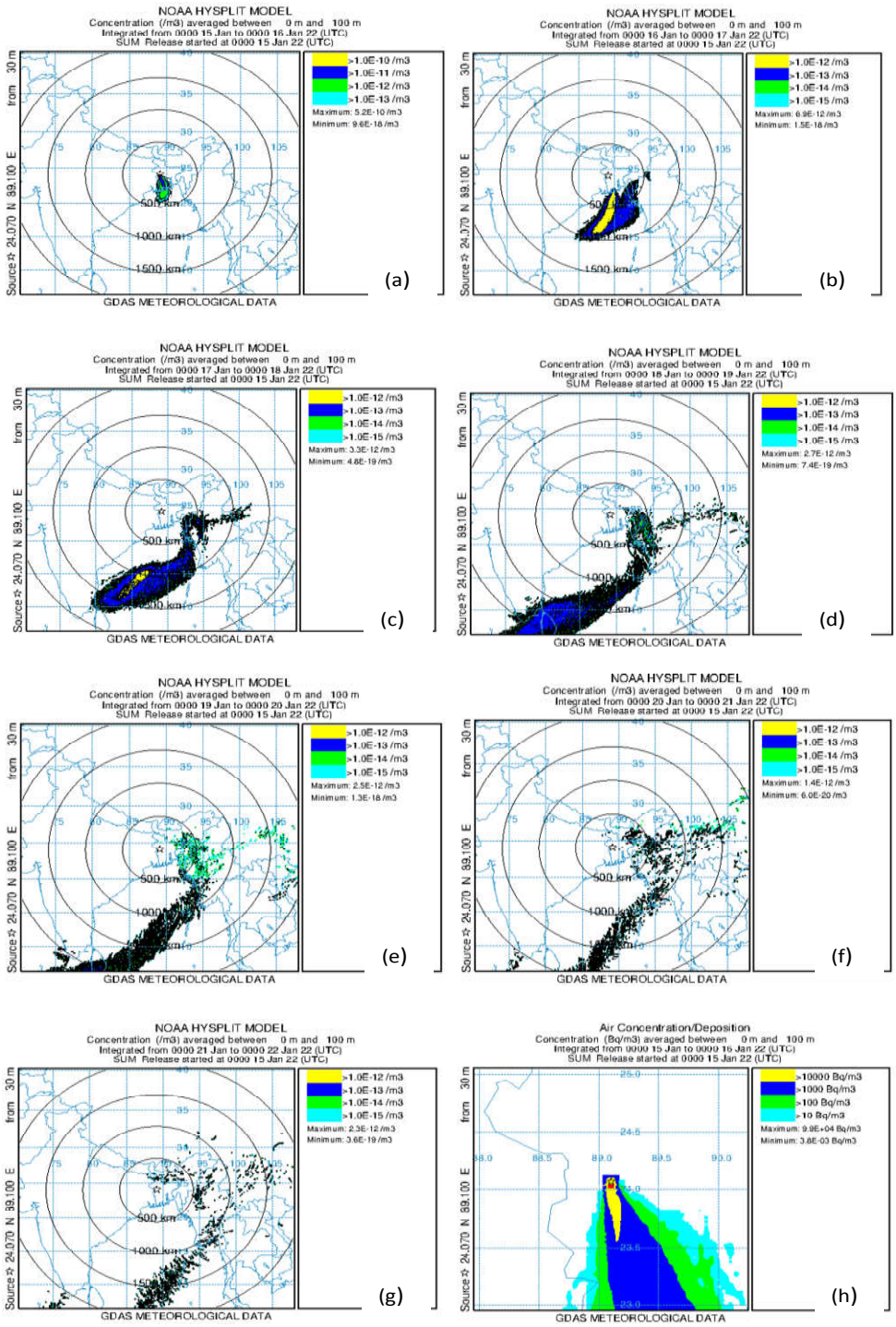

Figure 5-33: (a to g) Time-averaged normalized air concentration (/m^3) distribution respectively at 1st to 7th day **(dry weather month of January (15-21), 2022)** for the unit release rate (1 Bq/hr) and (h) **Volumetric air concentration** (Bq/m^3) distribution at 1st day for **10 hr release** during **CCM** LTSBO accident scenario from the **30 m release height** in **GDAS1 meteorological Data.**

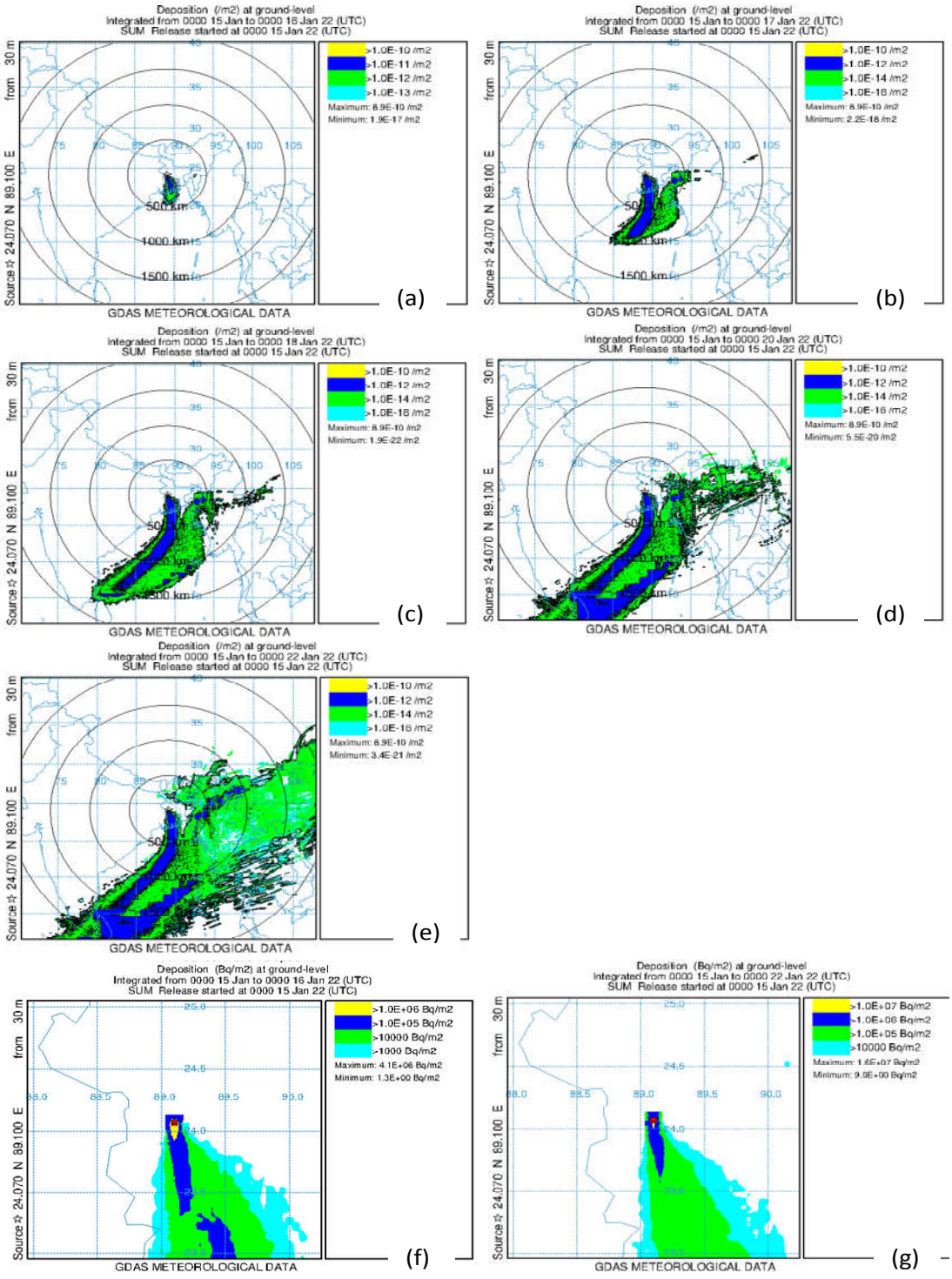

Figure 5-34: (a to e) Cumulative normalized ground deposition (/m^2) distribution respectively after 1 day, 2 days, 3 days, 5 days, and 7days from release starts at **dry weather month of 15th January 2022** for the unit release rate (1 Bq/hr) and (f & g) **cumulative ground deposition** (Bq/m^2) distribution after 1 day and 7 days for 10 hr release during **CCM** LTSBO accident scenario from the **30 m release height** in **GDAS1 meteorological Data.**

To accurately connect the observed air concentration and deposition patterns with meteorological conditions, we need to analyze air mass movements at various atmospheric levels rather than just at 30 meters high. **Figure 5-35** illustrates the forward trajectory patterns at 24-hour intervals, starting from altitudes of 30 m, 500 m, and 1,000 m under dry weather conditions. Two distinct meteorological datasets, GDAS1 and CDC1, were used to gather this data for January 15th of 2021 and 2022. The vertical profiles of these trajectories at each altitude are also displayed in the figure.

The **Figure 5-35** demonstrates that on most days, during 30 m release height, the radioactive plume follows a 30-meter trajectory, with a few deviations. When released at heights of 500 meters or 1,000 meters, the plume becomes more spread out and widens over time. Even though it starts at these higher altitudes, the plume tends to stay below 500 meters as days progress. Once released, the plume is influenced by wind patterns that correspond to its release altitude. While it may initially follow a specific path at 500 meters or 1,000 meters, it starts to expand both horizontally and vertically. This expansion causes some parts of the plume to be caught by air masses at different altitudes, which can have their own trajectories. As a result, while the main body of the plume may stick to its established path, smaller fragments of radioactive material can be carried in different directions by air masses at higher or lower altitudes. This dynamic explains why the area affected by the radioactive cloud expands over time and how radioactive deposition can occur in places not directly along the main trajectory.

The airborne concentration and ground deposition patterns mentioned earlier are affected by the spatial distribution of particle positions, along with the meteorological conditions present during the accident. As shown in **Figure 5-36**, over time, the number of simulated particles decreased significantly. On the first day, more than 10,000 particles were tracked within a 10-hour period, but by the seventh day, this number fell to just over 1,000. By the eighth day, no particles remained.

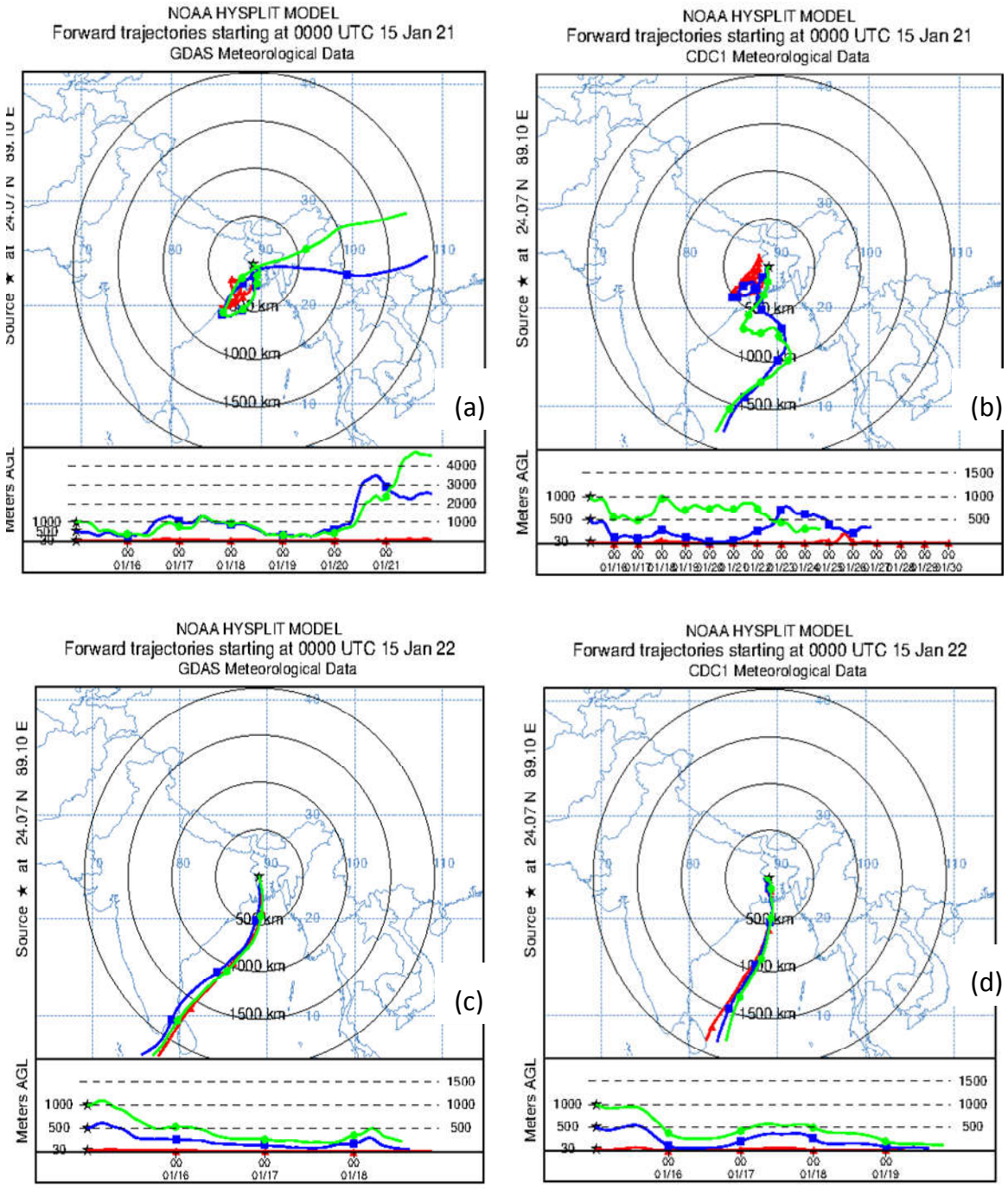

Figure 5-35: Airflow forward trajectories pattern at 24 hr intervals starting at 30 m, 500 m, 1000 m release height during **dry weather** month of **January 2021 and 2022** for two meteorological datasets with vertical profiles of trajectories.

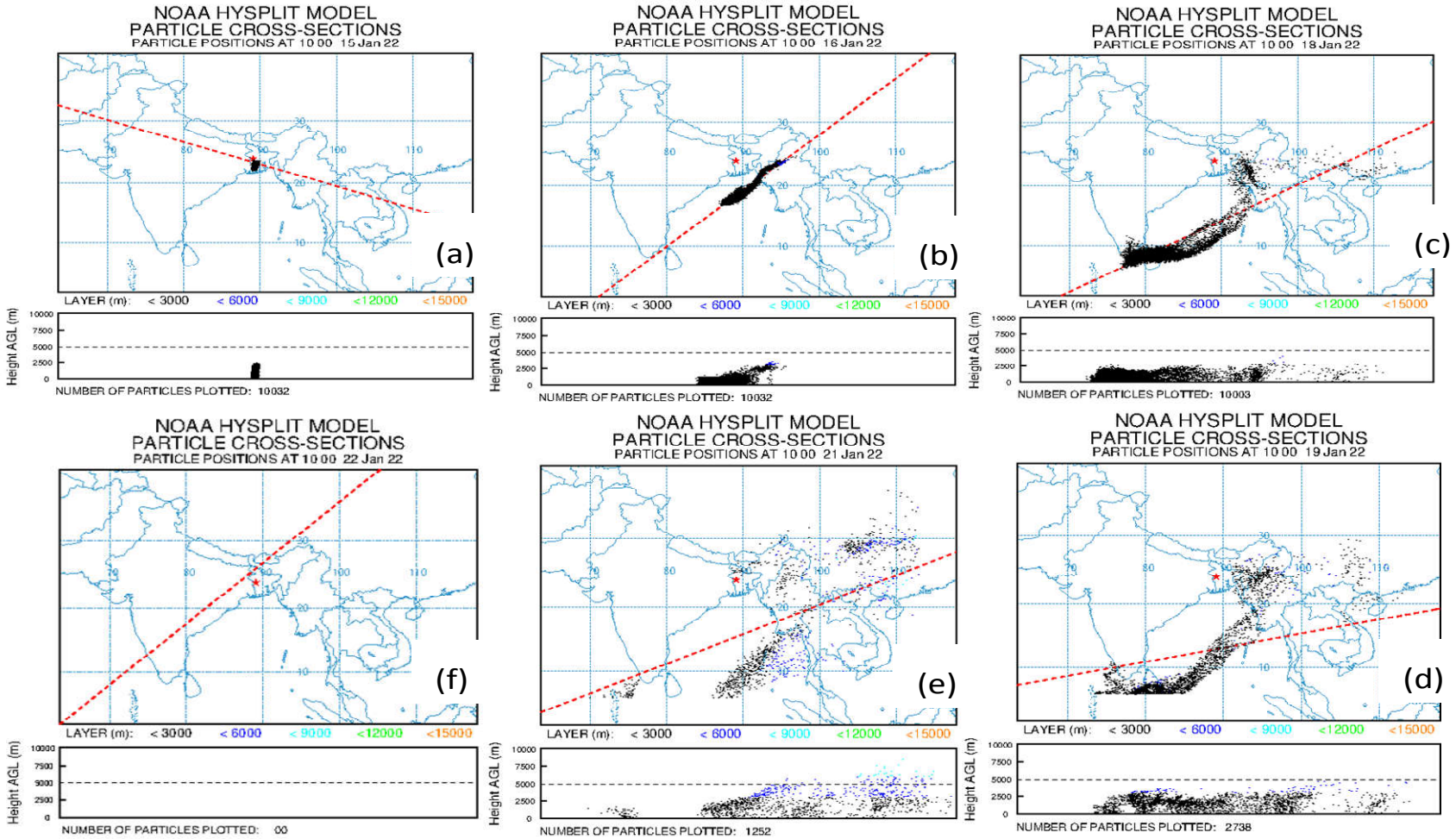

Figure 5-36: Particle cross-sections trajectory position after (a) 10 hr (b)2nd day (c) 4th day, (d) 5th day, (e) 7th day and (f) 8th day, simulation starting from **dry weather month of January 15th, 2022**.

5.1.13.2 Distribution Pattern in Wet Weather Month of July

Based on GDAS1 meteorological data, **Figure 5.37(a to h)** illustrates the changes in air concentration over the first seven days following the LTSBO-CCM event, which occurred in July 2022 during wet weather month. Figure **5-37(a & h)** show that the plume had an impact on Bangladesh's northwest on the first day. The most radioactive part was concentrated in a narrow strip spanning approximately 30 km across the Ishurdi–Pabna, Lalpur–Natore, and Bagha–Rajshahi areas. The peak volumetric air concentration levels near the release point is on the order of 10^4 Bq/m³. Within the first 24 hours, the radioactive plume spread approximately 800 km toward the north-central region of India. ,

By the second day, the plume's activity levels had decreased by two orders of magnitude in its most radioactive zone, ranging between factors of 10^{-12} and 10^{-15} m^{-3}, compared to 10^{-10} to 10^{-13} m^{-3} on the first day of time-averaged normalized air concentration. The most active portion of the plume had by then shifted to the north-central region of India, approximately 1,000 km from the accident site, affecting only the northern part of Bangladesh. On the third day, the plume continued to disperse toward the northwest, nearing the Pakistan border. At that time, the most active part of the plume exhibited a normalized air concentration of approximately 2.2×10^{-12} m^{-3}.

Figure 5-38(a to g) displays the cumulative ground deposition of radioactivity after the accident based on the meteorological data from GDAS during the wet weather month of July 2022. The oscillating movement of the radioactive cloud across the region caused significant deposition in northeastern India. According to **Figure 5-38(f),** after first day of the accidental release, the highest levels of deposition were found in northwestern Bangladesh, such as Ishurdi–Pabna, Lalpur, Boraigram–Natore, and Bagha–Charghat in the Rajshahi district recorded values exceeding 10^5 Bq/m² within a 60 km distance. The elevated deposition in northeastern Bangladesh resulted from the plume's location over this region during the initial 24 hours.

As shown in Figure **Figure 5-38(g),** seven days after the accident, the cumulative ground deposition affected areas up to 100 km from the release point in the order of 10^5 Bq/m². It crossed Bangladesh through the Chapainawabganj district, impacting regions like Ishurdi,

Natore, and Rajshahi. In northern West Bengal, particularly in Murshidabad, Berhampore, and parts of Jharkhand, cumulative ground deposition levels ranged from 1000 to 10000 Bq/m².

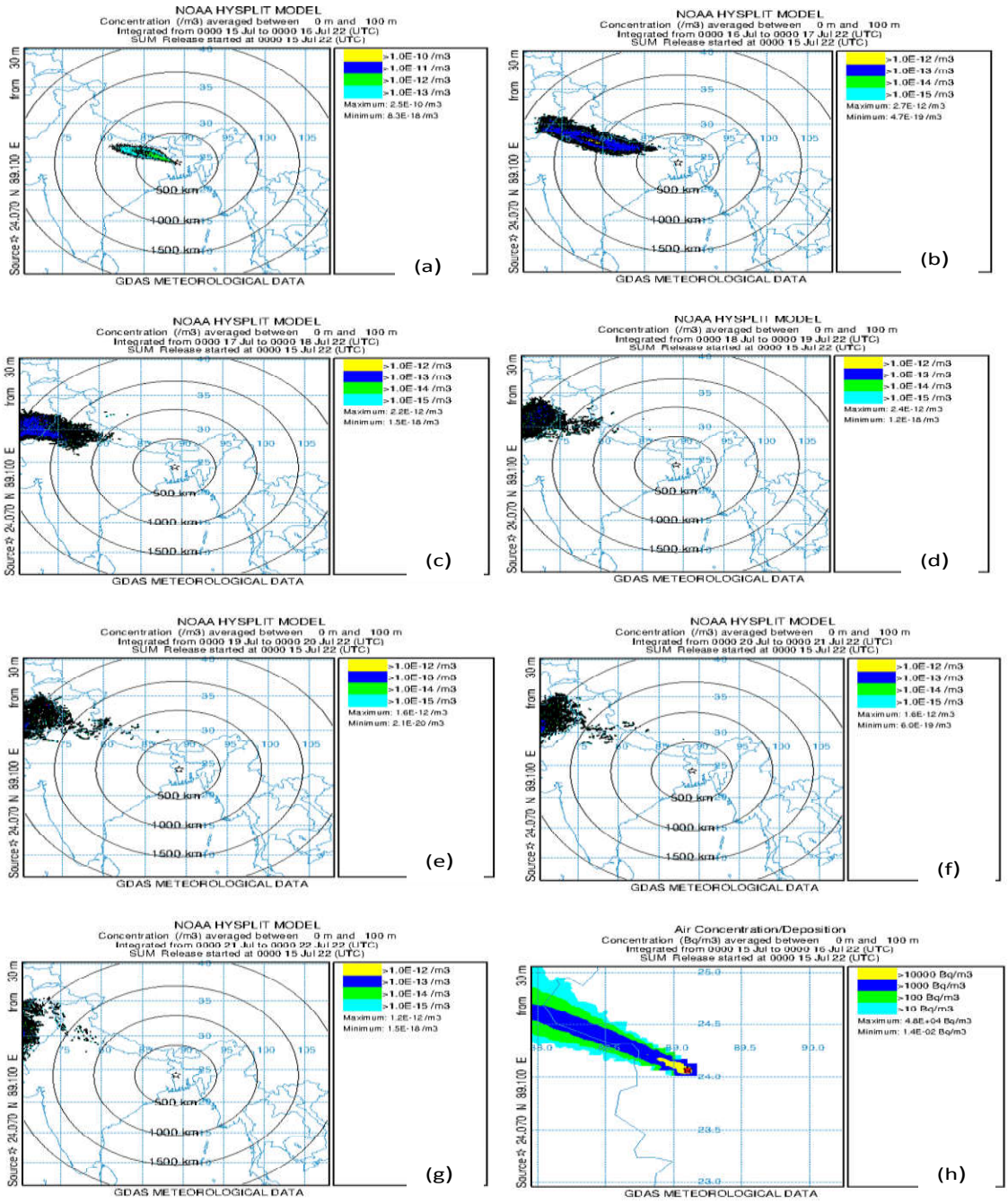

Figure 5-37: (a to g) Time-averaged normalized air concentration (/m^3) distribution respectively at 1st to 7th day **(wet weather month of July (15-21), 2022)** for the unit release rate (1 Bq/hr) and (h) **Volumetric air concentration** (Bq/m^3) distribution at 1st day for **10 hr release** during **CCM** LTSBO accident scenario from the **30 m release height** in **GDAS1 meteorological Data.**

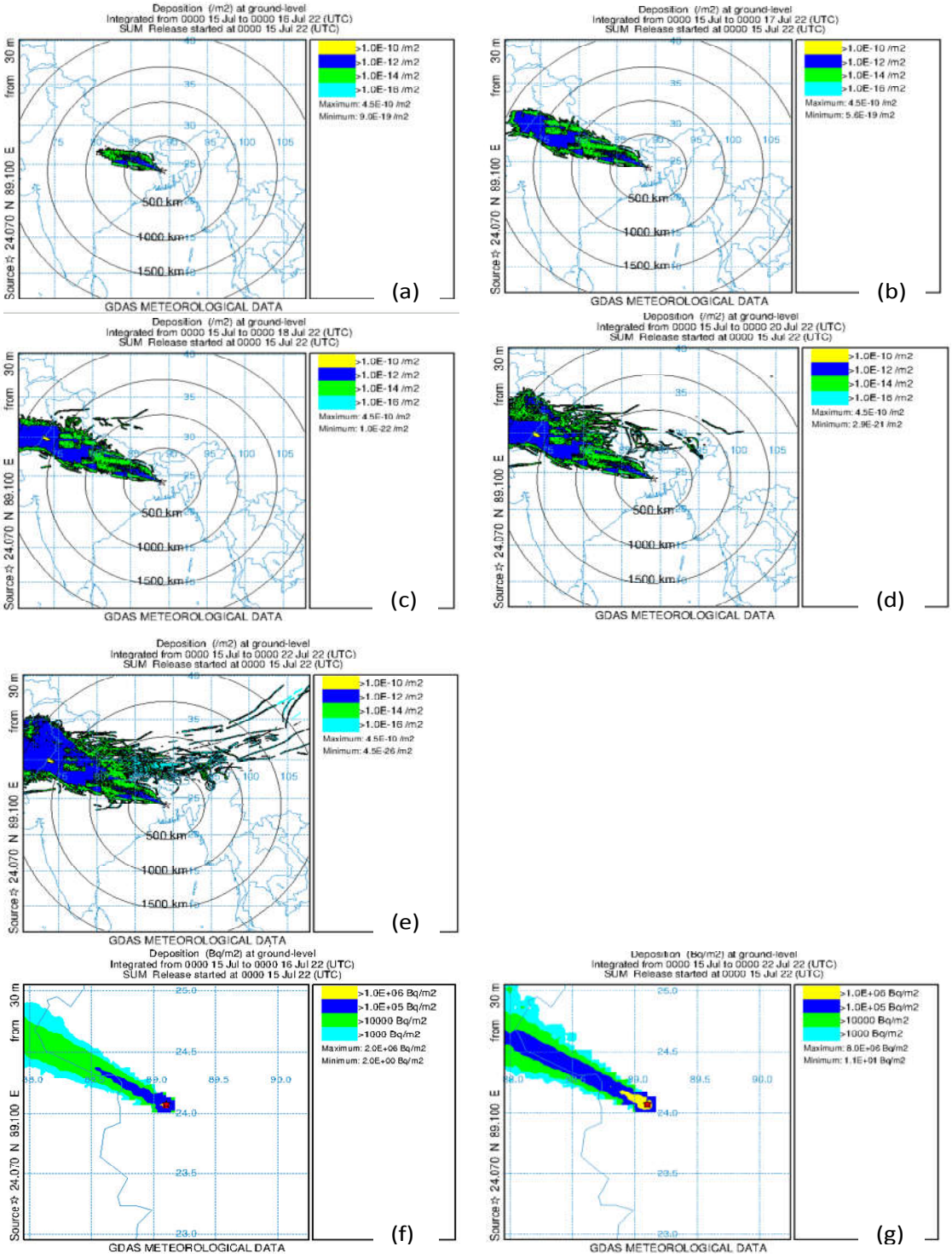

Figure 5-38: (a to e) Cumulative normalized ground deposition (/m^2) distribution respectively after 1 day, 2 days, 3 days, 5 days, and 7days from release starts at wet **weather** month of **15th July 2022** for the unit release rate (1 Bq/hr) and (f & g) **cumulative ground deposition** (Bq/m^2) distribution after 1 day and 7 days for 10 hr release during **CCM** LTSBO accident scenario from the **30 m release height** in **GDAS1 meteorological Data.**

Airflow forward trajectories of the radioactive cloud vary significantly under CDC1 and GDAS1 meteorological datasets in the year of 2021 and 2022 for the wet month of July are shown in **Figures 5-39**. These trajectories tend to rise to higher altitudes, often exceeding 5000 meters over time. In contrast, during dry month of January, trajectories stay lower and move more slowly. Air parcels mostly stayed over northern Bangladesh on the first day during July 2021 (**Figures 5-39(a & b)** trajectories), but in July 2022 (**Figures 5-39(c & d)** trajectories), the trajectories quickly crossed Bangladesh and entered West Bengal. However, in the wet weather month of July, the trajectories quickly exit the release area, traveling as far as 800 km in just one day. In contrast, it takes approximately two days to cover the same distance during the dry weather month of January.

On the third and fourth days, upper-atmospheric winds transported the radioactive cloud eastward. The plume was located over Assam and Thailand in the July 2021 scenario. Over the subsequent three days, the plume became more dispersed and was carried westward for CDC1 datasets, impacting a broad region bordered by India on the western side and extending the radioactive influence. By the end of the seven-day period, the trajectories for July 2021 extend as far as the southern regions of China, crossing Assam and Myanmar over a span of 1,000 km for GDAS1. For both datasets during July 2022, the trajectories cross central India and reach the eastern part of Pakistan.

Figure 5-40 illustrates how the quantity of simulated particles dramatically dropped over time. Over 10,000 particles were monitored in ten hours on the first day, but by the seventh day, that number had dropped over 3,000. There were no simulated particles left after the eighth day.

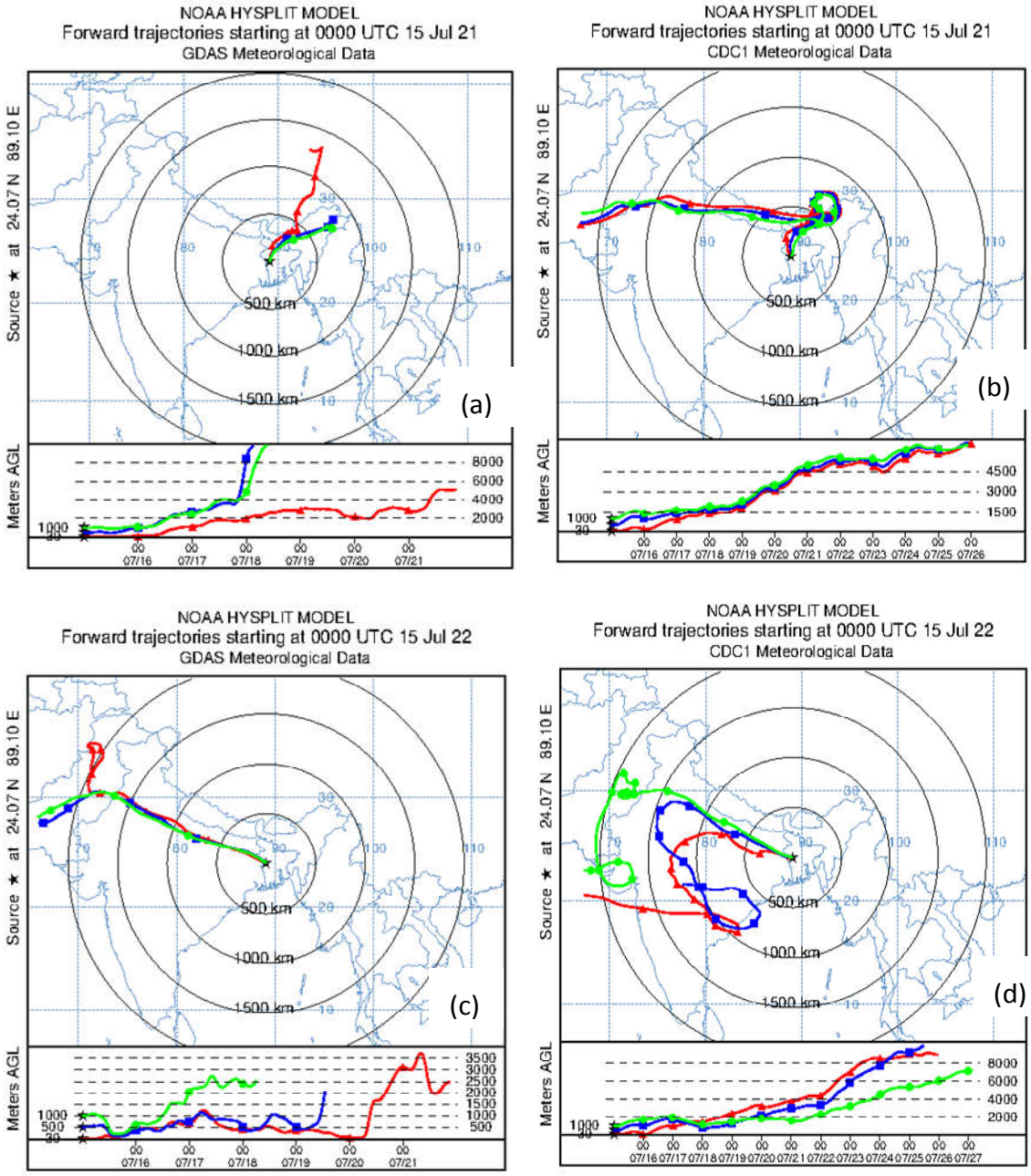

Figure 5-39: Airflow forward trajectories pattern at 24 hr intervals starting from **30 m, 500 m, 1000 m** release height during **wet weather m**onth of **July 2021 and 2022** for two meteorological datasets with vertical profiles of trajectories.

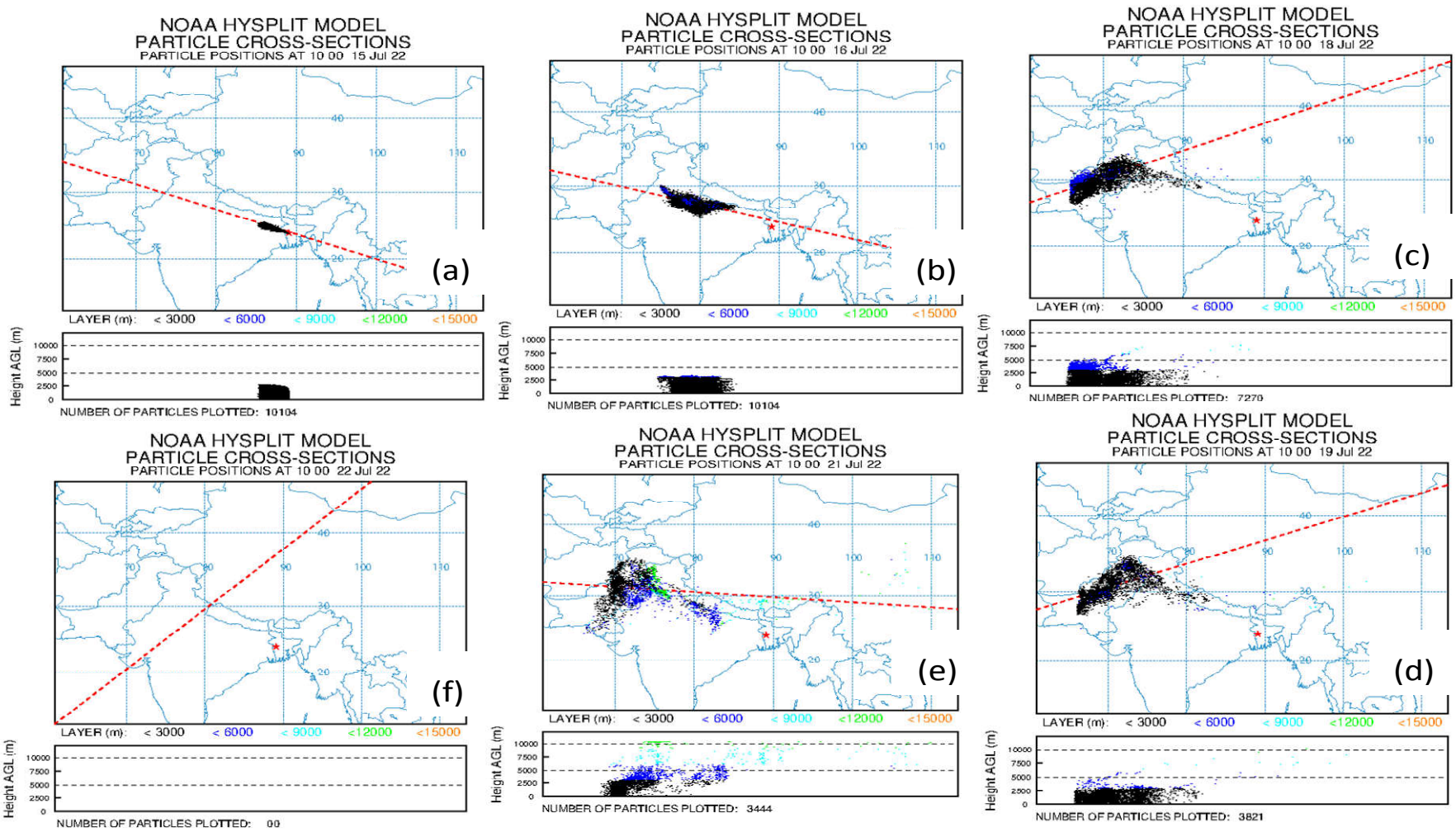

Figure 5-40: Particle cross-section trajectory position after (a) 10 hr (b)2nd day (c) 4th day, (d) 5th day, (e) 7th day and (f) 8th day, simulation starting from wet **weather month of July 15th, 2022**.

5.1.14 Release Height Effects in Air Concentration and Ground Deposition

The height of the release affects the atmospheric spread of radioactivity. Simulations were carried out at two elevations—30 meters (the equipment hatch position at 30 meters is the most likely to leak) and 500 meters (due to buoyant lift) above ground level—to assess the effect of release height. When radionuclides are released straight from the reactor building without any mechanical or buoyant lift, the release height is 30 meters. The 500-meter release height, on the other hand, allows for broader dispersion because of the higher elevation, simulating a scenario in which emissions are forcefully injected into the upper atmosphere.

Figures 5-41 and 5-42(b & d) depict the air concentration evolution and cumulative ground deposition patterns for the 500-meter release, respectively. The 30-meter release results for air concentration and ground deposition are shown in **Figure 5-33 and Figure 5-42(a & c)**, respectively. In comparison to the 500-meter release, the 30-meter scenario had roughly three times the maximum air concentrations and six times the ground deposition on the first day after the release. By the second day, both heights' spatial distributions of the plume and related air concentrations seemed comparable. In the next few days , significant variations in the time-averaged air concentration arose, demonstrating the complex connection between vertical release levels and atmospheric transport and plume behavior.

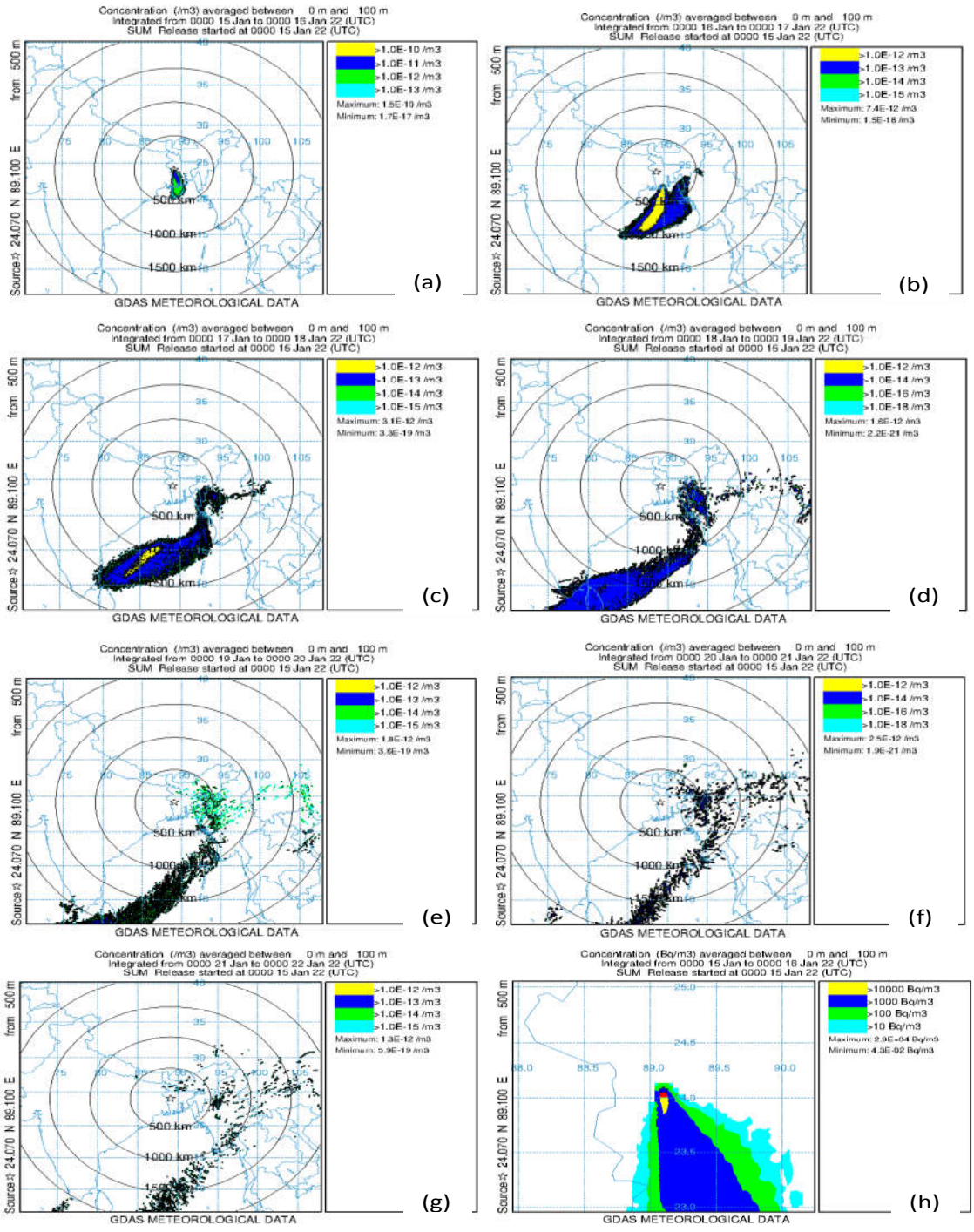

Figure 5-41: (a to g) Time-averaged normalized air concentration (/m^3) distribution respectively at 1st to 7th day **(dry weather month of January (15-21), 2022)** for the unit release rate (1 Bq/hr) and (h) **Volumetric air concentration** (Bq/m^3) distribution at 1st day of **10 hr release** during **CCM** LTSBO accident scenario from the **500 m release height** in **GDAS1 meteorological Data.**

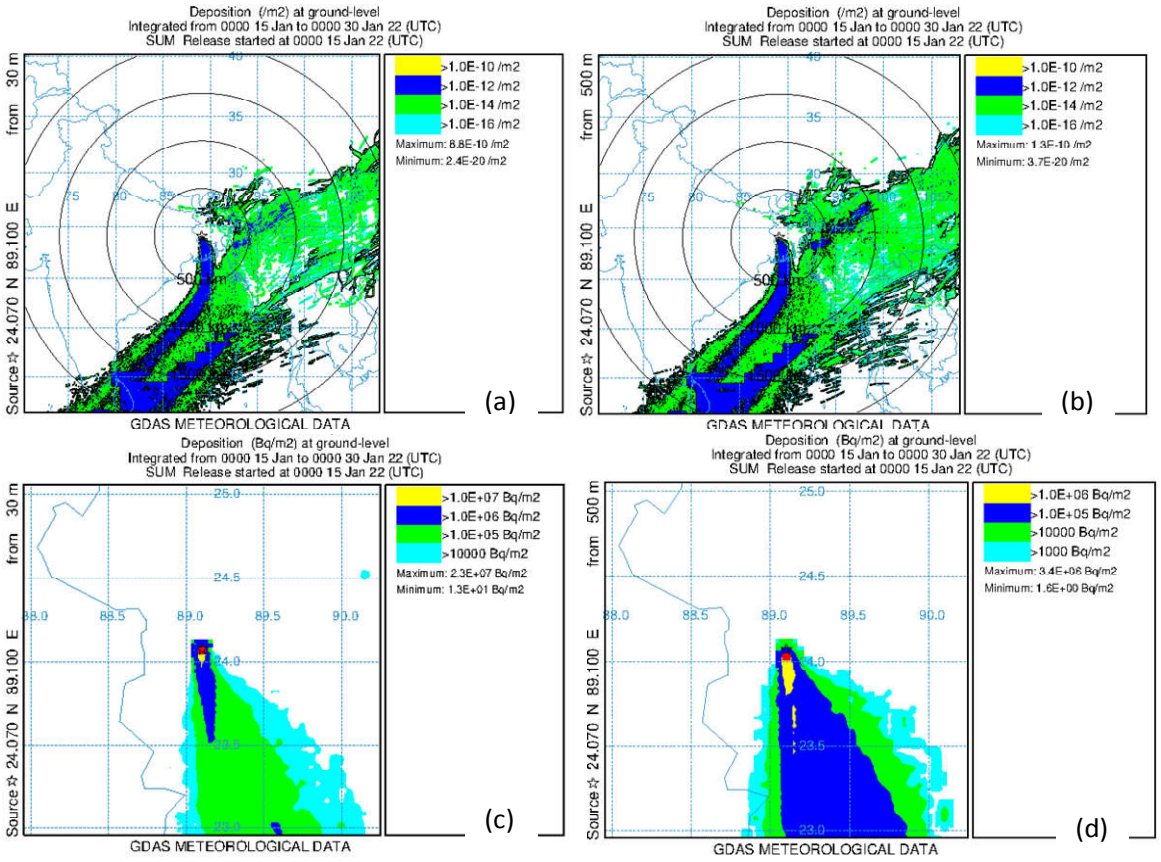

Figure 5-42: 15 days **after cumulative normalized ground deposition** (/m^2) patterns from (a**) 30 m height** (b) **500 m height** for unit release rate (1 Bq/hr) and **Cumulative ground deposition** (Bq/m^2) from (c) **30 m height** (d) **500 m height** for **CCM LTSBO** of **10 hr release** starting during **dry weather month of January 15th, 2022**.

5.1.15 Release Duration Effects in Air Concentration and Ground Deposition

The overall quantity of radioactive material carried from the source to possible receptors is influenced by the duration of release. A short-duration release that simulated a 3-hr accident (PCM) and a longer-duration release that simulated a 10-hr event (CCM) were the two scenarios that were investigated in this study. The air concentration development over the first seven days following the 3-hr release is depicted in **Figure 5-43**, and the results for the 10-hr scenario are shown in **Figure 5-37**. The results show that, in comparison to the 3-hr scenario, the 10-hr release produces noticeably higher air concentrations. This demonstrates how longer

release times raise atmospheric radioactivity, which may have more detrimental effects on the environment and human health.

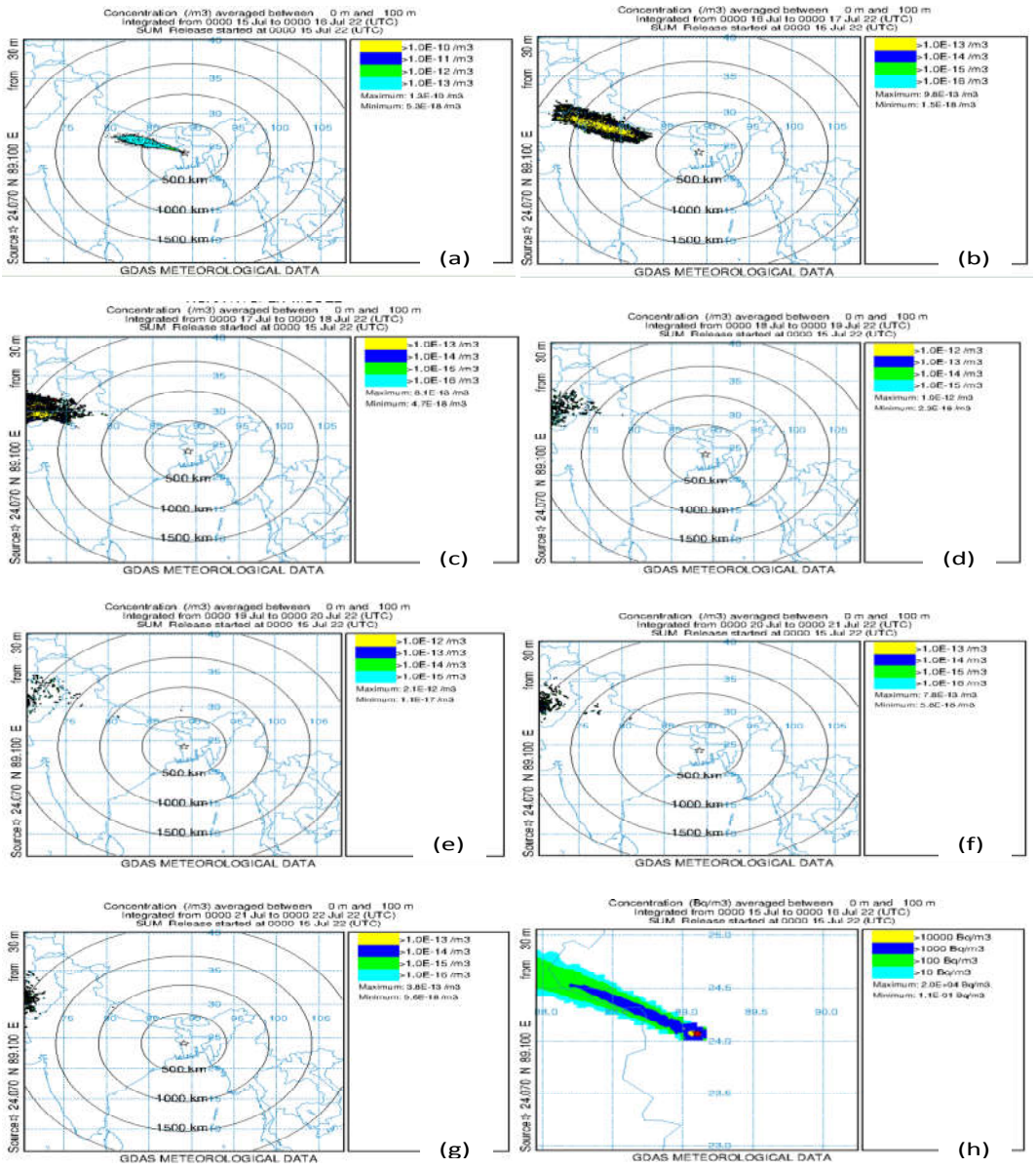

Figure 5-43: (a to g) Time-averaged normalized air concentration (/m^3) distribution respectively at 1st to 7th day **(wet weather month of July (15-21), 2022)** for the unit release rate (1 Bq/hr) and (h) **Volumetric air concentration** (Bq/m^3) distribution at 1st day of **3 hr release** during **PCM** LTSBO accident scenario from the **30 m release height** in **GDAS1 meteorological Data.**

Furthermore, for both release duration scenarios, **Figure 5-44** shows the cumulative ground deposition of radioactive material over a period of 15 days. In both instances, the highest

deposition occurs in the same area, which is located near the release site. In the 10-hr release scenario, the maximum cumulative ground deposition is 1.2×10^7 Bq/m². In contrast, the 3-hr release results maximum deposition of 4.9×10^6 Bq/m². This indicates that a longer release duration significantly increases ground contamination levels and expands the affected area. A longer emission period allows more radioactive material to be transported and deposited, which heightens the overall environmental impact.

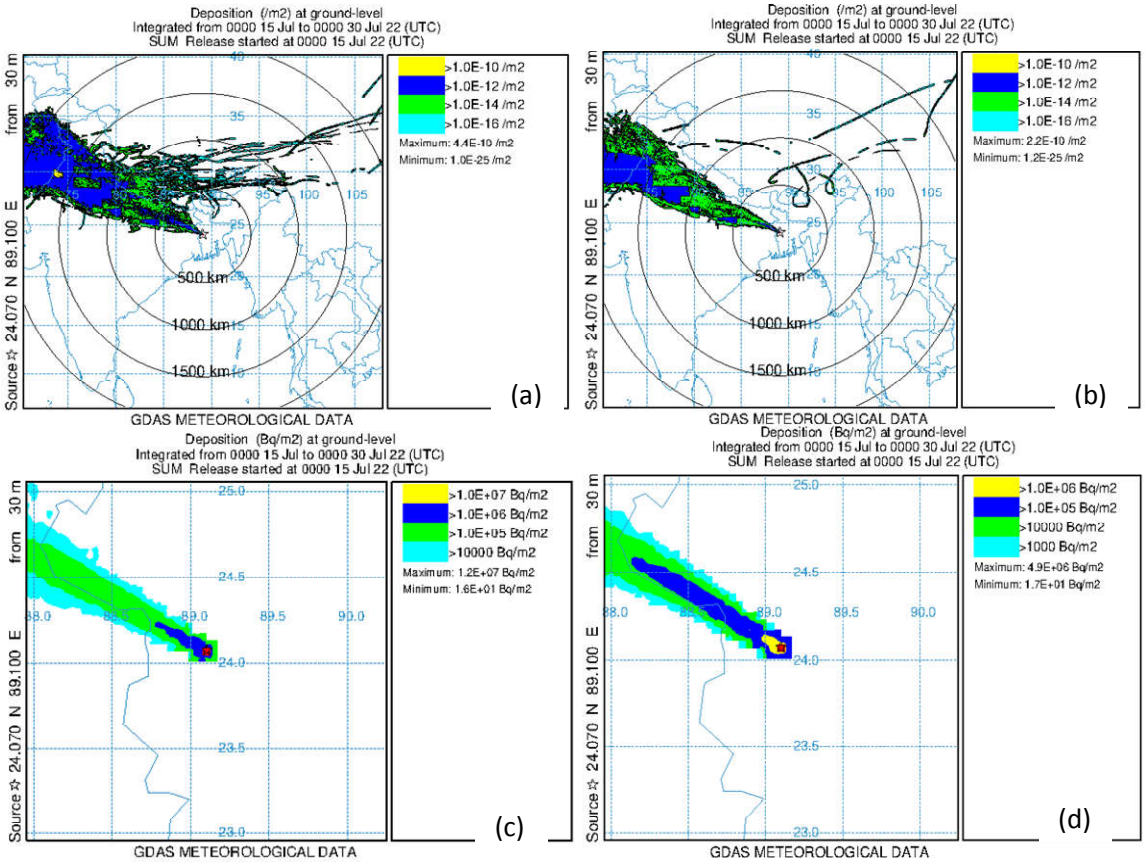

Figure 5-44: (a & b) 15 days **Cumulative normalized ground deposition** (/m^2) patterns for unit release rate (1 Bq/hr) in (a) CCM of **10 hr release** (b) PCM of **3 hr release** and **Cumulative ground deposition** (Bq/m^2) from accidental release during LTSBO event (c) CCM of 10 hr (d) PCM of 3 hr, release starting at **15th of wet weather month July 2022** from **30 m heights**.

5.1.16 GDAS1 and CDC1 Meteorological Dataset Effect

In both the CDC1 and GDAS1 meteorological datasets, respectively as shown in **Figures 5-45 and 5-33,** the radioactive cloud crossed the country by the second day following the release, primarily moving in a southwesterly direction in January and in a northwesterly direction in July (**Figure 5-37**). This rapid transport of air masses at all altitudes also accounts for the sharp decline in deposition flux values on either side of the plume's path. Therefore, the radioactive plume originating from the Rooppur accident predominantly impacted a limited region, largely determined by prevailing wind directions at the time of the release.

Figure 5-46 presents the development of ground deposition over the first 15 days of simulation using the CDC1 meteorological dataset, while corresponding results for the GDAS1 dataset under the same accident scenario and parameters are shown in **Figure 5-40**. The maximum deposition levels are significantly higher in the CDC1 case. In the first day after the accident, the CDC1 dataset predicts a peak cumulative ground deposition of 8.5×10^{7} Bq/m². In comparison, the GDAS dataset estimates a much lower peak of 2.0×10^{6} Bq/m² for a similar event. Additionally, the CDC1 dataset shows a larger affected area, underscoring how important meteorological input data is for atmospheric dispersion modeling.

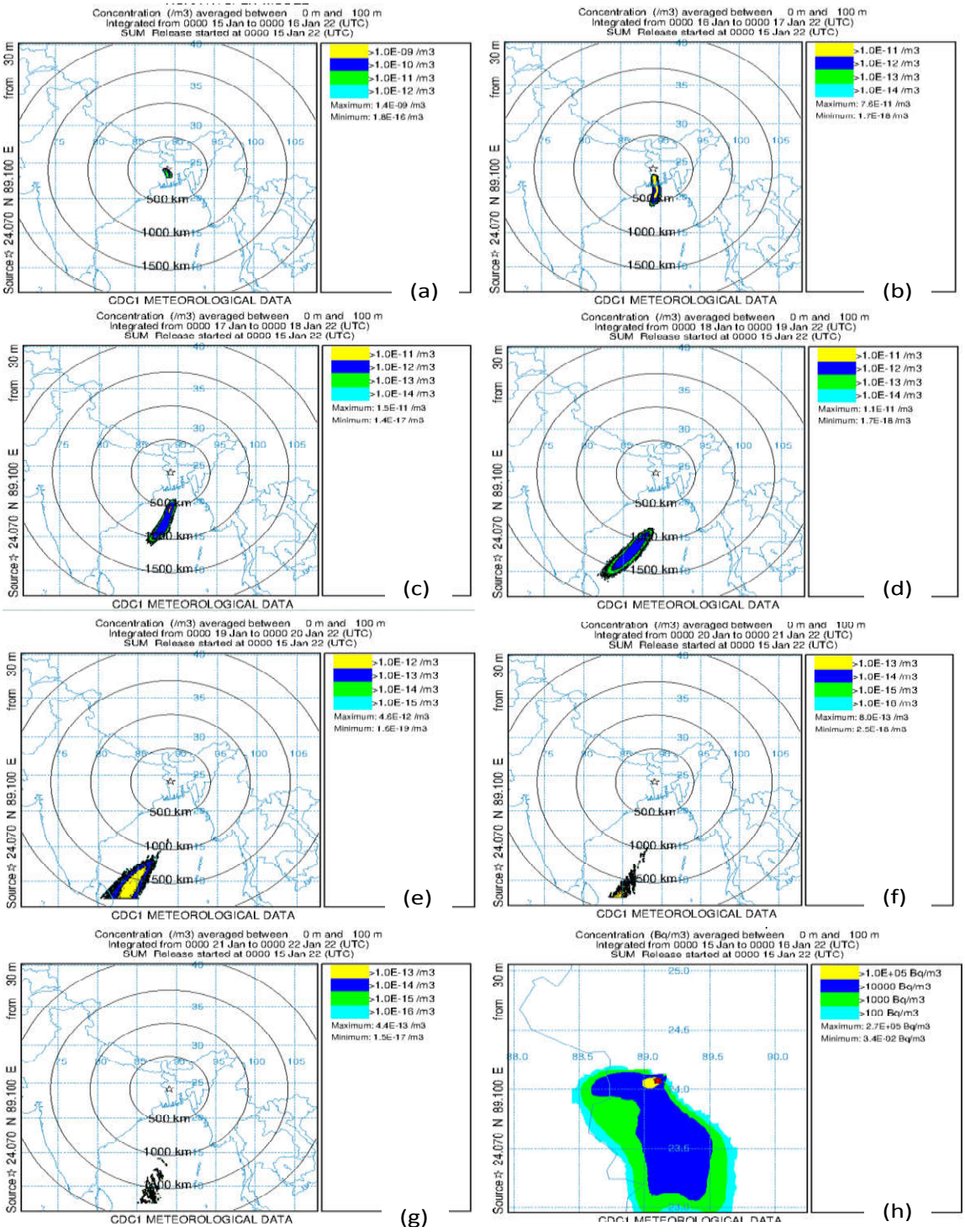

Figure 5-45: (a to g) Time-averaged normalized air concentration (/m^3) distribution respectively at 1st to 7th day **(dry weather month of January (15-21), 2022)** for the unit release rate (1 Bq/hr) and (h) **Volumetric air concentration** (Bq/m^3) distribution at 1st day of **10 hr release** during **CCM** LTSBO from the **30 m release height** in **CDC1 meteorological Data.**

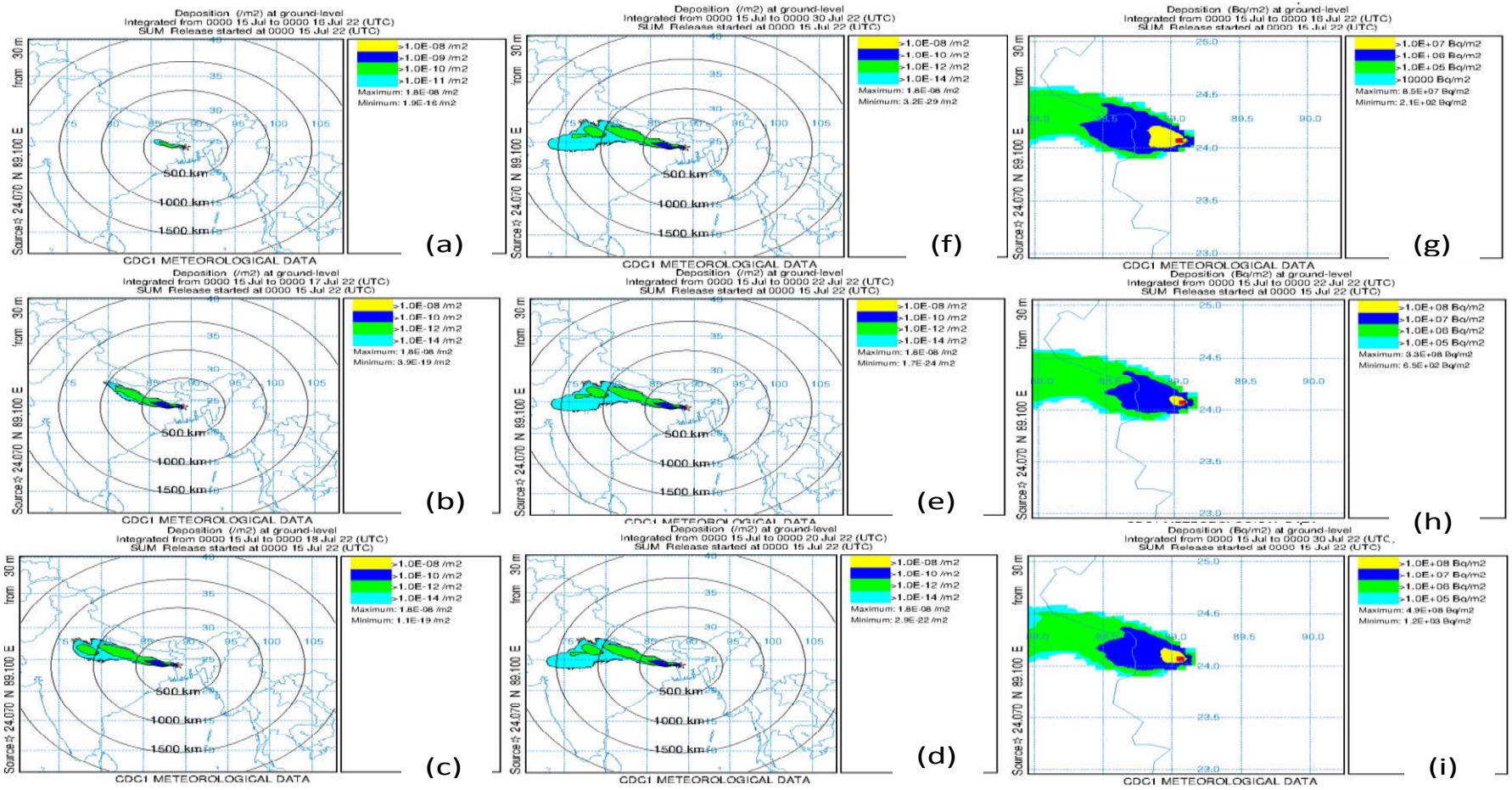

Figure 5-46: (a to f) Cumulative normalized ground deposition (/m^2) distribution respectively after 1 day, 2 days, 3 days, 5 days, 7days, and 15 days from release start at **wet weather of July 15th , 2022** for the unit release rate (1 Bq/hr) and (g &h) **Cumulative ground deposition** (Bq/m^2) distribution after 1 day, 7 days, and 15 days for **10 hr release** during **CCM** LTSBO from the **30 m release height** in **CDC1 meteorological Data.**

5.1.17 Air Concentration Uncertainty-Meteorological Data and Physics Model Ensemble

Figure 5-47(a & b) illustrates the probability distribution of air concentration based on meteorological data ensembles at an adjacent grid location near the Rooppur site along the plume direction with latitude and longitude coordinates of 24.0°N, 89.1°E for January and July. The concentration values come from the prob{xx} files of the ensemble analysis, which represent different points shown in the box plot. The 5^{th} and 95^{th} percentiles are indicated by the circles. The whiskers extend to reveal the 10^{th} and 90^{th} percentiles, while the box plot's boundaries show the inter-quartile range, more precisely the 25^{th} and 75^{th} percentiles. The line inside the box indicates the median concentration value, and a plus sign indicates the mean value. The plot depicts spanning 1-hr intervals. For the 10^{th} to 90^{th} percentile range, the concentration values vary by approximately one to three orders of magnitude for the month of January, whereas for the July dataset, the variation is above two orders of magnitude. This significant range is primarily due to the alteration of meteorological data by shifting one grid point, highlighting the sensitivity of concentration values to meteorological gradients.

Figure 5-48(a & b) displays box plots generated from the physics ensemble, which is based on 20 different variations. The ranges are narrower compared to those observed in the meteorological grid ensemble, within one to two orders of magnitude, particularly in the quartile range.

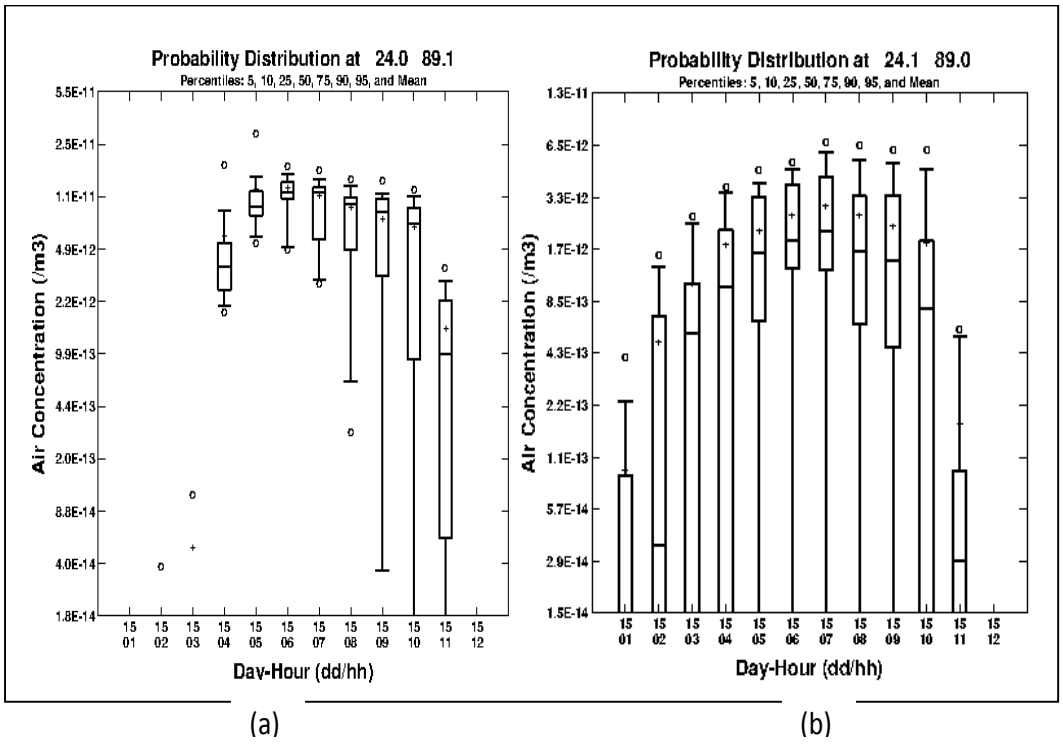

Figure 5-47: Air concentration Box plot distributions for Meteorological data Ensemble (a)dry (January) and (b) wet (July) months of 2022 in GDAS1 Meteorological Dataset.

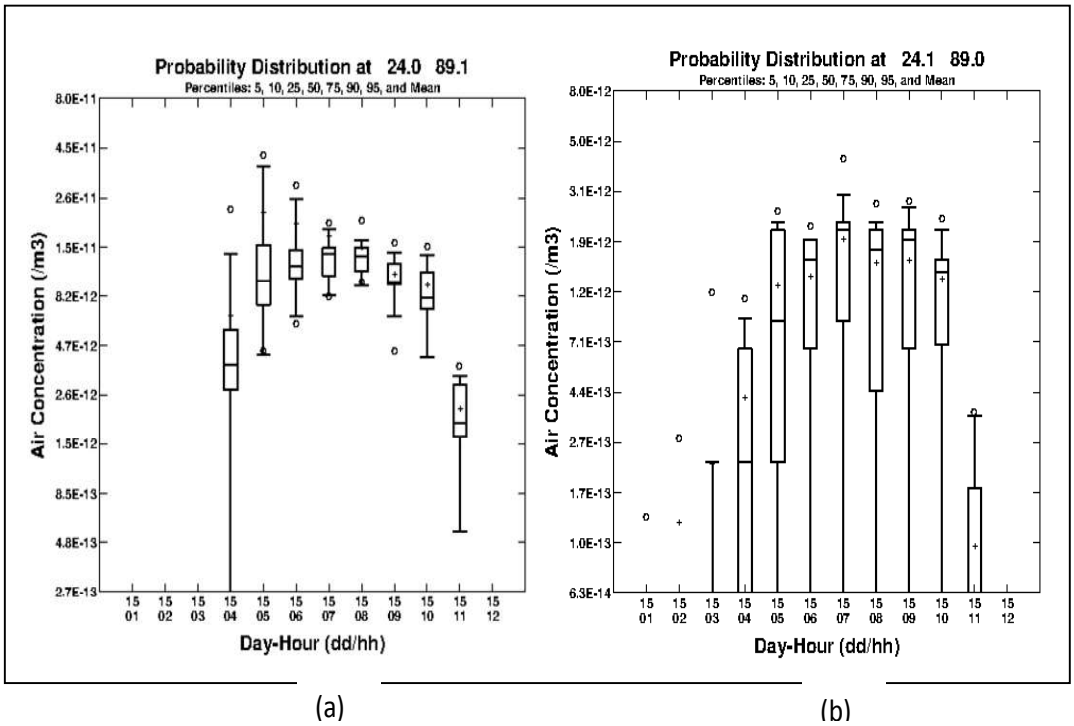

Figure 5-48: Air Concentration Box plot distributions for Physics Model Ensemble (a dry (January) and (b) wet (July) months of 2022 in GDAS1 Meteorological Dataset.

5.2 PART-B: Assessment of Emergency Planning Zones

For estimating the size of the EPZ, individual dispersion and dose assessments are performed for two assumed accident scenarios under 360 different weather conditions. The objective is to determine, with associated uncertainties, the required distances to satisfy the four dosimetric criteria for the PAZ and UPZ under various protective measures. The resulting exceedance distances are compiled into frequency distributions and cumulative histograms, showing the percentage of weather scenarios corresponding to each distance (Faisal et al., 2025*). Based on the distances exceeded in 95% of all scenarios and considering the effectiveness of emergency response measures, the approximate EPZ size for the Rooppur NPP is determined.

5.2.1 RBE Weighted Absorbed Dose to Red Bone Marrow ($AD_{\text{red bone marrow}}$)

5.2.1.1 Exceeded Distances for $AD_{\text{red bone marrow}}$ Dose Threshold

For PAZ size estimation, 1-day sheltering effects in red bone marrow dose are considered. Long-term sheltering effects (4-day sheltering) are also evaluated due to the large contribution of the ground shine in red bone marrow dose if early evacuation is not possible. **Figure 5-49(a & b)** shows the distances at which the PAZ dosimetric thresholds for 1 Gy of $AD_{\text{red bone marrow}}$ are exceeded to avoid severe deterministic effects in 360 weather scenarios with monthly/seasonal variation for LBLOCA and LTSBO events. If an individual is sheltered in a house for one day, the IAEA threshold of 1 Gy is projected to be exceeded within 0.3-2.6 km for daytime release and within 0.5-2.6 km for nighttime release in an LBLOCA event, whereas for an LTSBO event, the exceeded distances are within 0.4-3.7 km for daytime release and 0.8-3.8 km for nighttime release. During periods of moderate to heavy rainfall, the required distances increased for both scenarios. This is because rainfall enhances ground deposition further downwind, potentially expanding the area of concern for contamination control. Radiological doses via groundshine—one of the main exposure pathways to the red bone marrow—are considerably higher in rainy conditions, particularly between April and September, compared to dry weather periods from October to March. The threshold distances that exceed 1 Gy for acute doses of red bone marrow are nearly within 0.3-0.4 km for daytime and 0.5-0.8 km for nighttime release during no-rain scenarios in LBLOCA, while it is 0.4-1 km during LTSBO events.

---

* Article published from this thesis

If house sheltering is implemented for a longer period of time (4 days), the exceeded distances from the site are within 0.5-5.3 km in LBLOCA events and 0.7-7.5 km in LTSBO events. In the absence of rain, particularly during the dry weather, the exceeded distances are roughly 0.5-1.2 km for an individual sheltering 4 days in a house during LBLOCA release and 0.7-2.2 km in LTSBO. During rainy situations for 4 days of sheltering, the exceeding distances in LBLOCA reaches above 2.5 km and 4 km in LTSBO (Faisal et al., 2025*).

Distances are not exceeded beyond 0.5 km in LBLOCA and 0.7 km in LTSBO for an individual sheltering in a large building for one day. The exceeding distances for the four days of sheltering in a large building are within 0.9 km for LBLOCA events and 1.4 km for LTSBO events (Faisal et al., 2025*).

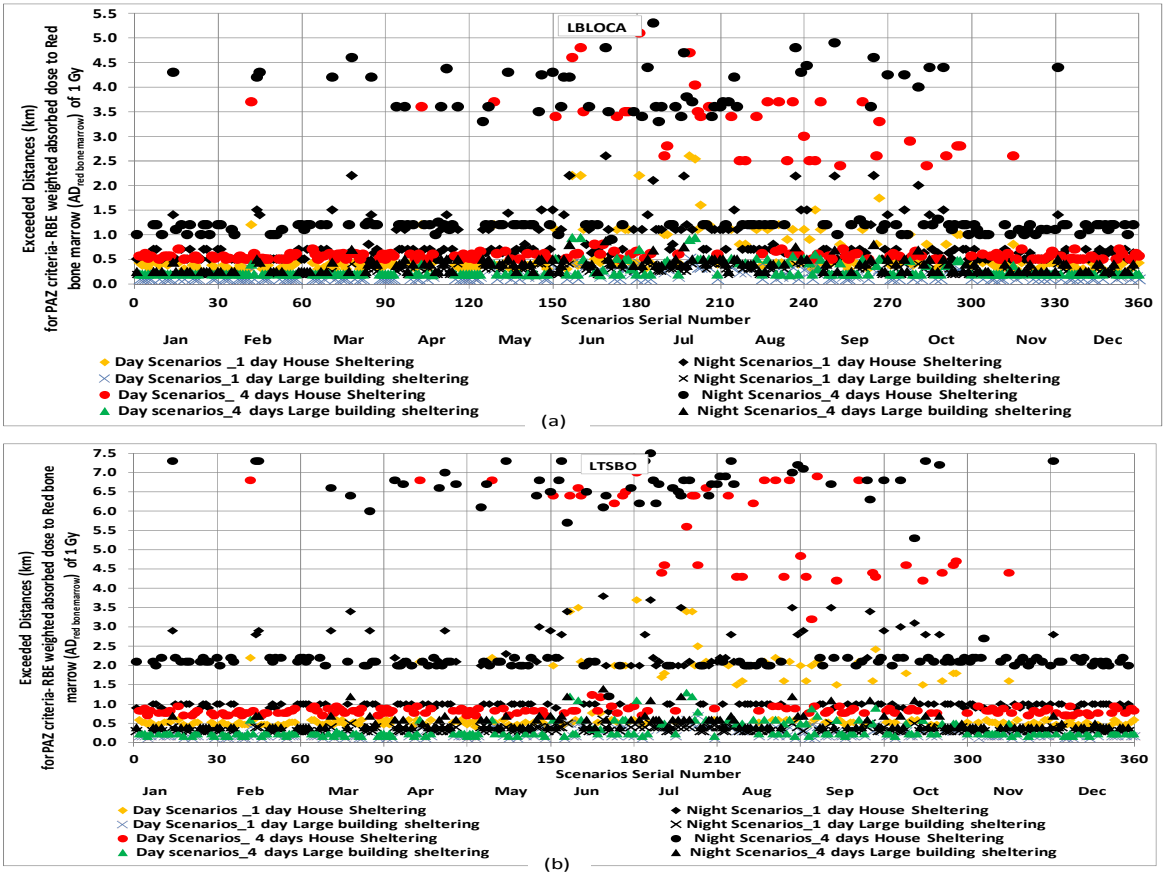

Figure 5-49: Month-wise 360 weather scenarios exceeded distances for PAZ dosimetric criteria (1 Gy of $AD_{red\ bone\ marrow}$) under different sheltering measures for (a) LBLOCA and (b) LTSBO (Faisal et al., 2025*).

* Article published from this thesis

The frequency distribution and covered percentage weather scenarios for exceeding the PAZ dosimetric criterion distances, receiving 1 Gy of $AD_{red\ bone\ marrow}$ in a day, experiencing 4 days of house sheltering, and the effects of large building sheltering for LBLOCA and LTSBO events are shown in **Figure 5-50(a to h)**. The percentage of weather scenarios covered as a function of distance is shown by cumulative histograms created based on the exceeded distances of the 360 weather scenarios in **Figure 5-49(a & b)**. The maximum distances at which red bone marrow threshold doses exceed 95% of all weather scenarios for 1-day house sheltering are 1.2-1.5 km in LBLOCA and 2.5-3.0 km in LTSBO; for 4-day sheltering, they are 4.0-4.5 km in LBLOCA and 6.5-7.0 km in LTSBO (Faisal et al., 2025*).

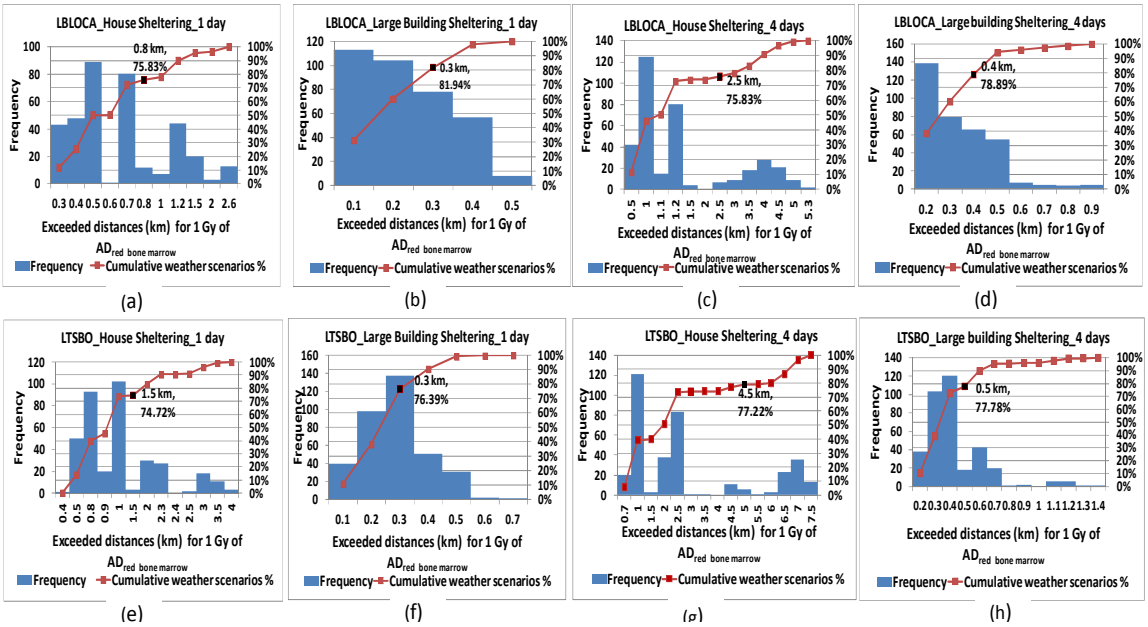

Figure 5-50: Frequency distribution of exceeded distances for 360 weather scenarios of PAZ dosimetric criteria (1 Gy of $AD_{red\ bone\ marrow}$) under different sheltering measures in (a to d) LBLOCA and (e to h) LTSBO postulated events with cumulative percentage coverage of exceeded distances.

5.2.1.2 Percentile Spatial Dose Distribution for $AD_{red\ bone\ marrow}$

Figures 5-51(a–d) present the 5th, 50th, and 95th percentile RBE-weighted absorbed doses to the red bone marrow ($AD_{red\ bone\ marrow}$) resulting from cloud shine, inhalation, one day of groundshine (sheltering_1 day), and four days of groundshine (sheltering_4 days) at varying distances, considering both house and large building sheltering during LBLOCA and LTSBO

* Article published from this thesis

scenarios. For one-day house sheltering, the dosimetric limit is exceeded at approximately 0.6 km for LBLOCA and 1.0 km for LTSBO based on the 50th percentile value. When sheltering in large buildings, these distances decrease to 0.2 km for LBLOCA and 0.3 km for LTSBO. Using the 95th percentile values, the exceeded distances for house sheltering reach about 1.5 km for LBLOCA and 3.0 km for LTSBO. In contrast, large building sheltering reduces these distances to 0.4 km and 0.5 km, respectively (Faisal et al., 2025*).

For four-day house sheltering, the 50th percentile exceeded distances are around 1.2 km for LBLOCA and 2.0 km for LTSBO. Under large building sheltering, these values reduce to 0.3 km and 0.4 km, respectively. At the 95th percentile, the exceeded distances for house sheltering range from 4–5 km for LBLOCA and 6–7 km for LTSBO, while large building sheltering limits them to approximately 0.4 km and 0.7 km, respectively. Overall, substantial dose reduction is achieved when sheltering in large buildings compared to houses (Faisal et al., 2025*).

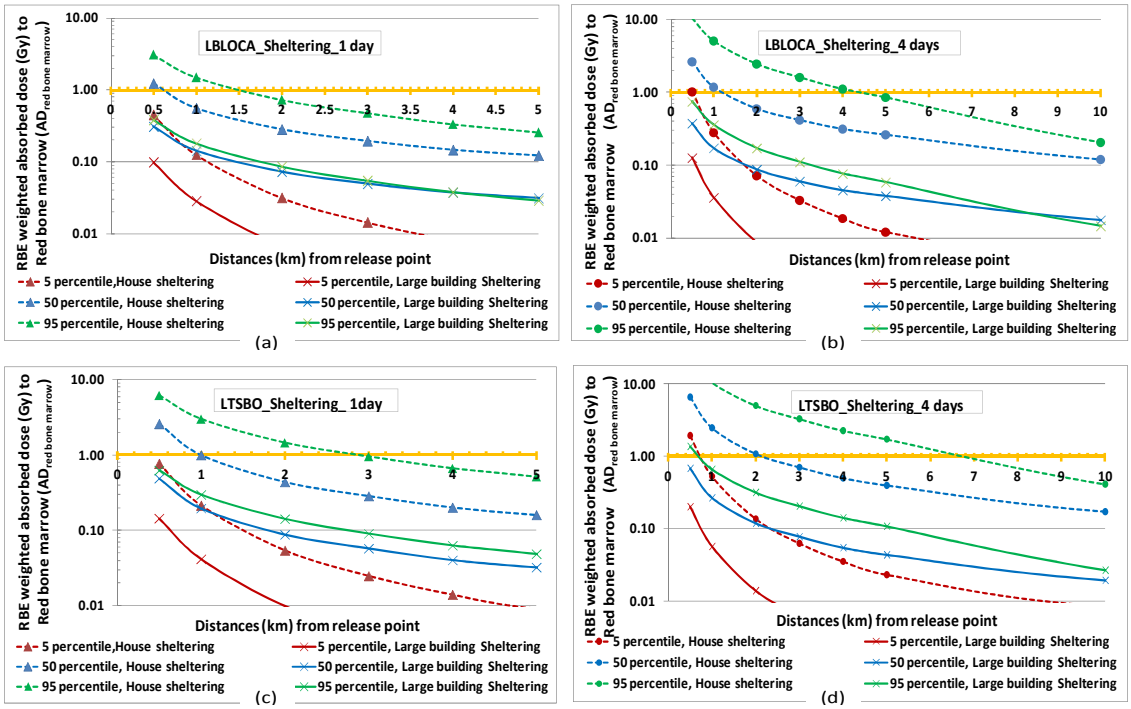

Figure 5-51: 5, 50 and 95 Percentile RBE weighted absorbed dose to the red bone marrow ($AD_{red\ bone\ marrow}$) vs. distances under different sheltering measures for (a & b) LBLOCA and (c & d) LTSBO; the solid yellow line indicates the IAEA criteria (Faisal et al., 2025*).

* Article published from this thesis

5.2.2 RBE Weighted Absorbed Dose to the Fetus from Inhalation ($AD_{fetus, inh}$)

5.2.2.1 Exceed Distances for $AD_{fetus, inh}$ Dose Threshold

Figures 5-52(a & b) illustrate the distances at which a fetal thyroid absorbed dose ($AD_{fetus, inh}$) of 1 Gy may be exceeded under different protective measures—house or large building sheltering, with and without the use of ITB—during LBLOCA and LTSBO scenarios.

For pregnant women sheltering in a house without ITB, distance exceeds within 2.7–5.3 km during daytime LBLOCA releases and 3.8–36 km at night. For LTSBO events, distances increase to 3.8–8.2 km during the day and 5–55 km at night. Nighttime releases show larger exceeded distances due to more stable atmospheric conditions (stability classes 'E' and 'F') compared to unstable daytime conditions (classes 'B' and 'C') (Faisal et al., 2025*). Additionally, inhalation doses decrease during rainy periods due to the washout of airborne radionuclides, particularly from June to August, reducing the distances where thresholds are exceeded.

When ITB is used in house sheltering, exceeded distances drop to 0.8–1.6 km for LBLOCA during the day and 1.3–9.1 km at night, while LTSBO events show distances of 1.2–2.1 km during daytime and 1.8–15.5 km at night. Under large building sheltering, distances further decrease to 0.5–4.3 km for LBLOCA and 0.7–7.3 km for LTSBO (Faisal et al., 2025*).

Figures 5-53(a to h) present the frequency distribution and cumulative included weather scenarios for exceeded distances of 1 Gy $AD_{fetus,inh}$ for sheltering with and without ITB in LBLOCA and LTSBO events.

5.2.2.2 Percentile Spatial Dose Distribution for $AD_{fetus, inh}$

Figures 5-54(a–d) present the variation of the RBE-weighted absorbed dose to the fetus from inhalation ($AD_{fetus, inh}$) with distance for LBLOCA and LTSBO events, considering the 5th, 50th, and 95th percentile weather scenarios. They also highlight the impact of different protective measures, including house sheltering, large building sheltering, and the use of ITB.

* Article published from this thesis

For house sheltering without ITB, the 1 Gy dosimetric limits is exceeded at approximately 5 km for LBLOCA and 7 km for LTSBO when using the 50th percentile value. Under large building sheltering, these distances are reduced to about 3 km for LBLOCA and 4 km for LTSBO. At the 95th percentile, the exceeded distances increase significantly, ranging from 30–35 km for LBLOCA and 40–45 km for LTSBO under house sheltering. For large building sheltering, the distances are notably lower, between 15–20 km for LBLOCA and 25–30 km for LTSBO (Faisal et al., 2025*).

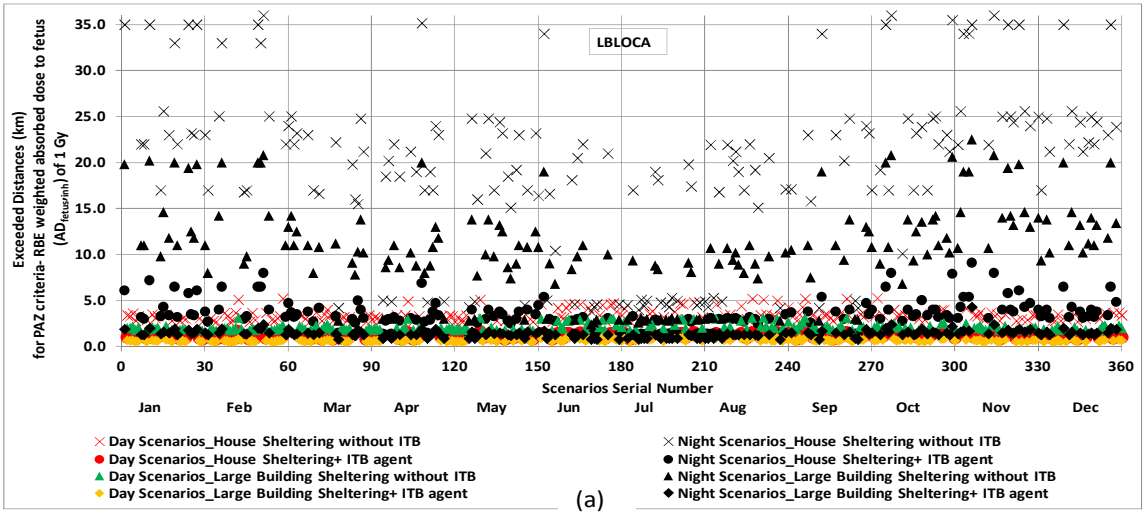

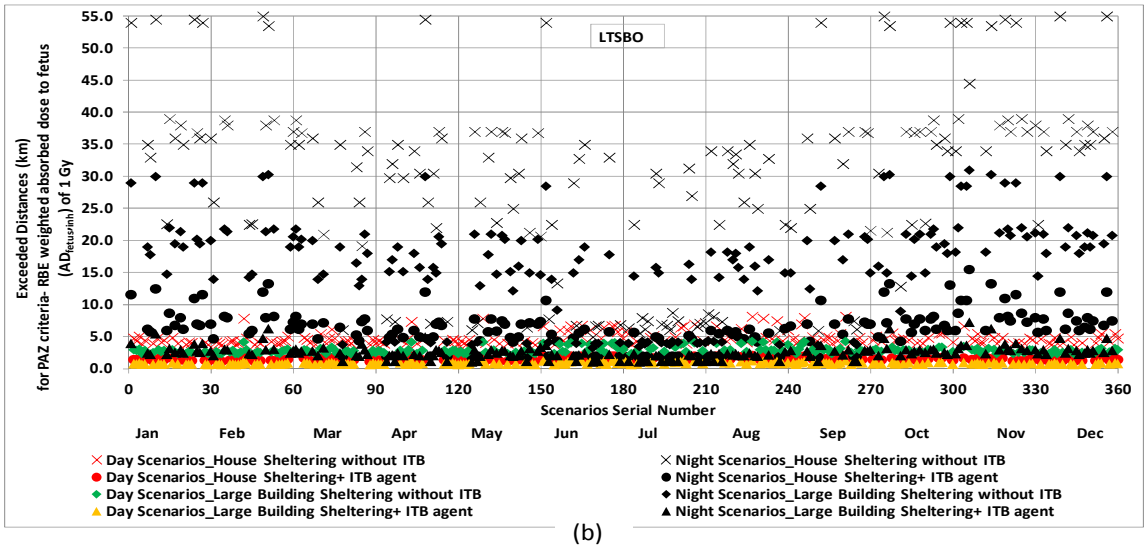

Figure 5-52: Month-wise 360 weather scenarios exceeded distances for PAZ criteria (1 Gy of $AD_{fetus,inh)}$ under different protective measures for (a) LBLOCA and (b) LTSBO (Faisal et al., 2025*).

* Article published from this thesis

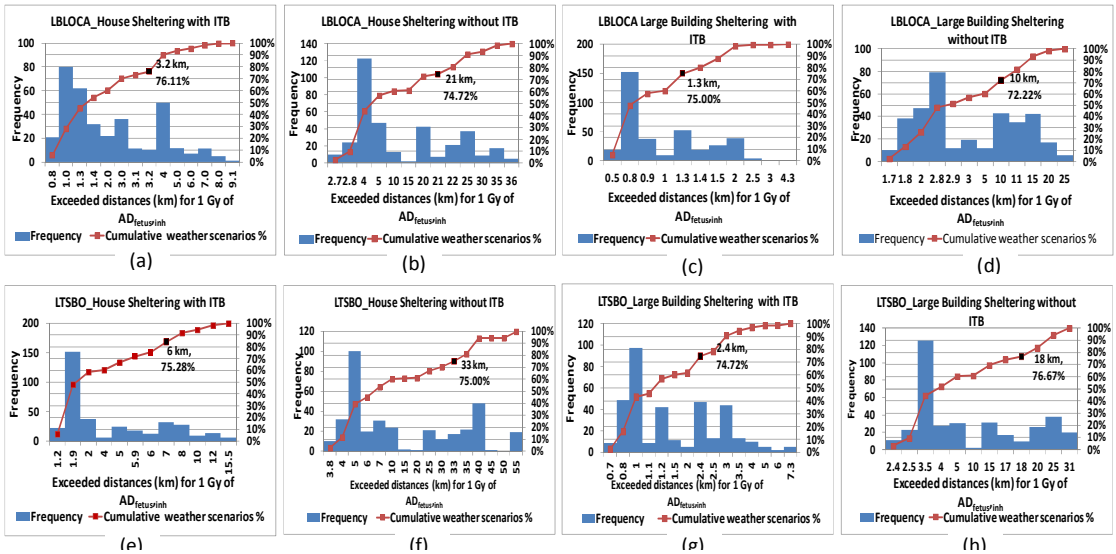

Figure 5-53: Frequency distribution of exceeded distances for 360 weather scenarios of PAZ criteria (1 Gy of $AD_{fetus,inh}$) under different protective measures in (a to d) LBLOCA and (e to h) LTSBO postulated events with cumulative percentage coverage exceeded distances.

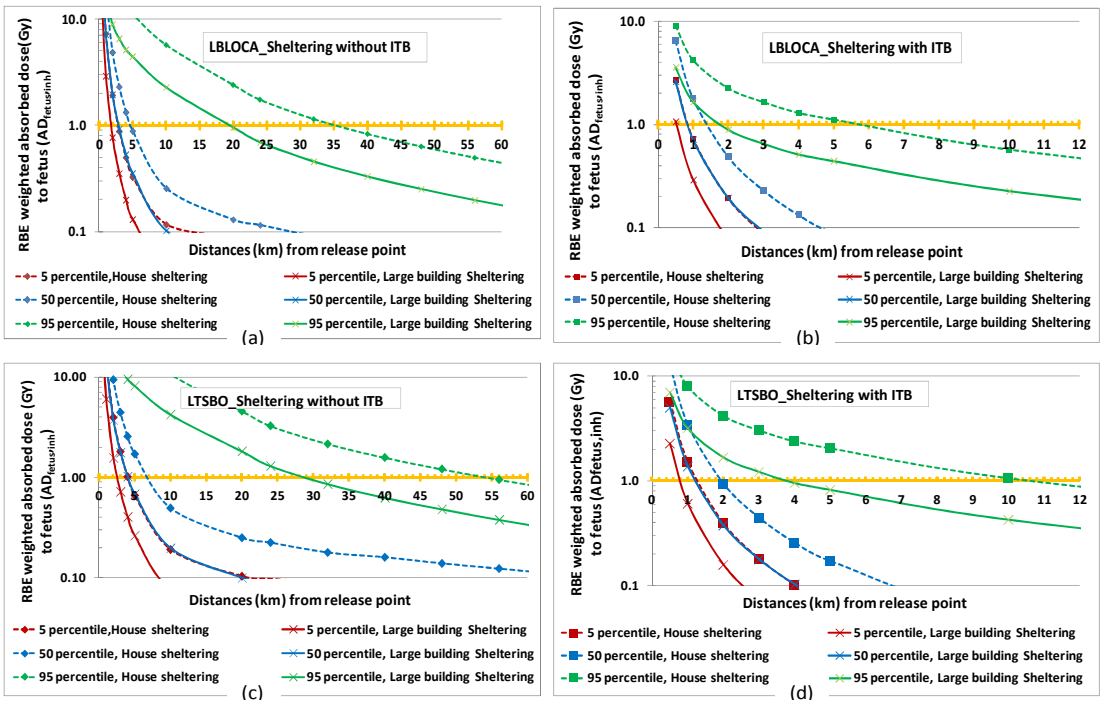

Figure 5-54: 5, 50 and 95 Percentile RBE-weighted absorbed dose to the fetus from inhalation ($AD_{fetus,inh}$) vs. distance under different protective measures for (a & b) LBLOCA and (c & d) LTSBO; the solid yellow line indicates the IAEA PAZ criteria (Faisal et al., 2025*).

* Article published from this thesis

Administration of ITB significantly reduces fetal dose exposure. When a pregnant woman shelters in a house and takes ITB before inhalation, the threshold dose for the fetal thyroid is exceeded only up to approximately 1.5 km for LBLOCA and 2 km for LTSBO at the 50th percentile. At the 95th percentile, these distances increase to 5–6 km for LBLOCA and 10–11 km for LTSBO (Faisal et al., 2025*).

For large building sheltering, the exceeded distances are further reduced to 1.5–2 km for LBLOCA and 3.5–4 km for LTSBO. Overall, the combination of ITB administration and large building sheltering results in a substantial reduction in absorbed fetal thyroid doses for both accident scenarios (Faisal et al., 2025*).

5.2.3 Decision of PAZ size

Table 5-4 shows the distances at which the 1 Gy absorbed dose criteria were exceeded to prevent severe deterministic effects from a severe release of about 4% of volatile fission products, for different protective actions and dosimetric criteria of PAZ. From this release occurring in 95% of all weather scenarios:

(i) **Precautionary evacuation** within a 5 km radius prior to a release ensures that red bone marrow doses remain below 1 Gy for LBLOCA and within 7 km for LTSBO scenarios (Faisal et al., 2025*).

(ii) **For fetal thyroid protection**, evacuation up to 4 km before a release is sufficient when sheltering in large buildings with ITB for both events. However, if sheltering conditions are less effective, evacuation distances of approximately 6 km for LBLOCA and 10 km for LTSBO are required (Faisal et al., 2025*).

(iii) **ITB administration** should be implemented prior to a release up to about 35 km for LBLOCA and 55 km for LTSBO during house sheltering. Under large building sheltering, ITB use is recommended within 20 km for LBLOCA and 30 km for LTSBO (Faisal et al., 2025*).

Table 5-4 Maximum exceeded distance ranges (km) for threshold doses of PAZ dosimetric criteria in different protective measures of LBLOCA and LTSBO postulated events in several percentile weather scenarios.

Criteria	Protective action	Weather scenario covered (%) & Exceeded distances (km) ranges		
		~50%	**~75%**	**~95%**

* Article published from this thesis

		LBLOCA	LTSBO	LBLOCA	LTSBO	LBLOCA	LTSBO
$AD_{red\ bone\ marrow}$ of 1 Gy	1 day House Sheltering	0.4-0.5	0.9-1.0	0.7-0.8	1.0-1.5	**1.2-1.5**	**2.5-3.0**
	1 day Large Building Sheltering	0.1-0.2	0.2-0.3	0.2-0.3	0.2-0.3	**0.3-0.4**	**0.4-0.5**
	4 days House Sheltering	1.0-1.1	1.5-2.0	2.0-2.5	3.5-4.5	**4.0-4.5**	**6.5-7.0**
	4 days Large Building Sheltering	0.2-0.3	0.3-0.4	0.3-0.4	0.4-0.5	**0.5-0.6**	**0.6-0.7**
$AD_{fetus,inh}$ of 1 Gy	House Sheltering with ITB	1.3-1.4	1.9-2.0	3.1-3.2	5.0-6.0	**5.0-6.0**	**8.0-9.0**
	House Sheltering without ITB	4.0-5.0	6.0-7.0	21-22	30-33	**30-35**	**35-40**
	Large Building Sheltering with ITB	0.8-0.9	1.1-1.2	1.3-1.4	2.2-2.5	**1.5-2.0**	**3.5-4.0**
	Large Building Sheltering without ITB	2.8-2.9	3.5-4.0	10-11	17-18	**15-20**	**20-25**

For 95% of all weather scenarios, a precautionary evacuation of approximately 5 km is sufficient to prevent an increased incidence of mortality associated with a 1 Gy absorbed dose to red bone marrow in the event of LBLOCA and LTSBO. In 95% of LBLOCA and 75% of LTSBO scenarios, the same 5 km evacuation effectively prevents a heightened risk of severe mental retardation in fetuses exposed to a 1 Gy absorbed dose. To achieve fetal protection in 95% of all LTSBO scenarios, evacuation must be extended to 9 km or supplemented with large building sheltering.

The PAZ's necessary range takes into account both the necessity of facilitating an efficient emergency response and the objective of avoiding severe deterministic effects. LTSBO events typically allow about 8 hours from shutdown, whereas LBLOCA events usually allow at least 3 hours before a release (Ramsdellet al., 2012). As a result, the PAZ's precautionary evacuation should be finished within three hours of the evacuation decision. Because of the dense population and the lack of transportation options, evacuation is difficult beyond 5 km from the Rooppur site.

This could make it more difficult to evacuate people who need the most immediate protection—those closest to the plant. However, under high-risk weather conditions, LTSBO-related evacuation may need to extend up to 10 km (Faisal et al., 2025*). The delayed core damage in LTSBO scenarios provides more time for evacuation or sheltering, improving overall safety. Even during the release phase (the plume), evacuating speed larger than at a walking speed of about 5 km/h is more effective than sheltering within 3–5 km of the plant (US NRC, 1990).

Using ITB agents alongside sheltering—especially in large buildings—greatly reduces radiation exposure to both the red bone marrow and the fetus. If immediate evacuation cannot be carried out safely, individuals near the plant should take ITB and remain sheltered until evacuation becomes possible (Faisal et al., 2025*). To ensure both the prevention of deterministic health effects and the effectiveness of emergency response, the PAZ for the Rooppur NPP should cover an area of about 5 km, consistent with IAEA guidelines for prompt evacuation (IAEA, 2013b).

5.2.4 Equivalent Dose to the Fetus ($H_{fetus, inh}$)

5.2.4.1 Exceeded Distances for $H_{fetus, inh}$

Figure 5-55(a & b) presents the 360 weather scenarios exceeded distances for UPZ dosimetric criteria of 100 mSv (0.1 Sv) of equivalent dose to fetus from inhalation ($H_{fetus,inh}$) in house sheltering with and without ITB, as well as large building sheltering effects of LBLOCA and LTSBO events. If a pregnant woman is sheltered in a house and the ITB agent is taken before inhalation, the IAEA criterion of 100 mSv is expected to be exceeded within 2.8–8.3 km for daytime releases and within 3.8–36 km for nighttime releases in the LBLOCA event, whereas for the LTSBO event, the exceeded distances are within 3.5–8.8 km for daytime releases and 5–55 km for nighttime releases. In both events, the maximum distance was observed in the ‘D’ class and ‘F’ class scenarios, respectively, for daytime and nighttime release.

However, if a pregnant woman is sheltered in a house and there is no ITB agent taken, the criterion is to be exceeded to a distance of within 8-36 km for daytime releases and 9.8-120

* Article published from this thesis

km for nighttime releases during LBLOCA, while it exceeds within 9.7-70 km for daytime releases and 13-160 km for nighttime releases during the LTSBO events. The maximum distances observed without ITB is in 'B' class scenarios with low wind speed for daytime release for both events, whereas in LBLOCA and LTSBO events, the maximum distance observed for nighttime release is in 'F' class and 'E' class no-rain scenarios, respectively. During wet scenarios, the threshold distance that exceeds 100 mSv equivalent doses to the fetus is lowered, and for nighttime releases, it is less than 50 km in LBLOCA and less than 60 km in LTSBO for home sheltering without ITB.

The exceeded distances for UPZ dosimetric criterion are within 1.7-3.7 km for a pregnant woman sheltering in a large building with ITB during the daytime release and 2.5-22.5 km for nighttime release in LBLOCA. However, it is 2.3-4.3 km for daytime release and 3.4-31.5 km for nighttime release during LTSBO events. Without ITB sheltering in a large building, the maximum exceeded distances for LBLOCA and LTSBO are 86 km and 111 km, respectively.

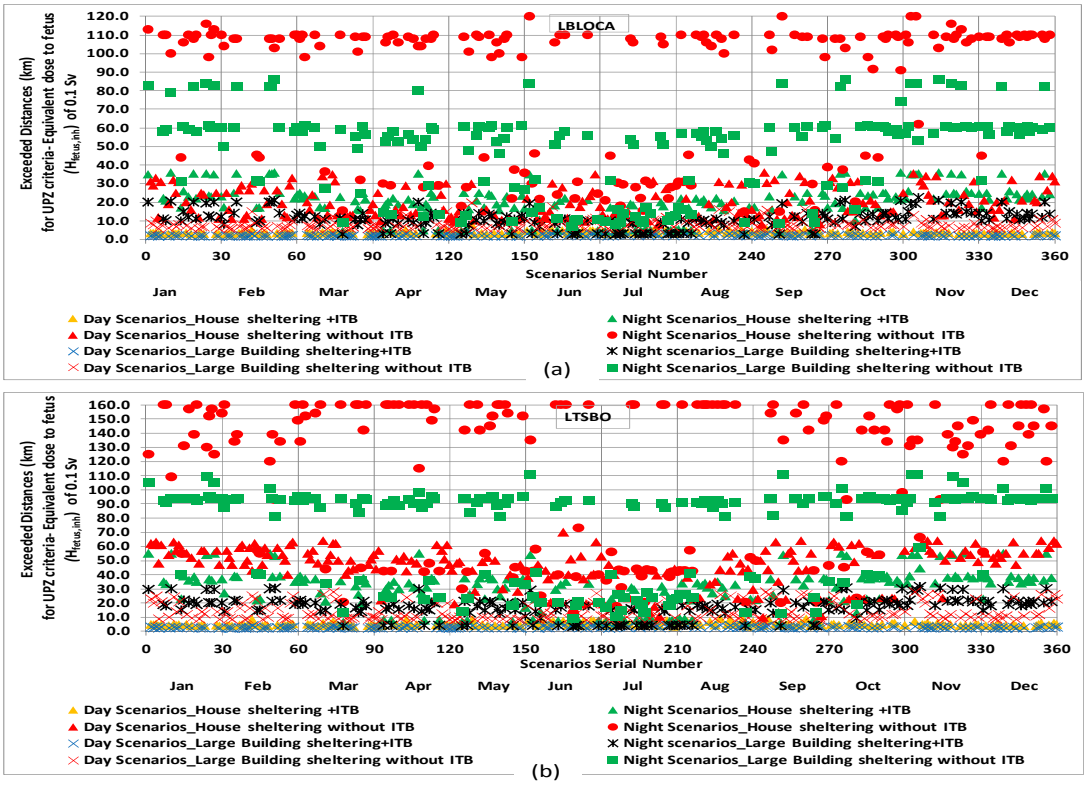

Figure 5-55: Month-wise 360 weather scenarios exceeded distances for UPZ dosimetric criteria (100 mSv of $H_{fetus,inh}$) under different protective measures of (a) LBLOCA and (b) LTSBO postulated events.

Figure 5-56(a to h) shows the frequency distribution and their cumulative weather scenarios for exceeded distances of 100 mSv $H_{fetus,inh}$ for house sheltering with and without ITB, as well as large building sheltering, in LBLOCA and LTSBO events. Maximum distances covering 95% of all weather scenarios exceed within 30-35 km in LBLOCA and 35-40 km in LTSBO for house sheltering with ITB, and 15-20 km in LBLOCA and 20-25 km in LTSBO for large building sheltering.

In 95% of all weather scenarios, house sheltering without ITB has maximum exceeded distances of 106-110 km for LBLOCA and 150-160 km for LTSBO, while large building sheltering without ITB has distances of 80-86 km and 90-100 km for LBLOCA and LTSBO events, respectively.

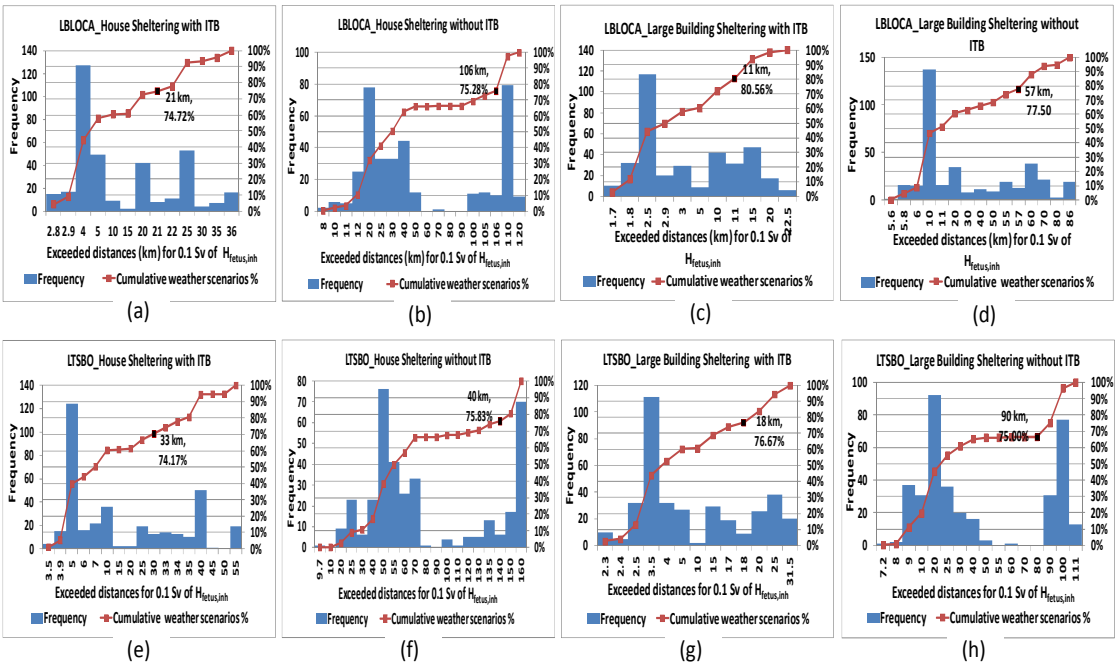

Figure 5-56: Frequency distribution of exceeded distances for 360 weather scenarios of UPZ dosimetric criteria (100 mSv of Hfetus,inh) under different protective measures in (a to d) LBLOCA and (e to h) LTSBO postulated events with cumulative percentage coverage exceeded distances.

5.2.4.2 Percentile Spatial Dose Distribution for $H_{fetus, inh}$

Figures 5-57(a & b) present the 5th, 50th, and 95th percentile equivalent doses to the fetus from

inhalation ($H_{fetus,\ inh}$) for LBLOCA and LTSBO scenarios, comparing conditions with and without ITB agents and different sheltering options (house and large building). Under house sheltering with ITB, the 100 mSv dose limit is exceeded at approximately 5 km for LBLOCA and 7 km for LTSBO at the 50th percentile. When sheltering in large buildings, these distances are reduced to about 3 km for LBLOCA and 4 km for LTSBO (Faisal et al., 2025*).

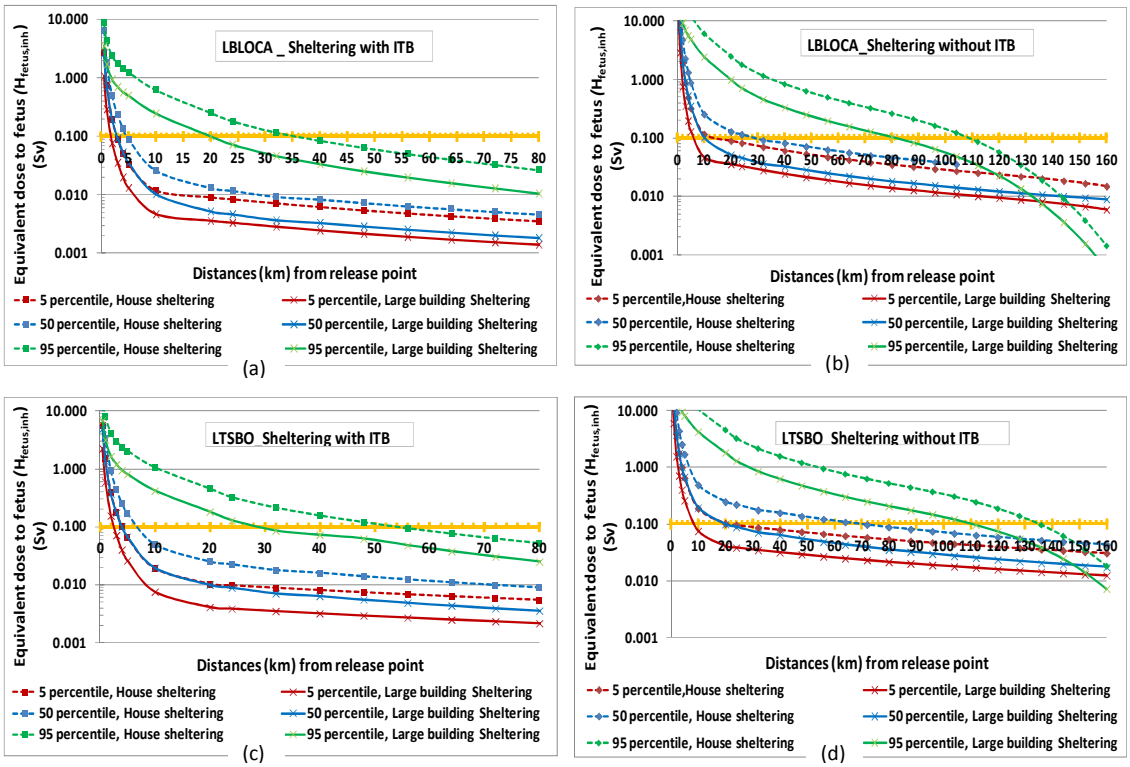

Figure 5-57: 5, 50 and 95 Percentile Equivalent dose to the fetus from inhalation ($H_{fetus,inh}$) with distances under different protective measures for (a & b) LBLOCA and (c & d) LTSBO; the solid yellow line indicates the IAEA UPZ criteria (Faisal et al., 2025*).

5.2.5 Effective Dose from Inhalation (E_{inh})

5.2.5.1 Exceeded Distances for E_{inh}

Exceeded distances of 360 weather scenarios for UPZ dosimetric criterion 'inhalation effective dose (E_{inh}) of 100 mSv (0.1 Sv) are shown in **Figure 5-58(a & b)** respectively for LBLOCA and LTSBO in-house sheltering as well as large building sheltering.

* Article published from this thesis

In the LBLOCA event, if an individual is sheltered in a house, the IAEA criterion is exceeded within 2.8-5 km for daytime release and 3.3-37.1 km for nighttime release, whereas the LTSBO event exceeds the distances within 3.4-7.1 km for daytime release and 4.1-54.5 km for nighttime release. In both events, the maximum distance was observed in the 'D' class scenario for daytime release and in the 'F' class scenario for night release. Due to the considerable inhalation dose reduction in rain scenarios, especially in the wet weather, in 'C' and 'D' classes, the threshold distance for an individual that exceeds 0.1 Sv is likewise reduced to less than 5 km in LBLOCA and less than 7 km in LTSBO for house sheltering.

In an 'E' class rain scenario, the threshold distance for LBLOCA falls below 15 km and for LTSBO falls below 20 km. During LTSBO events in large building shelters, it is within 2.3-4 km in daytime release and 2.9-30 km at midnight release.

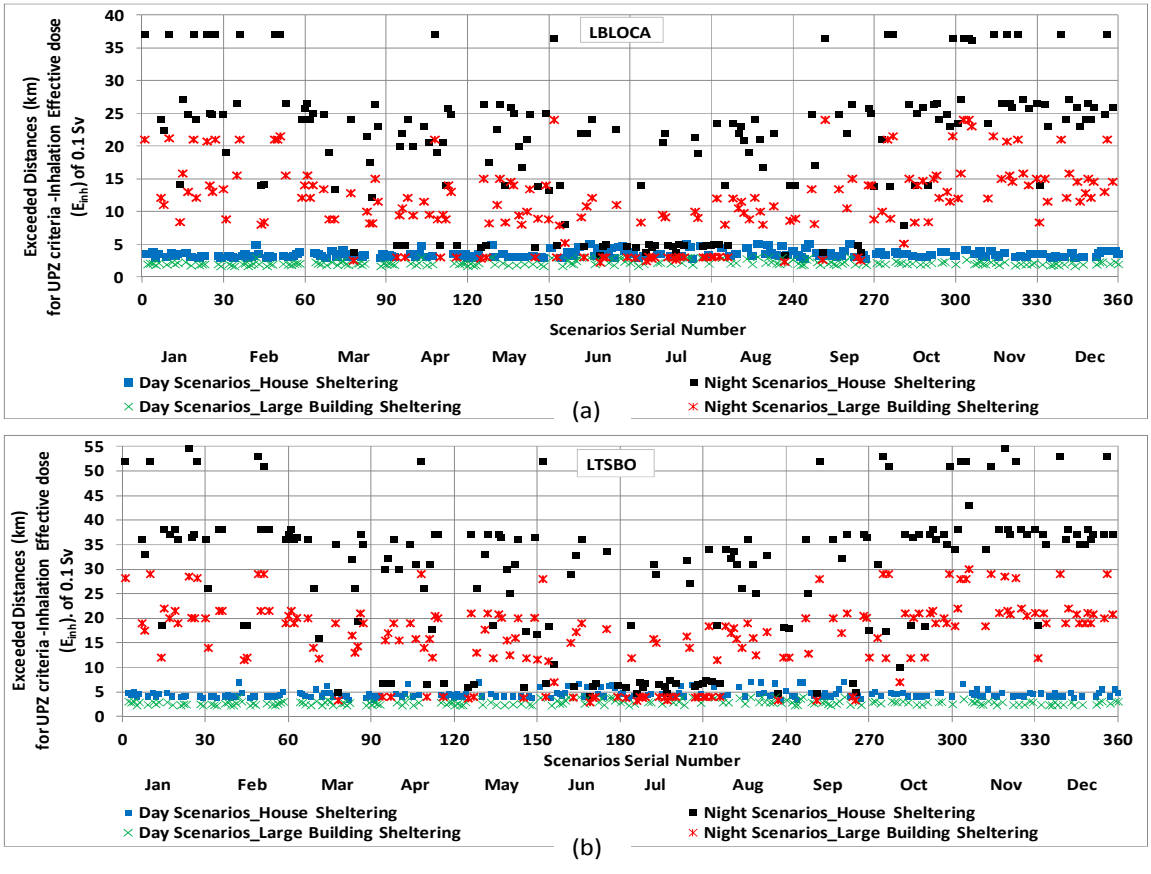

Figure 5-58: Month-wise 360 weather scenarios exceeded distances for UPZ dosimetric criteria (100 mSv of E_{inh}) under different sheltering measures of (a) LBLOCA and (b) LTSBO postulated events.

The frequency distribution and cumulative covered weather scenarios for exceeded distances of 100 mSv of effective inhalation dose for house sheltering and large building sheltering in LBLOCA and LTSBO events are shown in **Figure 5-59(a to d).** Maximum distances spanning 95% of all weather scenarios are 35-37.1 km in LBLOCA and 35-40 km in LTSBO for house sheltering and 20-24 km in LBLOCA and 20-25 km in LTSBO for large building sheltering

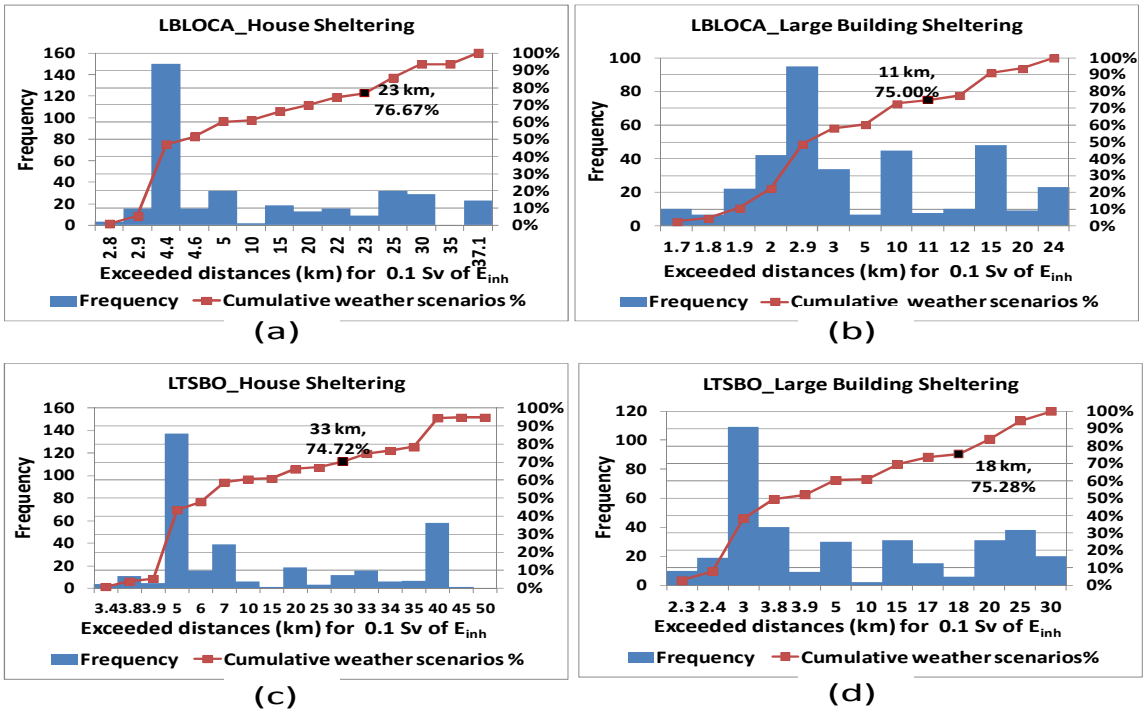

Figure 5-59: Frequency distribution of exceeded distances for 360 weather scenarios of UPZ dosimetric criteria (0.1 Sv of E_{inh}) under different sheltering measures in (a & b) LBLOCA and (c & d) LTSBO postulated events with cumulative percentage coverage exceeded distances.

5.2.5.2Percentile Spatial Dose Distribution for E_{inh}

Figure 5-60(a & b) shows the 5th, 50th, and 95th percentile values of effective inhalation dose for house and large building sheltering during LBLOCA and LTSBO scenarios. For house sheltering, the 100 mSv dose limit is exceeded at approximately 4.5 km for LBLOCA and 6 km for LTSBO at the 50th percentile. Under large building sheltering, these distances decrease to about 3 km and 4 km, respectively (Faisal et al., 2025*).

* Article published from this thesis

At the 95th percentile, exceedance distances increase significantly, reaching about 35 km for LBLOCA and 50 km for LTSBO under house sheltering. In comparison, large building sheltering reduces these distances to around 21 km for LBLOCA and 28 km for LTSBO (Faisal et al., 2025*).

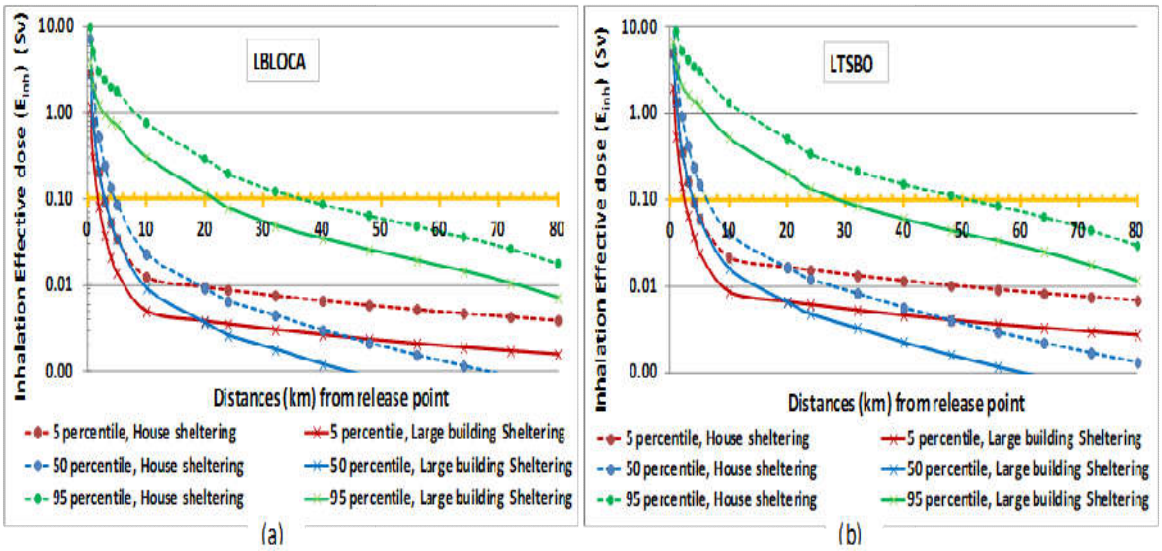

Figure 5-60: 5, 50 and 95 Percentile effective dose from inhalation (E_{inh}) vs. distances under different sheltering measures for (a) LBLOCA and (b) LTSBO; the solid yellow line indicates the IAEA UPZ criteria (Faisal et al., 2025*).

5.2.6 Decision of UPZ size

The size of the UPZ is established by identifying a compromise between decreasing the probability of stochastic effects and allowing for an effective response during an emergency. **Table 5-5** shows the distances at which the 100 mSv dose criteria were exceeded to avoid stochastic effects for different protective actions and dosimetric criteria of UPZ.

Table 5-5: Maximum exceeded distance ranges (km) for threshold doses of UPZ dosimetric criteria under different protective measures of LBLOCA and LTSBO postulated events in several percentile weather scenarios.

Criteria	Protective action	Weather scenario covered (%) & Exceeded distances (km) ranges					
		~50%		**~75%**		**~95%**	
		LBLOCA	LTSBO	LBLOCA	LTSBO	LBLOCA	LTSBO
(E_{inh})	House	4.4-4.6	6.9-7.0	22-23	33-34	35-37.1	35-40

* Article published from this thesis

	Sheltering						
	Large Building Sheltering	2.9-3.0	3.8-3.9	11-12	17-18	20-24	20-25
($H_{fetus,inh}$)	House Sheltering + ITB	4.0-5.0	5.0-7.0	21-22	33-34	30-35	35-40
	House Sheltering without ITB	25-30	55-60	105-106	135-140	106-110	150-160
	Large Building Sheltering + ITB	2.9-3.0	3.5-4.0	10.0-11.0	17-18	15-20	20-25
	Large Building Sheltering without ITB	10-11	20-25	55-57	90-100	80-86	90-100

To avoid stochastic effects from a severe release of about 4% of volatile fission products

(i) In LBLOCA and LTSBO events, evacuating to a distance of 25 km is adequate to ensure that inhalation-effective doses remain below 100 mSv in 95% of all weather scenarios during large building sheltering. Additionally, this distance is sufficient for 75% of weather scenarios while house sheltering for LBLOCA. In 95% of all weather scenarios, evacuation to a distance of approximately 35 km for LBLOCA and 40 km for LTSBO is sufficient to maintain doses below 100 mSv (Faisal et al., 2025*).

(ii) Evacuation out to a distance of 25 km is sufficient to keep the fetus's equivalent dose below 100 mSv in 95% of all occurring weather scenarios during large building sheltering with ITB for both events and adequately covers 75% of all weather scenarios in the LBLOCA event during house sheltering with ITB. In 95% of all weather scenarios, house sheltering with ITB and evacuation of around 35 km for LBLOCA and 40 km for LTSBO are sufficient to keep the fetus's equivalent dose below 100 mSv (Faisal et al., 2025*).

(iii) An ITB agent needs to be taken before a release at a distance of 110 km for LBLOCA and 160 km for LTSBO in-house sheltering for 95% of all weather scenarios, while it is 86 km for LBLOCA and 100 km for LTSBO during large building sheltering (Faisal et al., 2025*).

* Article published from this thesis

In the event of a severe release under 95% of weather scenarios, evacuating within 20 km for LBLOCA and 30 km for LTSBO ensures that fetal and inhalation-effective doses remain below the 100 mSv criterion during large building sheltering with ITB. For house sheltering, this requirement increases to about 35 km for LBLOCA and 50–55 km for LTSBO (Faisal et al., 2025*). It is worth considering extending the UPZ boundary beyond 30 km for two key reasons: Firstly, the additional benefit of dose reduction with increasing distance is relatively small. Secondly, delays in implementing protective measures may pose significant risks to the most vulnerable individuals near the plant (IAEA, 2013b). When meteorological forecasts indicate high-risk conditions, particularly stability classes 'E' and 'F', it is prudent to extend evacuation and protective actions beyond the UPZ boundary, especially during LTSBO scenarios.

If the evacuation takes so long due to the large area or to carry out many people either cannot be evacuated before the release or are evacuated during a large release. One possibility is large building sheltering combined with the intake of ITB during the release, followed by relocation dependent on ground deposition levels. This needs to prepare some large emergency buildings to shelter since the villages around the plant only have normal living houses, not large buildings. The UPZ should also be separated into areas that allow for evacuation of different sectors and distances based on the occurrence and the current scenario (Faisal et al., 2025*). Furthermore, the UPZ should be evacuated in phases based on the distance from the NPP, where the conditions dictate whether sheltering along with ITB intake is preferable to evacuation.

Overall, the suggested UPZ is approximately 25 km, aligning with IAEA guidelines that recommend a UPZ range of 15 to 30 km (IAEA, 2013b).

5.2.7 Validation of EPZ sizes based on Residual TEDE/Reference Dose Level

Figure 5-61(a & b) depicts the exceeded distances for the reference dose level (100 mSv) of residual TEDE in house sheltering as well as large building sheltering during LBLOCA and LTSBO events for 360 weather scenarios. If a person is sheltered in a house, the reference dose level is expected to be exceeded within 3.3-20 km for daytime release and within 5.9-39

* Article published from this thesis

km for nighttime release in the LBLOCA event, whereas the exceeded distances in the LTSBO event are within 4.3-22.1 km for daytime release and 8-56 km for nighttime release. In both events, the greatest distance was observed during the 'D' class light rain scenario for daytime release and the 'F' class scenario for nighttime release. As mentioned earlier, the radiological dose through the groundshine channel prevails in TEDE during the wet weather, specifically from April to September, while the inhalation dose dominates in TEDE during the dry weather, specifically from October to March.

The exceeded distances in LBLOCA are 1.8-4.2 km for an individual sheltering in a large building during the daytime and 3.1-23 km for nighttime release. During LTSBO events in large building shelters, it is within 2.4-6.6 km in daytime release and within 4-30 km at nighttime release.

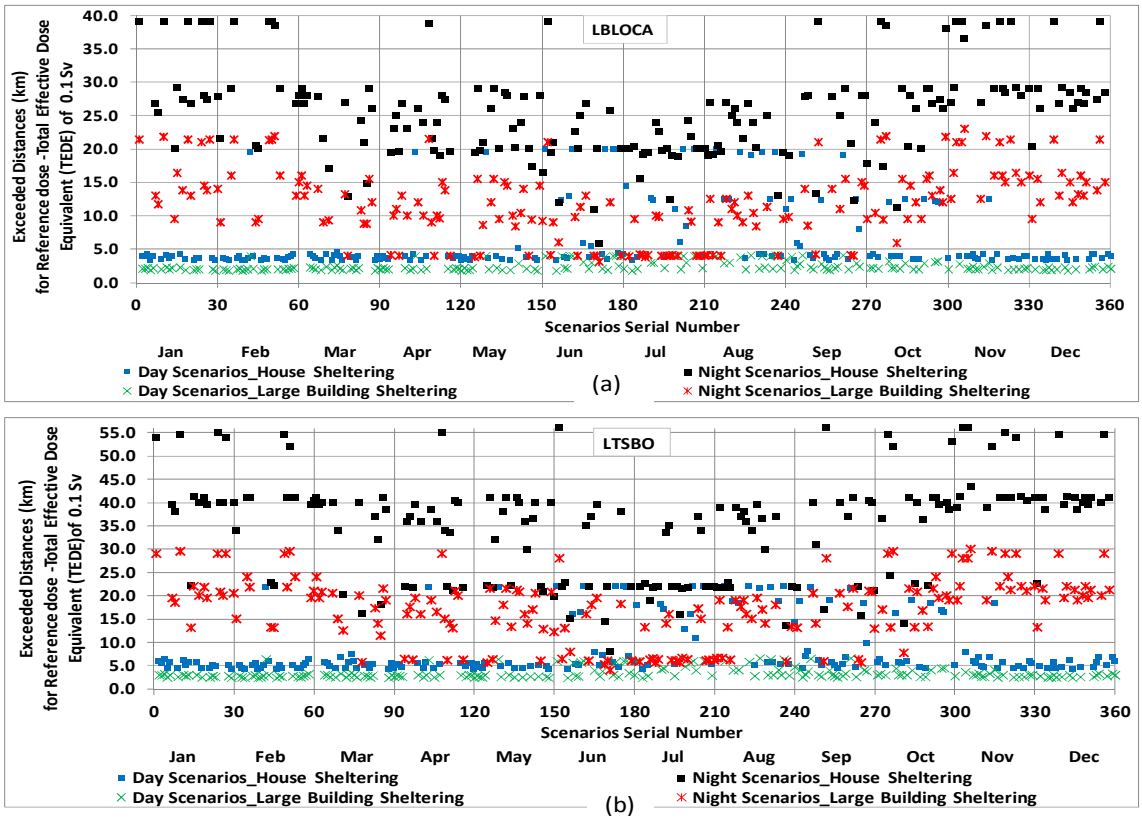

Figure 5-61: Month-wise 360 weather scenarios exceeded distances for Reference dose level of 100 mSv of TEDE under different sheltering measures of (a) LBOCA and (b) LTSBO postulated events.

Figure 5-62(a to d) shows the frequency distribution with cumulative covered weather scenarios in LBLOCA and LTSBO events for house sheltering and large building sheltering exceeding distances of 100 mSv reference dose. The maximum distances encompassing 95% of all weather scenarios where the reference dose is exceeded are 35-39 km in LBLOCA and 40-56 km in LTSBO for house sheltering, whereas they are 20-23 km in LBLOCA and 25-30 km in LTSBO for large building sheltering.

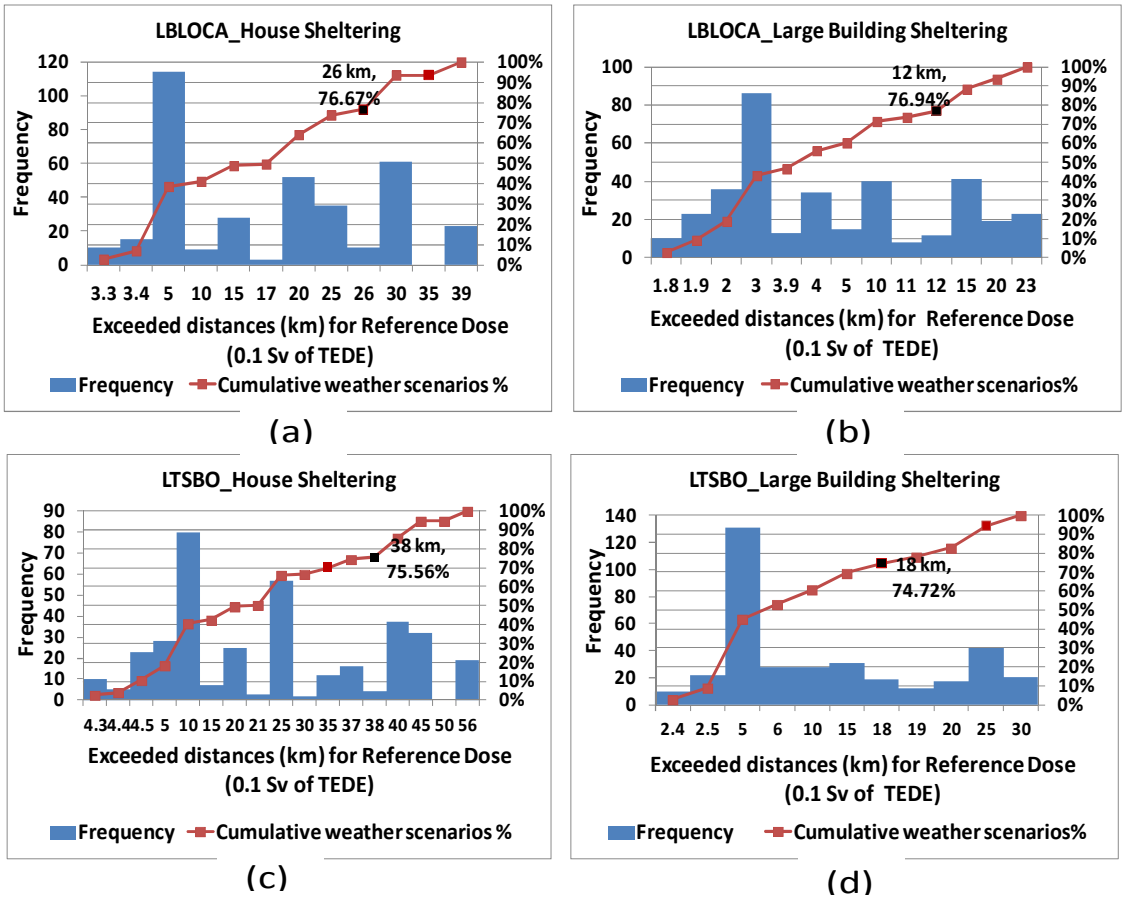

Figure 5-62: Frequency distribution of exceeded distances for 360 weather scenarios of reference dose level under different sheltering measures in (a & b) LBLOCA and (c & d) LTSBO postulated events with cumulative percentage coverage exceeded distances.

Figure 5.63(a & b) depicts the spatial dose variation for the 5th, 50th, 75th and 95th Percentile TEDE during LBLOCA and LTSBO events without and with protective measures (house sheltering and large building sheltering). According to **Figure 5-63(a & b)** and **Table 5-6**, a 25-km evacuation is sufficient to maintain the reference dose level below 100 mSv in LBLOCA and LTSBO events in 95% of all weather scenarios that occur during large building

sheltering. However, it covered 75% of weather scenarios in LBLOCA events during house sheltering. Evacuation out to a distance of nearly 35 km for LBLOCA and 40 km is enough for keeping the reference dose level below 100 mSv in 95% of all occurring weather scenarios during sheltering in a house. These results are comparable when compared to the exceeded distances of UPZ dosimetric criteria, which are 100 mSv of equivalent dose to the fetus from inhalation or the effective inhalation dose to an adult.

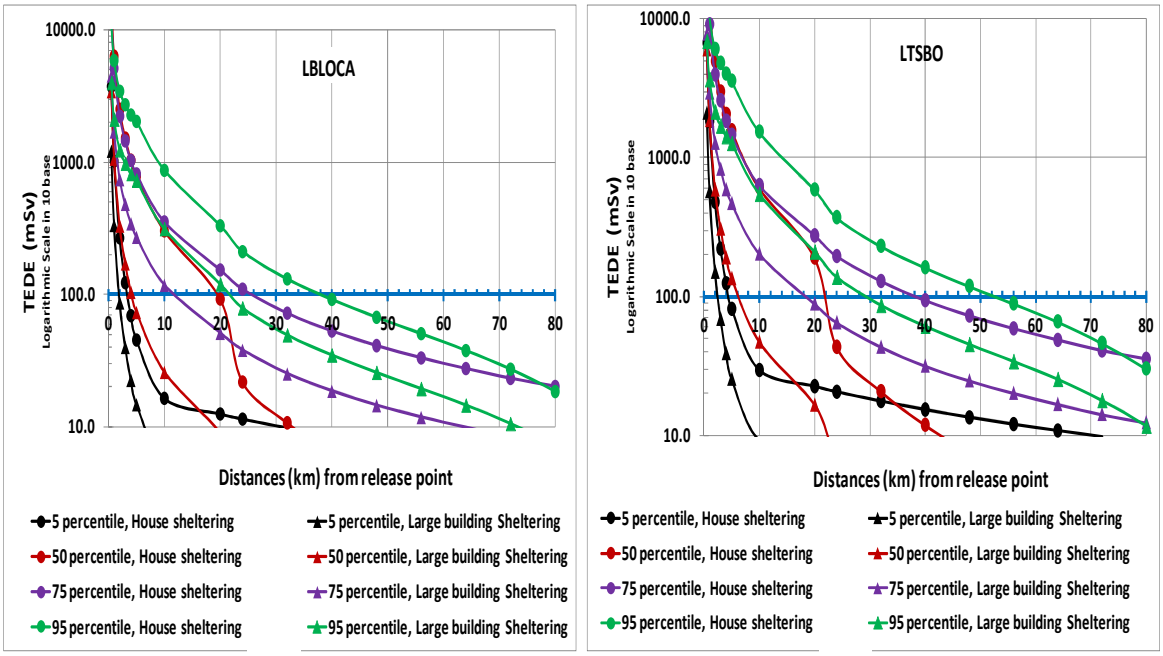

Figure 5-63: 5, 50, 75 and 95 Percentile TEDE vs. distances under different sheltering measures for (a) LBLOCA and (b) LTSBO; the solid blue line indicates the reference dose level.

Table 5-6: Maximum exceeded distance ranges (km) for threshold doses of Reference dose level under different sheltering measures of LBLOCA and LTSBO postulated events in several percentile weather scenarios.

Protective measures	Weather scenario covered (%) & Max. Exceeded distances (km)							
	Encompassed weather scenario based on exceeded 100 mSv reference dose of **Figure 5-61(a & b)**							
	~5%		~50%		~75%		~95%	
	LBLOCA	**LTSBO**	**LBLOCA**	**LTSBO**	**LBLOCA**	**LTSBO**	**LBLOCA**	**LTSBO**
House sheltering	3.3-3.4	4.4-4.5	15-17	25-26	25-26	25-30	35-39	40-56
Large building	1.8-1.9	2.4-2.5	3.9-4.0	11-12	11-12	10-15	20-23	25-30

sheltering								

5.2.8 Effect for Different Combinations of Protective Actions on EPZ sizes

Table 5-7 shows the residual TEDE and distances at which these are obtained to check whether the different combinations of protective actions allow doses to remain below the severe deterministic (1000 mSv) and reference dose levels (100 mSv). If the evacuation occurs before the release starts and in a site unaffected by the release, evacuation is intended to lower the radiation doses to zero, and sheltering reduces the radiation dose in accordance with the dose reduction factor for sheltered in-house and large buildings.

Table 5-7: Different combinations of protective measures and their corresponding residual TEDE with distances for several percentiles of weather scenarios

Combination of protective actions	Max. Residual dose (mSv)						Approx. Distance (km)
	Dry 'F' stability class(up to 95% weather scenarios)		Dry ' E' stability class (up to 75% weather scenarios)		Wet 'D' stability class(up to 50% weather scenarios		
	LBLOCA	LTSBO	LBLOCA	LTSBO	LBLOCA	LTSBO	
Evacuation (Evac.) : 3 km **House Sheltering (HS):** Beyond 3 km	2700	4800	1450	2550	1400	3000	**3**
Evac.: 5 km (Recommended PAZ) **HS:** Beyond 5 km	2000	3500	820	1450	730	1550	**5**
Evac.: 25 km (Recommended UPZ) **HS:** Beyond 25 km	200	320	**100**	180	20	35	**25**
Evac.: 30 km **HS:** Beyond 30 km	140	250	80	130	15	20	**30**
Evac.: 40 km **HS:** Beyond 40 km	**90**	160	50	**90**	7	12	**40**
Evac.: 3 km **Large Building Sheltering (LBS):** Beyond 3 km	980	1700	480	800	150	300	**3**
Evac.: 5 km (Recommended PAZ) **LBS:** Beyond 5 km	730	1250	270	450	70	130	**5**
Evac.: 12 km **LBS:** Beyond 12 km	230	420	**100**	170	20	40	**12**
Evac.: 20 km **LBS:** Beyond 20 km	120	200	50	**90**	8	20	**20**
Evac.: 25 km (Recommended UPZ) **HS:** Beyond 25 km	**70**	130	35	60	3	15	**25**

Referring to **Table 5-7**, a threshold dose of 1000 mSv for LBLOCA and LTSBO is not avoidable during severe weather conditions of 'F' class if the suggested PAZ (5 km) is evacuated before a release and simultaneous house sheltering is carried out in parts of the UPZ affected by the release. It can be avoidable for large buildings sheltering in the UPZ at a distance of about 5 km, where people would receive the highest effective dose of about 730 mSv for LBLOCA and 1250 mSv for LTSBO. In the case of the 'E' class, the maximum residual doses at 5 km for house sheltering are 820 mSv and 1450 mSv, respectively, for LBLOCA and LTSBO. In 'D' class rainy scenarios, if all parts of the PAZ (5 km) are likely to be evacuated, a house-sheltered population about 5 km away would receive the most effective dose of about 730 mSv for LBLOCA and 1550 mSv for LTSBO. However, the risk of an effective dose of 100 mSv (reference dose level) for house sheltering cannot be excluded during the 'F' class scenario, but it can be reduced in the 'E' class and 'D' class scenarios for evacuation of 25 km UPZ. In the case of large building sheltering, evacuation up to about 5 km, 12km, and 25 km is required to avoid the reference dose level of 100 mSv respectively for 'D', 'E', and 'F' class conditions in LBLOCA. Furthermore, an alternative option for evacuating all parts of the UPZ during severe weather scenarios ('E' or 'F' class) is to evacuate part of the zone at a distance of about 12 km, combined with shelter in the rest of the zone at a distance from 12 km to 25 km. This alternative is particularly favorable if sheltering can take place in large buildings that facilitate better protection than sheltering in wooden houses. It is concluded that the suggested ranges of the EPZs (PAZ 5 km, UPZ 25 km), combined with arrangements in the respective zones, allow dosing to be kept below an effective dose of 100 mSv reference levels for the postulated event.

5.3 PART-C: Consequences Analysis during Routine Operation

5.3.1 Month-wise Air Concentration and Ground Deposition during Monthly Continuous Routine Operation

Under the assumption of linear behavior, where a twofold increase in release leads to a twofold increase in concentration, HYSPLIT handles atmospheric transport and dispersion independently of the emission strength, allowing for simple scaling across various release scenarios. A unit release rate of 1 Bq/hr was used in this study, resulting in normalized model outputs that represent relative dispersion characteristics. During post-processing, the relevant real release rate is applied as a scaling factor to convert these unit-based results to actual air concentrations and dose values (Faisal & Islam, 2025*).

HYSPLIT is very flexible for post-processing analyses involving various source terms because it uses normalized concentrations. Additionally, if the number of reactors at the site changes in the future, this methodology makes it easy to update the assessment. Revisions pertaining to reactor configuration or variations in radionuclide release quantities can be incorporated without repeating the entire simulation, which is a major benefit of using normalized concentration and deposition in this study. By applying the actual release rate or activity corresponding to monthly or annual continuous routine operational emissions, the normalized results can be directly scaled to physical units like Bq/m^3, Bq/m^2, or mSv. HYSPLIT determines the normalized concentration for time-averaged outputs by dividing the integrated value (first expressed in hr/m^3) by the chosen averaging period, such as 744, 720, or 672 hours for a one-month interval (Faisal & Islam, 2025*).

* Article published from this thesis

Using GDAS1 meteorological data, **Figure 5-64** shows the cumulative, month-averaged normalized ground deposition patterns resulting from a continuous unit release of 1 Bq/hr over a full month, accounting for seasonal (12-month) variability in 2022. The maximum ground deposition was around 10^{-7} /m^2 for the majority of the months, with lower peak values of about 10^{-8} /m^2 recorded in March and April, mostly at or very near the Rooppur release location. **Figure 5-64** illustrates that during the wet season (April–September) compared to the dry season (October–March), deposition levels exceeding 10^{-9} /m^2 (highlighted in blue for ten months, with the exception of January shown in green and April) cover a notably larger area. (Faisal & Islam, 2025*).

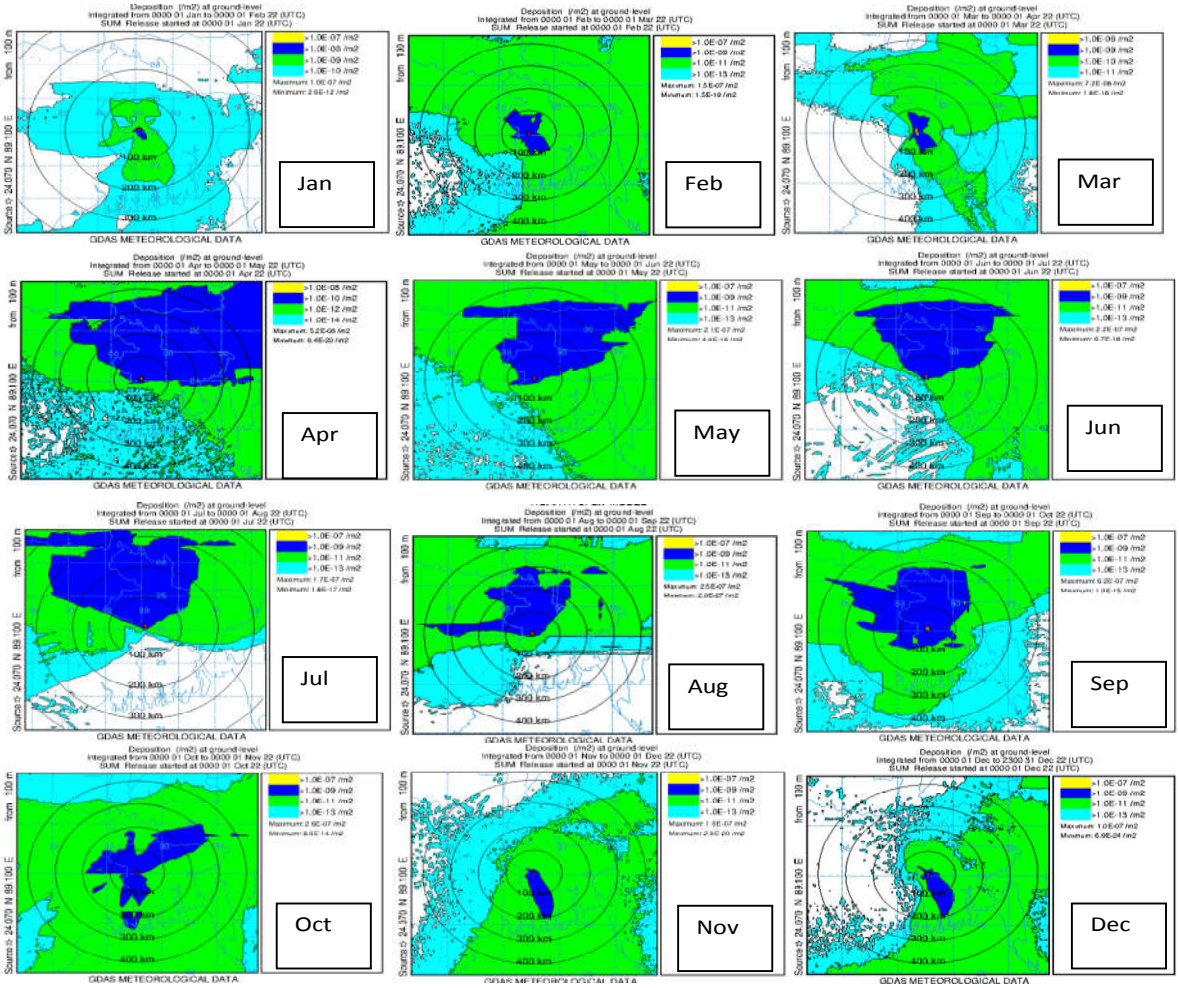

Figure 5-64: Cumulative (month-long) normalized ground deposition distribution patterns for continuous month-long unit release rate (1Bq/hr) for individual 12 months of the year 2022 during GDAS1 Met. Data (Faisal & Islam, 2025*).

* Article published from this thesis

The monthly variation of the estimated peak values of month-averaged normalized air concentrations and cumulative normalized ground depositions is shown in **Figure 5-65**. These findings are based on simulations using CDC1 and GDAS1 meteorological datasets for 2021 and 2022, assuming a continuous unit release of 1 Bq/hr over one month. To maintain a conservative assessment approach, the y-axis values in **Figure 5-65** only show the highest normalized air concentration or ground deposition predicted at any grid point, without reference to a specific location. (Faisal & Islam, 2025*).

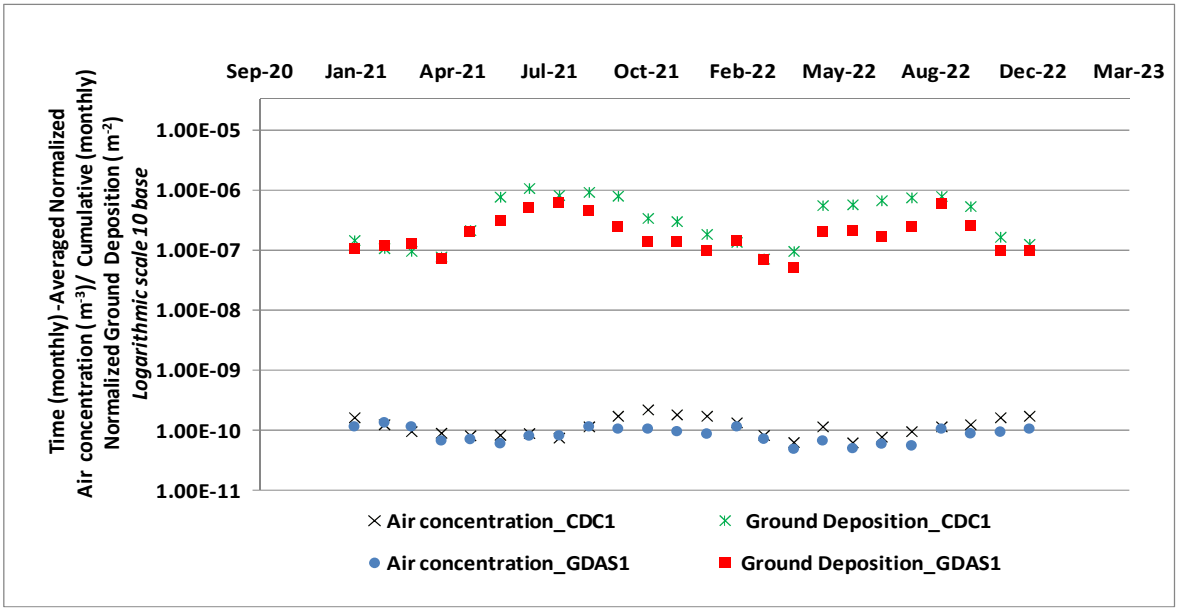

Figure 5-65: Month-wise peak estimated monthly-averaged normalized air concentration and cumulative normalized ground deposition for unit emission rate (1 Bq/hr) under CDC1 and GDAS1 meteorological datasets of the years 2021 and 2022 (Faisal & Islam, 2025*).

For each month with continuous routine releases, the monthly average air concentrations were first calculated in normalized form for a unit release and then converted to real values during the CON2REM post-processing step using the normal operational release data provided in the ACTIVITY.txt file. This process produced realistic monthly average air concentrations expressed in Bq/m³. **Figure 5-66** presents the spatial distribution of these monthly average air concentrations throughout 2022, from January to December, based on month-long continuous operational releases and GDAS1 meteorological data. The results clearly show a seasonal shift

* Article published from this thesis

in plume behavior: during the dry season (October to March), the radioactive plume is mainly transported toward the south, while in the wet season (April to September), the dispersion pattern shifts predominantly toward the west and north (Faisal & Islam, 2025*).

Over the entire year, the highest air concentrations were generally around 10^{-1} Bq/m³ and occurred at or near the Rooppur release point. As shown in **Figure 5-66**, areas with air concentrations above 0.01 Bq/m³ spread over a noticeably larger region during the dry season (October to March) than during the wet season (April to September). These higher concentration zones appear in green for eight months, while April, June, July, and December are shown in blue. (Faisal & Islam, 2025*).

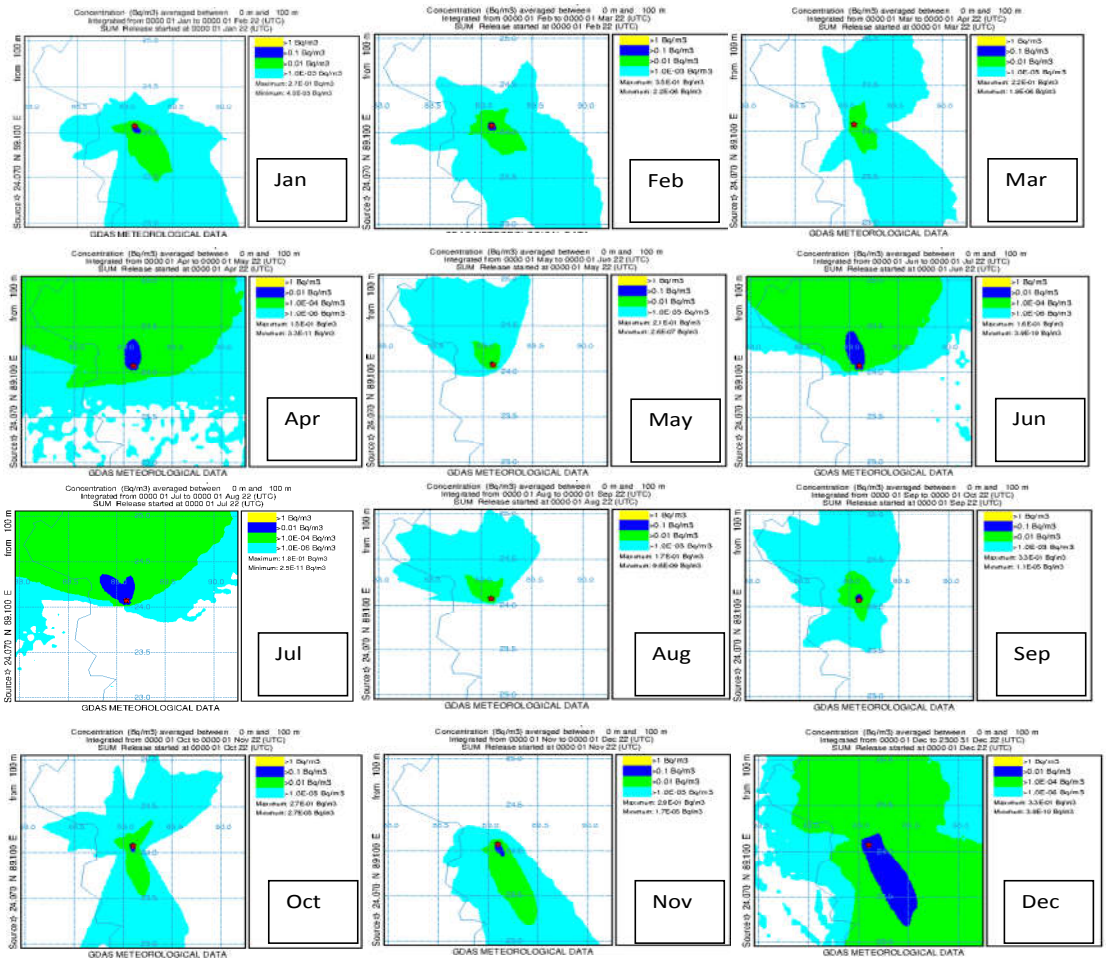

Figure 5-66: Monthly-averaged air concentration distribution patterns for continuous month-long routine operation release for individual 12 months of the year 2022 during GDAS1 Met. Data (Faisal & Islam, 2025*).

* Article published from this thesis

Figure 5-67 shows how the highest monthly air concentrations vary for the two meteorological datasets, along with their uncertainties and the ratio between them. Overall, air concentrations tend to be higher during the dry months from October to March. Notably, the CDC1-based results consistently predict higher concentrations than GDAS1, with peak values during November to January reaching nearly twice those estimated using GDAS1 (Faisal & Islam, 2025*).

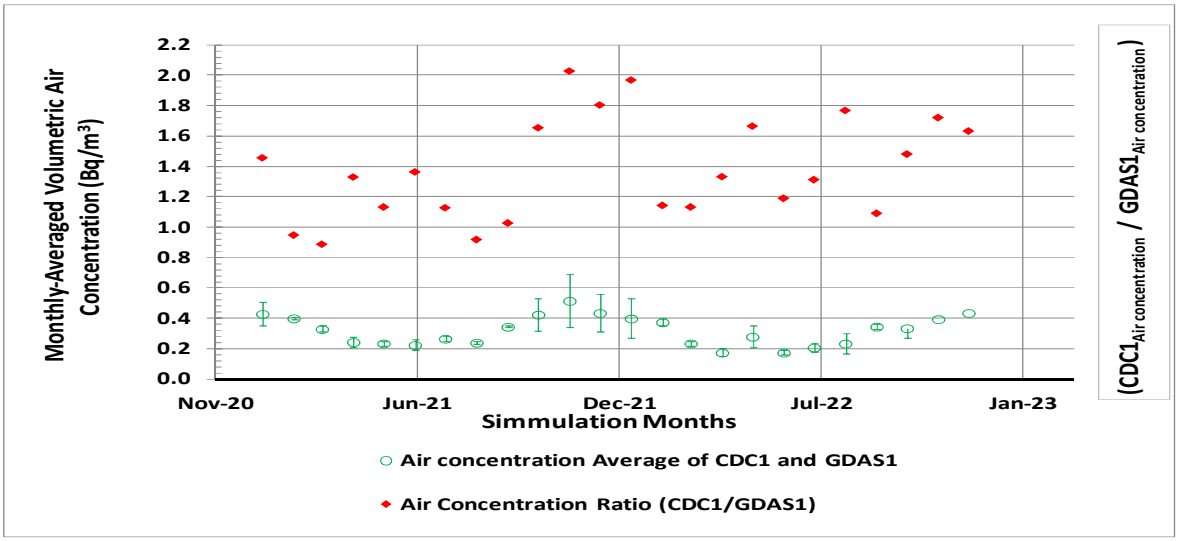

Figure 5-67: Month-wise peak monthly-averaged air concentration with uncertainty and ratios of two meteorological datasets during month-long routine operation release of year 2021 and 2022 (Faisal & Islam, 2025*).

5.3.2 Annual Air Concentration and Ground Deposition during Annual Continuous Routine Operation

Figure 5-68(a–d) shows the yearly average air concentration patterns for 2020, 2021, 2022, and 2023, based on continuous routine operational releases using CDC1 meteorological data. In each year, the highest concentrations were found at the release site, marked with red stars, reaching peak values of about 0.1 Bq/m³ (Faisal & Islam, 2025*).

Figure 5-69(a–d) shows the yearly cumulative ground deposition patterns from a continuous unit release of 1 Bq/h for 2020, 2021, 2022, and 2023, based on CDC1 meteorological data. In

* Article published from this thesis

each year, the highest deposition occurred near the release point, marked with red stars, with a slight shift toward the north, and peak values around 10^{-6} m^{-2}. Only iodine and cesium from the routine operation of the VVER-1200 reactor at Rooppur contribute to ground deposition, since noble gases do not settle. When scaled to the actual release activity of 10^4 Bq, the maximum iodine deposition is roughly (10^{-6} m^{-2} * 10^4 Bq)= 10^{-2} Bq/m² (Faisal & Islam, 2025*) .

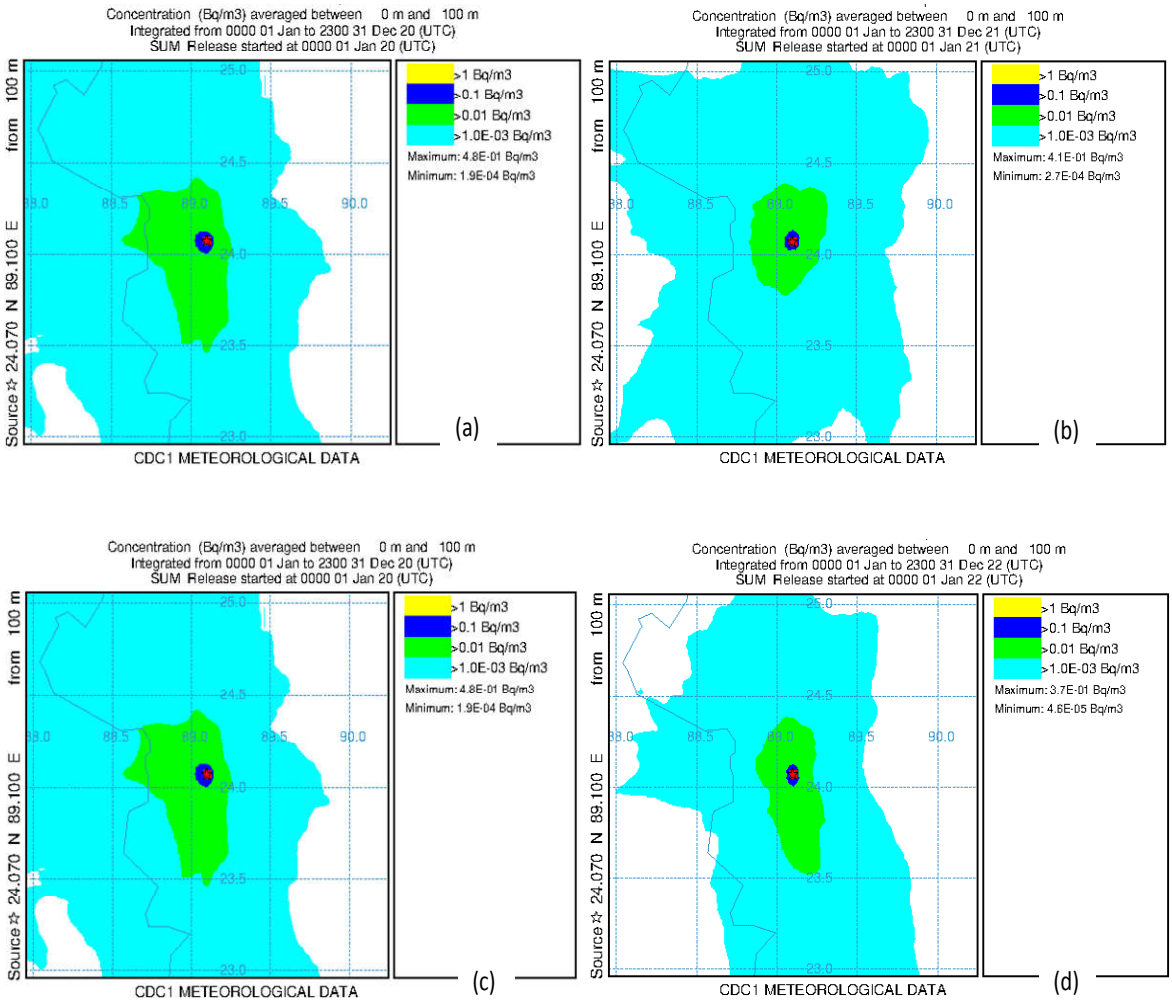

Figure 5-68: (a to d) Annual-averaged volumetric air concentration distribution during continuous year-long routine operation release of year 2020, 2021, 2022 and 2023 for CDC1 Met. Data (Faisal & Islam, 2025*).

* Article published from this thesis

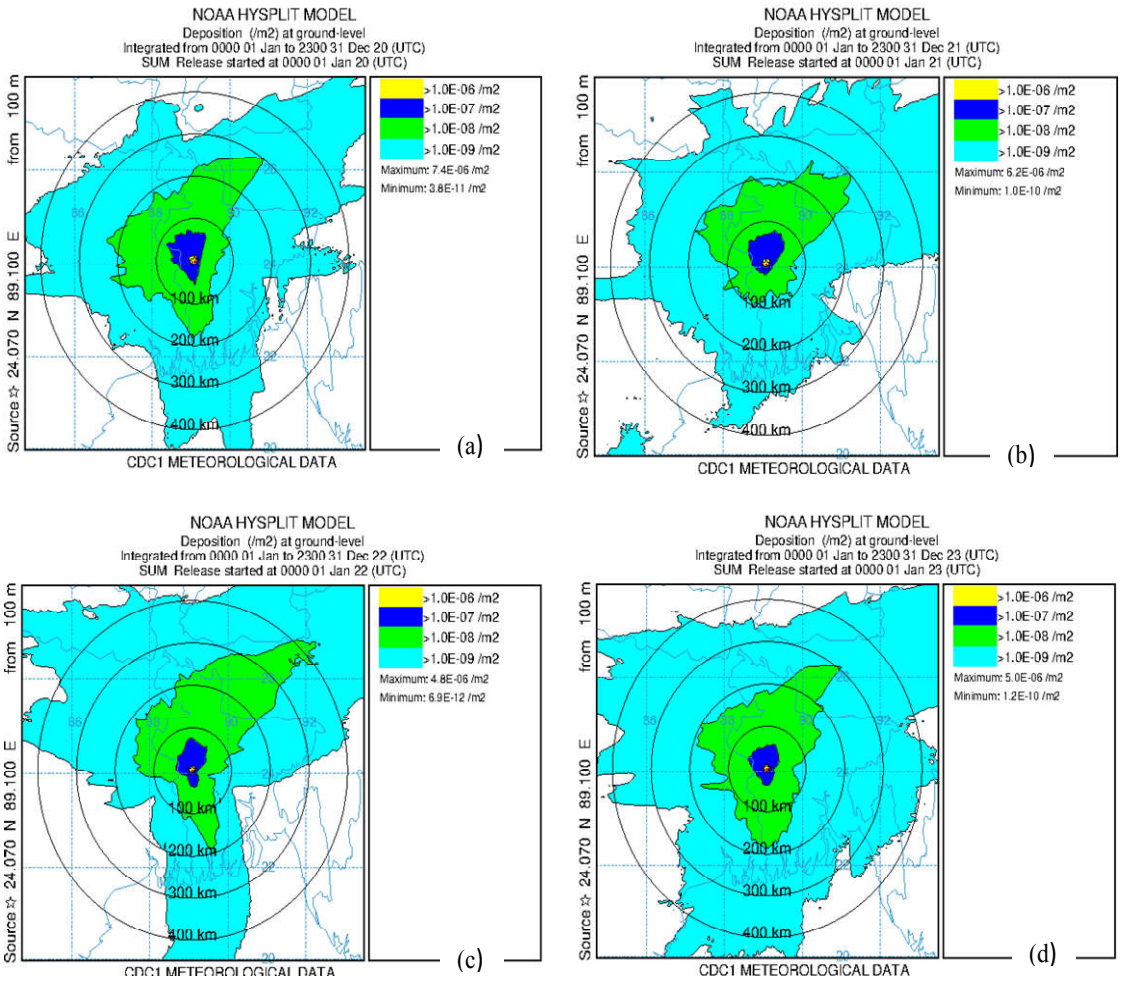

Figure 5-69: (a to d) Annual cumulative normalized ground deposition distributions during continuous year-long unit release rate (1 Bq/hr) of year 2020, 2021, 2022 and 2023 for CDC1 Met. Data (Faisal & Islam, 2025*).

* Article published from this thesis

5.3.3 Air Concentration Uncertainty

Figure 5-70(a–d) shows the probability distribution of air concentrations at a location near the release point (24.1°N, 89.1°E) using different meteorological data ensembles. The values come from the prob{xx} files and are summarized in a box plot. In the plot, the box shows the middle 50% of values (25^{th}–75^{th} percentiles), the whiskers cover the 10^{th}–90^{th} percentiles, and the circles mark the 5^{th} and 95^{th} percentiles. The median is indicated by a line inside the box, while the mean is shown with a plus sign. The data represent twelve 4-hour time intervals. For CDC1 data, concentrations within the 10^{th}–90^{th} percentile range vary by about two orders of magnitude, while for GDAS1, the variation is around one order of magnitude. This difference is mainly due to small shifts in the meteorological grid, showing how sensitive concentration estimates are to changes in weather conditions (Faisal & Islam, 2025*).

According to the 95^{th} percentile concentration map shown in **Figure 5-71(a to d),** only 5% of the ensemble members have concentrations that exceed this threshold. Specifically, only one or two members (about 5% of the 27 ensemble members) have concentrations above the yellow region of concentrations scaling factor greater than 10^{-11}.

Figure 5-72(a–d) shows box plots based on a physics ensemble with 20 different variations. The spread of values, especially within the middle 50% (inter-quartile range), is much smaller—about an order of magnitude less—than what is seen in the meteorological grid ensemble. This suggests that most of the uncertainty comes from how the meteorological data is gridded, while changes in physics assumptions have a much smaller effect (Faisal & Islam, 2025*).

* Article published from this thesis

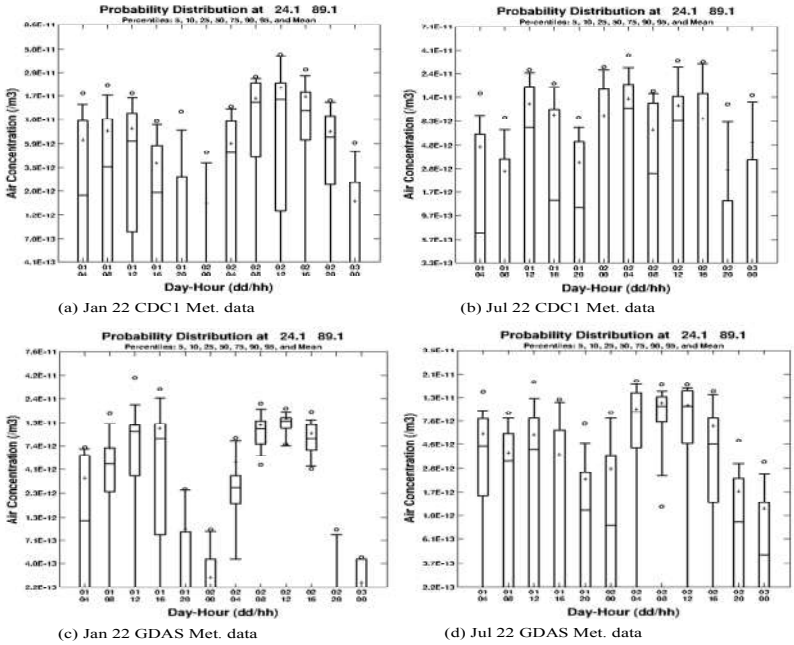

Figure 5-70: Box plot probability distributions for (a & b) CDC1, (c & d) GDAS1 Meteorological data ensemble air concentration at Rooppur site during dry (January) and wet month (July) of year 2022 (Faisal & Islam, 2025*).

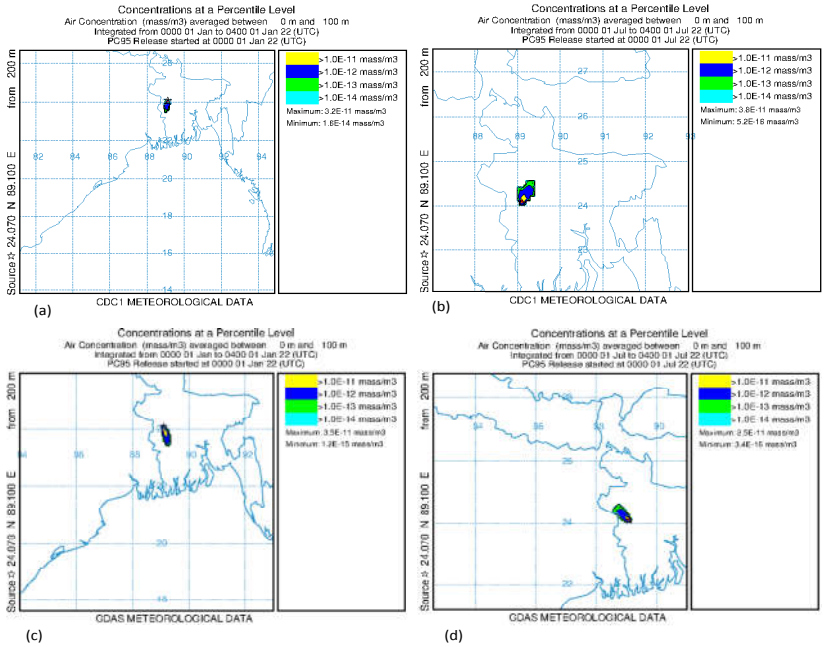

Figure 5-71: Meteorological data ensemble 95th percentile air concentration distributions (a & b) CDC1 and GDAS1 (c & d) at Rooppur site during dry (January) and wet month (July) of year 2022.

* Article published from this thesis

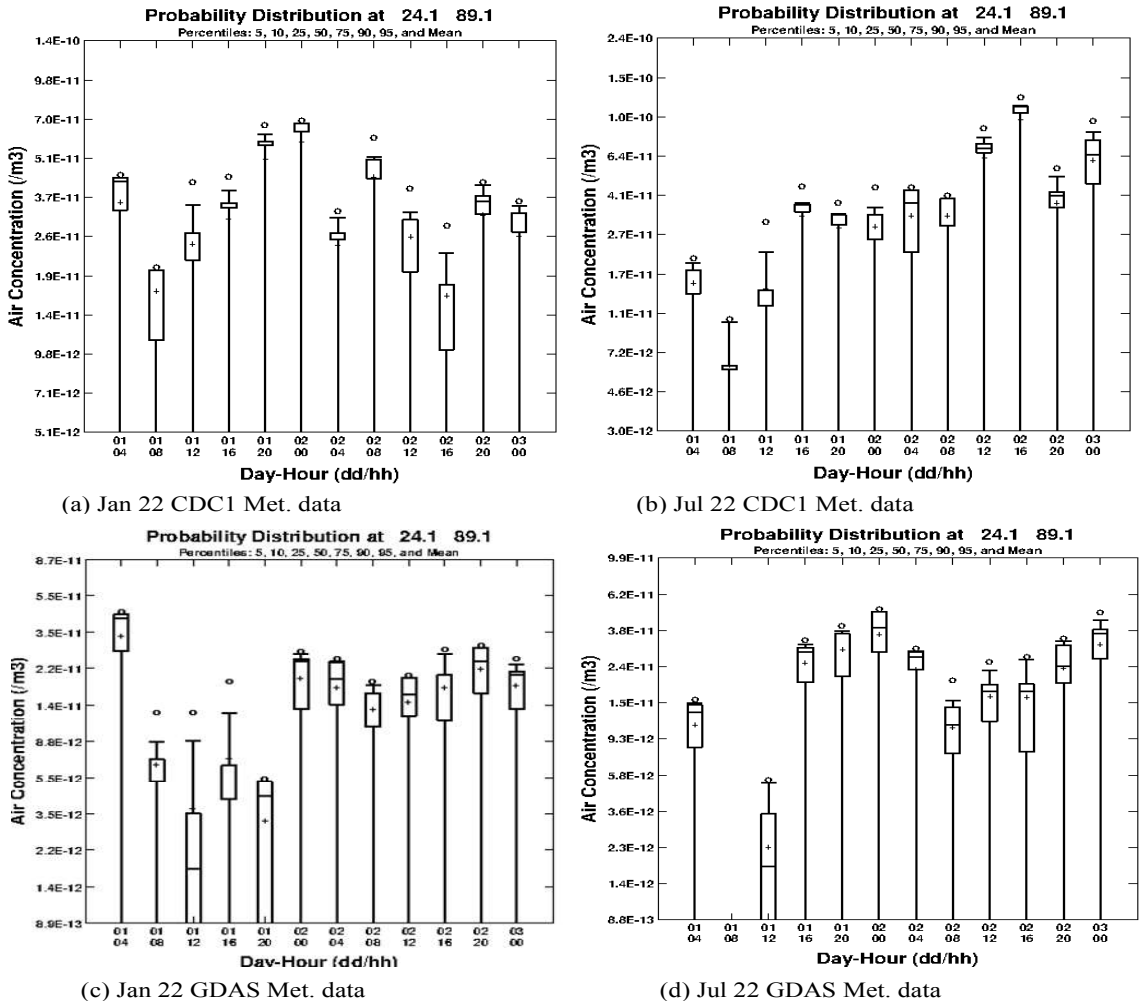

Figure 5-72: Physics model ensemble air concentration Box plot probability distributions for (a & b) CDC1, (c & d) GDAS1 Meteorological data at Rooppur site during dry month of January and wet month of July of year 2022 (Faisal & Islam, 2025*).

5.3.4 Monthly and Annual Effective Dose during Routine Operation

The estimated effective dose comes from two main exposure pathways: cloudshine and groundshine. To stay on the conservative side, this study didn't focus on specific locations where people might be. Instead, we looked at the highest dose values across the whole modeled area to represent worst-case exposure scenarios. As shown in **Figures 5-64, 5-66, 5-68, and 5-69,** the strongest air concentrations (cloudshine) and ground deposition (groundshine)

* Article published from this thesis

occurred at the release site or nearby. With a concentration grid of 0.05° × 0.05° (about 5 km × 5 km), the maximum values are found in the grid cell centered at the release point, near 24.1°N latitude and 89.1°E longitude (Faisal & Islam, 2025*).

Figure 5-73 (a & b) presents the monthly maximum cloudshine, groundshine, and overall effective doses for 2021 and 2022, based on simulations using the CDC1 and GDAS1 meteorological datasets. The monthly cloudshine dose was calculated by multiplying the average dose for each month by the number of hours in that month—744 hours for January, March, May, July, August, October, and December; 720 hours for April, June, September, and November; and 672 hours for February. The monthly groundshine dose was similarly estimated over the respective month-long simulation periods (Faisal & Islam, 2025*).

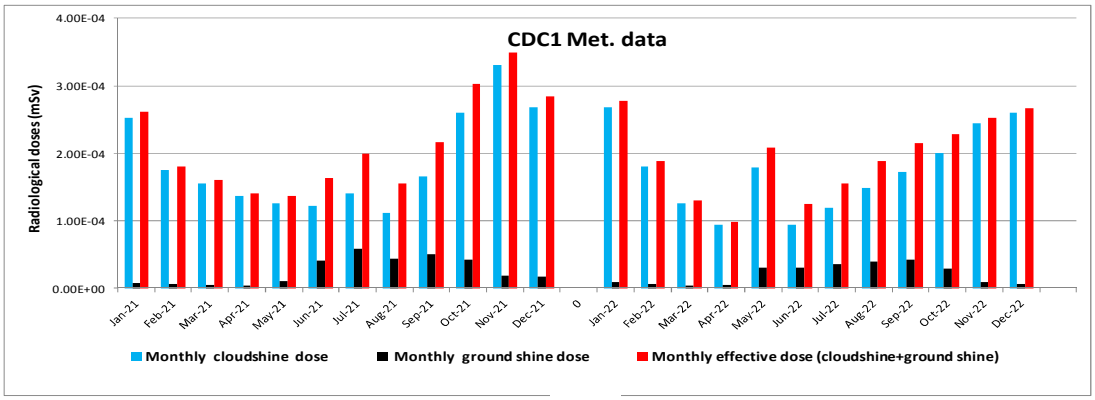

(a)

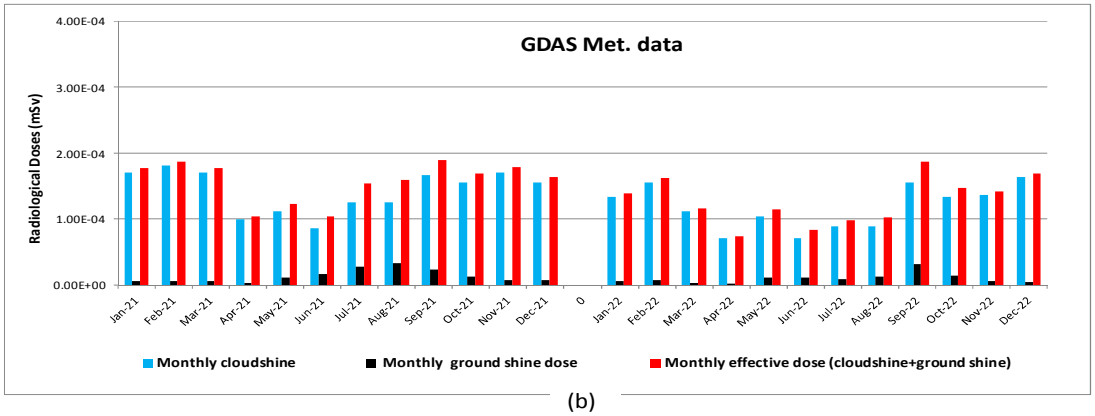

(b)

Figure 5-73: Month-wise cloud shine dose, ground shine dose and effective dose during routine operation release of year 2021 and 2022 for (a) CDC1 and (b) GDAS1 Met. Data (Faisal & Islam, 2025*).

* Article published from this thesis

The highest monthly cloudshine doses are seen during the dry season, from October to March, while the groundshine doses tend to be higher in the wet season, from May to October, mainly due to wet deposition. Overall, the effective dose is generally higher in the dry months. By adding up the monthly cloudshine and groundshine doses for the entire year, the annual effective doses for 2021 and 2022 were determined (Faisal & Islam, 2025*).

Figure 5-74 illustrates the distribution of average cloud shine and total ground shine doses for year-wise continuous operational release. The accumulated annual cloud shine dose distribution is calculated by multiplying the average air concentration by the year-wise averaging periods (8,759 hours for 2021, 2022, and 2023; 8,783 hours for 2020). The annual ground shine dose, which is summed over the year-long duration of the simulation.

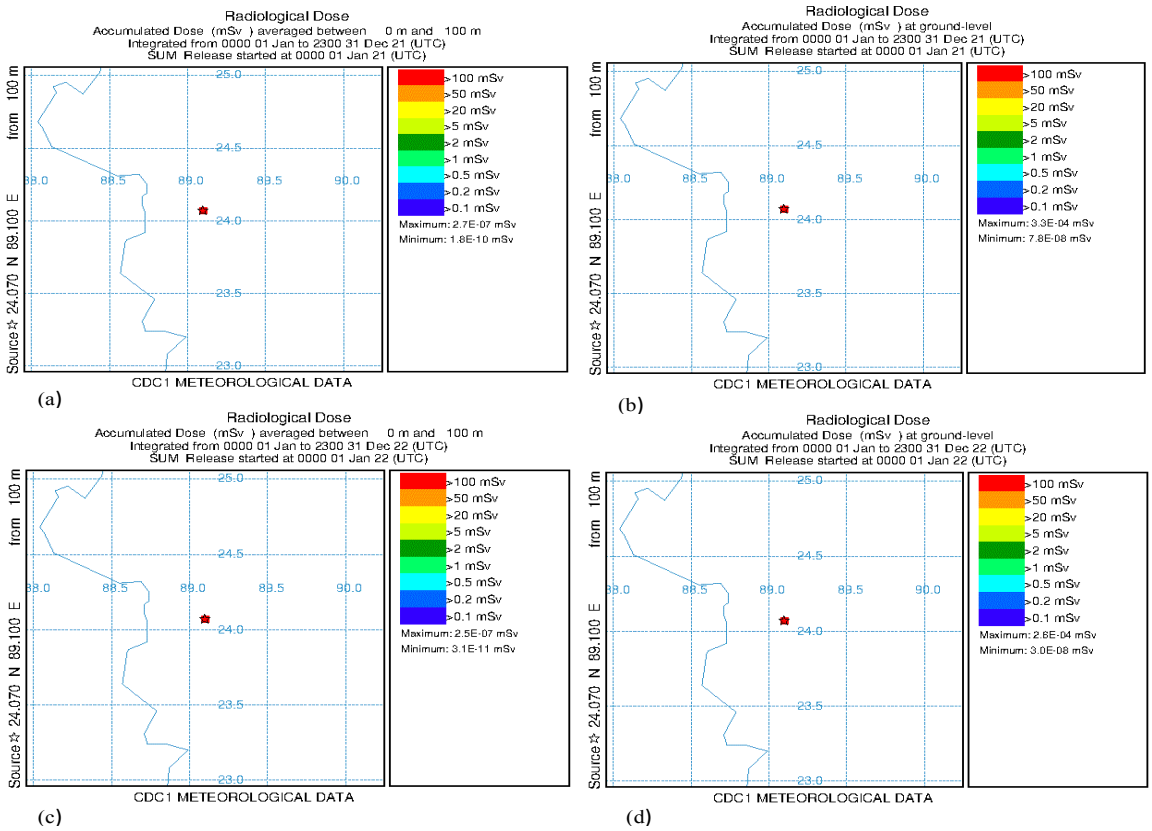

Figure 5-74: Comparative annual (a & c) average cloud shine dose and (b & d) cumulative ground shine dose distributions for CDC1 Meteorological Data of the year 2021 and 2022during routine operation release.

* Article published from this thesis

Figure 5-75 provides an overview of the radiological dose results from this study using two meteorological datasets, highlighting the separate contributions from cloudshine and groundshine. The annual cloudshine dose for the CDC1 dataset was estimated by multiplying the maximum average cloudshine dose by the total number of hours in each year (8,759 hours for 2021–2023 and 8,783 hours for 2020). The groundshine dose was calculated over the full one-year simulation period. Overall, cloudshine is the dominant contributor, accounting for about 90% of the total radiological dose (Faisal & Islam, 2025*).

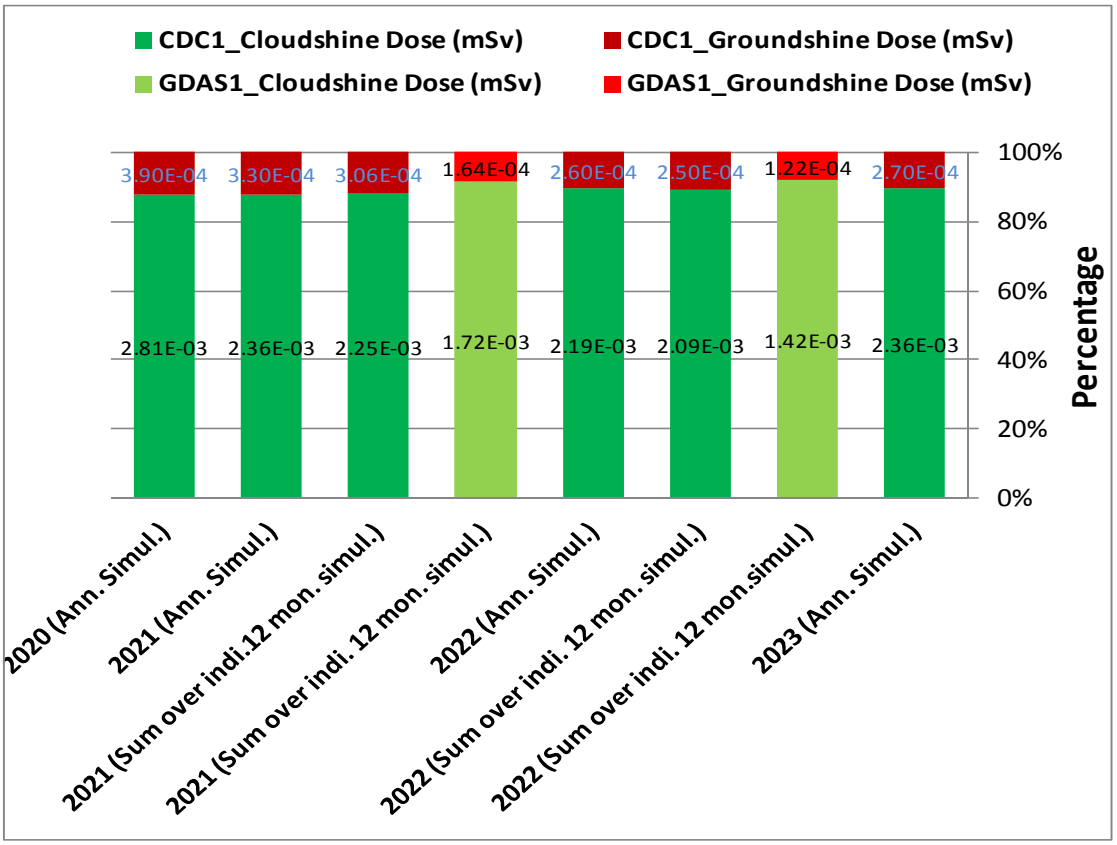

Figure 5-75: Comparative annual cloud shine and ground shine dose during routine operation release from VVER-1200 reactor (Faisal & Islam, 2025*)

Table 5-8 compares the annual dose estimated in this study with values reported in earlier studies for routine releases from different NPPs. The differences among the results mainly reflect the use of different calculation models, dose conversion factors, assumptions, and meteorological data from various years. As shown in the table, the annual effective dose estimated for the Rooppur site in this study is consistent with those reported elsewhere and falls

* Article published from this thesis

well within acceptable limits. On average, the annual dose is only about 0.3% of the public dose limit of 1 mSv per year, indicating that radiation exposure from routine operations at Rooppur NPP is very low and comfortably below regulatory requirements (Faisal & Islam, 2025*). It is also much lower than the natural background radiation level near the Rooppur site, reported as 0.96 mSv per year (Mollah & Chakraborty, 2009).

Table 5-8: Comparative annual effective dose Rooppur site with other studies during routine operation release (Faisal & Islam, 2025*).

NPP	Rooppur NPP 1 Present study	Rooppur NPP 1 (Sadhukhan & Synzynys, 2023)	Bushehr NPP-1 (Feyzinejad et al, 2019)	Bushehr NPP-1 (Pirouzmand et al., 2015)	Sebagin NPP site (Udiyani & Husnayani, 2017)	Barakah NPP-1 (Zubair et al., 2022)	Korean NPP (Kong et al., 2017)
Reactor type	VVER-1200	VVER-1200	VVER-1000	VVER-1000	1000 MW_e PWR	1400 APR	PWR, PHWR
Using Code	HYSPLIT	CROM	HYSPLIT	CAP 88 PC	PC-CREAM	GALE-86, HOTSPOT	KDOSE-60, XQDQWQ
Annual Effective dose (mSv)	2.41E-03	3.67E-03	2.1E-04	5.5E-04	5.3E-02	4.1E-03	~ 10^{-03}
(%) of Annual Dose limit	0.24	0.37	0.021	0.055	5.3	0.41	~0.1

* Article published from this thesis

CHAPTER 6.

POLICY IMPLICATIONS

This study identifies key strategies to strengthen Bangladesh's nuclear emergency preparedness and response framework.

(i) Emergency Protective Actions

Prioritize sheltering in secure structures and establish pre-planned evacuation protocols for communities within a 2–49 km radius of the plant.

Pre-distribute stable iodine tablets to populations within a 3–80 km zone to reduce thyroid exposure during radioiodine releases.

(ii) Infrastructure Enhancement

Utilize the extended grace period during events like LTSBO for timely evacuation or sheltering.

Construct large emergency shelters within the PAZ and encourage residents to reinforce housing structures for improved radiological protection.

(iii) Cross-Border Coordination

Develop formal collaboration with neighboring countries, particularly India, for real-time information sharing and joint emergency response.

(iv) Risk-Based Planning

Use study insights to enhance Severe Accident Management Guidelines (SAMGs) and design weather-dependent emergency plans to ensure realistic dose assessments.

These measures will strengthen nuclear safety frameworks, improve public health protection, and ensure compliance with international safety standards as Bangladesh expands its nuclear energy program.

CHAPTER 7.

CONCLUSION AND RECOMMENDATIONS

7.1 Radiological Doses and EPZ Assessment

This thesis presents a comprehensive assessment of the potential radiological consequences of severe BDBA of LTSBO scenarios, EPZ size and routine operational release at the under-construction Rooppur NPP, which houses two units of the VVER-1200 reactor. It uses modern accident consequences tools like RASCAL 4.3, HotSpot 3.1.2 and HYSPLIT codes, along with updated source terms, long-term weather data, and uncertainty analysis considering both dry (winter) and wet (monsoon) weather conditions.

7.1.1 LTSBO Consequences

The study evaluates radionuclide release, atmospheric dispersion, and public radiation exposure both in partial and complete core meltdown under INES level 6 and 7 events. This also investigated the contributions of radionuclides in different radiation exposure pathways and their delayed effects under six LTSBO cases (3 PCM and 3 CCM), both with and without passive safety systems of the ECCS. The HotSpot code is used for the comparison of the RASCAL 4.3 outputs. The findings show that effective passive safety systems and strong containment integrity significantly lower radiological risks. When ECCS operates for extended periods of time with intact containment, there is less release of radionuclide activity and lower radiation doses, reducing risks to the people and the environment. During wet weather, such as the monsoon season, increasing rainfall increases ground deposition owing to washout process. Conversely, dry conditions can cause larger airborne concentrations, increasing exposure to cloudshine doses. Also, during wet weather, dose distributions are often more concentrated around the plant site, *emphasizing the importance of emergency preparation that considers seasonal variations.*

Protective measures recommendations were made based on international (IAEA GSR Part 7) and national (Bangladesh NNREPRP) dose criteria. For the LTSBO accidents, the intervention distances—ranging from less than 1 km to over 100 km depending on weather and severity—

indicate the need for flexible, scenario-based emergency response planning. Also recommend Implementation of ITB within a wide range of areas extending up to 80 km or more, depending on weather conditions. The analysis demonstrates that variations between the RASCAL and HotSpot models' predictions are caused primarily by different dispersion algorithms, dose estimation methodologies, and rainout factors of the two codes. *This variation emphasizes the significance of carefully evaluating the results of these models.*

The 3-D HYSPLIT model assesses the long-range effects of radioactive material dispersion during LTSBO event in the atmosphere and on the ground, using meteorological datasets from CDC1 and GDAS1. Sensitivity assessments were carried out to establish the optimal settings for the HYSPLIT model, which included evaluation of variation of particle numbers, concentration grids, and release heights. The study discovered that estimations of air concentration and ground deposition differ greatly depending on the model's resolution and meteorological data used. Using a finer concentration grid of 0.010° (about 1 km x 1 km) can result in air concentration and ground deposition estimates that are 4 to 5 times greater than those derived with a coarser grid of 0.050° (roughly 5 km x 5 km). Furthermore, while both meteorological datasets demonstrated similar distribution patterns, CDC1 yielded air concentration and ground deposition estimates that were 2 to 4 times greater than GDAS1. CDC1's coarse resolution and large time intervals might impact the accuracy of dispersion patterns and deposition footprints, particularly in complex terrains or changing weather conditions. *This demonstrates the importance of meteorological data in the assessment process, since discrepancies between datasets can influence simulation outcomes even when other parameters remain equal.*

The HYSPLIT analysis of an LTSBO-CCM accident at the Rooppur NPP showed that in January's dry conditions, the radioactive plume initially moved south over the Bay of Bengal. As upper-level winds changed, the plume shifted to the north, ultimately impacting parts of Myanmar, Thailand, and China. In southwestern Bangladesh, particularly around Kushtia and Jashore, high levels of airborne radioactivity were detected, with the highest deposition reaching about 10^7 Bq/m² near Ishurdi. In contrast, during the wet month of July, the radioactive plume quickly moved northward into India within the first 24 hours, significantly affecting northwestern Bangladesh, including Ishurdi, Pabna, and Rajshahi. Rainfall and the plume's movement caused localized deposition, with levels surpassing 10^5 Bq/m² in several districts.

This study highlights the critical role of wind patterns and monthly weather conditions in the dispersion and fallout of radioactive materials following the accident.

7.1.2 EPZs

EPZs for the VVER-1200 reactor at the Rooppur site were evaluated using the RASCAL code, following both post-Fukushima IAEA guidelines and national dose criteria. Simulations were conducted for two potential severe accidents, assuming the release of approximately 4% of core inventory volatile and gaseous fission products under 360 different weather scenarios. For 95% of these scenarios, the maximum distances where PAZ dosimetric criteria are exceeded are estimated at around 3–4 km when sheltering in large buildings and 8–9 km when only houses are used. Similarly, UPZ dose criteria are exceeded at distances of 20–25 km for large building sheltering and 35–40 km for house-only sheltering. Exceeded distances were generally greater for the LTSBO event compared to the LBLOCA scenario for same containment release rate and weather conditions. To ensure protection against deterministic health effects while enabling an effective emergency response, a PAZ of 5 km and a UPZ of 25 km are suggested for the Rooppur site. *These are in line with the international guidelines and provide sufficient scientific and technical basis.*

7.1.3 Routine Operation

The modeling of normal operational releases using the HYSPLIT model; supported by two meteorological datasets spanning the year of 2020 to 2023 were performed. The results showed that the highest air concentration, contributing to the cloudshine dose, occurs during the dry seasonal months, while the highest ground deposition, contributing to the groundshine dose, is observed near the plant during the wet seasonal months. Cloudshine accounts for 90% of the total dose received. The study also found that the average annual effective dose to the public was approximately 10^{-03} mSv between 2020 and 2023, which is negligible compared to both the annual dose limit and the global average effective dose from natural background radiation. Since the Rooppur reactors are not yet operational, the study's findings were compared to those of other researches on different computational tools. The results for maximum simulated effective dose are consistent with studies on other NPPs, demonstrating that the HYSPLIT model is an effective tool for predicting dispersion and calculating doses under normal operating conditions

at Rooppur NPP. *The findings show the reliability of the method, evidence of successful model validation, and the establishment of a baseline for risk assessment of routine NPP operations.*

7.2 Limitations

This study has several limitations that need to be acknowledged. First, the RASCAL evaluation carries uncertainties, particularly in the overestimation of release magnitude, release speed, and projected radiological doses. The estimation of EPZ size for the Rooppur NPP was carried out using conservative assumptions, such as high leak rates and release fractions, which may not reflect real accident conditions. Consequently, while the approach ensures wide protective margins, the results may not be directly applicable to other reactor sites or designs without site-specific assessment.

Second, the analysis considered only adult radiation risk as representative of the population. Since children are generally more sensitive to radiation and often receive higher doses from the same exposure, the absence of age-specific dose assessments limits the comprehensiveness of the health impact evaluation. The use of HYSPLIT also restricted the inclusion of organ-specific and age-dependent dose coefficients. Furthermore, the model's 100×100 km grid resolution limits its ability to capture localized meteorological variations, particularly terrain-induced effects, though these are less significant for long-range transport.

Finally, in the routine operational analysis, the study focused only on external exposure from gaseous effluents, excluding liquid effluents and internal exposure pathways. This oversight is particularly relevant for radionuclides such as tritium and carbon-14, which are released through operational discharges and could contribute to internal dose. These constraints highlight areas where future studies could provide more detailed and comprehensive assessments.

7.3 Future Works

Although the findings improve our knowledge of emergency preparedness and protective action planning, there are still a number of topics that need more investigation.

First, for greater realism and accuracy, the modeling framework could be enhanced. Rather than depending on conservative release assumptions, future research should combine

atmospheric dispersion tools with severe accident progression codes such as MELCOR or MAAP to produce more realistic source terms. Predictive accuracy would also be increased by integrating real-time meteorological data from nearby weather stations into models like RASCAL, and HYSPLIT.

Second, the variety of accident scenarios taken into account should be increased in future studies. Assessments should cover multi-unit accidents, spent fuel pool accidents, and other hazards, both man-made (such as deliberate attacks) and natural (such as earthquakes and flooding), in addition to LBLOCA and LTSBO. A more thorough understanding of the effects on public health and the environment would be possible by looking into long-term effects like ground contamination, effects on the food chain, chronic exposure, and cancer risks.

There is a chance to improve policy development and emergency preparedness. The viability of constructing specialized radiation shelters in populated areas close to nuclear power plants, as well as the optimization of dynamic EPZs that adjust to shifting weather patterns, should be the main areas of research. Future research at the regional level should look at how serious accidents affect people across borders and offer models for coordinated emergency responses with nearby nations. Furthermore, considerable attention needs in how climate change affects nuclear plant vulnerability, plume dispersion, and extreme weather events.

Future studies that examine these topics may result in thorough risk assessments, enhanced protective action plans, and more robust nuclear safety planning in Bangladesh and across South Asia.

AI Credential Statement

This thesis was created by the author's original research concept, data analysis, and interpretation of findings. Artificial intelligence (AI) tools were used only for grammatical correction, language refinement. No artificial intelligence system was employed to create study material, data, or figures.

To ensure academic integrity, all information sources are referenced. The author examined the completed work to confirm correctness, originality, and conformity with the university's ethical standards. A plagiarism check was performed to ensure that the work met academic originality criteria.

REFERENCES

Ahangari, R., & Kalkhoran, O. N. (2019). A study of the protective actions for a hypothetical accident of the Bushehr nuclear power plant at different meteorological conditions. *Radiation and Environmental Biophysics*, *58*, 277–285.

Alam, R. (2024). Modeling of atmospheric dispersion and radiological dose consequences for a hypothetical accident in the perspective of Rooppur Nuclear Power Plant (RNPP). *Nuclear Engineering and Design*, *420*.

Altab, H., Sarim, S. K., Maruf, H. K., & Faraji, S. H. B. (2020). Radiological safety analysis of Rooppur Nuclear Power Plant site using atmospheric dispersion model. *International Journal of Low Radiation, 11*.

Ali, A. M., & Kakosimos, K. M. (2023). A receptor-centric decision support system for the mitigation of nuclear power atmospheric release incidents. *Reliability Engineering & System Safety, 238*, 109474.

Aliyu, A. S., Ramli, A. T., Garba, N. N., Ismaila, A., Abba, H. T., Saleh, M. A., & Aliyu, M. (2015). Assessment of environmental and human health impacts of a new nuclear power plant using hybrid single-particle Lagrangian air dispersion model. *Indian Journal of Science and Technology, 8*(S9), 489–500.

Alrammah, I., Saeed, I. M. M., Mhareb, M. H. A., & Alotiby, M. (2022). Atmospheric dispersion modeling and radiological environmental impact assessment for normal operation of a proposed pressurized water reactor in the eastern coast of Saudi Arabia. *Progress in Nuclear Energy, 145*, 10412.

Asmolov, V. G., Gusev, I. N., Kazanskiy, V. R., Povarov, V. P., & Statsura, D. B. (2017). New generation first-of-the-kind unit – VVER-1200 design features. *Nuclear Energy Technology, 3*, 260–269.

Athey, G. F., Brandon, L. K., & Ramsdell, J. V. J. (2013). *RASCAL 4.3 Workbook*. Washington, DC: U.S. Nuclear Regulatory Commission.

Auria, F. D., Suslov, A., Muellner, N., Petrangeli, G., & Cherubini, M. (2008). Accident management in VVER-1000. *Science and Technology of Nuclear Installations*.

Average-Weather-in-Ishurdi-Bangladesh-Year-Round#Figures-Summary. (Retrieved on 2023). (https://weatherspark.com/y/111701/)

Bakr, W. F., & Abdien, A. K. (2018). Assessing the emergency planning zones for the Egyptian nuclear power plant site. *Journal of Applied Physics, 10,* 76–85.

Bangladesh Atomic Energy Commission, Ministry of Science and Technology. (2022). *Installation of reactor pressure vessel for Rooppur nuclear power plant, unit-1*. Dhaka.http://rooppurnpp.portal.gov.bd/sites/default/files/files/rooppurnpp.portal.gov.bd/page/207f35cd_b9f3_44ff_9cf8_505f8834989e/2022-04-07-07-54-d83dd1331a30bb3cb4df44b02feb2b37.pdf

Barry, R., & Chorley, R. (2003). *Atmosphere, weather and climate* (8th ed.). Routledge.

Bateman, H. (1910). Solution of a system of differential equations occurring in the theory of radioactive decay transformation. *Proceedings of the Cambridge Philosophical Society, 15*, 423–427.

Belarussian NPP, Part 8.3. (2010). *NPP environmental impact assessment.*

Boeck, B. D. (2001). Prevention and mitigation measures to ensure containment integrity. *Nuclear Engineering and Design, 209*, 147–154.

Burgazzi, L., Fiorini, G. L., Magistris, F. D., Lensa, W. V., Staat, M., & Altes, J. (1998). Reliability assessment of passive safety systems. In *6th International Conference on Nuclear Engineering*, California.

Burson, E. G. (1975). *Structure shielding from cloud and fallout gamma-ray sources for assessing the consequences of reactor accident* (EGG-1183-1670).

Cao, B., Zheng, J., & Chen, X. (2016). Radiation dose calculations for a hypothetical accident in Xianning Nuclear Power Plant. *Science and Technology of Nuclear Installations*, Article ID 3105878.

Challa, V. S., Indrcanti, J., Baham, J. M., Rabarison, M. K. P. C., Young, J. H., Hughes, R., Swanier, S. J., Hardy, M. G., & Yerramilli, A. (2008). Sensitivity of atmospheric dispersion simulations by HYSPLIT to the meteorological predictions from a meso-scale model. *Environmental Fluid Mechanics, 8*, 367–387.

Chang, R., Schaperow, J., Ghosh, T., Barr, J., Tinkler, C., & Stutzke, M. (2012). *State-of-the-art reactor consequence analyses (SOARCA) Report* (NUREG-1935). Washington, DC: U.S. Nuclear Regulatory Commission.

CIEMAT (Centro de Investigaciones Energeticas Medioambientales y Tecnologicas). (2007). *CROM Code (Codigo de cRiba para evaluation de iMpacto) v6.0 Users guide*. Madrid, Spain: Editorial CIEMAT.

Clark, R. H. (1979). A model for short and medium range dispersion of radionuclides released to the atmosphere. *Technical Report NRPB-R91*, National Radiological Protection Board, UK.

Connan, O., Smith, K., Organo, C., Solier, L., Maro, D., & Hébert, D. (2013). Comparison of RIMPUFF, HYSPLIT, ADMS atmospheric dispersion model outputs using emergency response procedures, with 85Kr measurements made in the vicinity of nuclear reprocessing plant. *Journal of Environmental Radioactivity, 124*, 266–277.

Darnowski, P., Skrzypek, E., Mazgaj, P., Swirski, K., & Gandrille, P. (2015). Total loss of AC power analysis for EPR reactor. *Nuclear Engineering and Design, 289*, 8–18.

Draxler, R. R., & Hess, G. D. (1998). An overview of the HYSPLIT 4 modeling system for trajectories, dispersion, and deposition. *Australian Meteorological Magazine, 47*(4), 295–308.

Draxler, R. R., Arnold, D., Chino, M., Galmarini, S., Hort, M., Jones, A., & Saito, K. (2015). World Meteorological Organization's model simulations of the radionuclide

dispersion and deposition from the Fukushima Daiichi nuclear power plant accident. *Journal of Environmental Radioactivity, 139*, 172–184.

Draxler, R. R., Hess, G. D. (2015). *Description of the HYSPLIT 4 modeling system*. NOAA, Air Resources Laboratory.

Draxler, R., Stunder, B., Rolph, G., Stein, A., & Taylor, A. (2018). *HYSPLIT 4 User's Guides*. NOAA.

Draxler, R. R., Stunder, B., Rolph, G., & Stein, A. (2019). *HYSPLIT Tutorial*. NOAA Air Resources Laboratory.

https://www.ready.noaa.gov/documents/Tutorial_2019/html/index.html

Eckerman, K. F., Leggett, R. W. (2002). Dose *and risk coefficient file package for FGR-13*, FGR13PAK. TN: Oak Ridge National Laboratory.

Eckerman, K. F., Wolbarst, A. B., & Richardson, A. B. C. (1988). *Limiting values of radionuclide intake and air concentration and dose conversion factors for inhalation, submersion, and ingestion*. Federal Guidance Report No. 11, EPA-520/1-88-020. Washington, DC: U.S. Environmental Protection Agency.

Eckerman, K. F., Ryman, J. C. (1993). *External exposure to radionuclides in air, water, and soil*. Federal Guidance Report No. 12, EPA-402-R-93-081. Washington, DC: U.S. Environmental Protection Agency.

Environmental Impact Assessment. (2017). *Preliminary safety analysis report (PSAR), Rooppur NPP unit 1 and 2.*

Esfandiari, M., Jahanfarnia, G., Sepanloo, K., & Zarifi, E. (2019). Loss of offsite power accident analysis in a VVER-1000. *Nuclear Technology & Radiation Protection, 34*, 231–237.

Faisal, S. I, Soner, M. A. M., Islam, M. S., (2023). Prediction of radioactivity releases for a Long-Term Station Blackout event in the VVER-1200 nuclear reactor of Bangladesh. *Nuclear Engineering and Technology, 55*(2), 696-706.

Faisal, S. I, Ayoub, A., Soner, M. A. M., Islam, M. S., (2025). Deterministic assessment of emergency planning zones and radiological protective measures for Bangladesh's VVER-1200 reactor under severe postulated events. *Nuclear Engineering and Design*, *43.*

Faisal, S. I, Islam, M. S., (2025). Modeling and validation of airborne effluent dispersion and radiological doses from a VVER-1200 reactor routine operations using HYSPLIT. *Annals of Nuclear Energy,* 227, 111986.

Feyzinejad, M., Malakooti, H., Sadrinasab, M., & Ghader, S. (2019). Radiological dose assessment by means of a coupled WRF-HYSPLIT model under normal operation of Bushehr Nuclear Power Plant. *Pollution, 5*(2), 429–448.

German Commission on Radiological Protection. (2014). *Planning areas for emergency response near nuclear power plants*. Bonn.

Gifford, F. A. (1982). Horizontal diffusion in the atmosphere: A Lagrangian-dynamical theory. *Atmospheric Environment, 16*(3), 505–512.

Gyamfi, K., Birikorang, S. A., Ampomah-Amoako, E., & Fletcher, J. J. (2020a). Radiological risk assessment of a proposed site for a generic VVER-1000 using HotSpot and InterRas codes. *Progress in Nuclear Energy, 120*, 103239.

Gyamfi, K., Birikorang, S. A., Ampomah-Amoako, E., & Fletcher, J. J. (2020b). Radiological safety analysis for a hypothetical accident of a generic VVER-1000 nuclear power plant. *Science and Technology of Nuclear Installations*, Article ID 4721971.

Hanna, S. R., Briggs, G. A., & Hosker, R. P. (1982). *Handbook on atmospheric diffusion* (DOE/TIC-11223). U.S. Department of Energy.

Hanna, S., Briggs, R., & Britter, R. E. (2002). *Wind flow and vapor cloud dispersion at industrial and urban sites*. New York: Oxford University Press.

Homann, S. G., & Aluzzi, F. (2020). *HotSpot Health Physics Codes Version 3.1.2 User's Guide*. Livermore, CA: Lawrence Livermore National Laboratory.

https://www.ready.noaa.gov/ready2-bin/extract/extracta.pl

Huong, T. V., & Song, J. H. (2017). An analysis of containment responses during a station blackout accident. *Journal of Nuclear Science and Technology*.

ICRP. (1991). *1990 recommendations of the International Commission on Radiological Protection* (ICRP Publication 60, Annals ICRP 21(1–3)).

Inoue, M. (2012, February 13–15). *Overview of environmental contamination by radioactivity discharged from Fukushima Daiichi NPP*. Presented at the Japan/U.S. Department of Energy Workshop on Remediation.

Institute of Nuclear Power Operations. (2011). *Special report on the nuclear accident at the Fukushima Daiichi Nuclear Power Station* (INPO-11-005). Atlanta.

International Atomic Energy Agency. (1986). *Atmospheric dispersion models for application in relation to radionuclide releases* (IAEA-TECDOC-379). Vienna.

International Atomic Energy Agency. (2007). *Arrangements for preparedness for a nuclear or radiological emergency* (GS-G-2.1). Vienna.

International Atomic Energy Agency. (2011). *Status report 107 – VVER-1200 (V-392M)*. Vienna.

International Atomic Energy Agency. (2013a). *The International Nuclear and Radiological Event Scale User's Manual 2008 edition*. Vienna.

International Atomic Energy Agency. (2013b). *Actions to protect the public in an emergency due to severe conditions at a light water reactor* (EPR-NPP public protective actions). Vienna.

International Atomic Energy Agency. (2014). *Radiation protection and safety of radiation sources: International basic safety standards, General Safety Requirements (GSR) Part 3*. Vienna.

International Atomic Energy Agency. (2015a). *Preparedness and response for a nuclear and radiological emergency: General safety requirements Part 7*. Vienna.

International Atomic Energy Agency. (2015b). *The Fukushima Daiichi accident: Technical volume 4: Radiological consequences*. Vienna.
https://www-pub.iaea.org/MTCD/Publications/PDF/AdditionalVolumes/P1710/Pub1710-TV4-Web.pdf.

Jabbari, M., Hadad, K., & Pirouzmand, A. (2019). Re-assessment of station blackout accident in VVER-1000 NPP with additional measures following Fukushima accident using RELAP/Mod 3.2. *Annals of Nuclear Energy, 29*, 316–330.

Johansson, J., Kock, P., Boson, J., Karlsson, S., Isaksson, P., Lindgren, J., Tengborn, E., Maria, A., Buhr, B., & Bäverstam, U. (2018). *Review of Swedish emergency planning zones and distances*. Stockholm: Swedish Radiation Safety Authority.

Juyoul, K., & Moses, O. (2024). Radiological consequence assessment from long term station blackout nuclear accident on Buyende nuclear power plant of Uganda. *Annals of Nuclear Energy, 199*, 110366.

Juyoul, K., & Saleh, W. (2024). Enhancing resilience through nuclear emergency preparedness at El Dabaa site. *Science and Technology of Nuclear Installations*, Article ID 9345812.

Khai, N. T., & Cuong, L. D. (2015). Assessment of radioactive gaseous effluent released from Ninh Thuan 1 Nuclear Power Plant under scenario of INES-level 7 nuclear accident. *Communications in Physics, 25*, 375–382.

Khatun, M. A., Rashid, M. B., & Hygen, H. O. (2016). *Climate of Bangladesh* (Report no. 08/2016). Dhaka: Bangladesh Meteorological Department.

Kiehl, J. T., & Jacobson, M. Z. (2001). *Fundamentals of atmospheric modeling: Climatic change, 50*, 251–253.

Kim, H. J., Kim, J. S., Kim, K. P., Kwon, J. H., Kim, J. C., Jeong, J. Y., Yang, H. C., & Kim, Y. K. (2022). Radiological impact assessment of radioactive effluents emitted from nuclear power plants in Korea and China under normal operation. *Progress in Nuclear Energy, 153*, 104434.

Kong, T. Y., Kim, S., Lee, Y., Son, J. K., & Maeng, S. J. (2017). Radioactive effluents released from Korean nuclear power plants and the resulting radiation doses to members of the public. *Nuclear Engineering and Technology, 49*, 1772–1777.

Lamarsh, J. R., & Baratta, A. J. (2001). *Introduction to nuclear engineering* (3rd ed.). New Jersey: Prentice Hall.

Lee, H. L., Cho, J. L., Yoon, E. S., Cho, M., & Kim, D. G. (2016). Assessment of mass fraction and melting temperature for the application of limestone concrete and siliceous concrete to nuclear reactor basement considering molten core-concrete interaction. *Nuclear Engineering and Technology*, 448–456.

Lee, S. W., Hong, T. H., Seo, M. R., Lee, Y. S., & Kim, H. T. (2014). Extended station blackout coping capabilities of APR1400. *Science and Technology of Nuclear Installations*.

Marshall, J., & Plumb, R. A. (1965). *Atmosphere, ocean and climate dynamics: An introductory text* (Vol. 8). Academic Press.

McKenna, T. J., & Giitter, J. (1988). *Source term estimation during incident response to severe nuclear power plant accidents.* NUREG-1228, Washington, DC: U.S. Nuclear Regulatory Commission.

McMahon, C., Kelleher, K., cGinnity, P., Organo, C., Smith, K., Currivan, L., & Ryan, T. (2013). *Proposed nuclear power plants in the UK – potential radiological implications for Ireland*. Radiation Protection Institute of Ireland, RPII 13/01.

Ministry of Science and Technology. (2012). *Bangladesh Atomic Energy Regulatory Act (Act No. 19 of 2012)*. Dhaka, Bangladesh.

Ministry of Science and Technology. (2020). *National nuclear and radiological emergency and preparedness response plan*. Dhaka, Bangladesh

Mollah, A. S., & Chakraborty, S. R. (2009). Radioactivity and radiation levels in and around the proposed nuclear power plant site at Rooppur. *Japanese Journal of Health Physics, 44*(4), 408–413.

Muhammad, B. U. G., & Juyoul, K. (2019). Nuclear emergency management using accident consequence analysis code. *Journal of Korean Society for Hazard Mitigation, 19*, 215–225.

National Radiological Protection Board & Kernforschungszentrum Karlsruhe. (n.d.). *PC COSYMA* (EUR 16240 EN, NRPB-SR280).

Nath, P. D., Rahman, K. M., & Bari, M. A. A. (2020a). Thermal hydraulic analysis of a nuclear reactor due to loss of coolant accident with and without emergency core cooling system. *Journal of Engineering Advancements, 01*, 53–60.

Nath, P. D., Rahman, K. M., & Bari, M. A. A. (2020b). Investigation on thermal-hydraulic parameters of a nuclear reactor (VVER-1200) due to loss of coolant accident with station blackout and failure of emergency core cooling system. *Proceedings of the International Conference on Mechanical, Industrial and Energy Engineering*, Khulna.

Nielsen, S. T., Deme, S., & Mikkelsen, T. K. (1999). Description of the atmospheric dispersion module. *RIMPUFF, RODOS (WG2)-TN(98)-02*.

Omar, N., Koh, M. H., & Hashim, S. (2019). Radiological dose assessment due to hypothetical nuclear power plant operation in Mersing, Johor, Malaysia. *Malaysian Journal of Fundamental and Applied Sciences, 15*(4), 532–536.

Organization for Economic Co-operation and Development Nuclear Energy Agency. (2002). *Chernobyl: Assessment of radiological and health impact*. Paris, France.

Panofsky, H. A., & Dutton, J. A. (1984). *Atmospheric turbulence*. New York: John Wiley & Sons.

Pasquill, F. (1974). *Atmospheric diffusion* (2nd ed.). New York: John Wiley & Sons.

Perryman, L. J. (2005). Risk-informed emergency planning requirements for Koeberg Nuclear Power Station. *International Seminar on Emergency Risk Zoning around Nuclear Power Plants*.

Petersen, W. B., & Lavdas, L. G. (1986). INPUFF 2.0—*A multiple source Gaussian puff dispersion algorithm: User's guide*. EPA-600/8-86/024. Washington, DC: U.S. Environmental Protection Agency.

Pirouzmand, A., Dehghani, P., Hadad, K., & Nematollahi, M. (2015). Dose assessment of radionuclides dispersion from Bushehr nuclear power plant stack under normal operation and accident conditions. *International Journal of Hydrogen Energy, 40*(44), 15198–15205.

Pirouzmand, A., Kowsar, Z., & Dehghani, P. (2018). Atmospheric dispersion assessment of radioactive materials during severe accident conditions for Bushehr nuclear power plant using HYSPLIT code. *Progress in Nuclear Energy, 108*, 169–178.

Ramsdell, Jr., J. V., & Fosmire, C. J. (1998). Estimating concentrations in plumes released in the vicinity of buildings: Model development. *Atmospheric Environment, 32*, 1663–1677.

Ramsdell, J. V. J., Athey, G. F., McGuire, S. A., & Brandon, L. K. (2012). *RASCAL 4: Description of models and methods* (NUREG-1940). Washington, DC: U.S. Nuclear Regulatory Commission.

Ramsdell, J.V., Athey, Jr G.F., Rishel, J.P. (2013). *RASCAL 4.3: User's Guide (Draft.*,

Ramsdell, J. V. J., Athey, G. F., Rishel, J. P. (2015). *RASCAL 4.3: Description of models and methods* (NUREG-1940 Supplement 1). Washington, DC: U.S. Nuclear Regulatory Commission.

Raskob, W., & Gering, F. (2010). *Realtime online decision support system (RODOS)*. (http://www.rodos.fzk.de)

Rooppur Nuclear Power Plant Construction Project. (n.d.). A *snapshot on Rooppur Nuclear Power Plant Project*.
https://rooppurnpp.portal.gov.bd/sites/default/files/files/rooppurnpp.portal.gov.bd/notices/7e349f02_ec26_4a27_be29_66ef81041cb8/A%20snapshot%20on%20Rooppur%20Nuclear%20Power%20Plant%20Project.pdf

ROSATOM, *www. Rosatom.ru.*

Rosatom Technical Academy & National Research Nuclear University "MEPhI". (2019, May). *Course: Fundamentals of modern Russian designed NPP with VVER 1200 power reactor, Module 5: VVER safety systems*.

Sadhukhan, R. K., & Synzynys, B. I. (2023). Comprehensive assessment of radiation impact from natural radioactivity and tritium around Rooppur NPP before commissioning and predicted exposures of NPP operation. *Progress in Nuclear Energy, 164*, 104872.

Saeed, I. M. M., Saleh, M. A. M., Hashim, S., Hama, Y. M. S., Hamza, K., & Shatri, H. A. S. (2020). The radiological assessment, hazard evaluation, and spatial distribution for a hypothetical nuclear power plant accident at Baiji potential site. *Environmental Sciences Europe, 32*(6).

Sahadat, M. H., & Fairuz, A. (2020a). Assessment of the potential total effective dose (TED) and ground deposition (GD) following a hypothetical accident at the proposed Rooppur Nuclear Power Plant. *Applied Radiation and Isotopes, 158*.

Sahadat, M. H., & Fairuz, A. (2020b). Characterization of atmospheric radiological dispersion alongside risky location designation and shelter house proposition around the planned Rooppur Nuclear Power Plant. *ASME Journal of Nuclear Radiation Science, 6*(4), 042003.

Sahin, S., & Ali, M. (2016). Emergency planning zones estimation for Karachi-2 and Karachi-3 nuclear power plants using Gaussian puff model. *Science and Technology of Nuclear Installations*, Article ID 8549498.

Salari, F., Rabiee, A., & Faghihi, F. (2023). Assessment of the core-catcher in the VVER-1000 reactor containment under various severe accidents. *Nuclear Engineering and Technology, 55*, 144–155.

Scherpelz, R. I., Bander, T. J., Athey, G. F., & Ramsdell, J. V. (1986). *The MESORAD dose assessment model: Volume 1, Technical basis* (NUREG/CR-4000). Washington, DC: U.S. Nuclear Regulatory Commission.

Schulze, R. H., & Turner, D. (1996). *Practical guide to atmospheric dispersion modeling*. Texas: Trinity Consultants Inc.

Seinfeld, J. H. (1986). *Atmospheric chemistry and physics of air pollution*. New York: John Wiley & Sons.

Shamsuddin, S. D., Basri, N. A., Omar, N., Koh, M. H., Ramli, A. T., & Hassan, W. M. S. W. (2017). Radioactive dispersion analysis for hypothetical nuclear power plant (NPP) candidate site in Perak state, Malaysia. *EPJ Web of Conferences, 156*, 00009.

Shipler, D. B., Napier, B. A., Farris, W. T., & Freshley, M. D. (1996). Hanford Environmental Dose Reconstruction Project—An Overview. *Health Physics, 71*, 532–544.

Shiuli, S. S., Khaer, M. A., Islam, M. M., Hoq, M. A., Hossain, S. M., & Chowdhury, M. T., Rahman, M. M. (2022). Assessment of radiological safety and emergency response of VVER-1200 type reactor. *International Journal of Advanced Nuclear Reactor Design and Technology, 4*, 70–79.

Sjoreen, A. L., & McKenna, T. J., Julius, J. (1987). *Source term estimation using MENU-TACT* (NUREG/CR-4722). Washington, DC: U.S. Nuclear Regulatory Commission.

Slinn, W. G. N. (1984). Precipitation scavenging. In D. Randerson (Ed.), *Atmospheric Science and Power Production* (DOE/TIC-27601). Washington, DC: U.S. Department of Energy.

Soffer, L., Burson, S. B., Ferrell, C. M., & Lee, R. Y. (1995). *Accident source terms for light-water nuclear power plants* (NUREG-1465). Washington, DC: U.S. Nuclear Regulatory Commission.

Sohrabi, M., Parsouzi, Z., Amrollahi, R., Khamooshy, C., & Ghasemi, M. (2013). Public exposure from environmental release of radioactive material under normal operation of unit-1 Bushehr nuclear power plant. *Annals of Nuclear Energy, 55*, 351–358.

Souissi, R., Tawfik, F., Ramadan, A. B., & Reguigui, N. (2019). Atmospheric dispersion modeling of basis-design accident (LOCA) and radioactive dose assessment of two proposed sites for nuclear power plant in Tunisia. *International Journal of Engineering Applied Sciences and Technology, 4*(3), 2455–2143.

State Office for Nuclear Safety. (2001). *Assessment of beyond design and severe accidents consequences: Principles and methods of emergency planning and response at NPP Temelin*. Praha: State Office for Nuclear Safety.

Stein, A. F., Draxler, R. R., Rolph, G. D., Stunder, B. J. B., Cohen, M. D., & Ngan, F. (2015). NOAA's HYSPLIT atmospheric transport and dispersion modeling system. *Bulletin of the American Meteorological Society, 96 (12)*, 2059–2077.

Stull, R. B. (1998). *An introduction to boundary layer meteorology*. Boston: Kluwer Publication.

Tang, M. L., Tsuang, B. J., & Kuo, P. H. (2016). Dose estimation for nuclear power plant 4 accident in Taiwan at Fukushima nuclear meltdown emission level. *Journal of Environmental Radioactivity*, *155–156*, 71–83.

Tusheva, P., Reinke, N. (2007). Comparative analyses of thermal hydraulic behaviour of VVER-1000/V-320 for a station blackout accident scenario with ASTEC 1.2.1 and ATHLET 1.2. *Proceedings of Annual Meeting on Nuclear Technology*, Karlsruhe, Germany.

Tusheva, P., Schaefer, F., Rohde, U., & Reinke, N. (2009). Investigation on accident management measures for VVER-1000 reactors. *19th AER Symposium on VVER Reactor Physics and Reactor Safety*, St. Constantine and Elena Resort, Varna, September 21–25.

Tusheva, P., Schäfer, F., Reinke, N., Altstadt, E., & Kliem, S. (2012). Study on severe accidents and countermeasures for VVER-1000 reactors using the integral code ASTEC. *Kerntechnik, 77*(4), 271–277.

Udiyani, P. M., & Husnayani, I. (2017). Analysis of radiation safety in the nuclear power plant (NPP) site in normal operation condition, Sebagin site study. *Indonesian Journal of Nuclear Science and Technology, 18*(2), 73–84.

U.S. Environmental Protection Agency. (2017). *PAG manual: Protective action guides and planning guidance for radiological incidents*. Washington, DC.

U.S. Nuclear Regulatory Commission. (1980). *Criteria for preparation and evaluation of radiological emergency response plans and preparedness in support of nuclear power plants (NUREG-0654, FEMA-REP-1, Rev.1)*. Washington, DC.

U.S. Nuclear Regulatory Commission. (1982a). *Atmospheric dispersion models for potential accident consequence assessment at nuclear power plants* (Regulatory Guide 1.145, Rev. 1). Washington, DC.

U.S. Nuclear Regulatory Commission. (1982b). *Background and derivation of ANS-5.4 standard fission product release model* (NUREG/CR-2507). Washington, DC.

U.S. Nuclear Regulatory Commission. (1990). *Severe accident risks: An assessment for five U.S. nuclear power plants* (NUREG-1150). Washington, DC.

U.S. Nuclear Regulatory Commission. (2001). *MELCOR Computer Code Manual*, **NUREG/CR-6119.** Washington, DC.https://www.nrc.gov/docs/ML2104/ML21042B319.pdf.

U.S. Nuclear Regulatory Commission. (2010). *Criteria for protective actions recommendations for severe accidents: Review of NUREG-0654 Supplement 3 (NUREG/CR-6953)*. Washington, DC.

U.S. Nuclear Regulatory Commission. (2012). *Petition for rulemaking to improve emergency planning regulations (10 CFR 50.47)*. Washington, DC.

U.S. Nuclear Regulatory Commission. (2013a). *State-of-the-art reactor consequence analysis project: Volume 2, Surry bottom integrated analysis* (NUREG/CR-7110, Vol. 2, Rev. 1). Washington, DC.

U.S. Nuclear Regulatory Commission. (2013b). *Radiological Toolbox* [computer software]. Washington, DC.

Van der Hoven, I. (1968). Deposition of particles and gases. In D. H. Slade (Ed.), *Meteorology and atomic energy* (pp. 202–207). Washington, DC: U.S. Atomic Energy Commission.

Young, R. M., West, P. E., & Goh, S. G. K. (1990). PIGLET: A nuclear accident pathway model. *Nuclear Technology, 92*(1), 45–59.

Zali, A., Zafarghandi, M. S., Feghhi, S. A., & Taherian, A. M. (2017). Public member dose assessment of Bushehr Nuclear Power Plant under normal operation by modeling the fallout from stack using the HYSPLIT atmospheric dispersion model. *Journal of Environmental Radioactivity, 171*, 1–8.

Zubair, M., Eslam Ahmed, E., & Hartanto, D. (2022). Estimation of public exposure during normal operation of unit-1 Barakah Nuclear Power Plant using GALE and HOTSPOT. *South African Journal of Chemical Engineering, 41*, 235–243.

APPENDIX A

Nuclear Accident Classification and Past Severe Accidents

To classify nuclear accidents, the IAEA and the OECD's NEA created the INES. This scale ranges from Level 1 (anomaly) to Level 7 (severe accident), with each level representing an event that is roughly ten times more serious than the previous one. Levels 1 to 3 are considered incidents, while Levels 4 to 7 are classified as accidents (IAEA, 2013a) as shown in **Figure A-1.** The public often reacts with concern to radioactive leaks, particularly those rated at Level 3 or higher. **Figure A-2** shows the INES ranking procedure of Levels 4 to 7.

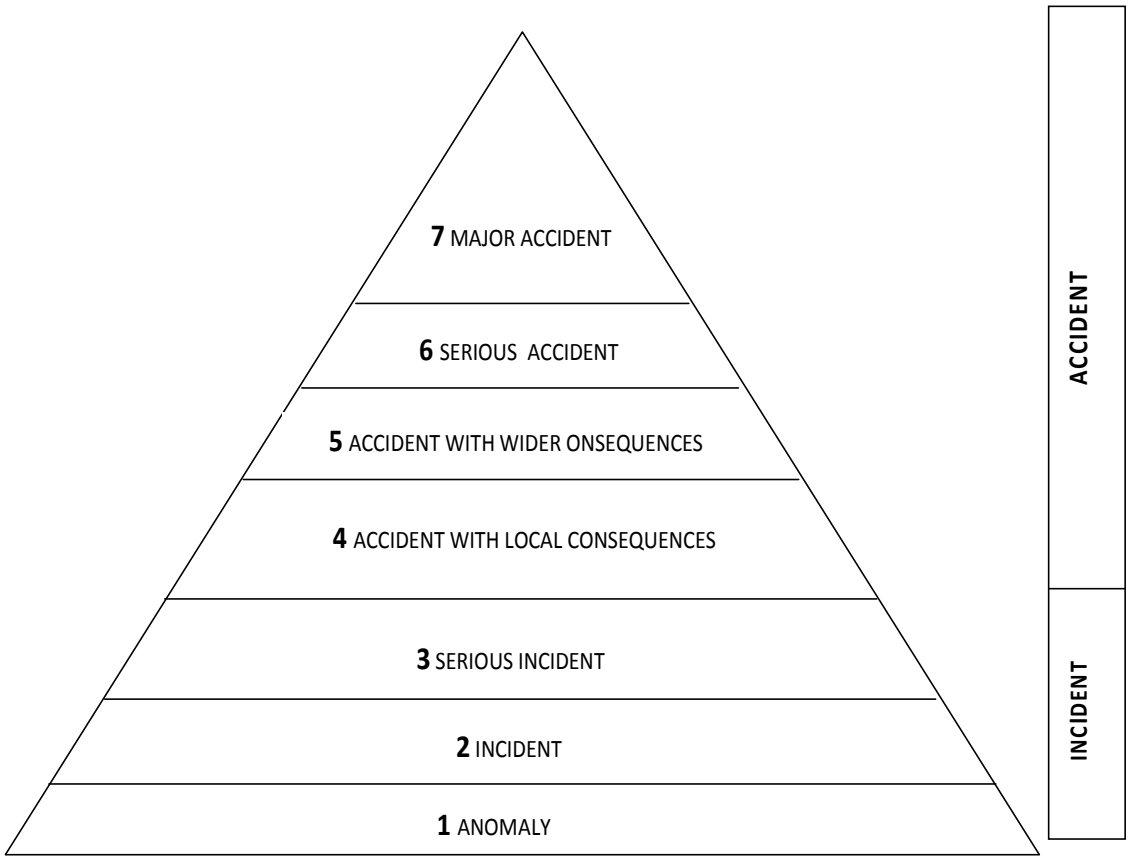

Figure A-1: INES Event Scale Rating.

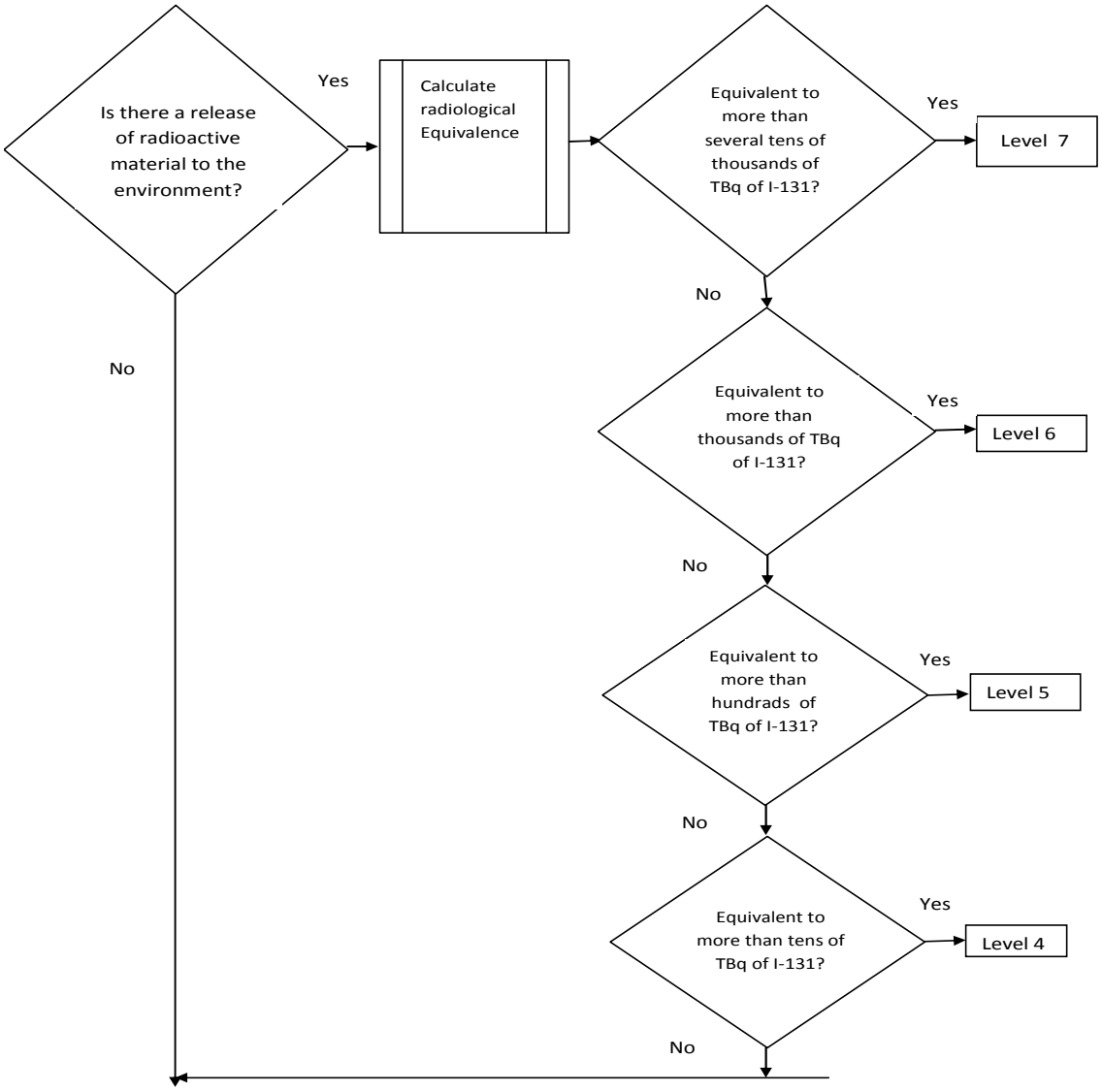

Figure A-2: INES Accident Rating Procedure (IAEA, 2013a).

Three Mile Island (USA), Chernobyl (Ukraine), and Fukushima Daiichi (Japan) are the three major nuclear reactor accidents in history that have caused large radioactive leaks.

On March 28, 1979, Unit 2 of a PWR in Pennsylvania experienced the **Three Mile Island (TMI)** accident. A mechanical problem and operator error caused a relief valve to become jammed open, leading to primary coolant loss and partial core meltdown (Clark, 1989). Even though the reactor was only in operation for a short time, noble gases such as xenon-135 and traces of iodine, cesium, and strontium were emitted, resulting in a lower inventory of fission

products. The containment building successfully retained most of the radionuclides, reducing the environmental damage significantly. The accident was classified as Level 5 on the INES.

On April 26, 1986, a turbine shutdown test at Unit 4 of the Chernobyl NPP resulted in the **Chernobyl accident**, the most catastrophic nuclear accident to date. The RBMK reactor design was intrinsically unstable at low power and lacked a suitable containment structure. During the test, operator actions such as removing control rods and reducing coolant flow caused a positive void effect, which resulted in a rapid power surge due to reduced neutron absorption. This resulted in two explosions that ruptured the reactor and ejected fuel and graphite into the atmosphere. Fires from exposed graphite burned for 10 days, dispersing radioactive materials over vast areas. Approximately 1.2×10^7 TBq of radionuclides were released, including all noble gases and significant fractions of volatile isotopes, while 3–4% of the reactor core was physically expelled (OECD NEA, 2002). Due to its scale and impact, the event was rated Level 7 on the INES.

The **Fukushima Daiichi accident** began on March 11, 2011, following a 9.0-magnitude earthquake and subsequent tsunami. These natural disasters caused total loss of on-site and off-site power—resulting in an SBO—and rendered emergency diesel generators and cooling systems inoperable across Units 1–3, all of which were operating at the time. Units 1, 2, and 3 experienced fuel damage, hydrogen production via zirconium-steam interactions, and hydrogen explosions due to the inability to remove decay heat, which caused core temperatures to rise. Radioactive materials were able to escape because of the substantial harm these explosions caused to containment structures. Mobile generators, water injection devices, and ground-based and helicopter cooling efforts were among the emergency response strategies. Air, ocean, drinking water, and food were all radioactively contaminated; high concentrations of iodine-131 and cesium-134/cesium-137 were detected (IAEA, 2015b). Due to the magnitude of radioactive emissions in the early phases of the crisis, the incident was first rated as Level 5, but it was subsequently elevated to Level 7.

APPENDIX B

Rooppur NPP

In 1961, the government first proposed the construction of a NPP to meet the nation's growing energy needs. Following extensive site evaluations based on global best practices, the Rooppur site—which is situated on the eastern bank of the Padma River, roughly 160 km northwest of Dhaka—was selected as the ideal location in 1963. It is about 21 km northwest of Pabna city and 8 km from the Ishurdi sub-district center. Geographically, the area is between latitudes 24°03′ and 24°04′ north and longitudes 89°02′ and 89°03′ east (Rooppur Nuclear Power Plant Construction Project, n.d.). The Rooppur NPP, the country's first nuclear power plant, represents a major shift in Bangladesh's energy system.

The facility consists of two 1,200 MW_e Generation III+ pressurized water reactors (PWR) plant of AES–2006 (VVER –1200, V-392M) technology. The plant design of Rooppur NPP reactor Units 1 and 2, incorporates the design, equipment manufacturing, construction, and commissioning experiences of Novovoronezh NPP-II'. It has advanced engineering features that are appropriate for Rooppur's specific seismic, hydrological, and climatic conditions. After extensive feasibility studies, environmental impact assessments, and project site evaluations, work began in 2013 (Bangladesh Atomic Energy Commission, 2022). **Figure B-1** shows the Google Earth image of the Rooppur site.

Figure B-1: Rooppur NPP Site view image taken from Google Earth

The Rooppur NPP uses a simplified and standardized reactor design, with each reactor unit having four coolant loops with horizontal steam generators and pumps. While turbine systems are intended to operate for 50 years, the main reactor equipment has a 60-year service life. The design also includes robust protection against environmental disasters such as earthquakes, floods, tornadoes, plane crashes, and fires (Rooppur Nuclear Power Plant Construction Project, n.d.). The Bangladesh Atomic Energy Regulatory Authority (BAERA) is responsible for regulatory oversight. In cooperation with Russian agencies and foreign organizations such as the IAEA, BAERA examined important documents such as the Quality Assurance (QA) program, Probabilistic Safety Assessment (PSA), and Preliminary Safety Analysis Report (PSAR). The project is expected to enhance energy security, reduce carbon emissions, foster regional development, and significantly increase Gross Domestic Product (GDP) growth through both direct and indirect economic benefits (Rooppur Nuclear Power Plant Construction Project, n.d.).

APPENDIX C

VVER-1200 Reactor System Overview

An improvement of the well-proven VVER-1000 technology is the VVER-1200 (V-392M) reactor with AES-2006 design, which is a member of the Generation III+ series. The design attempts to keep the likelihood of significant radioactive release and the probability of severe core damage below 1×10^{-6} per reactor-year and 1×10^{-6} per reactor-year, respectively (IAEA, 2011). The VVER-1200 reactor transfers thermal energy from the core to the secondary circuit by means of a closed-loop Reactor Coolant System (RCS). A pressurized water reactor (PWR), four circulation loops with steam generators, reactor coolant pumps (RCPs), and connected pipelines are all part of this system. **Figure C-1** presents the key components and interconnected equipments of the VVVER-1200 (AES 2006) reactor.

Primary System Components

Reactor Pressure Vessel

The reactor's internal components, which are contained in a vertical pressure vessel, include the core barrel, baffle, and protective tubes. There are control rod drives at the top of the head. In a reinforced concrete cavity with seismic barriers and thermal protection, the reactor vessel is securely fastened.

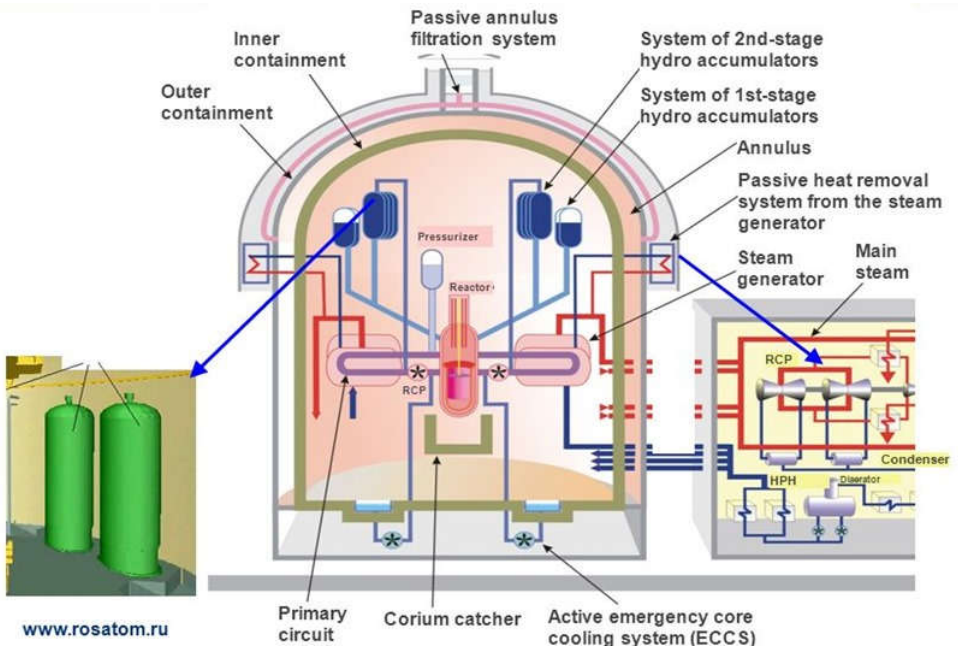

Figure C-1: Main Components of the VVER-1200 (AES 2006) Plant (ROSATOM, n.d.).

Steam Generator (SG)

A horizontal SG, consisting of bundles of heat-exchange tubes housed inside a cylindrical steel vessel, is installed in each loop. Hydraulic expansion of the U-shaped tubes creates primary collectors with corrosion-resistant coating and thick walls. The horizontal design reduces the height of the building and increases seismic stability. Heat-exchange tubes, which serve as a connection between the radioactive primary circuit and the SGs, prevent radioactive leakage.

Pressurizer

To ensure pressure stability in the primary circuit, the pressurizer, a vertical cylindrical vessel, is equipped with internal heaters and spray systems. It is essential for controlling system pressure in transient, steady-state, cooling, and startup situations.

Reactor Coolant Pump (RCP)

RCPs are made to coast down in the event of a power failure and circulate coolant continuously. They have a pressure head of 0.588 MPa and a flow rate of 21,500 m^3/h (IAEA, 2011).

Main Coolant Pipeline

The reactor, steam generators, and RCPs are all connected by the main coolant pipeline. Its 850 mm internal diameter and "leak-before-break" design principles assure optimal flow rates and low pressure loss. In order to minimize operating losses, it also has heat insulation and hot and cold legs.

Core and Fuel Design

Each of the 163 fuel assemblies (FAs) that comprise the reactor core contains 312 fuel rods filled with up to 5% enriched uranium dioxide (UO_2) pellets. For corrosion resistance and structural integrity, the rods are covered with zirconium alloy. For reactivity control, the core incorporates 121 control rod cluster assemblies (RCCAs), which are operated by actuators powered by electromagnets. 42 new FAs are normally reloaded each year, and the fuel can reach up to 60 MWd/kgU in burnup over a 12-month cycle. The average linear heat generation rate is 167.8 W/cm (IAEA, 2011).

Auxiliary Systems

Auxiliary systems help with primary operations by providing compressed air for valve actuation, nitrogen for gas blowdowns, hydrogen ignition systems to avoid explosive mixes, and ventilation systems to assure radiological and environmental safety. These auxiliary systems make maintenance easier, keep operations running smoothly, and keep people safe.

Operating Conditions

The VVER-1200 is designed for 100% nominal power under standard operation. It supports flexible load maneuvering and transient conditions without requiring reactor trips, with power ramp rates ranging from 0.017 to 3% of nominal power per minute. The reactor follows a once-through, open fuel cycle with refueling intervals of 12 months and a total cycle length of approximately 4 years. It is possible to operate for up to 20 months (IAEA, 2011).

Advanced Safety features of VVER-1200 Reactor

The VVER-1200 reactor has improved thermal power capacity and reliability in heat removal from the reactor core compared to the VVER-1000, due to enhancements in primary and secondary circuit parameters (pressure and temperature) and a 2000 m^3/h increase in main circulation pump performance (Asmolov,et al., 2017).

The VVER-1200 reactor incorporates a robust design with defense-in-depth, double containment with a ventilated gap, and a system to retain molten core material called core catcher. Reactor includes passive heat removal and core flooding systems with secondary hydraulic accumulators for cooling during blackouts (Asmolov et al., 2017). In the VVER-1200 reactor, the stage 1 and stage 2 passive safety hydraulic accumulators function independently for up to 24 hours and significantly longer (IAEA, 2011). Additionally, the four-channel Steam Generator Passive Heat Removal System (SG PHRS) in the secondary circuit can operate for up to 72 hours during accidents involving a complete station blackout, even in the absence of operator intervention for steam generator feed-water failures (Rosatom Technical Academy & National Research Nuclear University "MEPhI", 2019). A core-catcher at the containment base may manage core melt accidents by reducing pressure, temperature, hydrogen, and radioactive gases, preventing explosions.

To improve stability against rare events like Fukushima and enhance operational independence during BDBA, the VVER-1200 design includes additional measures such as spent fuel pool heat removal, alternative reactor cooling, and continuous safety monitoring. Additional systems for increased safety include a mobile emergency diesel generator, mobile pumping unit, ventilation cooling tower,

APPENDIX D

360 Weather Scenarios

Yearly Scenario No	Month	Monthly Scenarios No.	Monte Carlo random sampling wind speed (m/s) based on Table 4-4	Random Time	Random values (0-1) for rainfall	Precipitation type based on CONDITIONAL FORMULA of Table 4-4	Stability class based on Table 3-4
1	January	1	1.8	Night	0.5	No Precipitation	F
2		2	1.8	Day	0.5	No Precipitation	B
3		3	2.0	Day	0.7	No Precipitation	B
4		4	1.6	Day	0.9	No Precipitation	B
5		5	2.9	Day	0.2	No Precipitation	B
6		6	1.9	Day	0.9	No Precipitation	B
7		7	3.1	Night	0.4	No Precipitation	E
8		8	3.4	Night	0.5	No Precipitation	E
9		9	2.6	Day	0.1	No Precipitation	B
10		10	1.5	Night	0.6	No Precipitation	F
11		11	1.7	Day	0.2	No Precipitation	B
12		12	2.3	Day	0.6	No Precipitation	B
13		13	1.9	Day	0.8	No Precipitation	B
14		14	2.6	Night	1.0	light	E
15		15	2.1	Night	0.1	No Precipitation	E
16		16	3.1	Day	0.0	No Precipitation	C
17		17	2.9	Night	0.5	No Precipitation	E
18		18	2.7	Day	0.7	No Precipitation	B
19		19	2.3	Night	0.4	No Precipitation	E
20		20	3.1	Night	0.3	No Precipitation	E
21		21	2.9	Day	0.9	No Precipitation	B
22		22	3.0	Day	0.4	No Precipitation	B
23		23	2.4	Day	0.2	No Precipitation	B
24		24	1.9	Night	0.8	No Precipitation	F
25		25	2.7	Night	0.3	No Precipitation	E
26		26	2.9	Night	0.1	No Precipitation	E
27		27	1.8	Night	0.3	No Precipitation	F
28		28	2.3	Day	0.1	No Precipitation	B

29		29	2.3	Day	0.2	No Precipitation	B
30		30	2.8	Night	0.2	No Precipitation	E
31	February	1	4.4	Night	0.2	No Precipitation	E
32		2	2.3	Day	0.0	No Precipitation	B
33		3	2.7	Day	0.7	No Precipitation	B
34		4	3.0	Day	0.8	No Precipitation	B
35		5	2.2	Night	0.2	No Precipitation	E
36		6	2.3	Night	0.8	No Precipitation	E
37		7	2.2	Day	0.6	No Precipitation	B
38		8	2.0	Day	0.5	No Precipitation	B
39		9	3.0	Day	0.6	No Precipitation	B
40		10	2.8	Day	0.5	No Precipitation	B
41		11	2.2	Day	0.9	No Precipitation	B
42		12	3.4	Day	1.0	light	D
43		13	1.8	Day	0.5	No Precipitation	B
44		14	2.9	Night	1.0	light	E
45		15	2.6	Night	1.0	light	E
46		16	3.0	Day	0.3	No Precipitation	B
47		17	2.2	Day	0.6	No Precipitation	B
48		18	2.6	Day	0.9	No Precipitation	B
49		19	1.7	Night	0.3	No Precipitation	F
50		20	2.3	Night	0.7	No Precipitation	E
51		21	1.2	Night	0.7	No Precipitation	F
52		22	2.2	Day	0.5	No Precipitation	B
53		23	2.2	Night	0.8	No Precipitation	E
54		24	2.6	Day	0.3	No Precipitation	B
55		25	2.8	Day	0.6	No Precipitation	B
56		26	4.0	Day	0.1	No Precipitation	C
57		27	2.0	Day	0.1	No Precipitation	B
58		28	1.6	Day	0.1	No Precipitation	B
59		29	3.1	Night	0.8	No Precipitation	E
60		30	2.6	Night	0.8	No Precipitation	E
61		1	2.2	Night	0.1	No Precipitation	E
62		2	3.1	Night	0.6	No Precipitation	E
63		3	2.7	Night	0.4	No Precipitation	E
64		4	3.1	Day	0.1	No Precipitation	C
65		5	3.4	Day	0.5	No Precipitation	C
66		6	2.4	Day	0.0	No Precipitation	B
67		7	2.8	Night	0.1	No Precipitation	E
68		8	2.9	Day	0.9	No Precipitation	B
69		9	4.4	Night	0.2	No Precipitation	E
70		10	1.5	Day	0.4	No Precipitation	B
71		11	1.6	Night	0.9	light	E

72	March	12	2.8	Day	0.5	No Precipitation	B
73		13	3.2	Day	0.8	No Precipitation	C
74		14	1.3	Day	0.0	No Precipitation	B
75		15	1.8	Day	0.4	No Precipitation	B
76		16	2.8	Day	0.7	No Precipitation	B
77		17	3.0	Night	0.5	No Precipitation	E
78		18	3.4	Night	1.0	moderate	D
79		19	4.0	Day	0.0	No Precipitation	C
80		20	3.9	Day	0.1	No Precipitation	C
81		21	2.8	Day	0.5	No Precipitation	B
82		22	3.8	Day	0.6	No Precipitation	C
83		23	3.7	Night	0.4	No Precipitation	E
84		24	4.7	Night	0.1	No Precipitation	E
85		25	1.2	Night	0.9	light	E
86		26	2.4	Night	0.8	No Precipitation	E
87		27	3.3	Night	0.2	No Precipitation	E
88		28	3.0	Day	0.2	No Precipitation	B
89		29	3.4	Day	0.8	No Precipitation	C
90		30	2.6	Day	0.4	No Precipitation	B
91	April	1	3.8	Day	0.3	No Precipitation	C
92		2	2.3	Day	0.8	No Precipitation	B
93		3	4.8	Day	0.6	No Precipitation	C
94		4	3.5	Night	0.8	light	D
95		5	4.0	Night	0.1	No Precipitation	E
96		6	3.6	Night	0.2	No Precipitation	E
97		7	3.7	Night	0.8	light	D
98		8	3.1	Night	0.1	No Precipitation	E
99		9	3.4	Day	0.3	No Precipitation	C
100		10	4.0	Night	0.7	No Precipitation	E
101		11	2.8	Day	0.3	No Precipitation	B
102		12	3.3	Day	0.3	No Precipitation	C
103		13	3.7	Day	0.9	light	D
104		14	3.3	Night	0.2	No Precipitation	E
105		15	2.8	Day	0.7	No Precipitation	B
106		16	3.9	Night	0.0	No Precipitation	E
107		17	3.9	Night	0.5	No Precipitation	E
108		18	1.6	Night	0.1	No Precipitation	F
109		19	4.4	Night	0.3	No Precipitation	E
110		20	3.9	Night	0.9	light	D
111		21	3.6	Day	0.7	No Precipitation	C
112		22	1.9	Night	0.9	light	E
113		23	2.6	Night	0.1	No Precipitation	E
114		24	2.9	Night	0.8	No Precipitation	E

115		25	2.0	Day	0.3	No Precipitation	B
116		26	3.7	Night	0.9	light	D
117		27	2.4	Day	0.3	No Precipitation	B
118		28	3.4	Day	0.4	No Precipitation	B
119		29	2.0	Day	0.3	No Precipitation	B
120		30	3.0	Day	0.8	No Precipitation	B
121	May	1	3.9	Day	0.6	No Precipitation	C
122		2	5.0	Day	0.1	No Precipitation	C
123		3	2.9	Day	0.1	No Precipitation	B
124		4	3.5	Day	0.1	No Precipitation	C
125		5	5.5	Night	0.8	light	D
126		6	2.4	Night	0.0	No Precipitation	E
127		7	3.8	Night	0.8	light	D
128		8	4.7	Night	0.1	No Precipitation	E
129		9	3.2	Night	0.9	light	D
130		10	4.6	Day	0.3	No Precipitation	C
131		11	3.4	Night	0.1	No Precipitation	E
132		12	2.4	Night	0.3	No Precipitation	E
133		13	3.6	Night	0.0	No Precipitation	E
134		14	2.6	Night	0.8	light	E
135		15	2.7	Day	0.3	No Precipitation	B
136		16	2.5	Night	0.4	No Precipitation	E
137		17	2.7	Night	0.3	No Precipitation	E
138		18	2.8	Day	0.4	No Precipitation	B
139		19	4.0	Night	0.4	No Precipitation	E
140		20	4.9	Night	0.6	No Precipitation	E
141		21	4.5	Day	0.5	No Precipitation	C
142		22	3.8	Night	0.1	No Precipitation	E
143		23	2.8	Night	0.3	No Precipitation	E
144		24	4.1	Day	0.1	No Precipitation	C
145		25	4.7	Night	0.9	light	D
146		26	1.7	Night	0.9	light	E
147		27	4.6	Day	0.5	No Precipitation	C
148		28	3.0	Day	0.2	No Precipitation	C
149		29	2.7	Night	0.6	No Precipitation	E
150		30	1.5	Night	0.8	light	E
151		1	4.6	Day	0.8	light	D
152		2	2.0	Night	0.2	No Precipitation	F
153		3	3.5	Night	0.7	light	D
154		4	3.0	Night	0.8	light	E
155		5	3.0	Day	0.1	No Precipitation	B
156		6	2.4	Night	1.0	moderate	E
157		7	3.3	Day	1.0	moderate	D

158	June	8	3.9	Day	0.4	No Precipitation	C
159		9	4.2	Day	0.1	No Precipitation	C
160		10	3.6	Day	0.9	moderate	D
161		11	4.4	Day	0.8	light	D
162		12	4.1	Night	0.3	No Precipitation	E
163		13	4.3	Night	0.8	light	D
164		14	4.2	Night	0.0	No Precipitation	E
165		15	5.2	Day	0.3	No Precipitation	D
166		16	3.1	Night	0.4	No Precipitation	E
167		17	4.1	Day	0.5	No Precipitation	C
168		18	6.5	Day	0.1	No Precipitation	D
169		19	4.7	Night	1.0	Heavy	D
170		20	4.6	Night	0.7	light	D
171		21	5.1	Night	0.2	No Precipitation	D
172		22	3.3	Day	0.1	No Precipitation	C
173		23	4.9	Day	0.8	light	D
174		24	5.0	Day	0.5	No Precipitation	C
175		25	3.4	Night	0.2	No Precipitation	E
176		26	4.4	Day	0.7	light	D
177		27	4.2	Day	0.8	light	D
178		28	1.4	Day	0.1	No Precipitation	B
179		29	4.3	Night	0.8	light	D
180		30	3.3	Day	0.5	No Precipitation	C
181	July	1	4.6	Day	0.9	moderate	D
182		2	4.9	Night	0.8	light	D
183		3	3.0	Day	0.0	No Precipitation	B
184		4	2.7	Night	0.7	light	E
185		5	4.0	Day	0.3	No Precipitation	C
186		6	5.5	Night	0.9	moderate	D
187		7	3.3	Night	0.4	light	D
188		8	5.4	Night	0.7	light	D
189		9	3.6	Night	0.4	light	D
190		10	2.5	Day	0.4	light	C
191		11	2.1	Day	0.5	light	C
192		12	3.9	Night	0.1	No Precipitation	E
193		13	4.1	Night	0.3	No Precipitation	E
194		14	3.9	Night	0.8	light	D
195		15	3.9	Day	0.3	No Precipitation	C
196		16	4.5	Night	0.5	light	D
197		17	3.3	Night	0.9	moderate	D
198		18	3.1	Night	0.8	light	D
199		19	3.8	Day	1.0	Heavy	D
200		20	3.6	Night	0.5	light	D

201		21	4.2	Day	1.0	moderate	D
202		22	4.4	Day	0.4	light	D
203		23	2.9	Day	0.9	moderate	C
204		24	3.7	Night	0.2	No Precipitation	E
205		25	4.3	Night	0.2	No Precipitation	E
206		26	4.0	Day	0.5	light	D
207		27	4.6	Night	0.4	light	D
208		28	3.9	Night	0.4	light	D
209		29	3.8	Day	0.2	No Precipitation	C
210		30	3.8	Night	0.6	light	D
211	August	1	3.1	Night	0.5	light	D
212		2	3.2	Night	0.1	No Precipitation	E
213		3	3.2	Night	0.7	light	D
214		4	4.6	Day	0.6	light	D
215		5	2.9	Night	0.5	light	E
216		6	3.7	Night	0.5	light	D
217		7	2.9	Day	0.8	light	C
218		8	3.2	Night	0.3	No Precipitation	E
219		9	2.7	Day	0.6	light	C
220		10	3.6	Night	0.1	No Precipitation	E
221		11	3.3	Night	0.0	No Precipitation	E
222		12	3.9	Night	0.3	No Precipitation	E
223		13	5.2	Day	0.9	light	D
224		14	4.4	Night	0.4	No Precipitation	E
225		15	4.3	Day	0.0	No Precipitation	C
226		16	3.1	Night	0.3	No Precipitation	E
227		17	3.2	Day	0.8	light	D
228		18	3.8	Night	0.2	No Precipitation	E
229		19	4.9	Night	0.0	No Precipitation	E
230		20	3.3	Day	0.4	No Precipitation	C
231		21	4.1	Night	0.5	light	D
232		22	3.8	Night	0.4	No Precipitation	E
233		23	3.5	Night	0.3	No Precipitation	E
234		24	2.8	Day	0.6	light	C
235		25	3.6	Day	0.3	No Precipitation	C
236		26	3.8	Night	0.6	light	D
237		27	3.6	Night	1.0	moderate	D
238		28	3.6	Night	0.1	No Precipitation	E
239		29	2.3	Night	0.9	light	E
240		30	1.4	Day	0.9	light	C
241		1	2.1	Night	0.8	light	E
242		2	2.8	Day	0.8	light	C
243		3	2.8	Day	0.3	No Precipitation	B

244	September	4	1.0	Day	0.9	moderate	C
245		5	1.1	Day	0.3	No Precipitation	B
246		6	3.3	Day	0.7	light	D
247		7	2.8	Night	0.3	No Precipitation	E
248		8	4.8	Night	0.2	No Precipitation	E
249		9	1.7	Day	0.3	No Precipitation	B
250		10	4.3	Day	0.1	No Precipitation	C
251		11	3.8	Night	0.9	moderate	D
252		12	2.0	Night	0.3	No Precipitation	F
253		13	3.0	Day	0.7	light	C
254		14	3.1	Day	0.3	No Precipitation	C
255		15	2.3	Day	0.4	No Precipitation	B
256		16	2.8	Day	0.1	No Precipitation	B
257		17	2.8	Night	0.1	No Precipitation	E
258		18	3.9	Day	0.1	No Precipitation	C
259		19	0.1	Day	0.1	No Precipitation	B
260		20	3.6	Night	0.4	No Precipitation	E
261		21	3.2	Day	0.5	light	D
262		22	2.4	Night	0.4	No Precipitation	E
263		23	2.5	Day	0.2	No Precipitation	B
264		24	3.6	Night	0.8	light	D
265		25	3.2	Night	0.9	moderate	D
266		26	2.6	Day	0.7	light	C
267		27	2.3	Day	0.9	moderate	C
268		28	2.6	Night	0.1	No Precipitation	E
269		29	2.7	Night	0.2	No Precipitation	E
270		30	1.8	Night	0.8	light	E
271	October	1	1.9	Day	0.0	No Precipitation	B
272		2	1.6	Day	0.7	No Precipitation	B
273		3	3.8	Night	0.2	No Precipitation	E
274		4	2.1	Day	0.2	No Precipitation	B
275		5	1.7	Night	0.5	No Precipitation	F
276		6	1.7	Night	0.9	light	E
277		7	1.2	Night	0.4	No Precipitation	F
278		8	1.8	Day	0.8	light	C
279		9	1.9	Day	0.1	No Precipitation	B
280		10	3.5	Day	0.2	No Precipitation	C
281		11	2.1	Night	1.0	moderate	E
282		12	1.8	Day	0.6	No Precipitation	B
283		13	2.4	Night	0.3	No Precipitation	E
284		14	3.0	Day	0.8	light	C
285		15	2.7	Night	0.8	light	E
286		16	2.7	Night	0.1	No Precipitation	E

287		17	2.5	Day	0.1	No Precipitation	B
288		18	2.4	Night	0.7	No Precipitation	E
289		19	2.6	Day	0.5	No Precipitation	B
290		20	2.5	Night	0.8	light	E
291		21	2.6	Day	0.9	light	C
292		22	2.4	Night	0.7	No Precipitation	E
293		23	2.2	Night	0.3	No Precipitation	E
294		24	3.1	Night	0.3	No Precipitation	E
295		25	2.0	Day	0.9	light	C
296		26	1.9	Day	0.9	light	C
297		27	2.9	Night	0.3	No Precipitation	E
298		28	3.3	Night	0.3	No Precipitation	E
299		29	1.3	Night	0.4	No Precipitation	F
300		30	2.3	Day	0.7	No Precipitation	B
301	November	1	3.2	Night	0.5	No Precipitation	E
302		2	2.1	Night	0.8	No Precipitation	E
303		3	2.0	Night	0.7	No Precipitation	F
304		4	1.2	Day	0.3	No Precipitation	B
305		5	2.0	Night	0.5	No Precipitation	E
306		6	0.7	Night	0.8	No Precipitation	F
307		7	1.8	Day	0.4	No Precipitation	B
308		8	2.0	Day	0.3	No Precipitation	B
309		9	1.5	Day	0.1	No Precipitation	B
310		10	2.4	Day	0.8	No Precipitation	B
311		11	2.5	Day	0.6	No Precipitation	B
312		12	3.2	Night	0.6	No Precipitation	E
313		13	2.0	Day	0.2	No Precipitation	B
314		14	1.2	Night	0.4	No Precipitation	F
315		15	2.0	Day	0.2	No Precipitation	B
316		16	2.4	Day	0.1	No Precipitation	B
317		17	2.3	Night	0.4	No Precipitation	E
318		18	3.1	Day	0.9	No Precipitation	C
319		19	1.9	Night	0.3	No Precipitation	F
320		20	2.2	Night	0.7	No Precipitation	E
321		21	2.5	Night	0.7	No Precipitation	E
322		22	2.7	Day	0.0	No Precipitation	B
323		23	1.8	Night	0.9	No Precipitation	F
324		24	2.4	Day	0.3	No Precipitation	B
325		25	2.1	Night	0.2	No Precipitation	E
326		26	2.6	Day	0.2	No Precipitation	B
327		27	2.6	Night	0.9	No Precipitation	E
328		28	1.8	Day	0.4	No Precipitation	B
329		29	3.5	Day	0.0	No Precipitation	C

330		30	2.3	Night	0.4	No Precipitation	E
331	December	1	2.7	Night	1.0	light	E
332		2	2.5	Day	0.4	No Precipitation	B
333		3	2.4	Night	0.6	No Precipitation	E
334		4	3.3	Night	0.8	No Precipitation	E
335		5	2.7	Day	0.4	No Precipitation	B
336		6	2.9	Day	0.0	No Precipitation	B
337		7	3.1	Day	0.5	No Precipitation	C
338		8	2.7	Day	0.3	No Precipitation	B
339		9	1.7	Night	0.8	No Precipitation	F
340		10	2.5	Day	0.7	No Precipitation	B
341		11	3.1	Night	0.8	No Precipitation	E
342		12	2.1	Night	0.8	No Precipitation	E
343		13	1.7	Day	0.6	No Precipitation	B
344		14	3.0	Day	0.7	No Precipitation	B
345		15	2.5	Night	0.4	No Precipitation	E
346		16	3.3	Night	0.1	No Precipitation	E
347		17	2.5	Day	0.2	No Precipitation	B
348		18	3.0	Night	0.4	No Precipitation	E
349		19	2.3	Night	0.6	No Precipitation	E
350		20	3.1	Night	0.7	No Precipitation	E
351		21	2.5	Night	0.7	No Precipitation	E
352		22	2.5	Day	0.7	No Precipitation	B
353		23	3.1	Day	0.5	No Precipitation	C
354		24	1.5	Day	0.9	No Precipitation	B
355		25	2.9	Night	0.2	No Precipitation	E
356		26	1.7	Night	0.6	No Precipitation	F
357		27	2.2	Day	0.4	No Precipitation	B
358		28	2.5	Night	0.2	No Precipitation	E
359		29	1.5	Day	0.1	No Precipitation	B
360		30	1.8	Day	0.0	No Precipitation	B

APPENDIX E

Simulation Steps Snapshot

(a) RASCAL

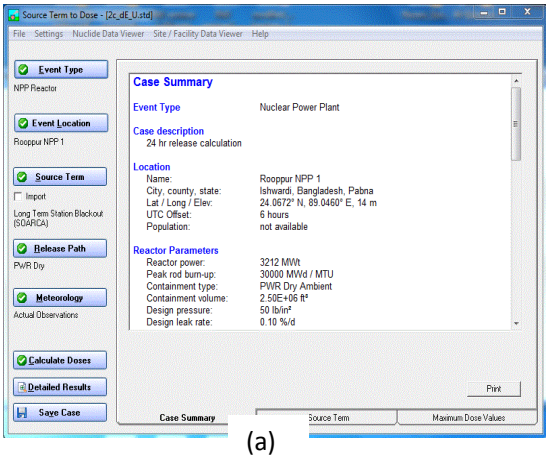

(a)

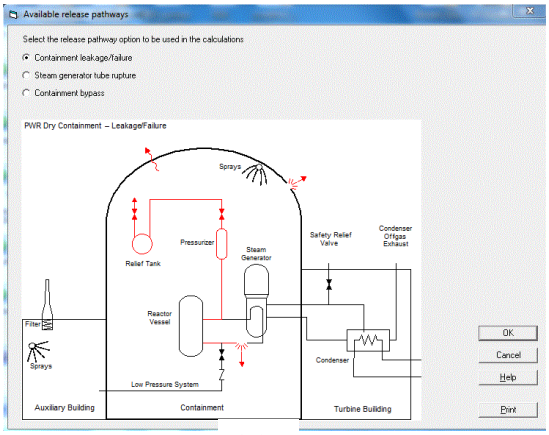

(d)

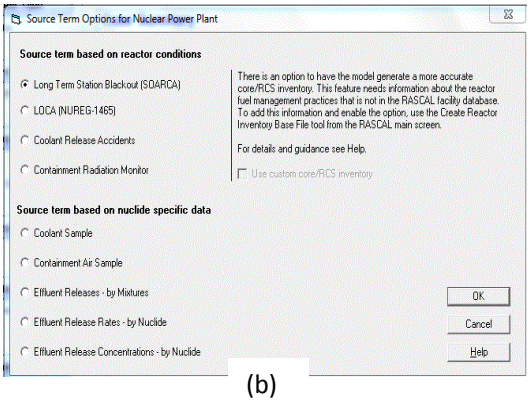

(b)

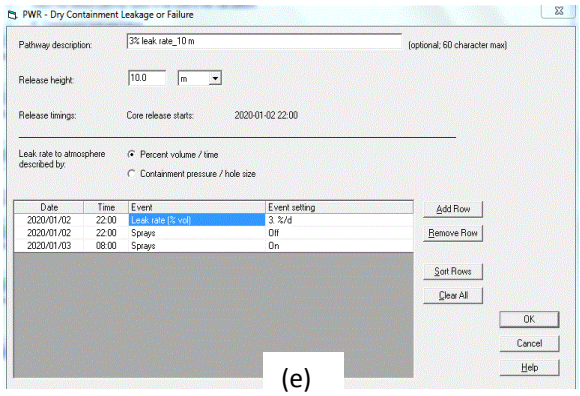

(e)

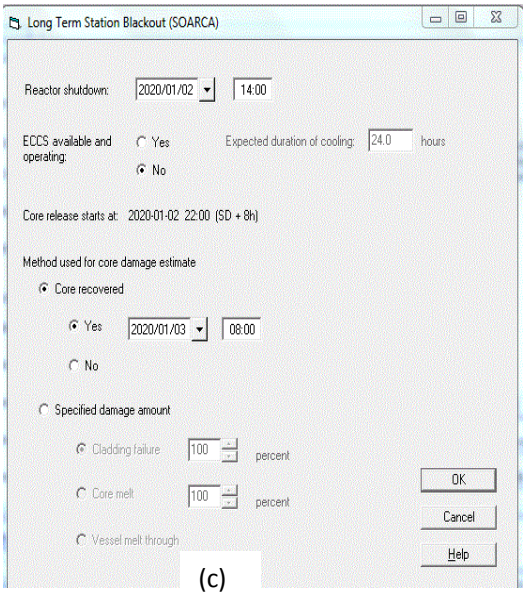

(c)

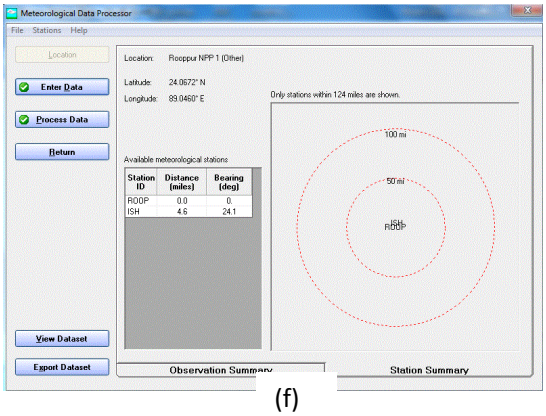

(f)

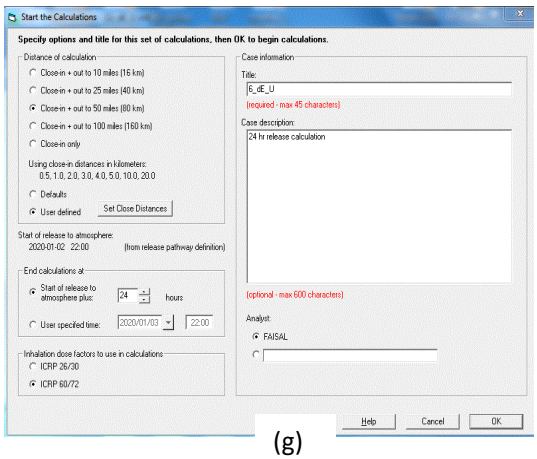

(g)

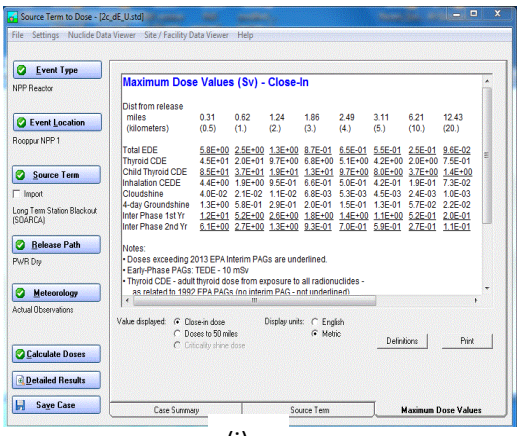

(i)

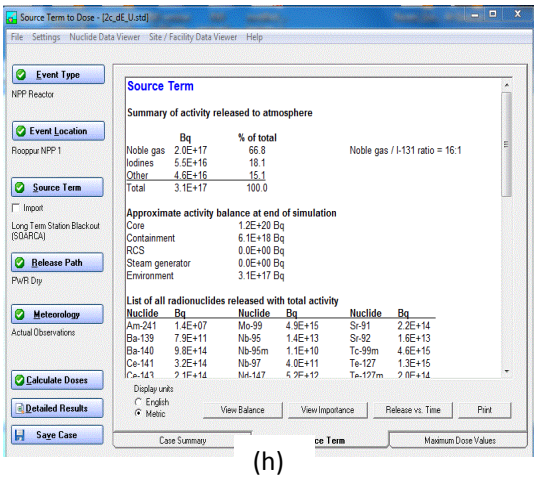

(h)

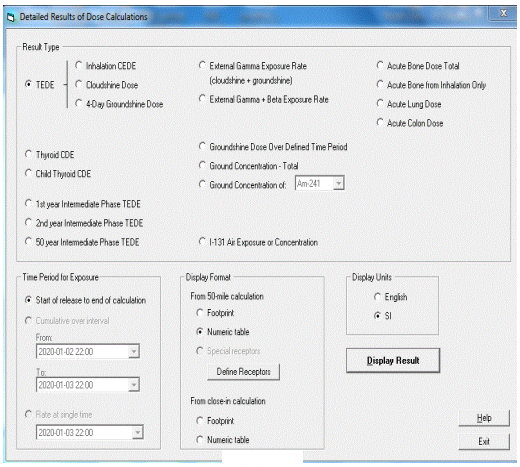

(j)

Figure E-1: (a) – (j) RASCAL simulation input and output steps

(b) HotSpot

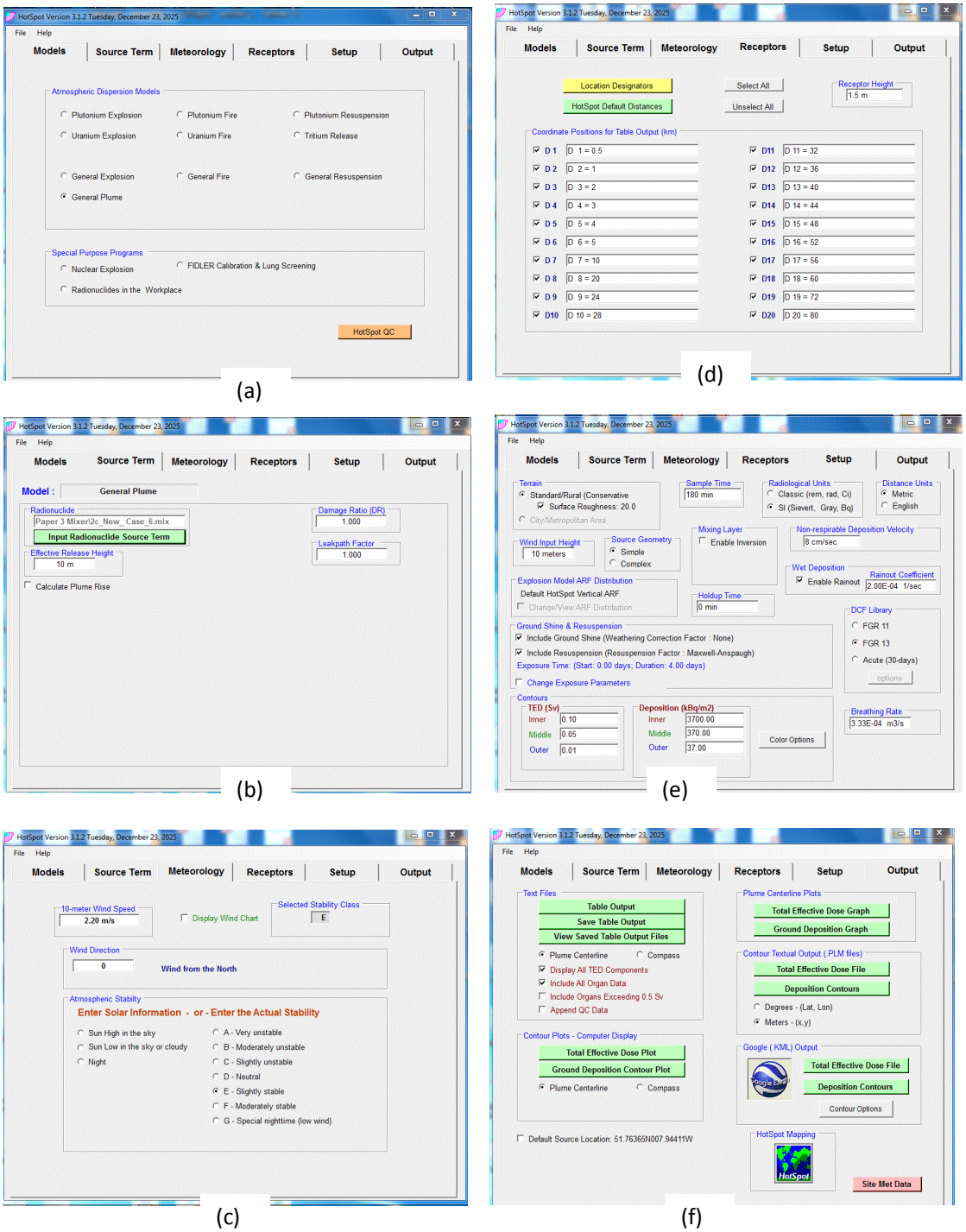

Figure E-2: (a) – (f) HotSpot simulation input and output steps

(c) HYSPLIT

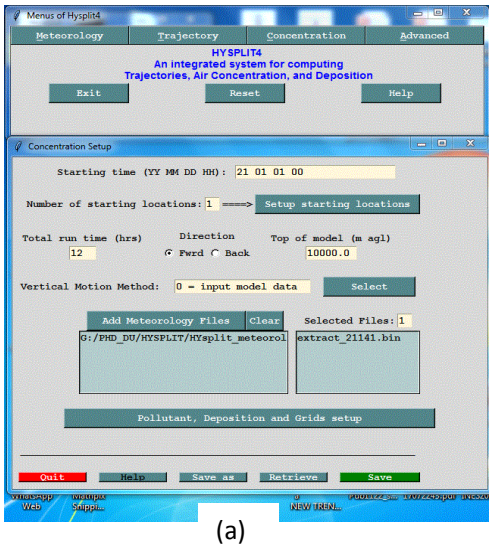

(a)

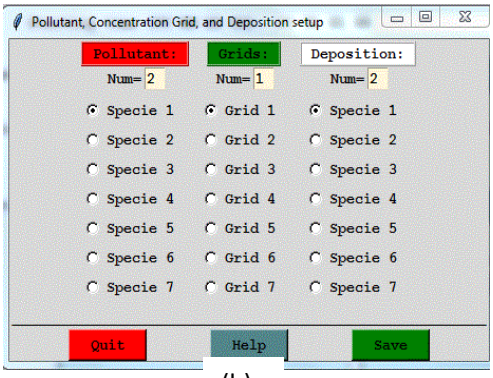

(b)

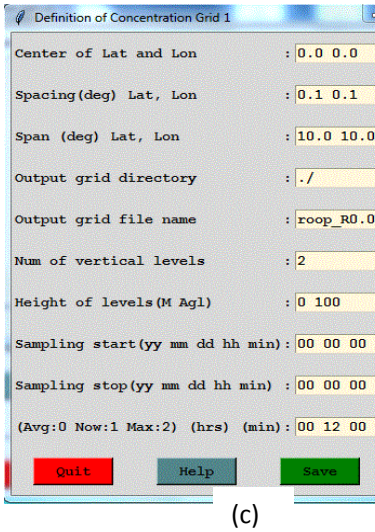

(c)

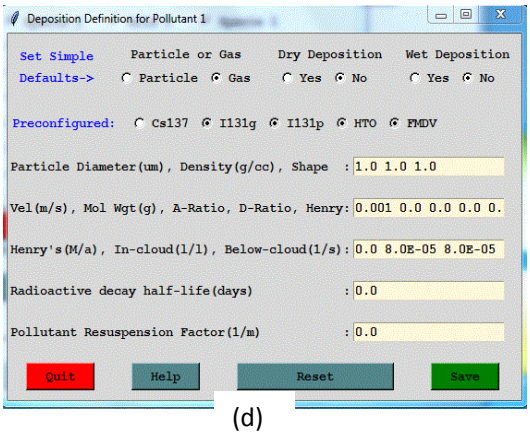

(d)

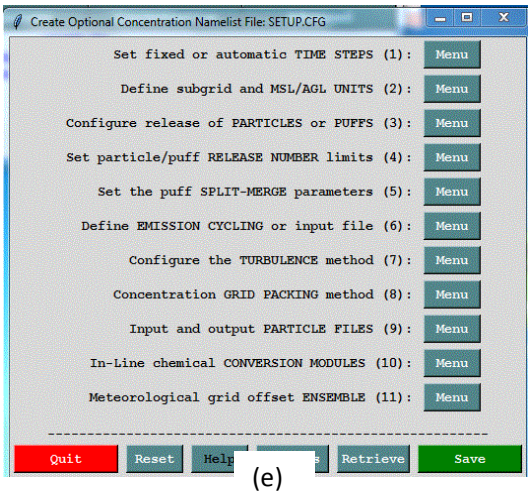

(e)

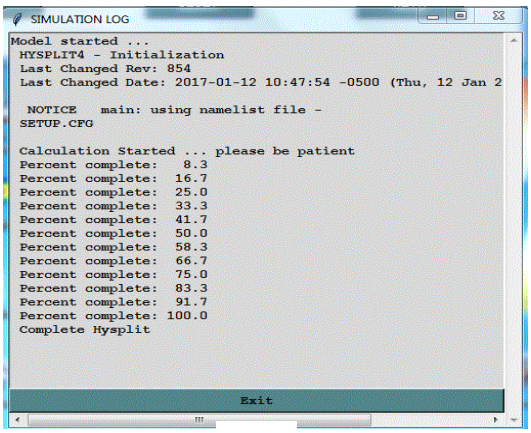

(f)

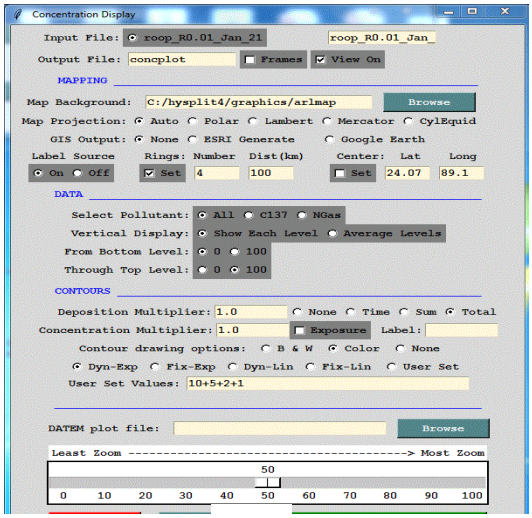

(g)

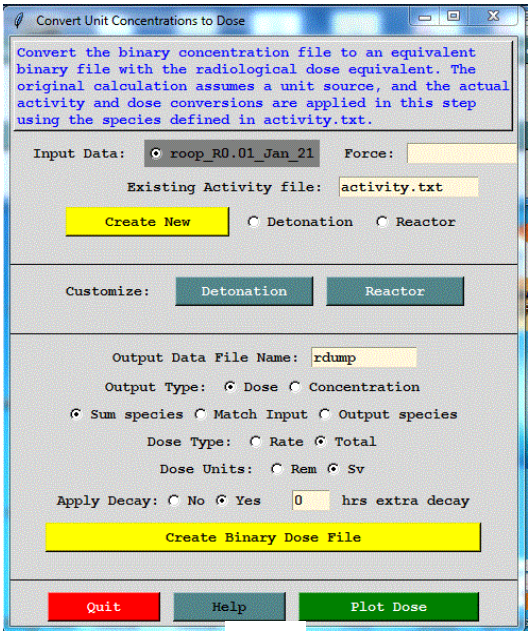

(i)

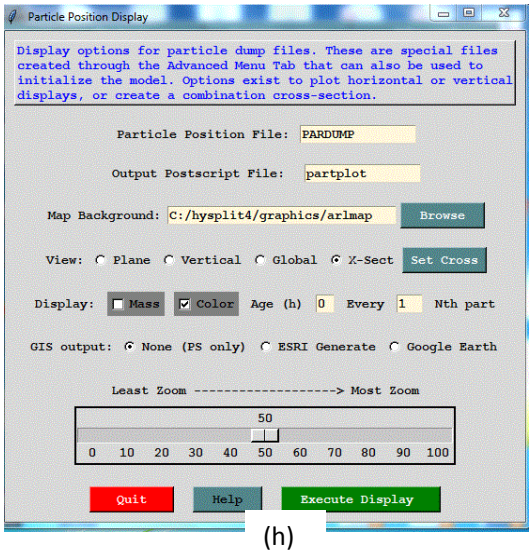

(h)

Figure E-3: (a) – (i) HYSPLIT simulation input and output steps

APPENDIX F Monthly Wind Rose Diagram for Year 2021 and 2022

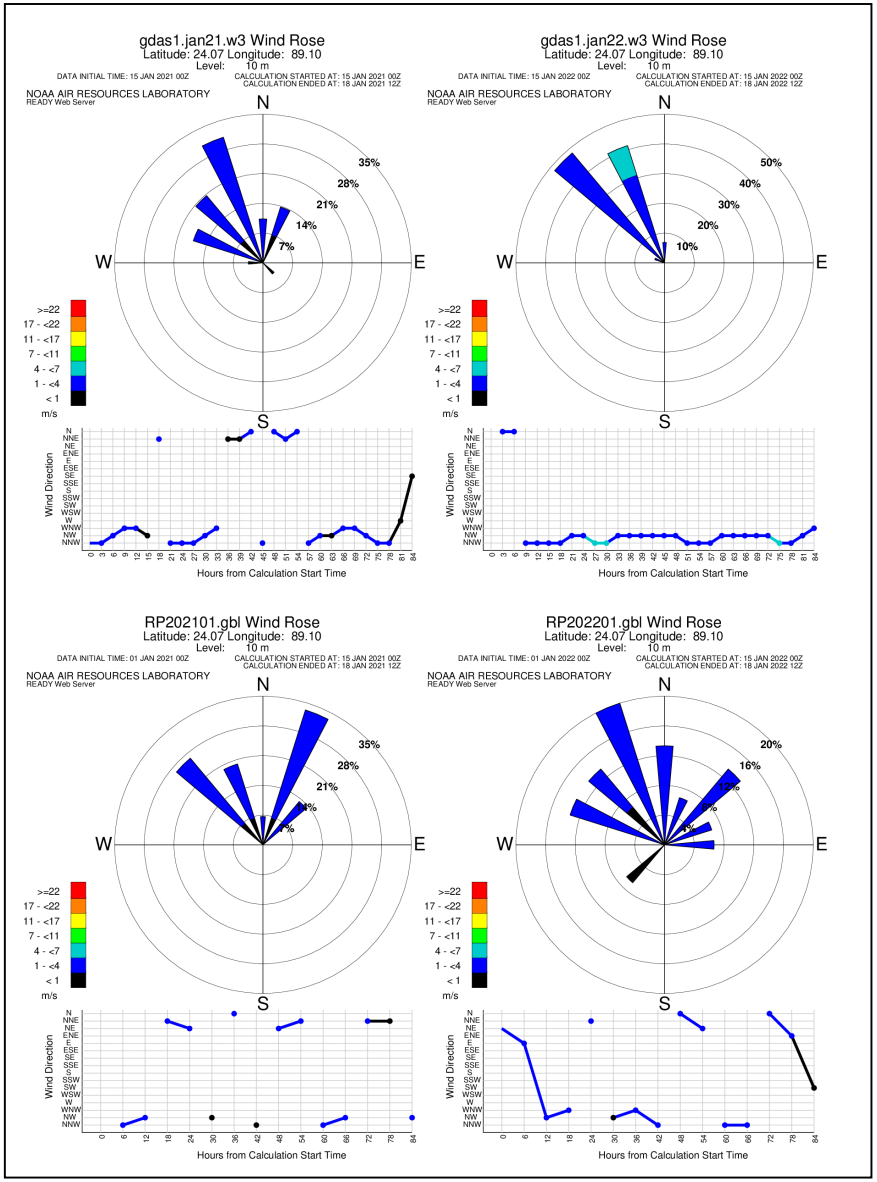

Figure F-1: Windrose- January

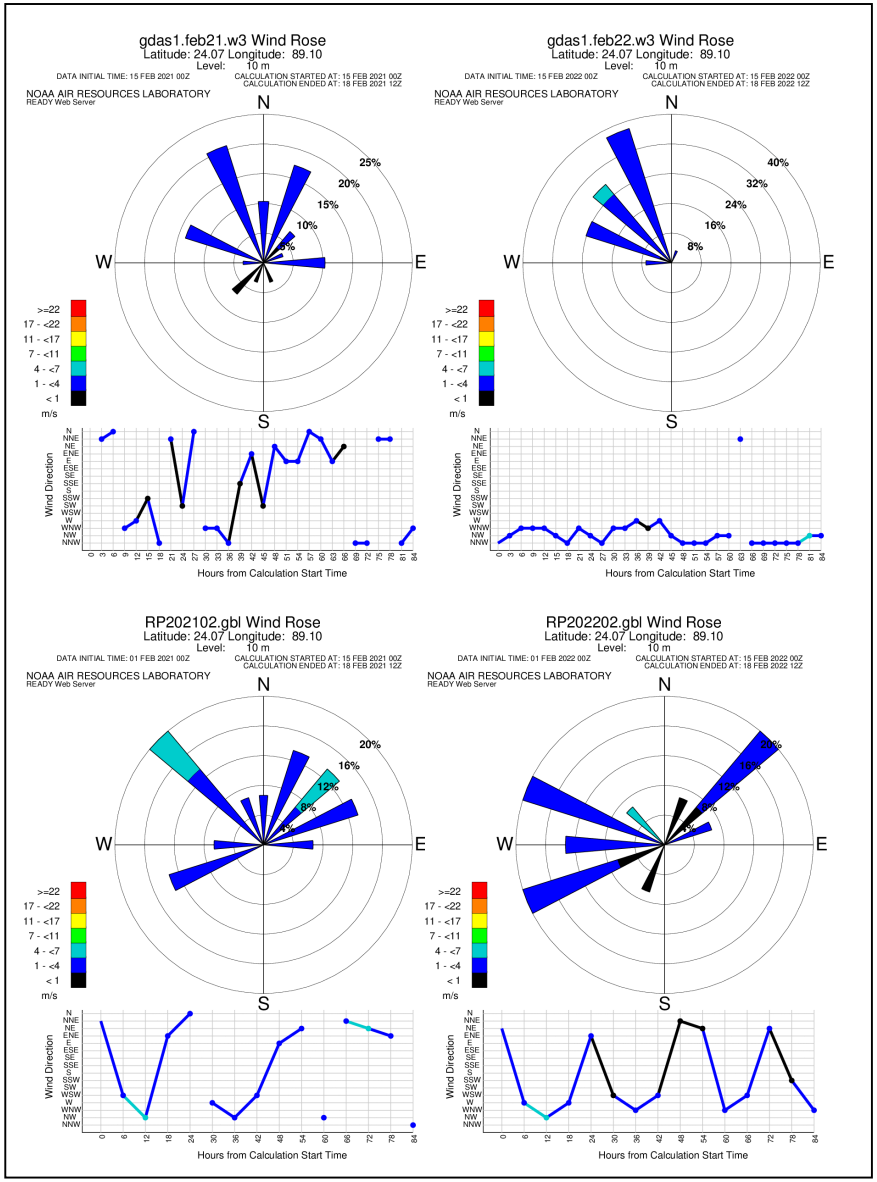

Figure F-2: Windrose- February

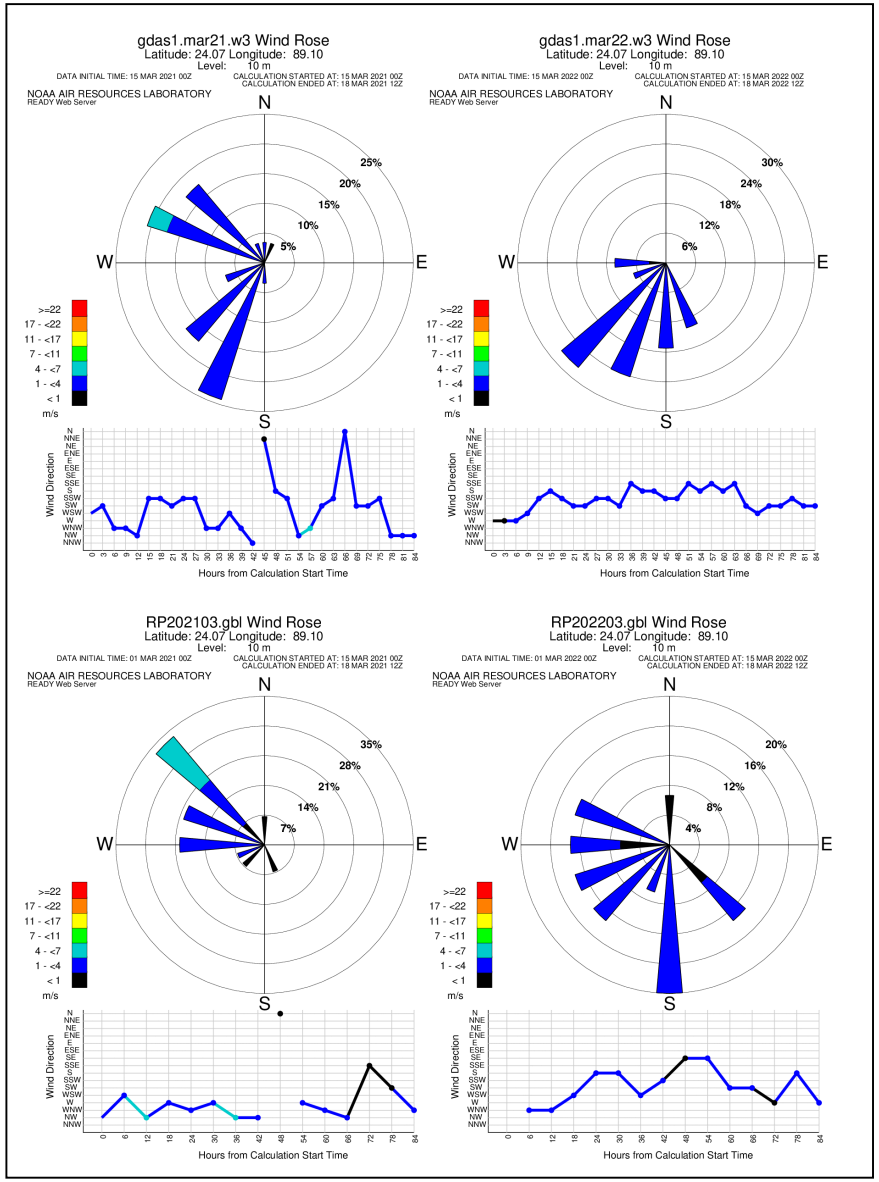

Figure F-3: Windrose- March

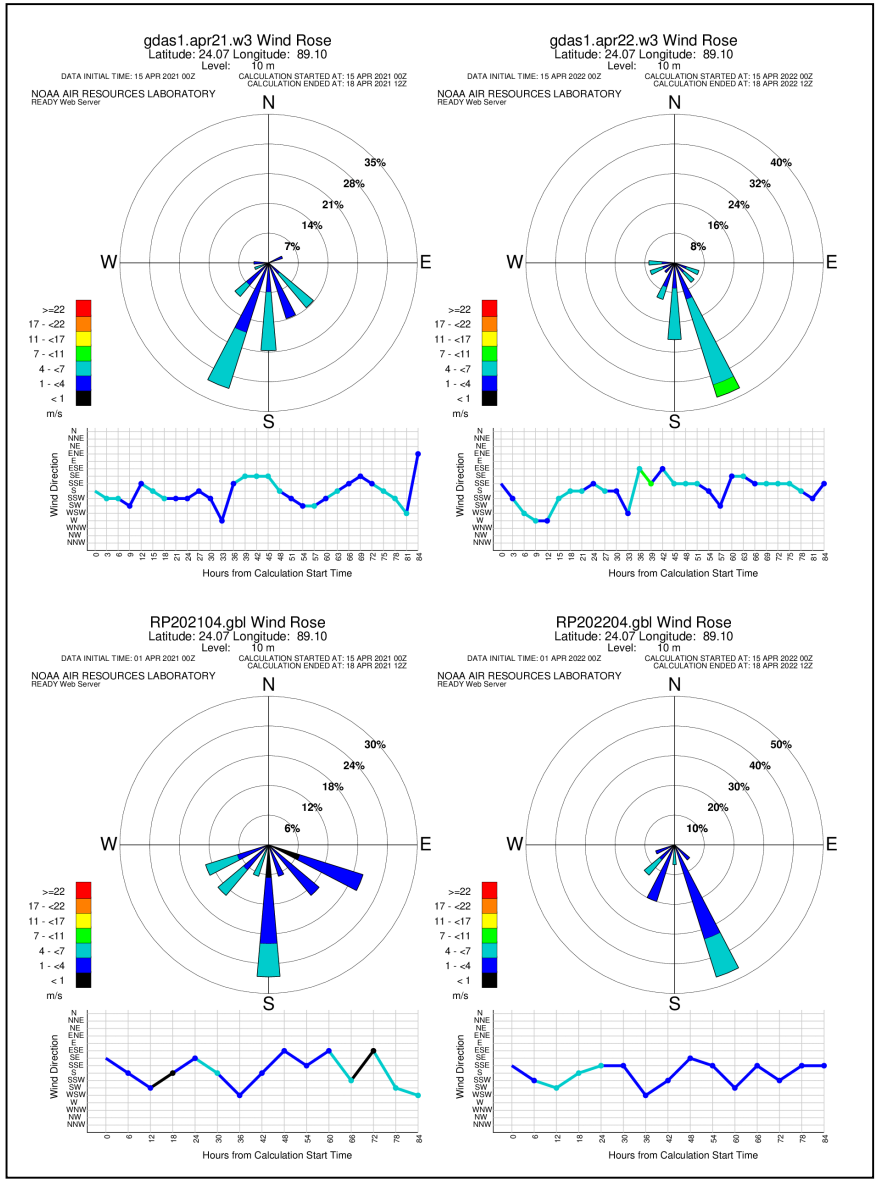

Figure F-4: Windrose- April

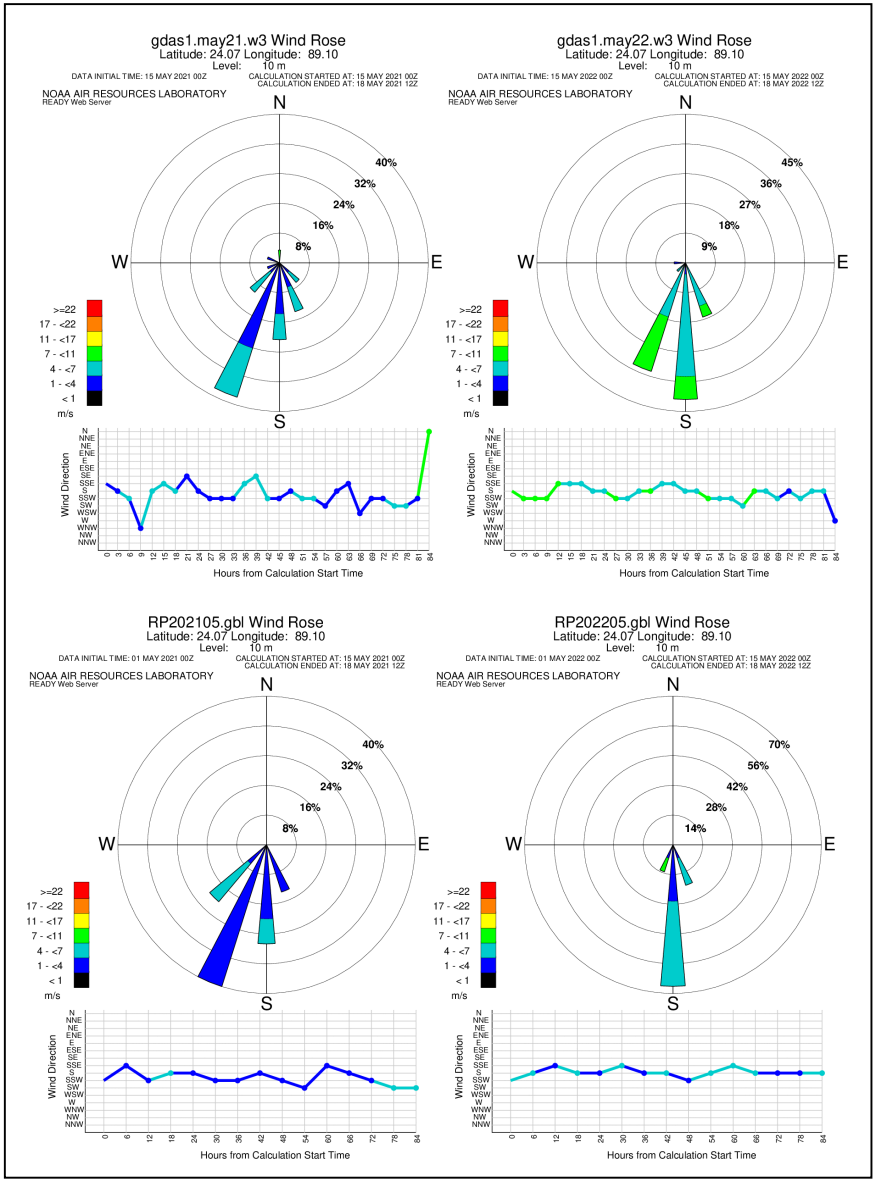

Figure F-5: Windrose- May

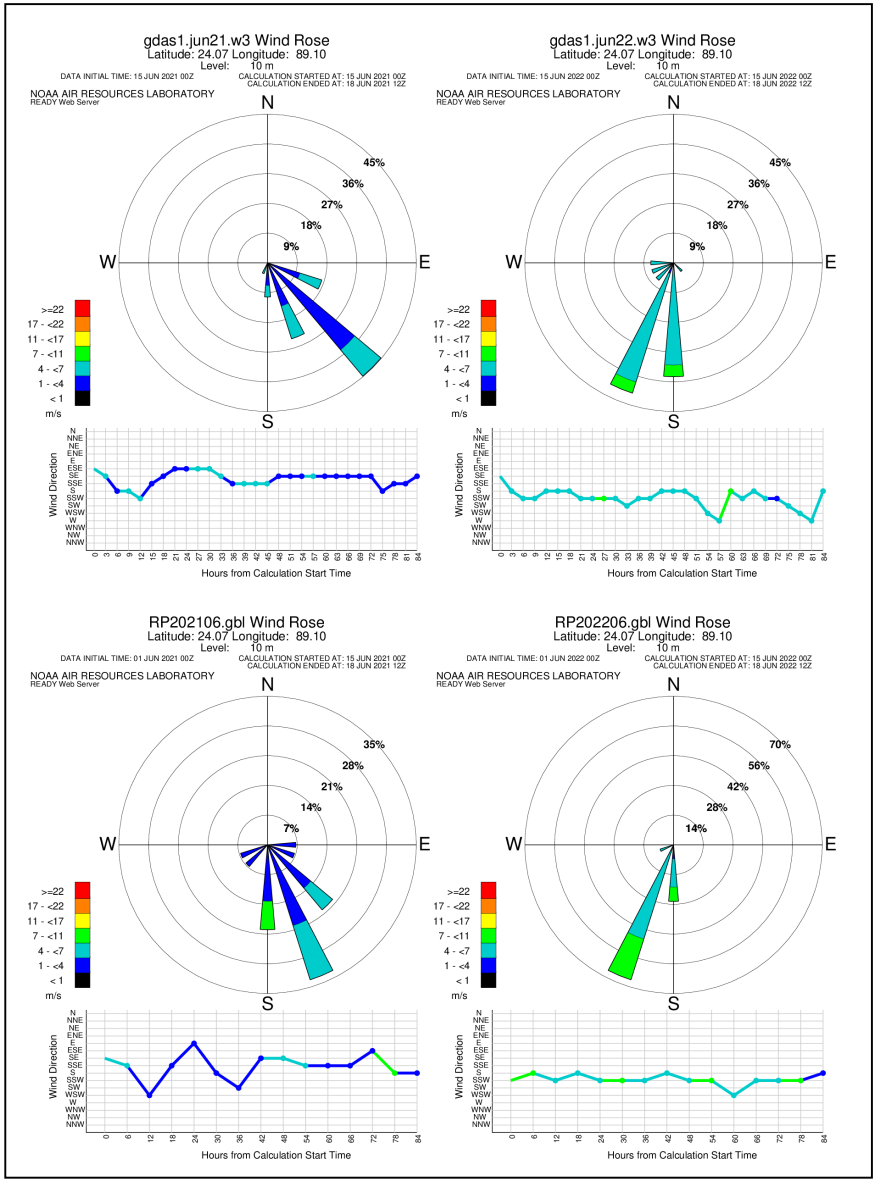

Figure F-6: Windrose- June

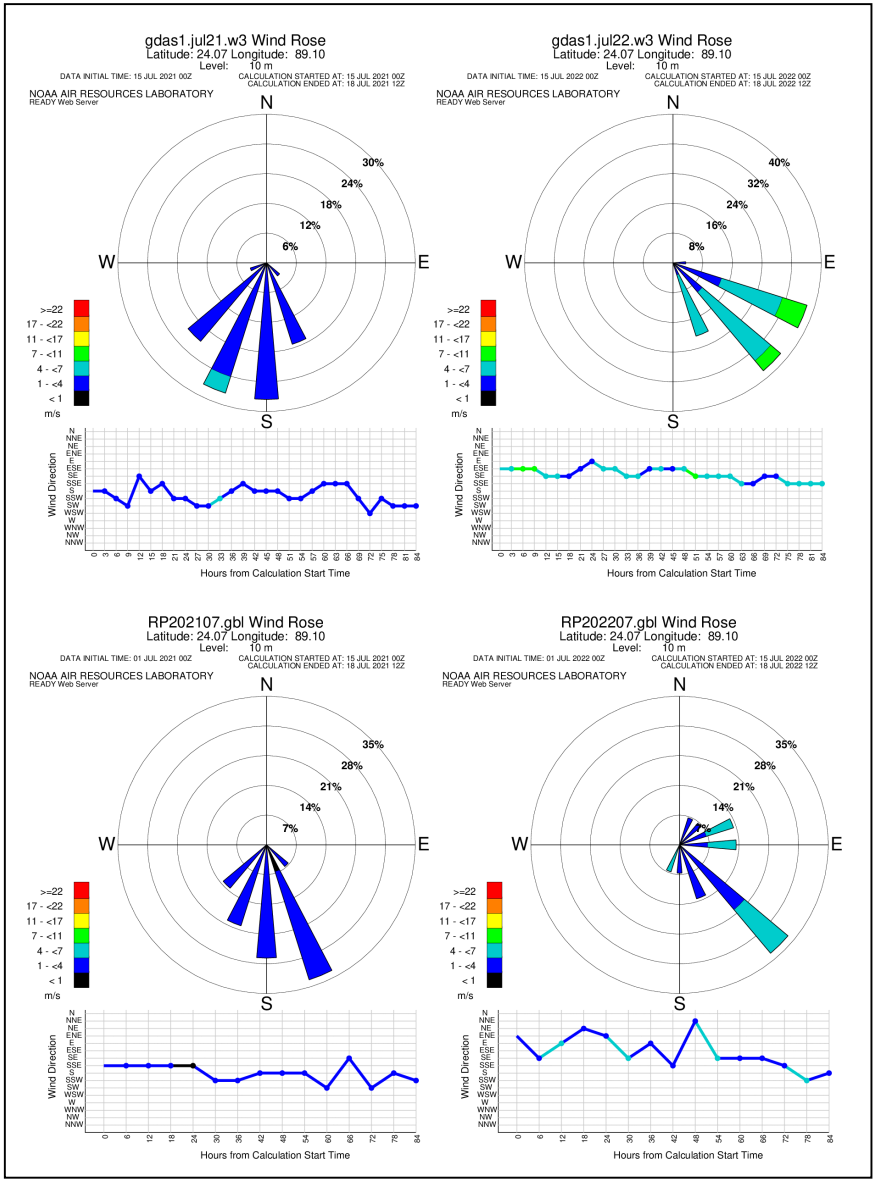

Figure F-7: Windrose- July

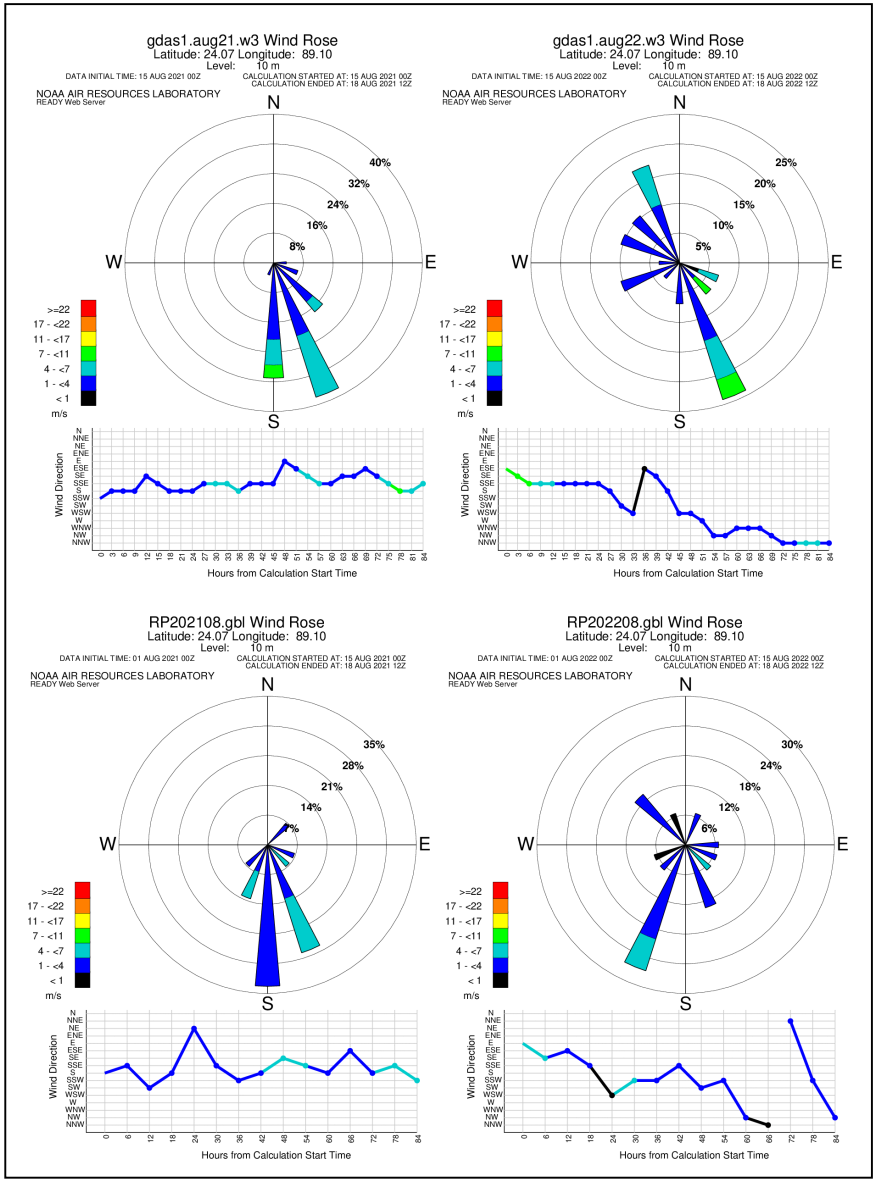

Figure F-8: Windrose- August

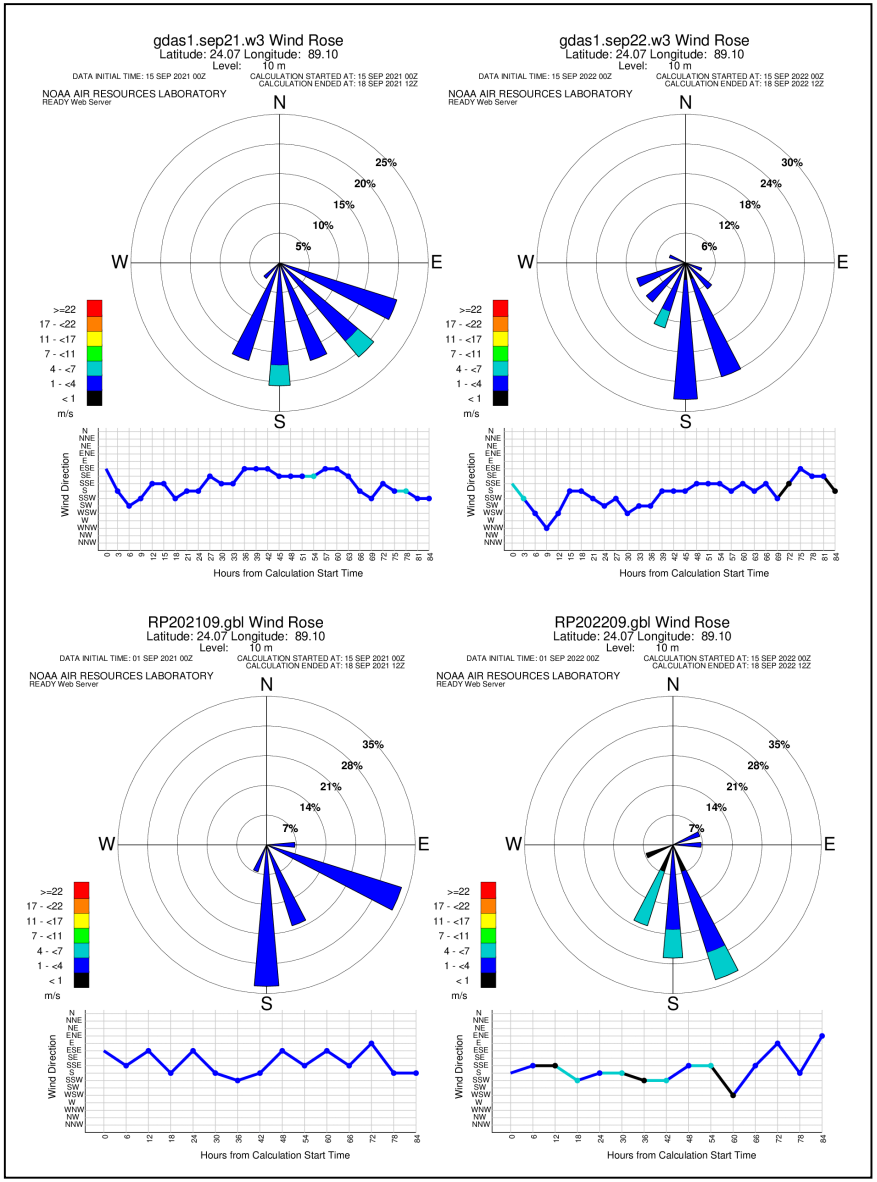

Figure F-9: Windrose- September

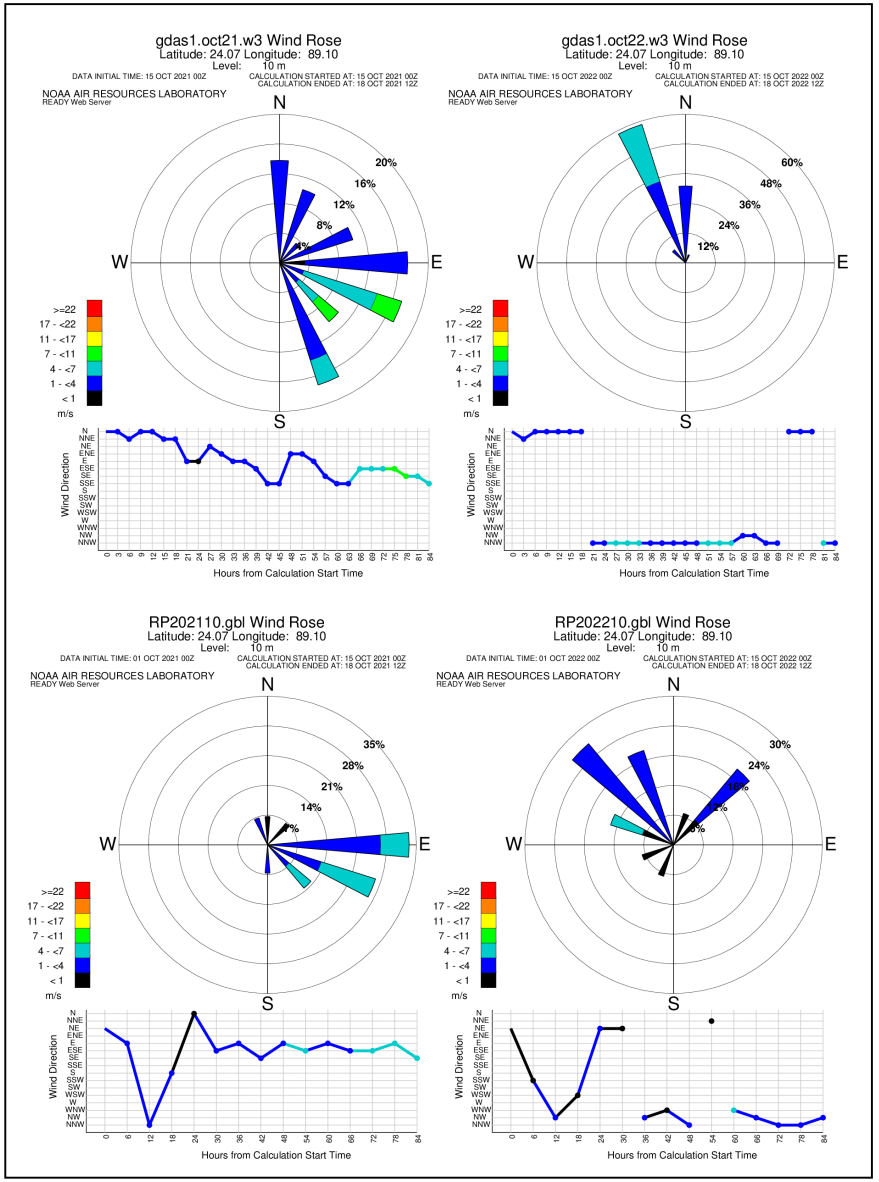

Figure F-10: Windrose- October

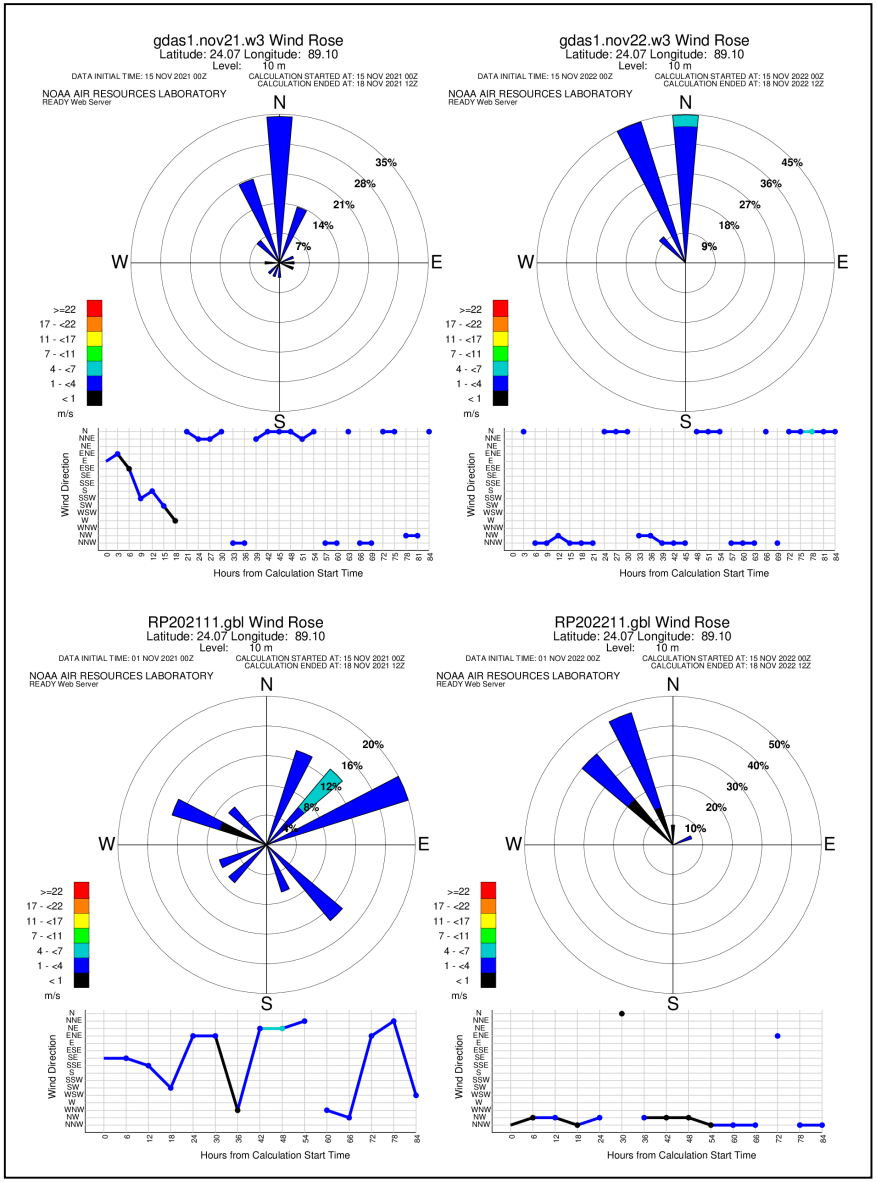

Figure F-11: Windrose- November

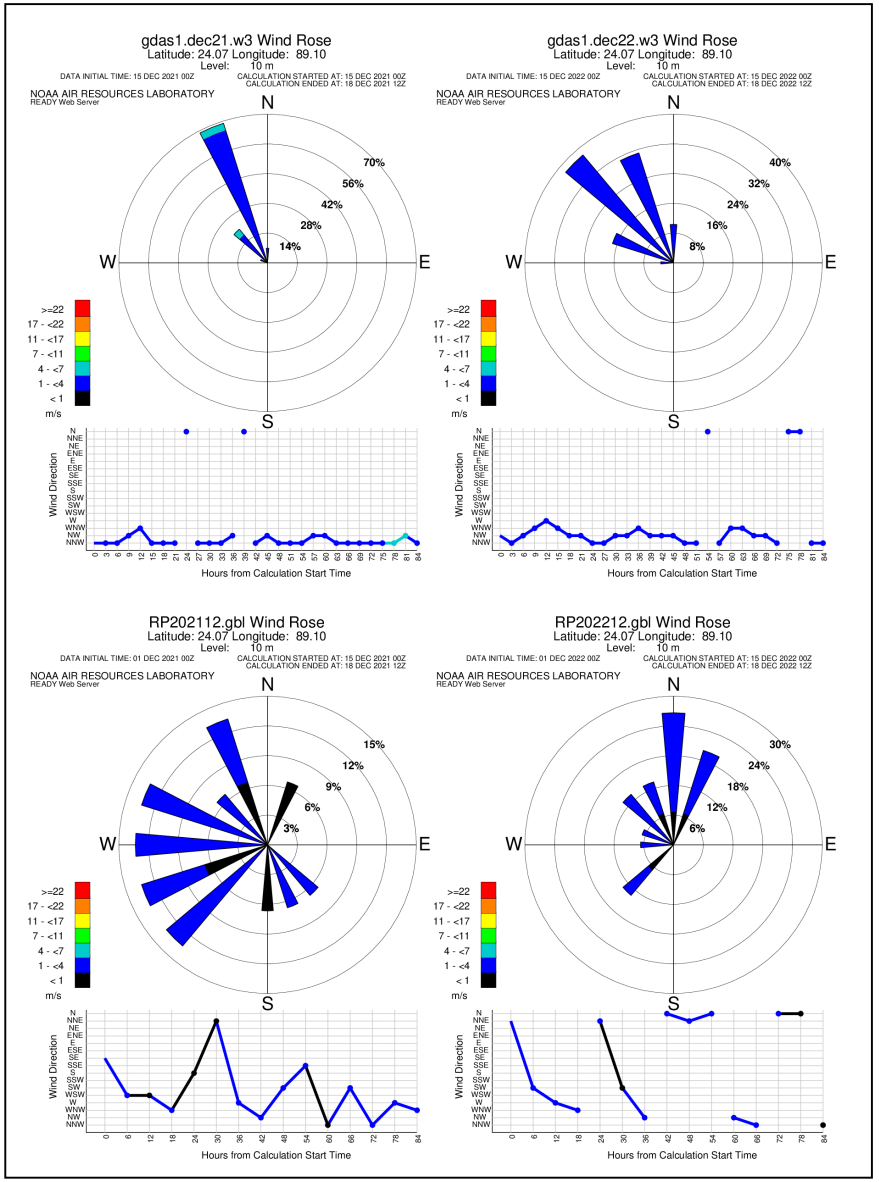

Figure F-12: Windrose- December

APPENDIX-G

Stability Class Variations over 84 Hours

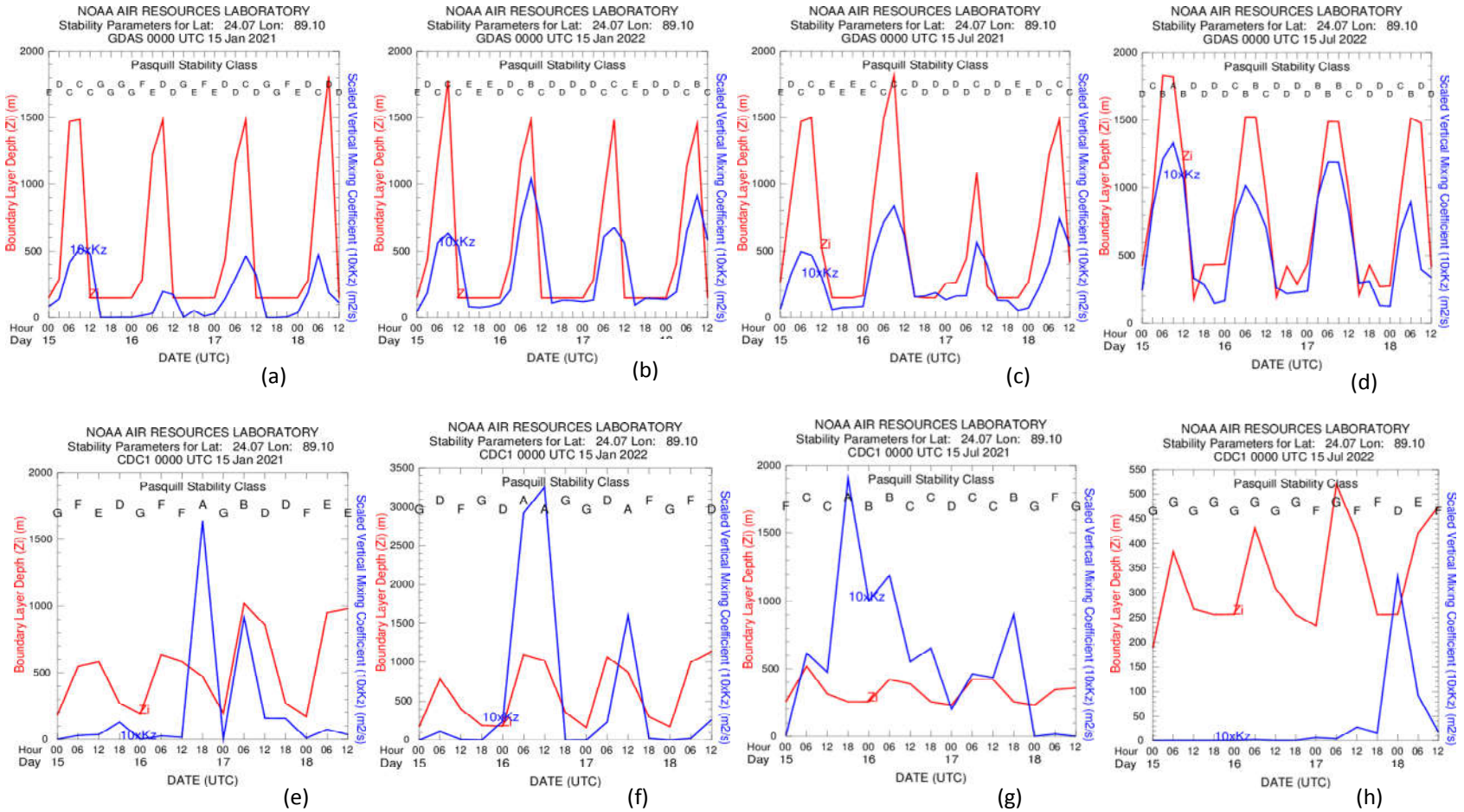

Figure G-1 Pasquill Stability Class Variations over 84 Hours starting from 15th January & July of the year 2021 and 2022 for GDAS1 and CDC1 Meteorological Data

APPENDIX- H

ACTIVITY.txt FILE for Air Concentration, Ground Deposition and Dose Conversion

Mass Nucl	T1/2	U235H	U235T	Pu239H	Pu239T	Cloudshine	Groundshine
Hr= 0.00	sec	Bq	Bq	Bq	Bq	rem/h Bq/m3	rem/h Bq/m2
85m Kr	1.61000E+04	1.20000E+15	1.20000E+15	1.20000E+15	1.20000E+15	3.19320E-09	5.65200E-11
85 Kr	3.37000E+08	8.90000E+14	8.90000E+14	8.90000E+14	8.90000E+14	8.64000E-11	3.78000E-12
87 Kr	4.57000E+03	1.60000E+13	1.60000E+13	1.60000E+13	1.60000E+13	1.42920E-08	3.02400E-10
88 Kr	1.02000E+04	9.10000E+14	9.10000E+14	9.10000E+14	9.10000E+14	3.49560E-08	6.22800E-10
133 Xe	4.53000E+05	1.60000E+17	1.60000E+17	1.60000E+17	1.60000E+17	4.78800E-10	1.42200E-11
135 Xe	3.28000E+04	3.90000E+16	3.90000E+16	3.90000E+16	3.90000E+16	3.96400E-09	9.00000E-11
138 Xe	8.53000E+02	2.00000E+03	2.00000E+03	2.00000E+03	2.00000E+03	1.97280E-08	3.85200E-10
131 I	6.94656E+05	1.80000E+16	1.80000E+16	1.80000E+16	1.80000E+16	6.08400E-09	1.31040E-10
132 I	8.28000E+03	2.40000E+16	3.20000E+15	2.40000E+16	3.20000E+15	9.93600E-09	2.22120E-10
133 I	7.49000E+04	2.30000E+16	2.30000E+16	2.30000E+16	2.30000E+16	9.94000E-09	2.22000E-10
134 I	3.17000E+03	2.60000E+12	2.60000E+12	2.60000E+12	2.60000E+12	4.39200E-08	9.10800E-10
135 I	2.38000E+04	7.80000E+15	7.80000E+15	7.80000E+15	7.80000E+15	2.71400E-08	5.29200E-10
134 Cs	6.50000E+07	3.00000E+15	3.00000E+15	3.00000E+15	3.00000E+15	2.54000E-08	5.33000E-10
136 Cs	1.13184E+06	9.10000E+14	9.10000E+14	9.10000E+14	9.10000E+14	3.57840E-08	7.30800E-10
137 Cs	9.52093E+08	2.10000E+15	2.10000E+15	2.10000E+15	2.10000E+15	3.34080E-11	1.07640E-12
127 Te	3.36600E+04	1.80000E+15	1.80000E+15	1.80000E+15	1.80000E+15	1.20240E-10	3.70800E-12
127m Te	9.41760E+06	2.80000E+14	2.80000E+14	2.80000E+14	2.80000E+14	4.03200E-11	3.08200E-12
129 Te	4.17600E+03	7.70000E+14	7.70000E+14	7.70000E+14	7.70000E+14	1.02960E-09	4.10400E-11
129m Te	2.90304E+06	1.20000E+15	1.20000E+15	1.20000E+15	1.20000E+15	5.61600E-10	2.05200E-11
131 Te	1.50000E+03	6.10000E+14	6.10000E+14	6.10000E+14	6.10000E+14	6.91200E-09	1.70600E-10
131m Te	1.08000E+05	2.70000E+15	2.70000E+15	2.70000E+15	2.70000E+15	2.35800E-08	4.82400E-10
132 Te	2.81520E+05	2.30000E+16	2.30000E+16	2.30000E+16	2.30000E+16	3.35520E-09	7.63200E-11
99 Mo	2.04120E+04	6.60000E+15	6.60000E+15	6.60000E+15	6.60000E+15	1.31040E-08	2.81000E-10
127 Sb	3.32640E+05	1.30000E+15	1.30000E+15	1.30000E+15	1.30000E+15	1.12320E-08	2.43400E-10
129 Sb	1.55520E+04	5.30000E+14	5.30000E+14	5.30000E+14	5.30000E+14	2.41560E-08	4.93200E-10
99m Tc	2.16720E+04	6.30000E+15	6.30000E+15	6.30000E+15	6.30000E+15	1.92600E-09	4.10400E-11
103 Ru	3.39379E+06	7.40000E+14	7.40000E+14	7.40000E+14	7.40000E+14	7.48800E-09	1.61600E-10
105 Ru	1.59840E+04	5.10000E+13	5.10000E+13	5.10000E+13	5.10000E+13	1.28160E-08	2.81500E-10
106 Ru	3.18124E+07	2.70000E+14	2.70000E+14	2.70000E+14	2.70000E+14	0.00000E+00	0.00000E+00
140 La	1.44979E+05	1.70000E+14	1.70000E+14	1.70000E+14	1.70000E+14	3.99600E-08	7.77600E-10
239 Np	2.03000E+05	6.20000E+15	6.20000E+15	6.20000E+15	6.20000E+15	2.50200E-09	5.54400E-11
241 Pu	4.54000E+08	5.90000E+13	5.90000E+13	5.90000E+13	5.90000E+13	2.27880E-14	6.15600E-16
140 Ba	1.10000E+06	1.70000E+15	1.70000E+15	1.70000E+15	1.70000E+15	2.90520E-09	6.84000E-11
141 Ce	2.81000E+06	6.00000E+14	6.00000E+14	6.00000E+14	6.00000E+14	1.11600E-09	2.49480E-11
143 Ce	2.81000E+06	3.70000E+14	3.70000E+14	3.70000E+14	3.70000E+14	4.35600E-09	1.08360E-10
144 Ce	2.46000E+07	4.90000E+14	3.70000E+14	3.70000E+14	3.70000E+14	2.74680E-10	6.62400E-12
89 Sr	4.36000E+06	9.10000E+14	9.10000E+14	9.10000E+14	9.10000E+14	1.57320E-10	2.46960E-11
90 Sr	9.18000E+08	9.10000E+13	9.10000E+13	9.10000E+13	9.10000E+13	3.53880E-11	5.90400E-13
143 Pr	1.17000E+06	2.70000E+13	2.70000E+13	2.70000E+13	2.70000E+13	6.98400E-11	7.41600E-12
144 Pr	1.04000E+03	4.50000E+14	4.50000E+14	4.50000E+14	4.50000E+14	1.63000E-16	5.86800E-11
95 Nb	3.04000E+06	2.60000E+13	2.60000E+13	2.60000E+13	2.60000E+13	1.25640E-08	2.62080E-10
95m Nb	3.12000E+05	2.50000E+10	2.50000E+10	2.50000E+10	2.50000E+10	9.86400E-10	2.12760E-11
97 Nb	4.32000E+03	6.50000E+11	6.50000E+11	6.50000E+11	6.50000E+11	6.75000E-16	2.43000E-10
95 Zr	5.53000E+06	2.50000E+13	2.50000E+13	2.50000E+13	2.50000E+13	1.20960E-08	2.53440E-10
97 Zr	6.08000E+04	1.10000E+13	1.10000E+13	1.10000E+13	1.10000E+13	3.20400E-09	9.00000E-11
90 Y	2.30000E+05	6.40000E+12	6.40000E+12	6.40000E+12	6.40000E+12	2.85120E-10	3.96000E-11

Figure H-1: 10 hr CCM LTSBO released radionuclides ACTIVITY.txt FILE

Mass Nucl	T1/2	U235H	U235T	Pu239H	Pu239T	Cloudshine	Groundshine
Hr= 0.00	sec	Bq	Bq	Bq	Bq	rem/h Bq/m3	rem/h Bq/m2
85m Kr	1.61000E+04	1.10000E+15	1.10000E+15	1.10000E+15	1.10000E+15	3.19320E-09	5.65200E-11
85 Kr	3.37000E+08	8.10000E+14	8.10000E+14	8.10000E+14	8.10000E+14	8.64000E-11	3.78000E-12
87 Kr	4.57000E+03	1.50000E+13	1.50000E+13	1.50000E+13	1.50000E+13	1.42920E-08	3.02400E-10
88 Kr	1.02000E+04	8.50000E+14	8.50000E+14	8.50000E+14	8.50000E+14	3.49560E-08	6.22800E-10
133 Xe	4.53000E+05	1.40000E+17	1.40000E+17	1.40000E+17	1.40000E+17	4.78800E-10	1.42200E-11
135 Xe	3.28000E+04	3.10000E+16	3.10000E+16	3.10000E+16	3.10000E+16	3.96400E-09	9.00000E-11
138 Xe	8.53000E+02	2.00000E+03	2.00000E+03	2.00000E+03	2.00000E+03	1.97280E-08	3.85200E-10
131 I	6.94656E+05	2.30000E+15	2.30000E+15	2.30000E+15	2.30000E+15	6.08400E-09	1.31040E-10
132 I	8.28000E+03	3.20000E+15	3.20000E+15	3.20000E+15	3.20000E+15	9.93600E-09	2.22120E-10
133 I	7.49000E+04	3.40000E+15	3.40000E+15	3.40000E+15	3.40000E+15	9.94000E-09	2.22000E-10
134 I	3.17000E+03	1.60000E+12	1.60000E+12	1.60000E+12	1.60000E+12	4.39200E-08	9.10800E-10
135 I	2.38000E+04	1.60000E+15	1.60000E+15	1.60000E+15	1.60000E+15	2.71400E-08	5.29200E-10
134 Cs	6.50000E+07	4.10000E+14	4.10000E+14	4.10000E+14	4.10000E+14	2.54000E-08	5.33000E-10
136 Cs	1.13184E+06	1.30000E+14	1.30000E+14	1.30000E+14	1.30000E+14	3.57840E-08	7.30800E-10
137 Cs	9.52093E+08	2.80000E+14	2.80000E+14	2.80000E+14	2.80000E+14	3.34080E-11	1.07640E-12
127 Te	3.36600E+04	2.20000E+14	2.20000E+14	2.20000E+14	2.20000E+14	1.20240E-10	3.70800E-12
127m Te	9.41760E+06	3.50000E+13	3.50000E+13	3.50000E+13	3.50000E+13	4.03200E-11	3.08200E-12
129 Te	4.17600E+03	9.60000E+13	9.60000E+13	9.60000E+13	9.60000E+13	1.02960E-09	4.10400E-11
129m Te	2.90304E+06	1.50000E+14	1.50000E+14	1.50000E+14	1.50000E+14	5.61600E-10	2.05200E-11
131 Te	1.50000E+03	8.40000E+13	8.40000E+13	8.40000E+13	8.40000E+13	6.91200E-09	1.70600E-10
131m Te	1.08000E+05	3.70000E+14	3.70000E+14	3.70000E+14	3.70000E+14	2.35800E-08	4.82400E-10
132 Te	2.81520E+05	3.00000E+15	3.00000E+15	3.00000E+15	3.00000E+15	3.35520E-09	7.63200E-11
90 Mo	2.04120E+04	9.60000E+14	9.60000E+14	9.60000E+14	9.60000E+14	1.31040E-08	2.81000E-10
127 Sb	3.32640E+05	1.50000E+14	1.50000E+14	1.50000E+14	1.50000E+14	1.12320E-08	2.43400E-10
129 Sb	1.55520E+04	1.10000E+14	1.10000E+14	1.10000E+14	1.10000E+14	2.41560E-08	4.93200E-10
99m Tc	2.16720E+04	9.00000E+14	9.00000E+14	9.00000E+14	9.00000E+14	1.92600E-09	4.10400E-11
103 Ru	3.39379E+06	5.20000E+13	5.20000E+13	5.20000E+13	5.20000E+13	7.48800E-09	1.61600E-10
105 Ru	1.59840E+04	7.30000E+12	7.30000E+12	7.30000E+12	7.30000E+12	1.28160E-08	2.81500E-10
106 Ru	3.18124E+07	1.90000E+13	1.90000E+13	1.90000E+13	1.90000E+13	0.00000E+00	0.00000E+00
140 La	1.44979E+05	1.30000E+11	1.30000E+11	1.30000E+11	1.30000E+11	3.99600E-08	7.77600E-10

Figure H-2: 3 hr PCM LTSBO released radionuclides ACTIVITY.txt FILE

Mass Nucl	T1/2	U235H	U235T	Pu239H	Pu239T	Cloudshine	Groundshine
Hr= 0.00	sec	Bq	Bq	Bq	Bq	rem/h Bq/m3	rem/h Bq/m2
85m Kr	1.61000E+04	1.19000E+08	1.19000E+08	1.19000E+08	1.19000E+08	2.47000E-09	5.65200E-11
85 Kr	3.37000E+08	3.52000E+05	3.52000E+05	3.52000E+05	3.52000E+05	8.64000E-11	3.78000E-12
87 Kr	4.57000E+03	1.23000E+08	1.23000E+08	1.23000E+08	1.23000E+08	1.42920E-08	3.02400E-10
88 Kr	1.02000E+04	3.12000E+08	3.12000E+08	3.12000E+08	3.12000E+08	3.49560E-08	6.22800E-10
133 Xe	4.53000E+05	1.63000E+09	1.63000E+09	1.63000E+09	1.63000E+09	4.78800E-10	1.42200E-11
135 Xe	3.28000E+04	1.64000E+08	1.64000E+08	1.64000E+08	1.64000E+08	3.96400E-09	9.00000E-11
138 Xe	8.53000E+02	6.28000E+07	6.28000E+07	6.28000E+07	6.28000E+07	1.97280E-08	3.85200E-10
131 I	6.94656E+05	1.89000E+04	1.89000E+04	1.89000E+04	1.89000E+04	6.08400E-09	1.31040E-10
132 I	8.28000E+03	1.26000E+04	1.26000E+04	1.26000E+04	1.26000E+04	3.78000E-08	7.92000E-10
133 I	7.49000E+04	1.21000E+04	1.21000E+04	1.21000E+04	1.21000E+04	9.94000E-09	2.22000E-10
134 I	3.17000E+03	2.50000E+04	2.50000E+04	2.50000E+04	2.50000E+04	4.39200E-08	9.10800E-10
135 I	2.38000E+04	1.47000E+04	1.47000E+04	1.47000E+04	1.47000E+04	2.71400E-08	5.29200E-10
134 Cs	6.50000E+07	1.06000E+03	1.06000E+03	1.06000E+03	1.06000E+03	2.54000E-08	5.33000E-10
137 Cs	9.52093E+08	1.50000E+03	1.50000E+03	1.50000E+03	1.50000E+03	3.34080E-11	1.07640E-12

Figure H-3: Normal Operation released radionuclides ACTIVITY.txt FILE

List of Publications, Article Submission and Conference Presentation Based on This Research Work

PART-A	1. ***Faisal, S. I, Soner, M. A. M., Islam, M. S., (2023)*** Prediction of radioactivity releases for a Long-Term Station Blackout event in the VVER-1200 nuclear reactor of Bangladesh. *Nuclear Engineering and Technology*, Volume 55, Issue 2, 696-706. https://doi.org/10.1016/j.net.2022.10.003 (ISI Indexed; 2022 Impact Factor: 2.7 2. Simulating protective interventions for the Rooppur VVER-1200 during Long-Term Station Blackout scenarios using RASCAL and HotSpot has been under review in the journal of *Heliyon* and second revision has been submitted. (ISI Indexed; 2025 Impact Factor: 3.6) 3. Simulation Study of Long Range Radionuclide Atmospheric Transport and Deposition Distribution for the INES Level 7 event of the Rooppur NPP has been prepared for submission. 4. Time-dependent release exposure behavior in Long Term Station Black out scenarios of VVER-1200 reactors, International Conference on Nuclear and Radiological Emergencies: Building the Future in an Evolving World, Riyadh, Saudi Arabia, 1–4 December 2025.
PART-B	1. ***Faisal, S. I, Ayoub, A., Soner, M. A. M., Islam, M. S., (2025*)** Deterministic assessment of emergency planning zones and radiological protective measures for Bangladesh's VVER-1200 reactor under severe postulated events. *Nuclear Engineering and Design*, Volume 433, 2025. https://doi.org/10.1016/j.nucengdes.2025.113841 (ISI Indexed; 2025 Impact Factor: 2.1) 2. Re-evaluation of the emergency planning zones of the Bangladesh Rooppur nuclear power plant, International Conference on Resilience of Nuclear Installations against External Events from a Safety Perspective – Focus on Climate Change, IAEA Headquarters, Vienna, Austria, 20–24 October 2025.
PART-C	1. ***Faisal, S. I, Islam, M. S., (2025)*** Modeling and validation of airborne effluent dispersion and radiological doses from a VVER-1200 reactor routine operations using HYSPLIT. *Annals of Nuclear Energy,* 227, 111986, https://doi.org/10.1016/j.anucene.2025.111986 (ISI Indexed; 2025 Impact Factor: 2.3)